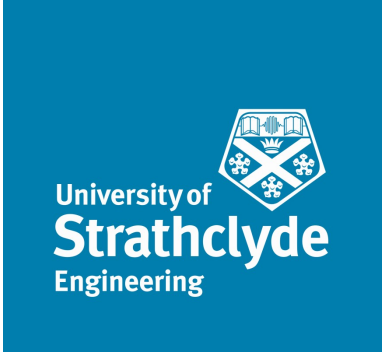

Rheological characterisation and numerical flow simulation of the human eye vitreous humour fluid

PhD Thesis

Andreia F. Silva

James Weir Fluids Laboratory
Mechanical and Aerospace Engineering
University of Strathclyde, Glasgow

February 2018

This thesis is the result of the author's original research. It has been composed by the author and has not been previously submitted for examination which has led to the award of a degree.

Andreia F. Silva

September 2017

This PhD is fully granted by the Portuguese Science and Technology Foundation (FCT - Fundação para a Ciência e a Tecnologia) through the Scholarship SFRH/BD/91147/2012

Abstract

In this work, the dynamics of vitreous humour (VH) and of a range of pharmacological fluids used to replace VH in eye surgery were investigated, both experimentally and numerically. Vitreous humour is a gel-like viscoelastic material that fills the majority of the ocular globe. Age-related changes occur in the VH, and as a consequence VH becomes progressively liquefied with age, which has an impact on the corresponding rheological properties, and leads to the appearance of vitreoretinal pathologies. The most effective treatment for such diseases is the injection of a VH substitute in the vitreous cavity. Most of the vitreous substitutes commercially available are silicone oils (SiO) and perfluorocarbon liquids (PFLC), but so far none of them proven to be used as a permanent substitute.

The results of the rheological characterisation of the VH and pharmacological fluids under shear and extensional flow conditions are presented in the first part of this thesis. Vitreous humour samples were obtained from New Zealand specimen rabbit eyes, whereas the pharmacological fluids were purchased from two different pharmaceutical companies.

Two distinct VH phases were analysed: a liquid and a gel phase. The average surface tension measured for the VH liquid phase was 47.8 mN/m, at $T = 21 \pm 2$ °C. Steady shear experiments demonstrated that VH liquid phase has a pronounced shear-thinning behaviour. Small amplitude oscillatory shear (SAOS) experiments showed that both gel and liquid VH phases present a solid-like behaviour, which is more dominant in the gel phase, and these results were corroborated by creep experiments. Experiments with the VH liquid phase under extensional flow yielded an average relaxation time of $\lambda = 9.7$ ms, at $T \simeq 37$ °C.

None of the pharmacological fluids tested showed a rheological behaviour close to the VH. The PFLCs and SiO-based fluids exhibit a Newtonian behaviour, with the exception of Siluron 2000 fluid, which under extensional flow presents a relaxation time of $\lambda = 6.8$ ms, at $T \simeq 20$ °C. The PFLCs have viscosities close to the viscosity of water, whereas the SiO-based fluids present viscosities between 0.73 and 4.57 Pa s, at $T = 37$ °C. Surface tension experiments showed that the PFLCs present lower values than the SiO-based fluids, and that the surface tension of the VH liquid phase is more than double of that measured for each of the pharmacological fluids tested. In contact with VH liquid phase from rabbit eyes, all the pharmacological fluids tested yielded interfacial tensions around 30 mN/m.

The dynamic response of VH during saccadic movements was studied numerically using the opensource software OpenFOAM®. A comparative study between the VH and pharmacological fluids was performed for a saccadic movement with an amplitude of 40°. The numerical results showed that the VH liquid and gel phases present distinct behaviour. The shear stresses at the walls for the VH gel phase are higher than those produced by the VH liquid phase. This shows that the phase balance in VH significantly affects the flow dynamics of the biofluid. The numerical results also showed that velocity and wall shear stress (WSS) profiles are significantly different for VH and pharmacological fluids, revealing that the latter are unable to mimic accurately the VH flow behaviour in conditions such as those experienced during saccadic eye movements. Finally, different degrees of saccadic movements were studied and the numerical results showed that, for all the fluids investigated, the momentum diffusion across the vitreous cavity and the WSS increase with the increase of the saccadic movement amplitude.

The new experimental results provided in this thesis, complemented by the dynamic behaviour computed numerically for saccadic eye movements, offer new insights for the improvement and development of new VH substitutes to be used in eye surgery, with particular focus on their mechanical functionality.

Keywords: Vitreous humour, Vitreous humour substitutes, Rheology, Biorheology, Shear flows, Extensional flows, Computational fluid dynamics, Saccadic movements

To my Family

No matter how far we can be from each other

You will always be my inspiration...

João, your smile and laugh will

live forever in my memory.

Acknowledgements

I would like to express my sincere gratitude to everyone who helped and supported me during the progress and completion of this thesis. This PhD was an unforgettable experience, and I will carry with me everything I have learned during these years.

First of all, I would like to acknowledge my supervisors, Doctor Mónica Oliveira and Professor Manuel Alves, for the expert guidance, strong support and continuous encouragement. I feel really lucky to have you as my supervisors. Mónica, I wouldn't have chosen anyone else to be my lead supervisor. Thanks for all the support and for always being eager to help. Manuel, thanks for all the discussions that showed me the right direction.

I would also like to acknowledge Fundação para a Ciência e a Tecnologia for the financial support through the PhD Scholarship SFRH/BD/91147/2012.

Obrigada to all of my colleagues from Centro de Estudos de Fenómenos de Transporte (CEFT), for always making me feel welcome and for providing a friendly work environment. I am deeply grateful to Doctor Patricia Sousa for all of her kindness and help. I would like to thank Francisco Pimenta for all the help and guidance regarding the OpenFOAM codes.

I would also like to acknowledge all the James Weir Fluids Laboratory (JWFL)/lunch group members. Our insane conversations actually helped me keep my sanity during all of this process. A special thanks to Thomas, for all the help with Linux, for providing me some extra cores every time I needed and for everything else.

To my Glasgow family, Ana, Inês, Nuno, Miguel, Kiko, Laura, Mari, Davide, Flo, Paula, Ivan and Dan. You really made my life in Glasgow much better, and I am thankful to all of you. Thanks Inês for receiving me in your house when I arrived, and

always made me feel welcomed. Ana, you were a great flatmate. I believe that you know more about rheology than you would like, just by listening to me talking/complaining about it!

To my MIB friends, thank you for all the moments, conversations, and for making me believe that surviving this was possible and everything would be alright. Some of you are Doctors now, or in the process of becoming one, and even being far from each other I believe we have managed to help and cheer each other through this years.

Ευχαριστώ Iasona for being there, in the good and dark days. Thank you for all of your patience, kindness and support. Life is better with you around.

Um obrigada muito especial para a minha familia, Mãe, Pai e Sofia vocês são os maiores. Obrigada por todo o apoio. Amo-vos muito. Obrigada também ao resto da familia (não vou por nomes senão isto iria tornar-se longo!). Embora a maioria não faça ideia acerca do topico deste Doutoramento, sempre me apoiaram e dão uma cor especial aos meus dias.

"*If we knew what it was we were doing, it would not be called research, would it?*"

Albert Einstein

Contents

List of Figures

List of Tables

Glossary

Greek Letters

α	Angle; Nonlinear parameter of the Giesekus model
β	Viscosity ratio
$\dot{\gamma}$	Shear-rate
$\dot{\gamma}_{\infty}$	Steady shear-rate
$\dot{\gamma}_r$	Shear-rate in the rim
γ_0	Strain amplitude
γ_r	Recoil strain
δ	Phase angle
Δt	Time-step
Δp	Pressure difference
$\Delta \rho$	Density difference
$\dot{\varepsilon}$	Strain rate
ε_H	Hencky strain
η	Shear viscosity
η_0	Zero-shear viscosity
η_E	Extensional viscosity
η_p	Polymer viscosity coefficient
η_s	Solvent viscosity
$\eta*$	Complex viscosity
θ_0	Cone angle
λ	Relaxation time

λ_p	Average relaxation time
μ	Dynamic viscosity
ρ	Density
ρ_d	Drop phase density
σ	Surface tension
τ	Shear stress
τ_0	Applied constant stress
τ_{11}	Normal stress
τ_{22}	Normal stress
$\boldsymbol{\tau}$	Extra-stress tensor
$\boldsymbol{\tau}_s$	Solvent-stress tensor
$\boldsymbol{\tau}_p$	Polymer-stress tensor
Ψ_1	First normal-stress coefficient
Ψ_2	Second normal-stress coefficient
Ω	Angular velocity
Ω_p	Peak angular velocity
ω	Angular frequency

Roman Letters

A	Amplitude; area
AR	Aspect ratio
CR	Contraction ratio
D	Diameter; caracteristic dimension
D_0	Diameter of the filament at time $t = 0$
D_p	Diameter of the plates
d	Slope
De	Deborah number
El	Elasticity number
F	Applied force
G	Elastic modulus

G'	Storage modulus
G''	Loss modulus
G^*	Complex modulus
$\boldsymbol{g}$	Gravitational acceleration
h	Depth of the microchannel; gap between plates
I	System inertia
i	Imaginary constant ($i^2 = -1$)
J	Compliance
J_s	Steady state compliance
K_σ	Geometry stress factor
K_γ	Geometry strain factor
L	Characteristic dimension; length
L_0	Initial length
L_f	Final length
M	Torque
M_0	Oscillatory torque amplitude
N_1	First normal-stress difference
N_2	Second normal-stress difference
p	Pressure
Q	Flow rate
R	Radius
Re	Reynolds number
t	Time
t_0	Initial time
t_c	Critical time
t_D	Saccadic movement duration
t_{diff}	Diffusive time scale
t_{flow}	Characteristic time of the flow
t_p	Aceleration time

t'	Elapsed time
Tr	Trouton ratio
U	Characteristic velocity; average velocity
$\mathbf{u}$	Velocity vector
$\mathbf{u}_g$	Grid velocity vector
$u_{\mathbf{p}}$	Peak angular velocity
WSS	Wall shear stress
w_c	Contraction lenght
w_u	Upstream channel lenght
Wi	Weissenberg number
x, y, z	Cartesian coordinates

Subscripts

ave	Average
k	Mode index
mag	Magnitude
max	Maximum
min	Minimum
x, y, z	Cartesian coordinates

Superscripts

T	Transpose

Acronyms

2D	Two-dimensional
3D	Three-dimensional
AGEs	Advanced glycation end products
AH	Aqueous humour
BSS	Balanced salt solution
CaBER	Capillary breakup extensional rheometer
CFD	Computational fluid dynamics
CS	Chondroitin sulphate
CUBISTA	Convergent and Universaly Bounded Interpolation Scheme for the Treatment of Advection
F4H6	Perfluorobutylhexane
F6H8	Perfluorohexyloctane
FEM	Finite element model
fps	Frames per second
FSiO	Fluorosilicone oil
FT-Raman	Fourier transform Raman
GAGs	Glycosaminoglycans
GNF	Generalised Newtonian fluid

HA	Hyaluronic acid
HMW	High molecular weight
HPF10	Fluorinated perfluorodecalin
HPF8	Perfluoro-n-octane
HSiO	Heavy silicone oil
IFT	Interfacial tension
IOP	Intraocular pressure
LMW	Low molecular weight
MAGME	Poly(methyl acrylamido glycolate methyl ether)
MRI	Magnetic resonance image
MW	Molecular weight
OSCER	Optimised Shape Cross-slot Extensional Rheometer
PAA	Poly(acrylamide)
PBS	Phosphate buffered saline
PDMS	Poly(dimethylsiloxane)
PDR	Proliferative diabetic retinophaty
PEO	Poly(ethylene oxide)
PFD	Perfluorodecalin
PFLC	Perfluorocarbon
PGMA	Poly(glyceril-methacrylate)
PHEMA	Poly(2-hidroxyethylmethacrylate)
PIV	Particle image velocimetry

PTT	Phan-Thien Tanner
PVA	Poly(vinyl alcohol)
PVD	Posterior vitreous detachment
PVP	Poly(1-vinyl-2-pyrrolidinone)
RD	Retinal detachment
RMN3	Mixed fluorinated and hydrocarbonated olefin
SAOS	Small amplitude oscillatory shear
SiFO	Silicone-Fluorosilicone oil
SIMPLE	Semi-Implicit Method for Pressure-Linked Equations
SIMPLEC	Semi-Implicit Method for Pressure-Linked Equations-Consistent
SiO	Silicone oil
SRM	Slow retraction method
ST	Surface tension
STMP	Sodium trimetaphosphate
UCM	Upper-Convected Maxwell
VH	Vitreous humour
WSS	Wall Shear Stress

"Everything is theoretically impossible, until it is done."

Robert A. Heinlein

Chapter 1

Introduction

This thesis topic, "*Rheological charaterisation and numerical flow simulation of the human eye vitreous humour fluid*", was motivated by the increase of eye diseases as a consequence of the increase of life expectancy [1]. It was found that there is a lack of studies presenting a detailed rheological characterisation of vitreous humour (VH), as well as numerical studies that try to understand how the rheological properties of the biofluid affect its flow behaviour. A more detailed knowledge of the rheological properties of the VH and how it behaves when subjected to everyday eye movements can actively help to find and improve solutions for health problems related with VH.

1.1 The Human eye and the process of sight

The eye is one of the most complex sensory organs in the Human body [2]. The eye has several components, each occupying a central role in sighting and processing what surround us. The main components of the eye are shown in Fig. 1.1.

The sclera is the white protective tissue around the eye. In the front of the eye, the cornea is the thin and transparent cover that protects the iris. It is the most sensitive tissue in the body. The iris is the coloured part of the eye and the amount of pigment

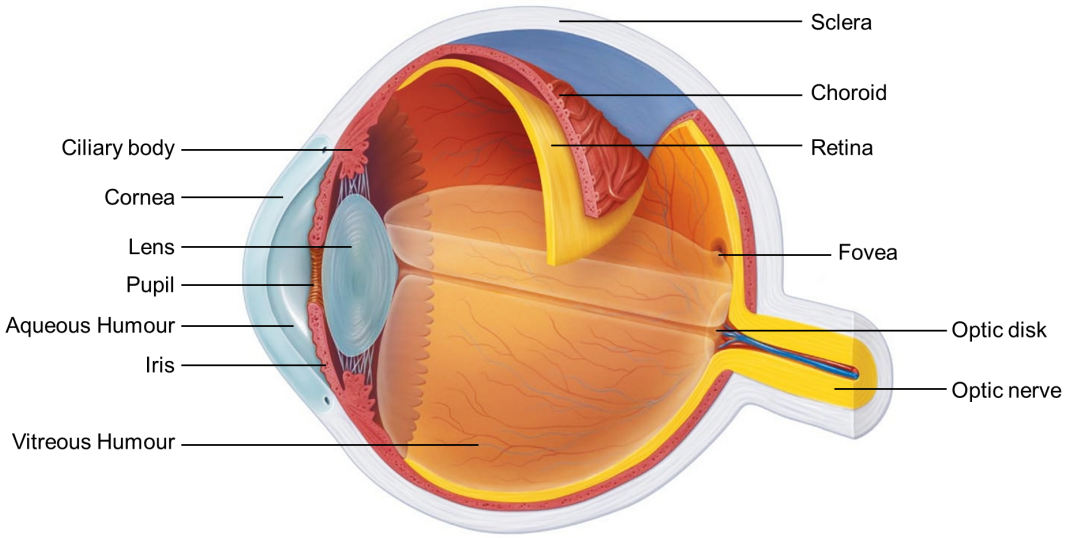

Figure 1.1. Anatomy of the eye and main structures involved in the sight process. Adapted from [3].

present determines the eye's colour. The pupil is the hole in the centre of the front of the eye. Curiously, most people commonly think that the pupil is black but indeed it is just an hole. The ciliary body includes the ciliary muscles that control the shape of the lens and the ciliary epithelium, which produces the aqueous humour (AH). AH is an optical transparent and alkaline fluid in constant circulation between the cornea and the lens. The lens is located right behind the iris and pupil and has the function of refracting the light to be focused on the retina. This part of the eye is surrounded by the two fluids of the eye: the AH and the vitreous humour (VH). VH is the transparent fluid that fills the eyeball between the lens and the retina. The retina is the inner surface of the eye and is mainly composed by rods and cones: the rods detect brightness and the cones detect colour. The fovea is a small pit in the retina composed mostly by cones. The network of the blood vessels that transport oxygen and other nutrients to the retinal pigment cells is called choroid. The optic disk is the structure in the retina (in the back of the eye) where all the nerve cells from the rods and cones connect with each other. Finally, behind the optic disk, the eye has the optic nerve that sends the signals to the brain [4–6].

The eye components are all interconnected and actively contribute to the process of sight. To be able to see, the first thing that the eyes need to do is to process light. The light reaches the eye and passes through the cornea, enters the pupil and then reaches the lens which adjusts its shape in order to focus. The cornea, pupil and lens combined produce a clear image that passes through the vitreous humour fluid and it is recognised by photoreceptors all over the retina, which is part of the central nervous system and it is located at the back of the eye. The main components of the retina have different functions: rods detect black and white light rays and cones detect colour rays. The size of the pupil, which regulates the amount of light that enters the eye, is controlled by the iris. The lens size and shape are controlled by muscles behind the iris and that is key to focus objects at different distances. The retina's photoreceptors bring together the visual information by absorbing the light, convert it into electric signals and sending those signals via the optic nerve to other parts of the brain, which ultimately processes the image and allows us to see [7]. As there are no rods or cones at the point where the optic nerve leaves the retina, the optic disk area (see Fig. 1.1) is also called blindspot [6].

One of the particularities of sight is that the image that reaches the retina is inverted. The left side of the image is actually processed by the right side of the brain and vice-versa.

1.2 Vitreous humour

The majority of the ocular globe is filled by a clear, colourless, gel-like viscoelastic material known as vitreous humour (VH). Some physical properties of VH are shown in Table 1.1. VH is a transparent gelatinous avascular structure that fills the space between the lens and the retina in the eye [8–12]. There have been various attempts to describe the vitreous structure and its composition [13–15], and it is now accepted that VH is composed approximately of 99% water, 0.9% of salts and 0.1% of a network of fine collagen fibrils and hyaluronan (HA) that form a scaffold [11, 16].

Several functions are attributed to VH: the biofluid helps to maintain the shape and consistency of the eye and pushes on the retina to hold it against the back of the

Table 1.1. Physical properties of the human VH fluid [17–19].

Property	Value
Volume (ml)	4
Weight(g)	4
Water content	99 %
pH	7.0 to 7.4
Osmolality (mOsm/kg)	288 to 323
Freezing point (°C)	-0.554 to -0.518
Density (g/cm^3)	1.0053 to 1.0089
Intrinsic viscosity (cm^3/g)	$3 - 5 \times 10^3$
Dynamic viscosity (cP)	1.6
Refractive index	1.3345 to 1.3348

eyeball; it also allows the light to pass through the lens to the retina during the process of sight; the vitreous serves as a metabolic repository for hyalocytes and neighbouring tissues, and controls the movement of solutes and solvents within the eye; and provides a system that absorbs mechanical stress and protects the surrounding tissues during eye movement and physical activity. This fluid is only produced during the embryonic stage and is not replenished throughout the entire life of a person [17]. It is known that as a consequence of ageing and/or some diseases the VH becomes progressively liquefied [18], with the corresponding rheological properties varying during lifetime.

Most Human eye diseases, such as retinal tears, rhegmatogenous or tractional retinal detachment, retinal edema, choroidal detachment or vitreous hemorrhage are associated with biological changes and consequent modifications in the viscoelastic properties of this biofluid [19].

1.3 Motivation

Ageing is nowadays a major cause of morbidity and mortality around the world [20]. With ageing, part of the body systems start changing, degradating and failing. Some are able to auto regenerate but others do not have such capacity. Eye diseases in which age is a major cause, like cataracts, glaucoma, diabetic retinophaty and age-related macular degeneration, are the main causes of reduced vision and blindness in humans [20]. All of these diseases are related with changes in VH and with the fact that this fluid is only

produced during the embryonic stage [17].

Nowadays, the treatment for such diseases involves eye surgery, more specifically the injection of surgical fluids in the vitreous chamber to try to correct the problem. Those fluids are commonly designated as vitreous substitutes. Unfortunately, until now, there is no fluid that can be used as a permanent vitreous substitute and all the fluids used in surgery have a short time residence inside the eye [18, 21].

The ideal vitreous substitutes should mimic specific characteristics of the VH, such as transparency, elasticity, buffer capacity, and biocompatibility, and avoid some of the negative properties associated with the native substance, such as liquefaction and biodegradation with age. It must also be able to mimic the VH behaviour when subjected to the different types of eyes movements. The development of this ideal substitute remains a goal still to be achieved [22].

As mentioned before, VH has complex viscoelastic properties. Although there have been several attempts to characterise its properties experimentally, the rheology of VH is not yet fully understood [18]. Additionally, the interaction between the vitreous components and their contribution to the overall viscoelastic properties is still poorly understood. So far, only a few computational fluid dynamics (CFD) studies involving the dynamics of VH in the eye have been performed (e.g. [23–26]), and these usually neglect the viscoelastic properties of the fluid and assume unrealistic shapes of the vitreous chamber.

This work investigates, both experimentally and numerically, the dynamics of the VH biofluid as well as of VH substitutes. The main objectives include:

- Performing a detailed rheological characterisation of VH biofluid;
- Characterising several pharmaceutical fluids used in eye surgery;
- Evaluating the impact of the viscoelastic properties on the dynamics of VH when the eyeball is subjected to saccadic movements and comparing the flow dynamics of the VH and the fluids used in surgery when subjected to saccadic movements.

1.4 Outline of the thesis

This thesis refers to the study of the rheology of VH and pharmacological fluids used in eye surgery, and also the flow behaviour of both types of fluids during saccadic movements. The current study had so far an outcome of one (1) publication in an international journal, and the main results of that work is presented in Chapter 4. Moreover, different parts of this research have been presented in seven (7) conferences, with four (4) oral presentations and three (3) posters, in order to disseminate the research performed, and discuss and receive feedback from experts in the field. The studies performed during this PhD are interconnected, thereby this thesis is divided in two sections: the first one includes the chapters related with the experimental work on the rheological characterisation of the fluids under study, whereas the second part contains the chapters associated with the computational fluid dynamics (CFD) work performed to understand the role of viscoelasticity during saccadic eye movements. A schematic representation of this thesis structure is presented in Fig. 1.2.

Chapter 2 presents a literature review on VH and, in particular, its rheological characterisation. The pharmacological fluids used in eye surgery, as well as the fluids that were and are currently under study for the same purpose, are also reviewed in this chapter. A discussion on important considerations that need to be taken into account when designing and creating VH substitutes is presented at the end of this chapter.

Chapter 3 starts with a description of the experimental techniques used during the experimental work to characterise the fluids, followed by the description of the experimental conditions considered in each set of experiments.

A detailed rheological characterisation of VH is presented in Chapter 4. The chapter starts with the results of the surface tension measurements, and is followed by shear rheology results, including steady shear and small amplitude oscillatory shear (SAOS) measurements. Creep experiments are also discussed and the chapter ends with the extensional rheological characterisation of VH. This research has been published in the *Rheologica Acta* journal, under the title "*Rheological behaviour of vitreous humour*" [27]. The corresponding rheological characterisation of the pharmacological fluids available

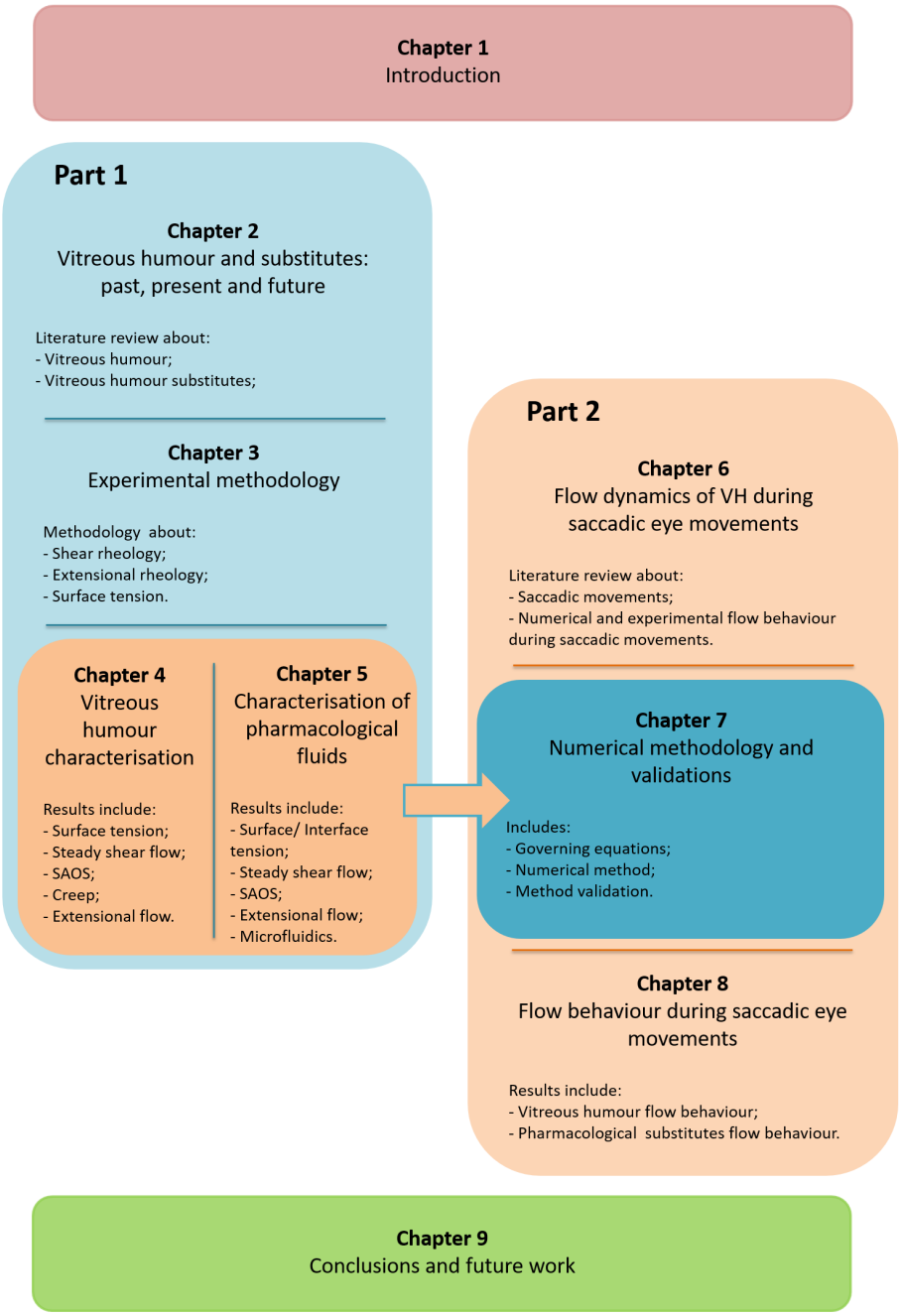

Figure 1.2. Schematic representation of this thesis structure and the relations between the different parts.

commercially is presented and discussed in Chapter 5.

The second part of this thesis starts with Chapter 6 where saccadic eye movements

are described, and a review of experimental and numerical work performed to study these movements in the eye are described.

The numerical methodology of the CFD work performed with the opensource software OpenFOAM® is presented in Chapter 7. Additionally, relevant validations performed with the solvers used are also described in this chapter.

Chapter 8 discusses the results of the numerical simulations, focusing on the comparison of the flow behaviour of VH and pharmacological fluids used in eye surgery. The fluids have different rheological behaviour and as a consequence distinct flow behaviour. The differences on the flow behaviour of VH and pharmacolgical fluids when subjected to different amplitudes of saccadic movements are also quantified and discussed.

This thesis ends with Chapter 9 where the main conclusions of this work are summarised and future work that is relevant in this research area is suggested.

"Failure defeats losers, failure inspires winners."

Robert T. Kiyosaki

Chapter 2

Vitreous humour and substitutes: past, present and future

This chapter presents a review of important studies of VH, from a rheological, chemical and physiological point of view. The VH substitutes used in eye surgery over the years are also described. The main polymers studied with the goal of finding a VH substitute that can remain in the eye permanently are also reviewed. Finally, a comparison between the VH properties from human and animals commonly used in studies *in vitro* and *in vivo* closes this chapter.

2.1 The vitreous humour

As described briefly in Section 1.2, the VH is a transparent gelatinous avascular structure that fills the space between the lens and the retina in the eye [8–12]. The gelatinous nature of the vitreous body is the result of long collagen fibrils suspended in patterns of hyaluronic acid or hyaluronan (HA) molecules and others glycosaminoglycans (GAGs), which surround and stabilise water molecules (see Fig. 2.1).

Various chemical studies were performed with VH over the years. In the "Handbook of Biomaterial Properties", Black [17] summarises the composition of the chemical com-

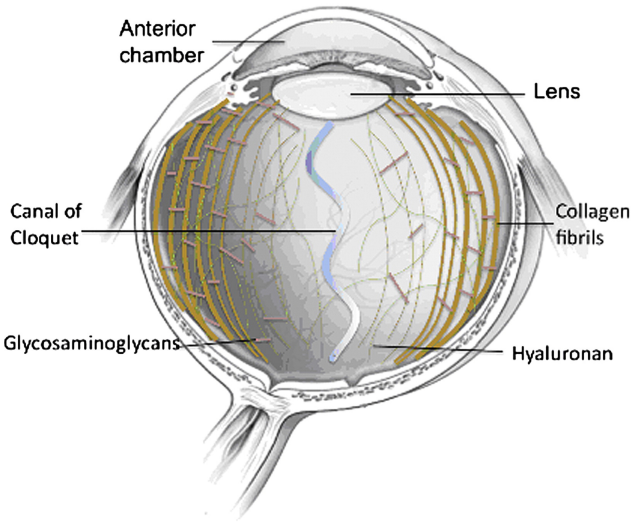

Figure 2.1. Vitreous humour structure (reprinted from [28] with permission from Elsevier).

pounds quantified until 1988, which are presented in Table 2.1. More recently, other authors have further quantified some of the chemical compounds of VH, and those values are also presented in Table 2.1.

The collagen concentration in VH is around $40 - 120\ \mu g/cm^3$ and collagen type II is the most abundant type of collagen in the eye [17,32]. HA is the major glycosaminoglycan in the VH structure [32,33] with a concentration of $100 - 400\ \mu g/cm^3$ [17].

The fibre networks increase in density away from the centre, especially so at the edge of the vitreous to form the bounding anterior and posterior hyaloid membranes [19]. In Human eyes, VH typically occupies a volume of 4 ml, has a neutral pH (between 7.0 and 7.4), a density in the range 1.0053-1.0089 g/cm^3 and a refractive index between 1.3345 and 1.3348 [17–19].

The presence of both HA and collagen together in the vitreous natural molecular architecture is responsible for the viscoelastic properties of the VH [22]. As a viscoelastic gel, the VH exhibits both solid and liquid-like behaviour [34]. Furthermore, the distribution of the collagen fiber network and the HA network is not homogeneous and consequently the rheological properties of VH vary along the vitreous cavity [17,19,22,34]. Lee [19] showed that the viscosity is higher in the posterior region and decreases toward the anterior segment. The author argues that the VH is more viscous at the posterior

Table 2.1. Chemical composition of VH.

Inorganic ions	[17]	[29]	[30]	[31]
Sodium	2.174-3.542 mg/cm^3	139.52 mmol/l	128.5 mmol/l	147.5 mmol/l
Potassium	130-470 μg/cm^3		16.91 mmol/l	5.92 mmol/l
Calcium	56-106 μg/cm^3		0.55 mmol/l	1.27 mmol/l
Phosphate	0.1-3.3 mEq/dm^3			
Chloride	3.155-5.140 mg/cm^3	130.12 mmol/l	114.8 mmol/l	122.5 mmol/l
Organic components				
Lipids	2 μg/ml			
Glucose	30-70 mg/dl	1.590 mmol/l	16.32 mg/dl	2.43 mmol/l
Lactic Acid	70 mg/dl		165.8 mg/dl	3.60 mmol/l
Urea	24-172 mg/dl	5.240 mmol/l	46.4 mg/dl	
Creatinine	0.3-3.0 mg/dl	84.90 mmol/l	1.02 mg/dl	
Citrate	1.9 mg/dl			
Pyruvic Acid	7.3 mg/dl			
Ascorbic Acid	36 mg/100g			
Total protein content	450-1100 μg/cm^3			
Hyaluronan	100-400 μg/cm^3			
Collagen	40-120 μg/cm^3			
Albumin	293 μg/cm^3			
Immunoglobulin	33.5 μg/cm^3			

segment in order to protect the retina and less viscous at the anterior segment in order to allow rapid accommodation.

In terms of the rheological characterisation of the VH, most studies focus on the measurement of the VH storage modulus (G') and loss modulus (G'') to characterise the viscoelastic behaviour [10,11,19,21,35,36], where G' represents the elastic or recoverable component, and G'' represents the viscous component related to the dissipated energy. Those studies reveal that VH has a higher storage modulus than loss modulus, indicating its viscoelastic solid-like behaviour. Nickerson *et al.* [10] developed a novel cleat geometry to overcome wall slip in shear rheometry and reported G' and G'' values measured right after dissection to be 32 Pa and 17 Pa for bovine VH, and 10 Pa and 3.9 Pa for porcine VH. They reported a storage modulus higher than all other sources, which was found to decrease with time after collection (i.e. when outside the eye) approaching steady- state values of $G' = 7.0$ Pa and $G'' = 2.2$ Pa for bovine, and $G' = 2.8$ Pa

and $G'' = 0.7$ Pa for porcine VH, suggesting that the moduli are even higher *in vivo*. Sharif-Kashani *et al.* [11] measured the dynamic deformation, the shear stress-strain flow and the creep compliance of porcine VH using a stress-controlled shear rheometer. For small amplitude oscillatory shear (SAOS) flow experiments, they concluded that only the results with frequencies in the range $\omega = 0.1$–10 rad/s were reliable and the average values obtained for the storage and loss moduli were $G' = 1.08 \pm 0.22$ Pa and $G'' = 0.25 \pm 0.07$ Pa, respectively. Regarding creep tests for VH, three distinct regions were described in the literature [11]: an elastic region (that lasts approximately 1 s), a retardation region ($\sim$ 80 s) and a viscous region. Based on this behaviour, the authors proposed a viscoelastic model consisting of two Voigt-Kelvin elements in series. Additionally, Filas *et al.* [36] measured both moduli for bovine and porcine eyes, in its natural conformation and also after digesting the samples with hyaluronidase and collagenase. The authors observed that bovine VH samples show higher moduli values than porcine VH ($G' \approx 10$ Pa and $G'' \approx 5$ Pa for bovine and $G' \approx 3$ Pa and $G'' \approx 1$ Pa for porcine). Additionally, when the sample was digested with collagenase (loss of collagen) the sample became more liquid, and when digested with hyaluronidase (loss of HA) the sample became more elastic.

Rearrangements of the macromolecular structure of VH occur with ageing, which results in the liquefaction of the vitreous: the VH undergoes liquefaction or transformation from a formed gel to a phase-separated fluid [37, 38]. Three different categories of rearrangements are reported: rheological, biochemical and structural [39, 40]. The gel portion of the vitreous collapses, a process called syneresis, leading to an increase of collagen and of the optical dense areas. Simultaneously, there is a progressive increase in the volume of liquefied spaces (synchysis) [38, 40]. Liquefaction is noticeable mainly in the central vitreous where collagen concentration is lower.

Balazs and Denlinger [37] found that at an age as early as 4 years old the vitreous may start to liquefy and by the time the eye reaches adult size (14-18 years old) 20% of the vitreous is liquid [16, 37, 41, 42]. After the age of 40 years old, they observed a continuous increase in liquid vitreous associated with a decrease in the gel volume [16]. The mechanism involved in the liquefaction of VH is still not clearly understood, but it

is believed to involve conformational changes of the collagen [43].

Sebag [39,44] employed a slit-lamp technique to analyse *post-mortem* eye structures and demonstrated that the vitreous of young people appeared homogeneous while for older people it was possible to observe collagen fibrils moving in the anterior chamber, as shown in Fig. 2.2. Walton *et al.* [40] showed that the eyes of young subjects were analogous to a ball filled with dense gelatine that moves with the movement of the globe. However, in the eyes of older subjects, the movement was less uniform, as a consequence of liquefaction and phase separation. The authors showed an unequal distribution of tractional forces exerted on the retina by less viscous vitreous of an aged eye, and concluded that the biomechanics of the vitreous, and consequently the tractional forces exerted by the vitreous on the retina and the fluid dynamics of the vitreous, suffer alterations due to the liquefaction process. Los *et al.* [38] investigated the morphologic aspects of the VH based mostly on the changes in fibrillar collagen and proteoglycans. The authors used light and transmission electron microscopy to observe the eyes and concluded that a break-down of collagen fibrils into smaller fragments seems to be crucial to the pathogenesis of age-related liquefaction of VH.

Goff and Bishop [42] described that, in early ages, the collagen fibrils form an extended network, being organised into small bundles that are interconnected by collagen fibrils running from one bundle to another. Within each bundle, the collagen fibrils are both connected together and spaced apart by the chondroitin sulphate (CS) chains of type IX collagen. With ageing there is a loss of type IX collagen from the fibril surfaces,

(a) **(b)** **(c)**

Figure 2.2. Vitreous structure from (a) a 33 week gestational age human, (b) a 58 years-old human and (c) an 88 years-old human (reprinted from [39] with permission from Macmillan Publishers Ltd, *Eye*).

which combined with an increased surface exposure of type II collagen results in collagen fibrillar aggregation. The authors report that liquefaction does not occur evenly in the vitreous cavity, with liquid pockets forming in the central vitreous which enlarge and coalesce. The liquefaction process leads to a decrease in the shock-absorbing ability of the vitreous and in addition the vitreous mass gradually shrinks and collapses. Increased liquefaction leads to changes in shear viscosity and elasticity and consequently causes variations in the fluid dynamics of the vitreous and its behaviour during eye movements [45].

The liquefaction process of the vitreous can lead to a decrease or even loss of the VH viscoelasticity, and to the appearance of diseases related with VH, such as retinal detachment and retinal tears [42, 46]. Various studies have also showed that some diseases can lead to modifications in the VH structure [15, 42, 46–48]. Sebag [44] performed a study to identify the morphological changes within the vitreous of diabetic patients. The study identified that hyperglycemia alters vitreous collagen, and that such changes might be responsible for vitreous degeneration. The author found that in a diabetic child, the vitreous structure contained prominent fibers, the appearance of which was similar to that found in middle-aged normal donors and not to the age matched controls. One year later, Sebag *et al.* [46] performed Fourier Transform Raman (FT-Raman) spectra of VH fluid from healthy donours and from diabetic donours, and found that the latter group presented significantly higher levels of the early glycation products. Lundquist and Osterlin [47] studied the concentration level of glucose in nondiabetic patients, diabetic patients with insulin-dependent *diabetes mellitus* and diabetic patients with non-insulin-dependent *diabetes mellitus*. They found that the glucose levels in the VH was higher for the last two groups, leading them to conclude that the high sugar levels in the diabetic groups increase the risk of collagen glycation in the vitreous of the diabetic patients. Stitt *et al.* [48] also attempted to correlate the glycation of the macromolecules present in the VH. The authors studied eyes from patients with different ages and eyes from diabetic patients and showed that advanced glycation end products (AGEs) occur in eyes with advanced age, but the occurrence of diabetes accelerates the process and consequently eyes of diabetic patients suffer glycation in

early ages, promoting the cross-linking of the VH collagen network.

As described before, there are histological/chemical studies showing that VH suffer rearrangements of the macromolecular structure, as a natural process of ageing or as a consequence of some diseases, which result in the liquefaction and separation of the fluid in two distinct phases: a *gel* and a *liquid phase*. However, and despite the study performed by Lee [19], all the previously described rheological studies performed with VH assume that the sample is a gel, and there is no reference about differences in the rheological characteristics of different phases of VH. Rheological information about the different phases can be crucial in order to help in the improvement and creation of health products directly or indirectly related with the VH biofluid.

2.2 Pharmacological fluids: past and present

Several functions are attributed to VH, including: the growth of the eye and the retinal pigment epithelium is dependent upon the growth of the vitreous and the forces generated by its growth; VH provides a transparent medium for the passage of light to the retina; VH serves as a metabolic repository for hyalocytes and neighbouring tissues, and controls the movement of solutes and solvents within the eye; the biofluid also provides a system that absorbs mechanical stress and protects the surrounding tissues during eye movement and physical activity [19]. Changes in the VH can have a serious impact in their functionality, leading to the appearance of several diseases, such as [19, 45]:

- Posterior vitreous detachment (PVD);
- Retinal tears, retinal detachements and vitreomacular traction;
- Diabetic retinopathy and vitreopathy;
- Cataract formation;
- Proliferative vitreoretinopathy;
- Age related macular degeneration.

For the normal operation of the eye, when some of those diseases appear, clinical treatments must be performed. The most effective treatment for most of these diseases is the injection of a fluid in the vitreous cavity. These substances, known as vitreous substitutes, can be used intraoperatively to push a detached retina to its normal position, to restore the volume of the vitreous cavity, and to help the surgeon in membrane dissection. Some of these agents can be used as post-operative adjuncts to provide internal tamponade after vitreous surgery [49]. Unfortunately, a substitute that can reproduce the properties of VH and remain for long periods or even permanently in the vitreous cavity has not yet been found. The ideal vitreous substitute should mimic the native vitreous in both form and function while being easily manipulated during surgery. In general, a suitable VH substitute is expected to [8, 21, 22]:

- have rheological properties similar to VH;
- maintain intraocular pressure and support intraocular tissues;
- allow the movement of ions and electrolytes through the biofluid;
- be transparent;
- have buffer capacity;
- be biocompatible with the surrounding tissues;
- have density and refractive index similar to the natural vitreous;
- be amphiphilic, but not soluble in water;
- ensure low (superior breaks) and high (inferior breaks) specific gravity;
- avoid liquefaction and biodegradation with time (one of the biggest negative problems of VH);
- be able to stay permanently in the vitreous chamber;
- be easily available;
- be stable during storage;

- be injectable through a small syringe needle;
- guarantee that the forces generated by the presence of a new fluid will not compromise the normal functionalities of the real VH.

Past and current available VH substitutes can be divided in gases (air, sulfur hexafluoride, or perfluoropropane) and liquids (water and salt solutions, perfluorocarbons - PFLC, semifluorinated alkanes, fluorosilicone oils - FSiO, and silicone oils - SiO). Currently, none of them can be used as a long term VH substitutes (all commercial VH substitutes so far have a residence time smaller than 6 months) and a description of those fluids is presented in Section 2.2.1 and Section 2.2.2.

2.2.1 Gas VH substitutes

Gases were the first fluids used as a vitreous substitute. Table 2.2 presents a list of the gases used in eye surgery over the years.

The advantages of using gases as a VH substitute was related to their high surface tension, allowing them to maintain a tamponade effect, but only in the absence of movement of the head, and the fact that gases do not require a surgical procedure for its removal as they disappear by themselves. These fluids showed an unsatisfactory behaviour when left in the eye for long periods. Jacobs *et al.* [51] showed there is a volume loss along time for bubbles of air, sulphur hexafluoride, perfluoropropane (and mixtures of these gases) when used in eye surgery. Depending of the gas used, the

Table 2.2. Gases used as VH substitutes [18, 50]

Substance	Year	Residence time	Problems
Air	1911	1-4 days	Rapid diffusion, loss of tamponade effect
Perfluorocarbons	1980	1-2 weeks	Increase IOP, central retinal artery occlusion, postoperative position
Perfluoropropane	1970	1-2 weeks	Increase IOP, central retinal artery occlusion, postoperative position
Octafluorocyclobutane	1975	1-2 weeks	Cataracts, edematous conjunctiva

maximum time required for the bubble to disappear from the eye was 60 days. The residence time of gases was not the only problem associated with these VH substitutes, and in fact most importantly gases increase the intraocular pressure (IOP) and as a consequence patients ended up having post-operatory complications [18, 50].

Gases are still used nowadays in vitreoretinal surgery. However, because of all the problems associated with them, their use is limited to very specific cases and they are considered a short term substitute [18].

2.2.2 Liquid VH substitutes

Over the years, several liquids have been studied for vitreous replacement (see Table 2.3). Some of them are currently used in eye surgery with success. Nowadays, perfluorocarbons (PFLC) and silicone oil (SiO) based fluids are the only VH substitutes regulated and approved by the European Medicines Agency (EMA) - Europe, and Food and Drug Association (FDA) - United States of America, for use in surgery in the posterior segment of the eye. Note that the heavy silicone oils (HSiO) are approved and used in Europe, but not in the United States of America.

Perfluorocarbons are clear, transparent and can dissolve gas, although being immiscible with aqueous solutions. The action in the eye of PFLCs is purely mechanical. Perfluorocarbons are mostly used in retinal detachments and are immediately removed from the eye after the retina is restored to its normal position. If left in the eye for long periods, PFCLs can induce morphological changes in the inferior retina caused by mechanical compression. Their high density and low viscosity, together with a low interfacial tension against the liquefied vitreous and the eye facilitate intraocular dispersion of PFCLs during head motion [49]. Imamura *et al.* [52] reviewed the proliferative diabetic retinopathy (PDR) surgical records performed in Osaka Medical College, between April 1999 and October 2001. During that period, 18 eyes were treated with PFLC fluids, with 16 showing clinical success. The PFLCs were removed at the end of surgery. The study corroborates the fact that, for short periods of time, the injection of PFLCs can be used successfully in eye surgery.

SiO started being studied during the 1950's. In 1958, Stone [53] reported the first *in*

vivo study with SiO: liquid silicone was injected into the vitreous cavity of rabbits. The results were promising and in 1962, the first clinical study with Humans was reported, with 33 patient eyes being injected with liquid silicone [54]. SiO are the most used VH substitutes showing suitable properties such as stability, transparency, and high interfacial surface energy with the eye tissues. The first SiO used in eye surgery were composed by SiO molecules of just one molecular weight (MW). Different viscosities were available, between 1 and 5 Pa s, corresponding to SiO with MW between 25 and 50 kD.

SiO with lower viscosities have the advantages of requiring smaller needles and a shorter injection time during the surgical procedure [55]. However, the emulsification rate of the SiO with lower viscosities is higher than for the ones with higher viscosity. Light [56] reported a case study with a 59 years old patient that had a retinal detachment repair. The patient showed emulsified SiO that had migrated from the posterior to the anterior chamber (see Fig. 2.3), requiring the removal of the SiO from the vitreous cavity after the retina was reattached. SiO emulsification can affect the retina, optic nerve,

Table 2.3. Liquids used as VH substitutes [45].

Substance	Year	Density (g/cm^3)	Viscosity (cSt)	RI*	Residence time
Balanced salt solution (BSS)	1948	1.08	1	1.333	–
Silicone Oil (SiO)	1962	0.97	1000-5000	1.404	2-3 months (maximum of 6)
Silicone-Fluorosilicone Oils (SiFO)	–	1.16	170-200	1.390	2 months
Fluorosilicone Oil (FSiO)	1990	1.29	1000-10000	1.382	2 months
Perfluoro-n-octane	1988	1.73	0.8	1.280	–
Perfluorodecalin (PFD)	1988	1.94	2.7	1.310	2 weeks
Perfluorohexyloctane	2002	1.35	1.342	1.330	–
Silicone Oil/ Perfluorohexyloctane	2005	1.06	1.48	1.387	maximum of 6 months

*RI - Refractive index

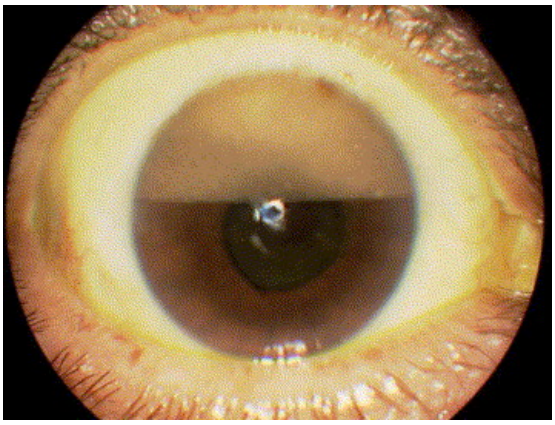

Figure 2.3. Silicone oil droplets in the superior anterior chamber of the eye (reprinted from [56] with permission from Elsevier).

and even extraocular structures, and is also associated with various complications, such as glaucoma or corneal decompensation, which can lead to blindness. Chan *et al.* [57] tested the emulsification of SiO during eye movements. A cylindrical chamber was used to resemble the vitreous cavity and saccadic movements with an angular displacement around 9° and a maximum angular velocity of approximately 400°/s were tested. The study showed that SiO with higher viscosity tend to move with the eye chamber, and as a consequence have less relative movement which could be one of the reasons for their lower tendency to emulsify.

To try to overcome the emulsification problems, new SiO composed by two different MWs were created. Based on the information provided by the manufacturers and in the literature [57–60], adding a small amount of SiO with a high molecular weight (HMW) to a SiO with short chains increases the resistance of the fluid to emulsification: the viscosity of the fluid increase when compared with the SiO with only the short chains, but not enough to significantly increase the injection time during surgery; additionally, the HMW chains give the fluid some elastic properties and increase the elongational viscosity of the fluid, as it becomes more elongated and aligned with the flow direction [59]. Day *et al.* [61] measured the shear and extensional rheology of SiO with low molecular weight (LMW) and mixtures with SiO with LMW and HMW. Extensional rheology tests showed that the mid-filament diameter decays linearly with time, consistent with Newtonian fluid behaviour. Caramoy *et al.* [58, 59] performed different studies to test

the emulsification rates of conventional and HMW SiOs. In [58] the authors tested SiOs commercially available for eye surgery. In [59] besides the comercially available SiOs, new samples with different percentages of a HMW SiO (7%, 10% and 15%) were added to a SiO with a viscosity of approximately 1 Pa s, known as Siluron 1000 which is commercially available (Fluoron GmbH). Different emulsifier agents were used. Overall, their results showed that the samples with HMW chains presented a lower percentage of emulsified area. Additionally, in [59] the elastic and viscous moduli, and the viscosity of the fluids were measured, using a piezoelectric axial vibrator. The experimental results showed that all the fluids presented measurable elastic and viscous moduli and the elasticity increased with the insertion of HMW chains up to a percentage of 10%. Williams *et al.* [60] also observed that increasing the extensional viscosity of SiO reduces their tendency for emulsification. The shear and extensional viscosity of SiO with a shear viscosity of 1 and 5 Pa s, a 50:50 mixture of 1 and 5 Pa s and 5% and 10% of HMW SiO, respectively, were measured using capillary breakup extensional rheometry, rotational shear rheometry, and capillary extrusion rheometry. The authors concluded that adding low concentrations of HMW chains of the same chemistry as the bulk oil has the potential to increase the emulsification resistance of the tamponade agents, while maintaining their ease injection and removal. Note that ultimately, independently of being composed by a single MW or being a mix of different MWs, all the SiO fluids available for eye surgery need to be removed from the eye.

Heavy silicone oils (HSiO) were also introduced in eye surgery. Because of their increased density, they provide a better tamponade effect than the common SiO for the treatment of inferior retinal detachment. Different HSiO are available, such as the fluids Densiron 68 and Densiron Xtra (Fluoron GmbH), or Oxane HD (Bausch + Lomb). Densiron 68 and Densiron Xtra are a combination of SiO with a viscosity of 5 Pa s and perfluorohexyloctane (F6H8) in a proportion of approximately 70/30 [62]. Densiron Xtra also has SiO with HMW. Oxane HD is composed by 11.9% of a mixed fluorinated and hydrocarbonated olefin (RMN3) and 88.1% of SiO with a viscosity around 5.7 Pa s. These fluids show good results when used in surgery and longer residence times than the common SiO. Schwarzer *et al.* [63] performed a retrospective study including 100 eyes

that had vitreoretinal surgey with HSiO. The HSiO was removed after a mean period of 20.2 weeks, except in 18 eyes where the fluid remained in the eye (the follow-up time was in average 35.9 weeks). Even though the tests showed satisfatory results, some complications were recorded leading the authors to conclude that the removal of the fluid after an appropriate time is crucial. Ozdec *et al.* [64] performed a similar study, with 41 patients with retinal detachment. The study showed a high success rate and the removal of the fluid was performed in average 4.7 months after the surgical procedure. Nevertheless, as showed by Caramoy *et al.* [58], in terms of emulsification they show a similar behaviour with the SiO: Densiron Xtra as is composed also by HMW chains of SiO shows an increased resistance to emulsification when compared with Densiron 68.

Fluorosilicone Oils (FSiO) are viscous and hydrophobic materials with properties similar to silicone oils. Based on the success of SiO, and since its density is higher than that of silicone oil, FSiOs were introduced with the hope of being a more efficient tamponade agent that could be used for longer periods of time. FSiO have low molecular-weight (<700 Da) and have a density approximately twice of that of water. Unfortunately, Gremillion *et al.* [65] showed a high level of emulsification associated with the use of FSiO in the eye, which makes this fluid unsuitable for use in surgery.

Beyond the products presented in Table 2.3, a VH substitute known as HWS 46-3000 is currently in test phase. The components of this product are silicone oil plus perfluorobutylhexane (F4H6). The fluid has a density of 1.105 g/cm^3, a refractive index of 1.37, a viscosity of 2.9 Pa s, surface tension of 18.8 mN/m and an interface tension with water of 41.3 mN/m [66].

PFLCs and SiO-based fluids are so far the only liquids used in surgery, that are in direct contact with VH inside the vitreous cavity. Despite all the clinical and experimental studies performed with those fluids, there is still a lack of rheological studies that quantify their flow behaviour.

2.3 Polymeric solutions, hydrogels and the future of vitreous humour substitutes

Due to the shortcoming of current VH substitutes, as discussed in the previous section, studies to develop new VH substitutes continue to be carried out. Polymeric solutions and hydrogels are currently the most studied as prospective VH substitutes and it is believed that they are the fututre of VH substitutes [34, 45]. Experimental tests with polymers have so far proven that they are capable of matching some of the VH properties [34]. An overview of polymers studied with the purpose of replacing VH is presented in Table 2.4.

As the main components of the natural VH, collagen and HA were the target of extensive studies. However, both of them failed as a suitable VH substitutes. Hyaluronic acid solutions showed a short residence time and high levels of degradation in the vitreous cavity [18]. Collagen also showed a short residence time, and it is believed that

Table 2.4. Polymers studied for vitreous humour replacement [45].

Type	Polymer
Modified natural polymer	Hyaluronic acid solutions
	Collagen
	Collagen/Hyaluronic acid mixture
	Methylated collagen
	Hyaluronic acid/Gellan Gum
	Polygeline
Synthetic polymer	Poly(acrylamide)
	Poly(glyceryl methacrylate)
	Poly(2-hydroxyethyl methacrylate)
	Poly(2-hydroxyethyl acrylate)
	Hydroxypropyl methylcellulose
	Pluronic polyol F-127
	Poly(1-vinyl-2-pyrrolidone)
	Poly(vinyl alcohol)
	Methacrylated poly(vinyl alcohol)
	Poly(methyl acrylamidoglycolate methyl ether)
	Silicone Gel
	Semifluorinated alkanes (CnF2n‘1)CmH2m‘1
	Poly(methyl2-acrylamido-2-methoxyacetate)
	Poly(ethylene oxide)

one of the reasons why collagen did not work effectively as a substitute is related to the differences in type and chain size of the collagen inserted in the eye when compared with the native one. Liang *et al.* [67] tried to modify the chemical nature of collagen, using methylation, protease digestion or ultraviolet (UV) irradiation to increase the intravitreal residence time, but the results were not promising. Mixtures of collagen/HA were also tested, but again the results were not encouraging: the solution became more like a viscous solution rather than a gel over time, resulting in a poor tamponade effect on the retina [45, 68]. One of the reasons for the failure of this combination could be the inability to reproduce the type of interaction between collagen and HA as in the natural vitreous. Also, inflammatory and immunological responses were observed as a consequence of the samples implanted in the human vitreous cavity being originally from other humans or animals [69]. Nevertheless, cross-linked HA are currently under study and preliminary results are promising, but so far only *in vitro* tests were performed [18].

Based on the fact that SiO are used as VH substitutes, studies were carried out to test the feasibility of silicone gels as VH substitutes. However, such gels showed the same drawbacks of SiO, as they exert a poor tamponade effect in the retina [18, 34].

According to Baino [18], poly(1-vinyl-2-pyrrolidinone) (PVP) was the first synthetic polymer to be tested as a VH substitute, during the 1950's. In the 1990's, Chirila and co-workers [8, 70–74] developed several studies with PVP as a vitreous substitute. Some of the formulations used in their studies resulted in a clear gel, transparent, insoluble in water, which exhibited mechanical properties similar to those of natural vitreous. However, the process of injection of the polymer in the vitreous cavity by a small gauge needle caused polymer fragmentation, resulting in a decrease in the polymer mechanical properties [71]. Additionally, some tests showed phagocytosis of the biomaterial [73, 74].

Methacrylate-based polymers, such as poly(glyceril-methacrylate) (PGMA) and poly(2-hidroxyethyl methacrylate) (PHEMA) were used in studies *in vivo* by Refojo *et al.* [75, 76], showing high biocompatibility and overall good results in rabbit eyes. However, both PGMA and PHEMA were considered unsuitable for clinical use because it is not possible to inject them and, consequently, the biomaterial needed to be implanted in the eye through a small surgical incision, which was traumatic for the eye.

Poly(methyl acrylamide glycolate methyl ether) (MAGME) was the first polymer studied that showed high cytotoxicity. Chirila *et al.* [77] implanted the gel in rabbit eyes and post-operative clinical complications were reported, such as inflammation and even damage of the optic nerve. As a result, cytotoxicity tests started to be performed as a criterion for selection of a material as a VH substitute [45, 68].

Even if most of the polymers presented in Table 2.4 failed the purpose of being used as VH substitutes, for various reasons, some others showed promising results.

Currently, polyacrylamide (PAA) is one of the most studied polymers to use as a VH substitute. It was first studied during the 1960's and 1970's by Mueller-Jensen *et al.* [78, 79]. Although acrylamide has the potential of becoming toxic, the final polymer exhibits good biocompatibility after complete polymerization. Mueller-Jensen *et al.* [78, 79] showed that if properly polymerized, PAA remained clear until the animals were sacrificed, 14 months after the implantation. More recently, new studies involving this polymer emerged (*eg.* Swindle *et al.* and Foster *et al.* [80, 81]), in which PAA gels were created directly in the eye, under physiological conditions, and the injected fluid did not show signs of fragmentation. These promising results justify further investigations with PAA as a vitreous substitute.

Poly(vinyl alcohol) (PVA) is another polymer being considered as a vitreous substitute. Several studies were reported [82–86] using this biomaterial and the results are promising. A good outcome of the studies performed with this polymer is the fact that no inflammation or damage to the retina was observed. It was also observed that the IOP and retinal activity remained normal, *in vitro* cytotoxicity assays were normal, and they showed long-term biocompatibility. Maruoka *et al.* [85] studied *in vivo* the properties of PVA hydrogels cross-linked by γ irradiation. Six eyes of three male crab-eating macaques were used: PVA hydrogel was injected in the right eye (3 eyes) and saline in the left eye (3 eyes) as a control. For a follow-up period of 3 months, histopathologic, intraocular pressure and electroretinogram tests showed that PVA was in general well tolerated (even if some vacuolations of the inner retina were found in some specimens)(see Fig. 2.4). In the study of Leone *et al.* [83] PVA hydrogels were cross-linked with trisodium trimetaphosphate (STMP). Several concentrations of poly-

mer/crosslinker were tested and the molar ratio STMP/PVA 1:8 showed rheological characteristics similar to VH. Moreover, this hydrogel showed good properties in terms of light transmittance, water content, citotoxicity, and good performance when injected with a small needle. Poly(vinyl alcohol) hydrogels are promising candidates for vitreous substitutes, but more studies still need to be performed to collect more data about their mechanical properties, retention time, and ability to act as a tamponade agent.

Poly(ethylene oxide) (PEO) has also been studied, both as a solution and as a hydrogel, to be used as VH substitutes [87, 88]. When used as a polymeric solution and implated in rabbit eyes, Pritchard *et al.* [87] showed that precipitation can occur after the fluid is implanted in the eye; however, the transparency of the fluid in general was maintained. The authors believed that the conformation studied was not suitable as VH substitutes, but they also argued that the cross-linking of the polymer to create hydrogels may improve biocompatibility and retention time, as well as the mechanical properties. Annaka *et al.* [88] studied the physiological and mechanical properties of PEO-based hydrogels, which were composed of thermosensitive amphiphilic polymer to be capable of forming a transparent gel in the vitreous cavity, after injection. The elastic and viscous moduli of the hydrogel was 3 orders of magnitude higher than the VH. However, the authors believe that weak gels will not act as an effective vitreous tampon-

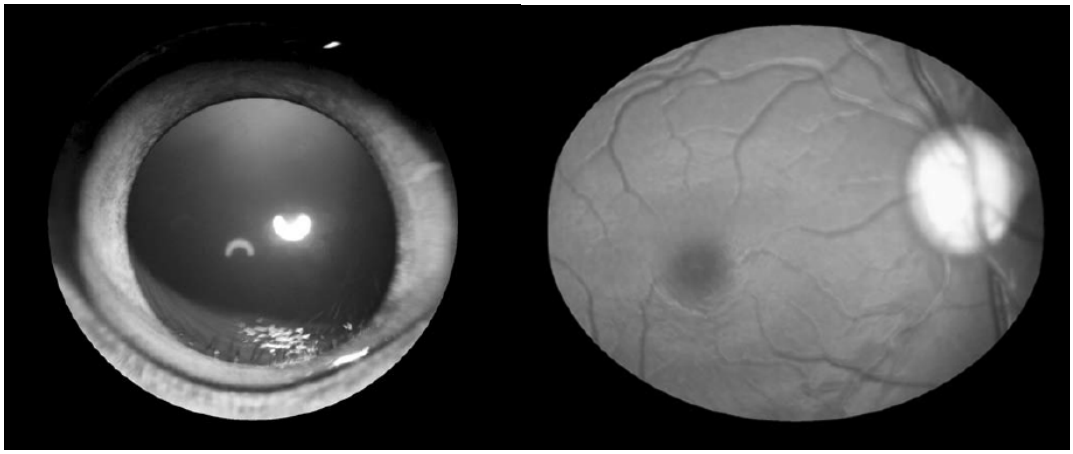

(a) **(b)**

Figure 2.4. (a) Anterior segment and (b) posterior fundus of a PVA injected eye, 3 months after the surgery (reprinted from [85] with permission from Taylor & Francis).

ade agent to restore the volume and internal pressure of the ocular globe. The results of this study show that, with a suitable treatment, this polymer has some potential to be used as a VH substitute.

Some of the fluids studied previously show biocompatibility, good tamponade effect, transparency, have buffer capacity, etc.; however, at the present stage of development they all failed as a permanent VH substitute. The author of this work believes that the incomplete knowledge regarding the rheological properties can be an important factor for the failure of the proposed formulations, and so far, the development of an ideal VH substitute remains a goal still to be achieved. However, and considering the studies performed up to date, it is believed that, arguably, the most promising polymers for vitreous substitutes are PAA, PVA and PEO. Nevertheless, more studies involving these polymers are clearly needed to confirm or discard their potential.

2.4 *In vivo* studies: differences between Human and other mammals

Before tests in Humans can be conducted, tests *in vitro* followed by tests *in vivo* with other specimen are often the common procedure. To test the properties and biocompatibily of the polymers described in the previous section, both *in vitro* and *in vivo* studies were performed. To be able to relate the collected data and make correlations with Humans, it is important to know the properties and differences of the VH from the animals normally used. VH from different species is mostly composed by the same matrix of elements. However, the concentration of the components varies between species [19]. Biochemical and physiological characteristics of vitreous in different species are shown in Table 2.5.

Table 2.5. Comparative biochemical and physiological characteristics of VH in different species [22].

	Human	**Rabbit**	**Pig**	**Monkey**
Volume (mL)	4-5	1-2	3.2	3-4
Collagen content (µg/mL)	40-120	75-900	20	N/A
HA content (µg/mL)	100-400	20-60	70-80	100-200
Protein content (µg/mL)	450-1100	44-81	1000-1200	210-220

The Human eye is the one with the higher volume of fluid (4 to 5 ml) of all the species typically considered (rabbit, pig, monkey). Regarding the main components of the fluid, collagen and HA, rabbit eyes have a significant higher concentration of collagen, in comparison with all the rest, and is also the animal with the lowest amount of HA content. In terms of protein content the value is significantly different between all the animals.

Differences in the MW of components, such as collagen and HA, also affect the conformation and mechanical properties of the biofluid. Regarding the MW of HA, adult Humans, rabbits and bovines present values of approximately 3×10^6 Da, $2-3 \times 10^6$ Da and $5 - 8 \times 10^5$ Da, respectively [89, 90].

Collagen is a protein that can be divided in at least 27 different types, depending on the structure and lenght of the chain. In the VH it is possible to find mostly collagen types II, IX and V/XI [42]. Consequently, the MW of this protein varies in a wide range. Unfortunately, it was not possible to find studies which provide information about the differences in the MW of Humans and other animals.

Despite anatomical differences between Human and Rabbit eyes, rabbits are the most used animal model for studies involving vitreous and retina pathologies [91]. Even though when comparing specific structures between both species shows some visible differences, similarities in the matrix structure between the two species makes VH from rabbit eyes a suitable animal model to study VH properties [22, 91, 92]. Los [91] showed that VH from rabbit eyes also suffers degeneration and consequently liquefaction during life, and that the changes observed in ageing rabbit eyes resembles the liquefying changes also found in humans. Therefore, rabbit eyes are good models to study the differences of vitreous structure and liquefaction in more detail, and will be used in this work.

"A scientist in his laboratory is not only a technician: he is also a child placed before natural phenomena which impress him like a fairy tale."

Marie Curie

Chapter 3

Experimental methodology

A detailed description of the experimental techniques employed in this research work is presented in this chapter. The methodology followed to obtain the VH samples is presented. The dimensionless numbers used to characterise different flow regimes are also described. The experimental procedures followed for the characterisation of the fluids under study are described and key rheology and flow concepts are introduced.

3.1 Background

The term Rheology was coined by E. C. Bingham in 1929, and has its origin in the greek words $\rho\acute{\epsilon}\omega < rh\acute{e}\bar{o} >$, meaning "flow", and $\lambda o\gamma\acute{\iota}\alpha < -logia >$, meaning "study of", being defined as the science that studies the deformation and flow of matter when subjected to an applied force [93].

Consider a fluid between two parallel plates, with the bottom plate stationary and the top plate moving at a constant velocity. The tangential force (F) per unit area (A) necessary to mantain the constant velocity of the upper plate is the shear stress, τ,

$$\tau = \frac{F}{A} \tag{3.1}$$

Fluids move continuously under an applied shear stress. The shear rate is defined as the rate of change of velocity between layers of fluid, and for this ideal flow is given by

$$\dot{\gamma} = \frac{v}{h} \tag{3.2}$$

where h is the gap between plates and v is the velocity of the upper plate.

The shear viscosity is a material function that provides a measure of a fluid's resistance to flow and is calculated as the ratio between the shear stress and the shear rate,

$$\eta = \frac{\tau}{\dot{\gamma}} \tag{3.3}$$

In daily life, we are surrounded by fluids and their flows: rivers flow, cooking processes involve different types of flow, while having showers, petroleum transport in pipelines, flow in thermal and cooling systems, etc. Body fluids and other fluids in most biological systems are also subjected to different types of flow: blood is continuously flowing inside the body, the synovial fluid in the knee joints flows while walking, and VH flows inside the eye cavity during eye movements. Therefore, rheological studies are key to improve industrial processes, in the creation and improvement of fluids used in daily life, and even for the improvement of health systems.

3.2 Newtonian and non-Newtonian fluids

Based on the stress and deformation relationship, fluids are commonly divided in two different groups: Newtonian and non-Newtonian fluids. A diagram showing different type of fluids is presented in Fig. 3.1.

An incompressible Newtonian fluid is a purely viscous fluid that follows the linear equation proposed by Sir Isaac Newton, where the shear stress is proportional to the shear rate:

$$\tau = \eta\dot{\gamma} \tag{3.4}$$

While Newtonian fluids exhibit a constant shear viscosity, most non-Newtonian fluids exhibit a shear-rate dependent viscosity, $\eta(\dot{\gamma})$, thus $\tau = \eta(\dot{\gamma})\dot{\gamma}$ (see Fig. 3.2a). Non-Newtonian fluids can be divided in three main groups (*cf.* Fig. 3.1): time-independent fluids (also called generalized Newtonian fluids, GNF), time-dependent fluids, and viscoelastic fluids [93–95].

One of the well-known time-independent materials with yield-stress is the Bingham fluid (named after Professor Bingham). This type of fluid behaves like a viscous fluid during flow at high shear stresses, but for lower shear stresses it behaves as a rigid body, as shown in Fig. 3.2a. Most of the non-Newtonian fluids are shear-thinning (or pseudoplastic) and their viscosity decreases with the increase of shear rate. The fluids that have an apparent viscosity increasing with shear rate are called shear-thickening fluids or dilatant fluids.

Time-dependent fluids display a variable shear stress along time for a constant shear rate and constant temperature (see Fig. 3.2b). The initial properties of the fluid are recovered some time after the shear rate has returned to zero. Time-dependent fluids

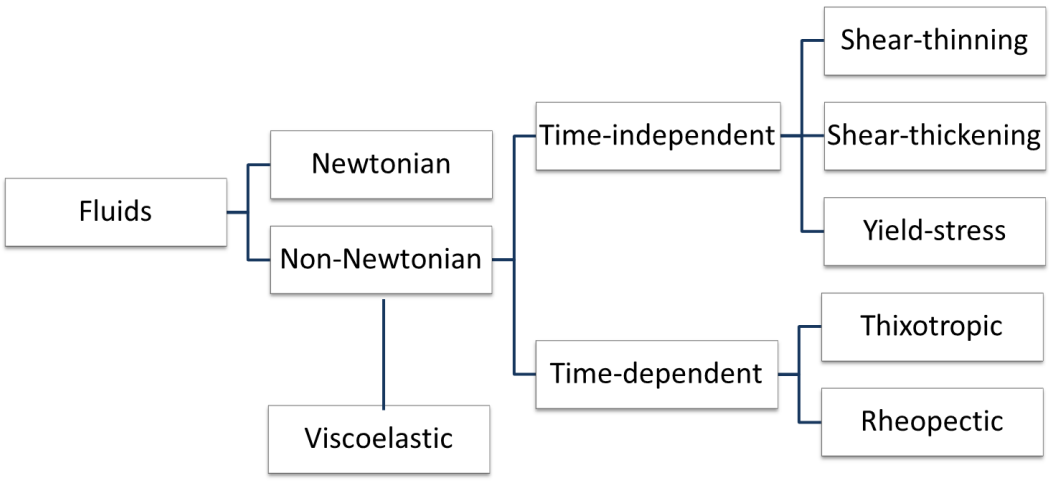

Figure 3.1. Scheme of the different types of fluids.

are classified either as thixotropic fluids, for which the shear stress decreases over time at a constant shear rate, or as rheopectic fluids, which shows an increase of shear stress along time for an applied constant shear rate. Thixotropic fluids are usually associated with the occurence of hysteresis, see Fig. 3.3, a phenomenon that describes the fluids energy loss during a deformation cycle (zero shear rate $\longrightarrow$ final shear rate $\longrightarrow$ zero shear rate).

Viscoelastic fluids are the last group of non-Newtonian fluids presented in Fig. 3.1. The rheological response of those fluids depends on the deformation history of the material. When a material (liquid or solid) is subjected to a shear stress, it deforms. The initial elastic deformation disappears after the shear stress is removed; however, a permanent deformation (the plastic deformation) remains. Viscoelastic fluids show both solid-like and liquid-like behaviour and cannot be described by a simple relationship between shear stress and shear rate, as both variables are time-dependent.

In general, the non-Newtonian behaviour of a fluid can be more complex than described previously and have simultaneously properties of more than one type. The insight of the material rheological characteristics and its characteristics as function of shear rate and shear stress is key to understand how the fluid behaves and to choose

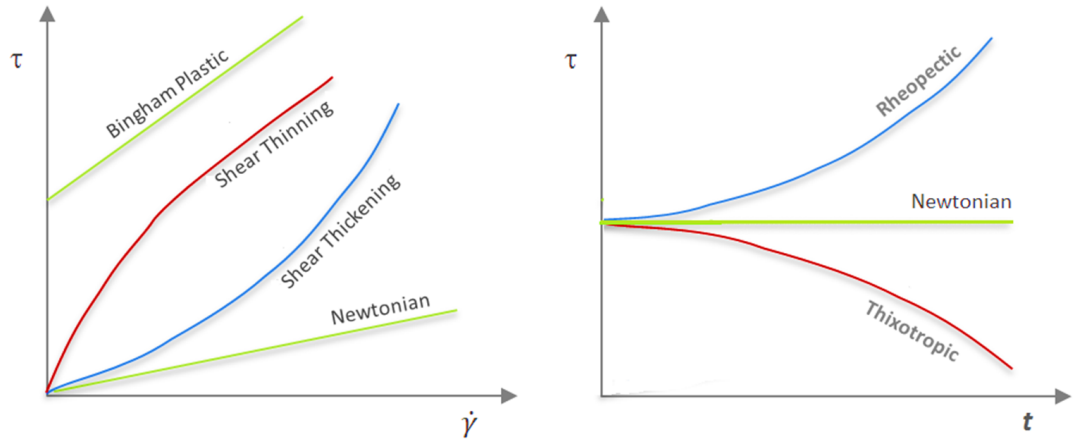

(a) **(b)**

Figure 3.2. (a) Shear stress-shear rate relationship for time-independent fluids, and (b) shear stress as a function of time for time-dependent fluids, at constant shear rate.

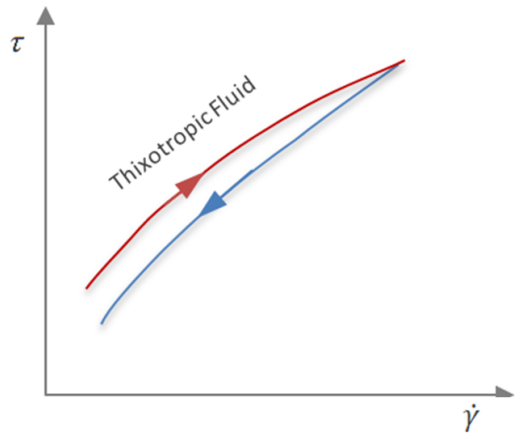

Figure 3.3. Shear stress versus shear rate relationship for a thixotropic fluid. The up and down curves are not coincident as a consequence of hysteresis.

proper constitutive models to describe the rheological behaviour of the fluid.

3.2.1 Sample selection and preparation

Different fluids with different properties were characterised during this study, including the biofluid VH and different pharmacological fluids used in eye surgery.

The VH samples were collected from healthy New Zealand white rabbit specimen, aged 18 ± 3 weeks and weighing between 2.8 and 3.0 kg. Vitreous humour in rabbit eyes occupies 1 to 2 ml, has a collagen content of $75 - 900$ μg/cm^3 and HA content of $20 - 60$ μg/cm^3 [22]. As discussed in Section 2.4, it is acceptable to use VH from rabbit eyes and correlate the results with Human VH, as the VH from rabbit eyes is considered a reliable model of VH from Human eyes [22, 91, 92]. All rabbit eye samples were collected on the day of the experiments and the tests were performed within 5 hours *post-mortem*. The rabbits were euthanised and the eyes were used in parallel with other research projects to minimise animal usage. During the dissection, it was possible to observe two distinct phases: a liquid and a gel phase. Note that the samples start to change their conformation as a result of being highly fragile in nature [15]. Nickerson *et al.* [10] suggested that the collagen and some amount of hyaluronan remain in the gel phase while the exudate fluid contains mostly hyaluronan, as illustrated in

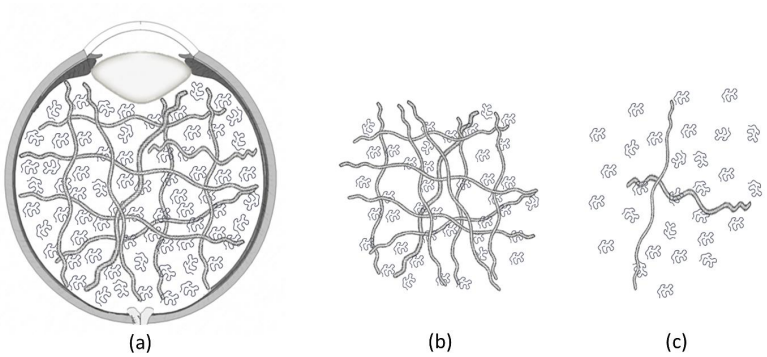

Figure 3.4. (a) Schematics of vitreous humour enclosure in the eye (native state) and after separation in two different phases: (b) *gel phase* mostly composed by collagen fibrils and a small amount of hyaluronan and (c) *liquid phase* mostly composed by hyaluronan. Adapted from [10].

Fig. 3.4. Three different conformations of VH were considered in this work: the gel phase right after dissection, the gel phase hours after dissection and the liquid phase hours after dissection. The first experiments with the VH gel phase samples started less than 5 minutes after the dissection of the sample, and the fluid was moved from a closed environment, the vitreous cavity, to another closed environment, between the rheometer plates with a solvent trap. The delayed measurements of both the gel and liquid phases of VH were performed within a maximum of 4 ± 1 hours after the dissection of the eyes.

Six different pharmacological fluids were used during this study, including: three Silicone oils (SiO), RS-Oil 1000 from Alchimia (Padova, Italy), Siluron 2000 and Siluron 5000 both from Fluoron (Ulm, Germany); Densiron 68 from Fluoron (Ulm, Germany), which is a mixture of 70% of SiO with a viscosity of approximately 5 Pa s with 30% of perfluorohexyloctane; and two Perfluorocarbons (PFLCs), fluorinated perfluoro-n-octane (HPF8) and fluorinated perfluorodecalin (HPF10) both from Alchimia (Padova, Italy). Note that all the SiO are composed by polymer chains of the same MW, except Siluron 2000 that is composed of 95% of short molecular chains and 5% of a ultra-long molecular chains with a viscosity around 2500 Pa s.

Silicone is the common name given to the polymer poly(dimethylsiloxane) (PDMS). Poly(dimethylsiloxane) is optically clear, inert, non-toxic and biocompatible. The chemical structure of PDMS is shown in Fig. 3.5. The polymer can be produced with different viscosities and is hydrophobic.

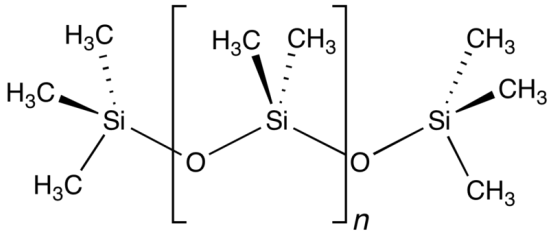

Figure 3.5. Chemical strucutre of the repeating and end units of poly(dimethylsiloxane).

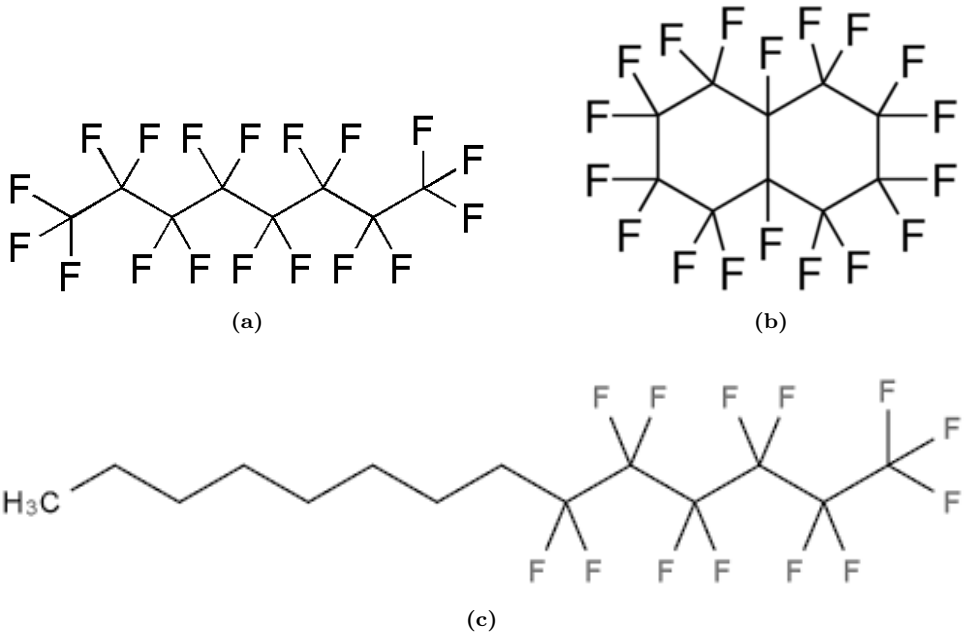

Figure 3.6. Chemical strucutre of (a) perfluoro-n-octane, (b) perfluorodecalin and (c) perfluorohexyloctane.

Perfluorocarbons are synthetic compounds that consist in carbon and fluorine molecules. PFLCs are hydrophobic, clear and colourless [96]. This family of molecules has been studied for different medical applications, such as blood substitutes [97], contact lenses when combined with SiO [96], etc. The chemical strucutre of the PFLCs used in eye surgery are shown in Fig. 3.6.

3.3 Dimensionless numbers

In fluid systems, the use of dimensionless numbers is useful in order to characterise different flow regimes. These dimensionless groups express the relative importance of

various competing effects that act in a fluid. Different dimensionless numbers are used in this thesis, thus it is convenient to provide an introduction to those numbers.

3.3.1 Reynolds number

Arguably, the most used dimensionless number for fluid flows is the *Reynolds number*, Re. It was first introduced in 1851 by Stokes, but it became popular and was named after Osborne Reynolds [98]. This number measures the ratio between inertial and viscous forces per unit volume

$$\mathrm{Re} = \frac{\text{inertial forces}}{\text{viscous forces}} = \frac{\rho U D}{\eta} \tag{3.5}$$

where U is a characteristic velocity, D is a characteristic lengthscale of the geometry and ρ is the density of the fluid. For very small Re (Re $<<$ 1), inertial effects can be ignored and the flow is called creeping or inertialess flow; if Re is high, inertial effects are dominant and the nonlinear terms in the momentum equation predominate leading to turbulent flow. Note that the rheological behaviour of viscoelastic fluids cannot be described solely with the Reynolds number. Due to the fluids elasticity, to characterise viscoelastic fluid flows other dimensionless numbers are required, as described next.

3.3.2 Deborah number

Based on the prophetess Deborah words *"The mountains flowed before the Lord"* (Old Testament) in 1964, Reiner [99] introduced the *Deborah number* De, defined as the ratio between the relaxation time λ of the fluid and the time of observation,

$$\mathrm{De} = \frac{\text{relaxation time}}{\text{time of observation}} = \frac{\lambda}{t_{flow}} = \frac{\lambda U}{D} \tag{3.6}$$

Reiner assumed that any material is able to flow, depending of the timeframe of observation. If the Deborah number is very small (De $<<$ 1), elastic effects can be neglected and the fluid has a Newtonian-like behaviour. When the Deborah number is very high, elastic effects are predominant, which occurs typically for De $>$ 1.

3.3.3 Weissenberg number

The *Weissenberg number* Wi was introduced by White [100], who wrote the momentum equation for second-order fluids and identified this dimensionless number. It gives a relationship between inherent relaxation properties and the rate of deformation of a material, and is defined as the ratio between elastic and viscous forces,

$$\mathrm{Wi} = \frac{\text{elastic forces}}{\text{viscous forces}} = \lambda\dot{\gamma} \tag{3.7}$$

The Weissenberg number is similar and often confused with the Deborah number, but they have different physical interpretations. The Weissenberg number indicates the degree of anisotropy generated by the deformation, and describes flows with a constant stretch history. The Deborah number is used to describe flows with a non-constant stretch history, and represents a ratio of time-scales [101].

3.3.4 Elasticity number

The ratio between elastic and inertial forces is given by the *Elasticity number*, El. It is usually defined as the ratio between the Wi and Re numbers:

$$\mathrm{El} = \frac{\mathrm{Wi}}{\mathrm{Re}} = \frac{\lambda\eta}{\rho D^2} \tag{3.8}$$

As both Wi and Re vary linearly with the characteristic velocity, the Elasticity number is independent of the flow kinematics [102].

3.4 Shear rheology

Performing measurements of rheological material functions is the subject of rheometry. Experimental measurements of the bulk rheological properties of a fluid can be done using rheometers or adequate microfluidic devices. Depending on the deformation applied to the fluid, two types of flow are usually considered: shear and extensional flows (see Fig. 3.7).

Shear measurements are usually performed with rotational rheometers, that can be

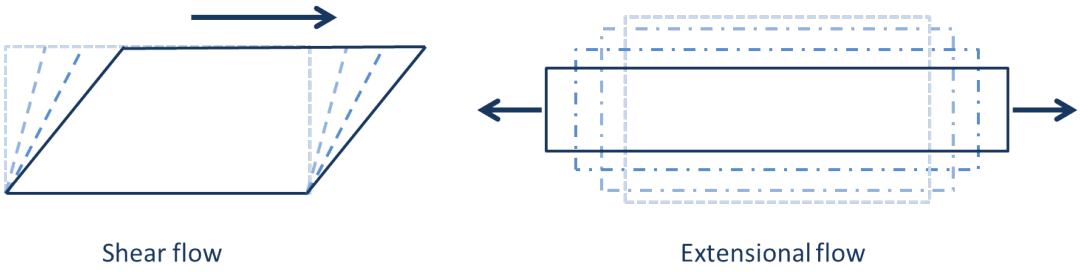

Figure 3.7. Schematic representation of a shear and an extensional flow deformation.

stress- or strain-controlled. To measure the properties of the fluids, rheometers typically use three main different geometries: parallel-plate, cone-and-plate, and concentric cylinders. For the parallel-plate and the cone-and-plate geometries, typically the top plate rotates with a constant or variable angular velocity (depending on the test), while the bottom plate remains static. The bottom plate and the top plate (or cone) are separated by a fixed distance. For the concentric cylinders geometry, the sample is placed between two concentric cylinders, which are in relative motion. Commonly, the inner cylinder rotates at constant angular velocity and the outer cylinder remains static.

Shear rheometers typically have an accurate temperature control in isothermal tests and a good torque resolution and are able to perform measurements under both steady shear and oscillatory flow [95, 103].

3.4.1 Steady shear measurements

Steady shear flows are important in situations where the shear viscosity is the dominant material property [103]. Fig. 3.8 shows a schematic representation of the cone-and-plate and parallel plates geometries, which have been used during this work. Depending on the geometry used, calculations of shear rate, shear stress and consequently the shear viscosity differ. The equations to calculate those variables with the cone-and-plate and parallel-plate geometries are presented in Table 3.1. In the parallel-plate configuration, the shear rate varies between the centre and the rim of the plate, and as a consequence, a correction procedure (also shown in Table 3.1) needs to be applied in order to overcome this error.

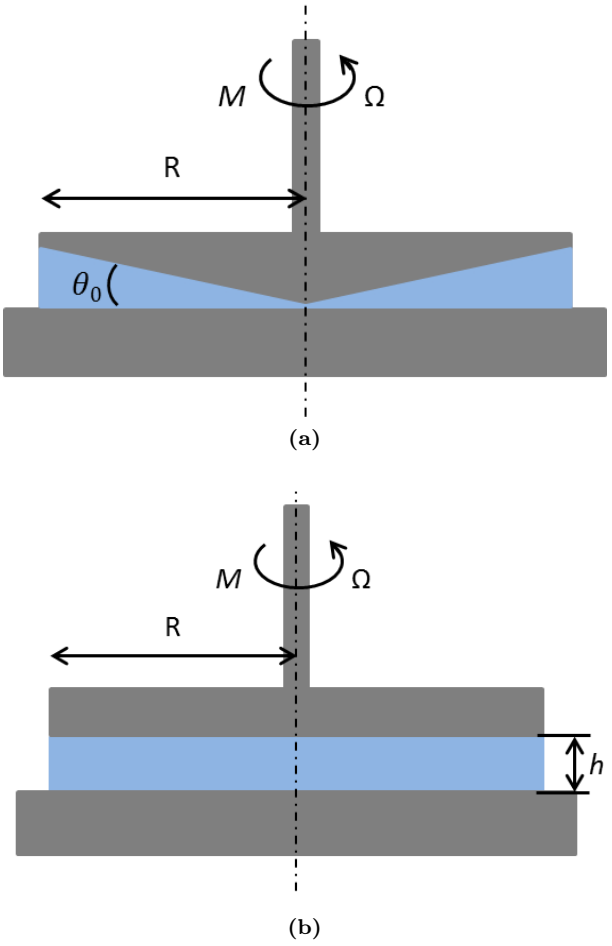

Figure 3.8. Illustration of (a) cone-and-plate and (b) parallel-plate configurations.

Table 3.1. Equations to calculate the shear rate, shear stress and shear viscosity with the cone-plate and the paralell-plate geometries.

	Cone-and-plate	**Parallel-plate**
Shear rate, $\dot{\gamma}$	$\dot{\gamma} = \frac{\Omega}{\theta_0}$ (3.9)	$\dot{\gamma}_R = \frac{R\Omega}{h}$ (3.10)
	where Ω is the angular velocity and θ_0 the angle between the cone and the plate	where shear rate is higher in the rim, $\dot{\gamma}_R$, and zero in the centre
Shear stress, τ	$\tau = \frac{3M}{2\pi R^3}$ (3.11)	$\tau = \frac{2M}{\pi R^3}\left(\frac{3}{4} + \frac{1}{4}\frac{\mathrm{d}\ln M}{\mathrm{d}\ln \dot{\gamma}_R}\right)$ (3.12)
	where M is the torque and R the radius of the cone	where the term in brackets is the correction factor for the variable shear rate profile
Shear viscosity, η	$\eta = \frac{3M\theta_0}{2\Omega\pi R^3}$ (3.13)	$\eta(\dot{\gamma}_R) = \frac{2M}{\dot{\gamma}_R}\pi R^3\left(\frac{3}{4} + \frac{1d\ln M}{4d\ln \dot{\gamma}_R}\right)$ (3.14)

There are situations when normal stresses are significant and can produce significant changes in the flow patterns. Those effects are mainly a result of the tensile stress along the streamlines that is generated during the flow of viscoelastic fluids and are much less relevant in Newtonian fluids. In steady shear rheology, two independent normal stresses differences can be defined, which are called the first (N_1) and second (N_2) normal stress differences. Both material functions are function of shear rate, and can be calculated as

$$N_1 = \tau_{11} - \tau_{22} \tag{3.15}$$

$$N_2 = \tau_{22} - \tau_{33} \tag{3.16}$$

Based on the normal stresses differences, the first (Ψ_1) and second (Ψ_2) normal stress coefficients are obtained as

$$\Psi_1 = \frac{N_1}{\dot{\gamma}^2} \tag{3.17}$$

$$\Psi_2 = \frac{N_2}{\dot{\gamma}^2} \tag{3.18}$$

For dilute and semi-dilute polymeric solutions N_2 is typically very low and is not easy to measure experimentally, requiring several repetitions with both cone-and-plate and parallel-plate geometries, to ensure reliable measurements. For viscoelastic fluids, Ψ_2 is usually much lower than Ψ_1, and usually these quantities have opposite sign [94].

During this study, shear measurements were performed using a DHR-2 rotational rheometer (TA Instruments) and two geometries were used: a cone-and-plate with 60 mm diameter and 1° cone angle; and a 40 mm diameter parallel-plate system.

Regarding the VH measurements, both the cone-and-plate and the parallel-plate geometries were used to perform the experiments with the liquid phase and the parallel-plate geometry was covered with 500 grit silicon carbide sandpaper to minimise wall slip and provide an effective no-slip boundary condition [10, 11]. The flow curve mea-

surements for the liquid phase were performed with a solvent trap maintaining a water-saturated atmosphere at the operating temperature.

All the pharmacological fluids were measured with a cone-and-plate configuration with 60 mm diameter and an angle of 1°. Flow curve measurements were performed at $T = 20$ °C and $T = 37$ °C with a shear rate from 0.01 to 1000 s^{-1} for RS-Oil 5000, Densiron 2000, RS-Oil 1000 and Densiron 68 and with a shear rate from 1 to 1000 s^{-1} for HPF8 and HPF10 fluids.

For all the flow curves, the lower and upper limits of $\dot{\gamma}$ were computed to ensure that the experiments are accurate. Considering 20 times the minimum measurable torque (1x10^{-8} N m) for the DHR-2 rheometer, the lower shear viscosity values considered for the measurements performed with the cone-and-plate geometry are given by

$$\eta = \frac{3(20M_{min})}{2\pi R^3}\frac{1}{\dot{\gamma}} \tag{3.19}$$

and by

$$\eta = \frac{2h(20M_{min})}{\pi R^4 \Omega} \tag{3.20}$$

if using the parallel plates geometry, where M_{min} is the minimum measurable torque and Ω the angular velocity.

The upper limit of a measurable shear viscosity, based on the onset of inertial instabilities is given by [104]

$$\eta = \frac{\Omega\theta^2\rho R^2}{6} \tag{3.21}$$

for the cone-and-plate geometry, and by

$$\eta = \frac{\Omega\rho h^2}{6} \tag{3.22}$$

for the parallel-plate configurations.

Unlike in the constant strain rate experiments, where the shear stress is measured under steady flow, in the creep experiments the time-dependent deformation of the

sample is measured during the transient flow, for a prescribed applied constant shear stress, τ_0 [103]. The material function that is obtained in a creep test is denominated creep compliante, J, and is defined as

$$J(t, \tau_0) = \frac{\gamma}{\tau_0} \tag{3.23}$$

For long times, the strain varies linearly with time and the flow reaches the steady-state. At this point, the slope of the compliance as function of time is given by

$$\dot{J}(t, \tau_0) \approx \frac{\dot{\gamma}_\infty}{\tau_0} \tag{3.24}$$

where $\dot{\gamma}_\infty$ is the steady-state shear rate, and the ratio is the inverse of the steady shear viscosity. Based on that, the steady-state compliance, J_s, is defined as the difference between the compliance function at steady-state for a particular time t and the steady flow contribution at that time $J_s(\tau_0) = J(t, \tau_0)|_{steady\ state} - \frac{t}{\eta(\dot{\gamma}_\infty)}$ and it can be calculated by extrapolating the linear part of $J(t, \tau_0)$ to $t = 0$.

After the creep deformation reaches steady-state, the shear stress can be removed, and depending on the elasticity and viscosity, the material will recover a certain amount of strain. This experiment is called creep recovery and the amount of the strain recovered is called recovered or recoil strain, $\gamma_r(t')$. The ultimate strain recovered after the sample returns back to rest is defined as recoverable shear, γ_∞, and is given by

$$\gamma_\infty = \lim_{t' \to \infty} \gamma_r(t') \tag{3.25}$$

where t' corresponds to the time elapsed since the shear stress was removed.

Creep tests are usually relevant to understand the long term behaviour of a sample, as the behaviour at low frequencies are difficult to test with other type of rheometric experiments. For viscoelastic materials, especially the ones that present solid-like behaviour, creep and creep recovery experiments are important to evaluate the behaviour of cross-linked polymers and gels [105].

During this work, creep compliance experiments were performed for both VH phases, at $T = 37$ °C for a duration of 2000 s, at constant applied shear stresses of $\tau_0 = 1$ and 2 Pa.

The geometries used were the same as for the flow curve measurements previously described. A solvent trap was also used during all the experiments to maintain a water-saturated atmosphere.

3.4.2 Oscillatory measurements

Small amplitude oscillatory shear (SAOS) flow measurements are commonly used for viscoelastic fluids. In an oscillatory shear experiment, the sample is exposed to a sinusoidal oscillating strain, γ, with an angular frequency, ω,

$$\gamma(\omega, t) = \gamma_0 \sin(\omega t) \tag{3.26}$$

where γ_0 is the imposed strain amplitude.

The resultant shear stress in SAOS is also sinusoidal and can be described by

$$\tau(\omega, t) = \tau_0 \sin(\omega t + \delta(\omega)) \tag{3.27}$$

where $\delta(\omega)$ is the phase angle that depending on the elastic properties of the fluid can vary between 0° and 90°: for a purely elastic sample the applied strain is in phase with the measured stress ($\delta = 0°$), a purely viscous fluid exhibits a stress response 90° out of phase, and a viscoelastic fluid presents a response such that $0° < \delta < 90°$, depending on the degree of elasticity of the fluid. The response of a viscoelastic fluid can be decomposed in a viscous component and an elastic component, and Eq. (3.27) can be rewritten as

$$\tau(\omega, t) = \tau_0 \left[\cos(\delta(\omega))\sin(\omega t) + \sin(\delta(\omega))\cos(\omega t)\right] \tag{3.28}$$

or

$$\tau(\omega, t) = \gamma_0 \left[G'\sin(\omega t) + G''\cos(\omega t)\right] \tag{3.29}$$

where G' is the storage or elastic modulus and G'' the loss or viscous modulus, defined as

$$G' = \frac{\tau_0}{\gamma_0}\cos(\delta) \tag{3.30}$$

$$G'' = \frac{\tau_0}{\gamma_0}\sin(\delta) \tag{3.31}$$

The storage modulus and the loss modulus characterise, respectively, the solid-like and fluid-like contributions of the measured shear stress response. The relative importance of energy dissipation and energy storage of a fluid is given by the loss tangent, $\tan(\delta)$,

$$\tan(\delta) = \frac{G''}{G'} \tag{3.32}$$

Based on the measurements of G' and G'', the dynamic or complex modulus can be obtained by

$$|G^*| = \sqrt{(G')^2 + (G'')^2} \tag{3.33}$$

and the complex viscosity can be defined as

$$\eta^* = \frac{G^*}{\omega} = \frac{G''}{\omega} - \left(\frac{G'}{\omega}\right) i \tag{3.34}$$

were i is the imaginary constant.

The equations to calculate G' and G'', taking into account the inertia corrections performed by the rheometer used (DHR-2 TA Instruments), with the cone-and-plate and parallel-plate geometries are presented in Table 3.2. Note that the software of the rheometer performs both a correction of the measuring system inertia and a contribution from the sample inertia.

Table 3.2. Equations to calculate G' and G'' with the cone-and-plate and the paralell-plate geometries.

	Cone-and-plate	**Parallel-plate**
Elastic modulus G'	$G' = \frac{K_\sigma}{K_\gamma \theta_0}(M_0 \cos(\delta_{raw}) + I\omega^2) + \frac{2R^2\alpha^2\omega^2\rho}{15}$ (3.35)	$G' = \frac{K_\sigma}{K_\gamma \theta_0}(M_0 \cos(\delta_{raw}) + I\omega^2) + \frac{h^2\omega^2\rho}{3}$ (3.36)
Viscous modulus G''	$G'' = \frac{K_\sigma M_0}{K_\gamma \theta_0} \sin(\delta_{raw})$ (3.37)	

where K_σ is the geometry stress factor, K_γ is the geometry strain factor, I is the system inertia, M_0 the oscillatory torque amplitude, θ_0 the oscillatory displacement amplitude, δ_{raw} the raw phase angle, ω the angular frequency, R is the radius of the geometry, ρ is the density of the fluid, α is the cone angle and h is the gap in the plate-plate system

For VH liquid and gel phases, SAOS measurements were performed at $T = 20$ °C and $T = 37$ °C, closer to the normal body temperature, for a strain $\gamma = 1\%$ and frequency $\omega = 1$ rad/s or $\omega = 10$ rad/s. No meaningful differences were found between the experiments performed at both temperatures. The dynamic moduli as a function of strain was measured for $\gamma = 0.1 - 50\%$ and a frequency $\omega = 10$ rad/s. It was found that for a low strain of $\gamma = 1\%$ the sample exhibits a linear viscoelastic behaviour, as both $G'(\gamma)$ and $G''(\gamma)$ curves display a plateau value. The cone-and-plate configuration was used to perform some of the experiments with the liquid phase and the parallel-plate geometry (covered with sandpaper) was used to perform experiments with the gel and liquid phases.

All the pharmacological fluids were measured with the 60 mm cone-and-plate geometry with angle of 1°. Experiments were performed both at $T = 20$ °C and $T = 37$ °C, for a strain between 1% and 40%, depending on the fluid. The dynamic moduli as a function of strain was measured for $\gamma = 0.1 - 100\%$ and a frequency $\omega = 10$ rad/s. It was found that for strains between 1 and 40% the measurements were in the linear viscoelastic regime.

3.4.3 The Cox-Merz rule

Cox and Merz [106] showed that the shear viscosity curve versus the shear rate measured with a capillary viscometer was similar to the curve of the complex viscosity plotted as a function of frequency. Based on that observation they proposed an empirical rule, known as the Cox-Merz rule, that relates these linear and non-linear rheological quantities. The Cox-Merz rule has been proven to work well for different fluids, such as colloidal dispersions, polymer melts, and also for entangled and branched polymers [107]. According to the Cox-Merz rule, SAOS and steady shear viscosity can be correlated as

$$\eta(\dot{\gamma}) = |\eta^*(\omega)| = \frac{|G^*|}{\omega}, \text{ for } \dot{\gamma} = \omega \tag{3.38}$$

One advantage of using this empirical rule is the smaller number of experiments that needs to be performed to characterise a sample, as linear and non-linear characteristics

can be estimated based on the same experiment.

The Cox-Merz rule was used to correlate the VH liquid phase steady shear and oscillatory measurements.

3.5 Extensional rheology

Extensional rheological studies are not as common as shear rheology measurements. This happens, not because elongational studies are less important, but mostly because due to the very large and rapid deformation of the fluid elements, extensional rheology is difficult to measure, especially for low viscosity fluids [103].

In extensional flow, the elements of a fluid are stretched or squeezed, depending on the direction of the applied deformation. Although different techniques can be used to achieve an extensional flow, in this thesis the capillary breakup extensional rheometry technique was used, and therefore the main theoretical principles behind it are briefly described next. In a Capillary Breakup Extensional rheometer (CaBER), the flow is generated by placing a sample of fluid between two cylindrical plates and imposing a fast axial step strain to create an unstable filament, that will subsequently thin and breakup, as shown in Fig. 3.9.

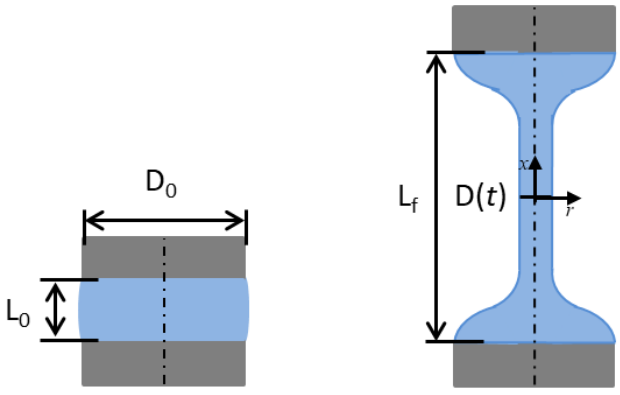

Figure 3.9. Principle of operation of the CaBER device.

During this process, it is usually assumed that the filament profile remains similar for each point, so the dynamics can be characterised by measuring a single point of the thinning filament [95, 103, 108]. For an uniaxial extension of a fluid at a constant strain rate, the velocity components are given by

$$u_x = \dot{\varepsilon} x \tag{3.39}$$

$$u_r = -\frac{1}{2}\dot{\varepsilon} r \tag{3.40}$$

where $\dot{\varepsilon}$ represents the extensional strain rate, which ideally would be a constant value during the filament thinning process.

The cylindrical filament is typically stretched rapidly (typically within 50 ms), to a final lenght L_f, and the total deformation of the fluid is given by the Hencky strain, $\varepsilon_H = \ln(L_f/L_0)$. The stretch is then stopped, the thinning filament diameter $D(t)$ is monitorised and the extensional strain rate can be computed as

$$\dot{\varepsilon} = -\frac{2}{D(t)}\frac{\mathrm{d}D(t)}{\mathrm{d}t} \tag{3.41}$$

and the uniaxial extensional viscosity is given by

$$\eta_E = \frac{\tau_{xx} - \tau_{rr}}{\dot{\varepsilon}} \tag{3.42}$$

where $\tau_{xx} - \tau_{rr}$ is the normal stress difference. Finally, it is possible to relate the uniaxial extensional viscosity with the shear viscosity, defining the Trouton ratio Tr, as

$$Tr \equiv \frac{\eta_E(\dot{\varepsilon})}{\eta_0(\dot{\gamma})} \tag{3.43}$$

where the shear viscosity is evaluated at the characteristic shear rate of $\dot{\gamma} = \sqrt{3}\dot{\varepsilon}$. For a Newtonian fluid in uniaxial extensional flow the Trouton ratio is $Tr = 3$, but for viscoelastic fluids the Trouton ratio can be orders of magnitude greater.

Entov and Hinch [109] showed that the filament diameter of a Newtonian fluid

decreases linearly with time,

$$\frac{D(t)}{D_0} = \frac{\sigma}{6\eta D_0}(t_c - t) \tag{3.44}$$

while for a viscoelastic fluid $D(t)$ decreases exponentially with time,

$$\frac{D(t)}{D_0} = \frac{GD_0}{\sigma} e^{-t/(3\lambda)} \tag{3.45}$$

where t_c is the critical time for the Newtonian fluid to breakup, σ the surface tension, G is the elastic modulus of the viscoelastic fluid with relaxation time λ.

In the present work, a uniaxial extensional flow was applied to the samples under study in order to measure their relaxation time under extensional flow. Different techniques were applied: VH liquid phase was studied with a CaBER device (HAAKE^{TM} CaBER^{TM} 1), and the pharmacological fluids were subjected to the slow retraction method (SRM) [110] using an in-house miniaturised filament breakup device [111]. The SRM technique is an extensional rheometry technique that allows to investigate filament thinning of fluids with low viscosity and/or very low relaxation times, applying a slow plate separation (instead of the step strain deformation), which allows positioning the plates close to the critical point when a stable liquid bridge still exists [110, 112].

The VH liquid phase was characterised in the CaBER 1 device and was subjected to a step strain with 50 ms duration. All measurements were performed at $T \simeq 37$ °C for imposed strains of 1.23 and 1.64. The plates used have either a diamater of $D_p = 4$ mm or $D_p = 6$ mm. The evolution of the thinning fluid filament was measured using a laser and confirmed using a high speed camera.

The pharmacological fluids were measured with cylindrical plates with diameter $D_p = 2$ mm and an initial gap of $L_0 = 0.5$ mm (initial aspect ratio of $\wedge_i = L_0/D_p = 0.25$) for the silicone oils, and $L_0 = 0.25$ mm ($\wedge_i = 0.125$) for the PFLCs. The SRM measurements were performed with a plate separation velocity of 5 μm/s at temperatures between 18.6 °C and 23.3 °C. During the experiments, the evolution of the thinning fluid filament formed between the plates was monitored with video imaging using a high-speed CMOS camera (FASTCAM MINI UX100) operated at 5000, 20000 and

40000 frames per second (fps). At 5 000 fps the spatial resolution and the exposure time are 1280x1000 pixels and 50 μs, respectively. Increasing the frame rate decreases the spacial resolution and the exposure time, and for the maximum frame rate (40000fps) the spacial resolution is 1280x120 pixels and the exposure time is 5 μs. The camera was connected to a magnifying optical lenses (H) (OPTEM Zoom 70 XL) that allow a variable magnification from 1$\times$ to 5.5$\times$. All the images were recorded with a magnification of 4$\times$ which corresponds to 0.86 μm/pixel. The video images were afterwards analysed in Matlab (MathWorks, version R2014b), in order to obtain the filament diameter as a function of time, and to determine the filament breakup time. All the data presented corresponds to times for which the filament exhibits a quasi-cylindrical shape.

3.6 Surface and interfacial tension

Surface tension (ST) is caused by the attraction between the molecules in a liquid, and is defined as the force along a line of unit length perpendicular to the surface. In the bulk of the liquid, individual molecules are pulled equally in all directions by neighbouring molecules, resulting in a zero net force. However, as shown in Fig. 3.10, at the surface the molecules in the liquid are pulled inbound by the other molecules inside the liquid, but there are no liquid molecules on the outside to balance these forces, so the surface molecules are subject to a net inbound force. Interfacial tension (IFT) is somehow similar to surface tension, where the cohesive forces between the surface of two different immiscible fluids are involved [113].

The knowledge of ST and IFT of a material plays an important role in different processes, such as assessing the biocompatibility of polymers, wetting, adsorption and emulsification cases, etc [114].

In this work, the pendant drop method was adopted to measure the ST and IFT. Classified as a gravity-distorted drop method, the pendant drop consists of suspending a liquid drop from a needle in a liquid or gas environment. The ST (or IFT) together with the gravity effect, origin a drop with a specific shape and radius. The pressure inside the drop increases as a result of the ST or IFT. The Young-Laplace equation

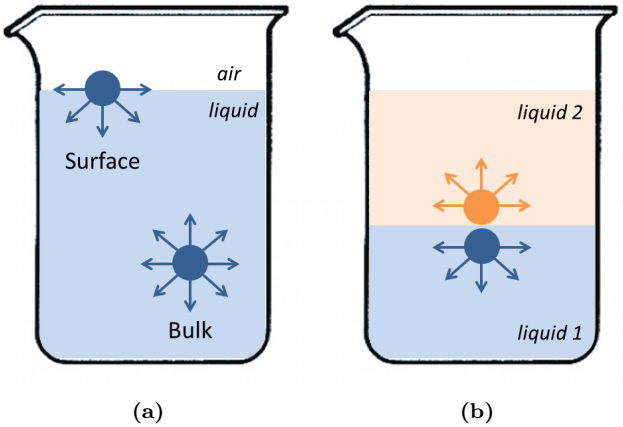

Figure 3.10. (a) Bulk, surface and (b) interfacial tension of a liquid.

relates the SF or IFT (σ), the pressure differences (Δ_p) and the radii of curvature r_1 and r_2 as

$$\Delta p = P_{int} - P_{ext} = \sigma \left(\frac{1}{r_1} + \frac{1}{r_2} \right) \tag{3.46}$$

Gravitational effects cause a pressure variation along the z-axis. Consequently, the Laplace pressure $\Delta p(z)$ at a distance z from an arbitrary reference plane with Laplace pressure Δp_0 is given by

$$\Delta p(z) = \Delta p_0 - \Delta \rho g z \tag{3.47}$$

with $\Delta\rho = \rho_d - \rho$ being the density difference, where ρ_d is the drop phase density and ρ is the continuous phase density.

For the lowest point of the pendant drop, the principal radius of curvature at the vertex is $r = r_1 = r_2$. For every point above it $r_2 = x/\sin\Phi$ (see Fig. 3.11), giving

$$\frac{1}{r_1} + \frac{\sin\Phi}{x} = \frac{2}{r} - \frac{\Delta\rho g z}{\sigma} \tag{3.48}$$

Eq. (3.48) is then parameterised using the arc lenght s of the drop shape resulting in a set of three first-order differential equations and three boundary conditions, as follows:

$$\begin{cases} \frac{\mathrm{d}\Phi}{\mathrm{d}s} = -\frac{\sin\Phi}{x} + \frac{2}{r} - \frac{\Delta\rho g z}{\sigma} \\ \frac{\mathrm{d}x}{\mathrm{d}s} = \cos\Phi \\ \frac{\mathrm{d}z}{\mathrm{d}s} = \sin\Phi \\ x(s=0) = z(s=0) = \Phi(s=0) = 0 \end{cases} \tag{3.49}$$

Solving the previous system of equations allows to abtain the theoretical drop profile which can be compared with the experimental drop profile, with the first being calculated with the surface tension as one of the adjustable parameters. The best match identifies the fluid surface tension [113].

The drop shape method has the advantages of offering no limitations on the ST or IFT values to be measured, only needing a small amount of sample, working well for a wide range of materials with distinct viscosities, and also for a significant range of temperatures [115]. The main disadvantages of the method are the fact that densities of the liquids under study need to be accurately predetermined, and for fluids with similar densities it may not be possible to obtain accurate results [113,116]. To achieve

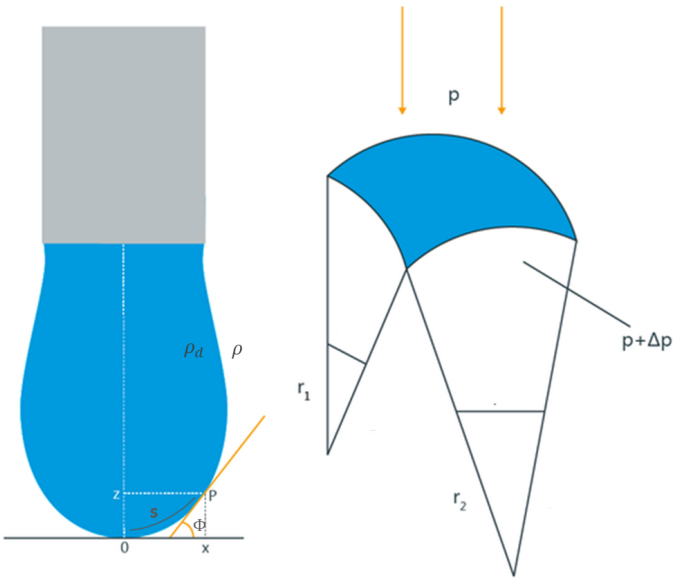

Figure 3.11. Schematic representation of a pendant drop, and the determination of the local radii of curvature for a given pressure difference.

accurate measurements, the drop should be as large as possible, without compromising its stability.

During this study, the surface tension measurements were performed with a drop shape analyser (model DSA25, Krüss).

For VH, measurements were performed only for the liquid phase, in different days and with different samples, to assess the repeatability. The measurements were performed at constant temperature, $T = 21 \pm 2$ °C. The shape of the pendant drop was fitted to the Young-Laplace equation, Eq. 3.46, and σ was determined.

The surface tension of the pharmacological fluids was measured at $T = 20 \pm 2$ °C.

All the interfacial tension measurements between the VH fluid and the pharmacological fluids were also measured with the drop shape analyser, at $T = 22 \pm 1$ °C. For all the measurements, VH was the environment fluid and the drop was the pharmacological fluid. Experiments with the HPF8 and HPF10 fluids were done with a needle of 0.309 mm in diameter, while a needle of 0.660 mm in diameter coated with Teflon was used for Densiron 68, RS-Oil 1000, Siluron 2000 and RS-Oil 5000 fluids. The densities presented in Table 3.3 were used to calibrate the system.

Table 3.3. Densities of the different fluids analised.

Fluid	Density (g/cm^3) [17, 18]
Vitreous Humour	1.0053-1.0089
HPF8	1.76
HPF10	1.94
Densiron 68	1.06
Silicone Oils	0.97

3.7 Microfluidics

Microfluidics refers to the study of different types of flow circulating in artifical microsystems, where the channels have micrometric characteristic dimensions, typically between 1 and 1000 μm. Due to the low amount of sample and reagents required, the cost efficiency, the reduction of the waste generated and portability, this technique has become popular in the last decades. Microfluidics is commonly used for different appli-

cations in different fields such as lab-on-a chip diagnosis for different types of diseases, micro-rheology, inkjet printing, particle crystalization, among others [117, 118].

Microfluidics is a common technique to study the flow patterns of Newtonian and non-Newtonian fluids in low Re flow conditions. One geometry often used is a contraction-expansion channel. Even though it is a simple geometry, it shows complex flow patterns that present both shearing and elongational regions: close to the walls the flow is shear-dominated, whereas in the centreline it is mostly extensional and shear-free [117].

During this study a planar contraction-expansion of approximately $390-50-390$ μm and a constant depth of 100 μm was used[1]. The shape and main dimensions of the microchannel are shown in Fig. 3.12. The contraction ratio $CR = w_u/w_c$ between the expansion and the contraction is $CR = 7.8$ and the aspect ratio is $AR = h/w_c = 2$. The microchannels were made of PDMS, using standard soft-lithography techniques (details about the method are presented in Refs. [119, 120]). Visualizations of the flow patterns were performed with *long-time* exposure photography. The imaging experimental set-up includes an inverted fluorescence phase contrast microscope (model IX71, Olympus) equipped with a filter cube set in order to isolate the 535 peak of the fluorescent light source (Lumen 200, Prior scientific), and the resultant particle fluorescence signal (580

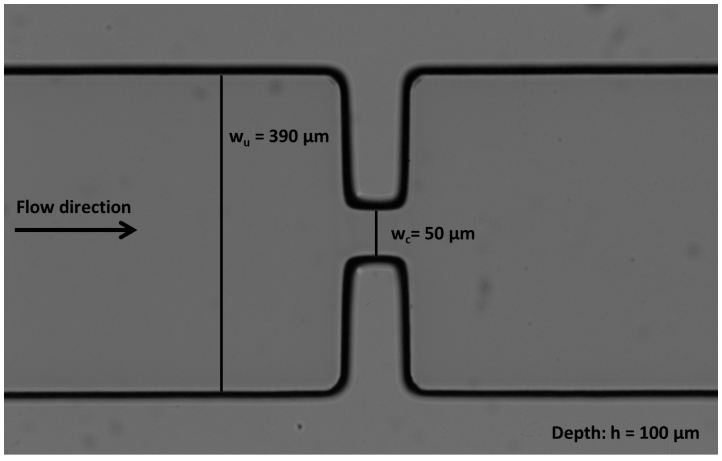

Figure 3.12. Optical transmission microscope image of an approximately $390-50-390$ μm planar contraction-expansion showing the main characteristic dimensions.

[1]The microchannels were kindly fabricated by the PhD student Joana Fidalgo

nm) is captured by a CCD camera (model XM10, Olympus).The flow rate was controled with a neMESYS (Cetoni) syringe pump system.

The pharmaceutical fluids Densiron 68, Siluron 2000 and Siluron 5000 were studied. All the fluids were seeded with 1 μm fluorescent tracer particles (Fluorospheres, Molecular Probes, Invitrogen, Ex/Em: 535/575 nm), and an exposure time of 700 ms was used to obtain the flow pathlines, which were then recorded for further analysis.

"An experiment is a question which science poses to Nature, and a measurement is the recording of Nature's answer."

Max Planck

Chapter 4

Vitreous humour characterisation[†]

This chapter presents a detailed rheological characterisation of the two phases of the VH under shear and extensional flow conditions. The results show that VH *liquid phase* exhibits a surface tension of $47.8\ \mathrm{mN/m}$, a shear thinning behaviour reaching a viscosity plateau around 10^{-3} Pa s for shear rates above $\sim 1000\ \mathrm{s}^{-1}$, and an average extensional relaxation time of 9.7 ms. Interestingly, both VH phases present higher storage modulus than loss modulus, and the measurements performed with VH gel phase 4 ± 1 hours after dissection exhibit the highest moduli values. The compliance measurements for the *gel phase* show a viscoelastic gel behaviour and that compliance values decrease substantially with time after dissection.

4.1 Surface tension

The average surface tension measured for the VH liquid phase was $\sigma = 47.8 \pm 3.8\ \mathrm{mN/m}$ (see Table 4.1). There was no significant difference observed in the measurements

[†]Part of this chapter has been published in:
A. F. Silva, M. A. Alves and M. S. N. Oliveira, "*Rheological behaviour of vitreous humour*", Rheologica Acta, volume **56** number **4**, 2017

right after dissection or a few hours after dissection (average values of 47.1 mN/m and 48.6 mN/m, respectively). Fig. 4.1 shows an example of a pendant drop of the VH liquid phase visualised during the surface tension experiments. To the best of the author knowledge only Ross *et al.* [121] presented measurements with the VH collected from rabbits, reporting an average surface tension of 60.6 ± 2.6 mN/m. The measurements presented here for the liquid phase exhibit lower values of surface tension, but closer to the results presented by Li and collaborators for HA solutions [122], which is consistent with the main component of the liquid phase being hyaluronan [10]. Li *et al.* [122] performed a series of surface tension measurements with hyaluronic acid solutions at different concentrations and in solutions with gelatine and/or N,N-dimethylformamide, showing that for aqueous solutions of hyaluronic acid (1.3 and 1.5 HA w/v%) the surface tension measured varied between 52 and 53 mN/m.

Table 4.1. Surface tension obtained for VH liquid phase at $T = 21 \pm 2$ °C, using the Young-Laplace equation with a pendant drop.

	Average surface tension (mN/m)	Standard deviation (mN/m)
Measurements immediately after dissection	47.1	2.8
Delayed measurement within 4±1 hours after dissection	48.6	4.4
All measurements	47.8	3.8

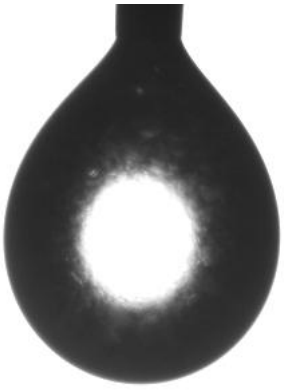

Figure 4.1. Example of an image of a pendant drop of VH liquid phase captured for the determination of the surface tension.

4.2 Steady shear flow experiments

Fig. 4.2 shows the steady shear experiments performed with the VH liquid phase, measured at $T = 37$ °C.

In the stress-controlled experiments (see Fig. 4.2a), for shear stresses below 0.2 Pa the measured viscosity of the VH liquid phase is very high (above 200 Pa s) and the corresponding shear rate is very small. For a shear stress around 0.2 Pa, a sudden decrease in the shear viscosity of more than four orders of magnitude is observed, from above 200 Pa s to a value around 0.003 Pa s, while the shear rate increases abruptly. For the shear rate-controlled experiments (see Fig. 4.2b), the viscosity exhibits shear-thinning with a power-law behaviour, $\tau \propto \dot{\gamma}^{-1}$, with a value around 20 Pa s for a shear rate of 0.01 s^{-1} reaching a value around 10^{-3} Pa s for shear rates above ~ 1000 s^{-1}. Although the author of this work is not aware of any comparable studies in the literature, it is instructive to compare the results obtained with some studies with HA solutions [123, 124], which is believed to be one of the main components of the liquid phase, and with some biological fluids in which the main constituent is HA [125–128]. HA solutions are shear-thinning and the values and the characteristics of the flow curve are dependent of the concentration of HA, the molecular weight and conformation of HA and, consequently, the interactions between them [123–128]. Fam *et al.* [126] measured the rheological properties of different concentrations of hyaluronic acid/bovine calf serum solutions that can be used as analogues of synovial or periprosthetic fluids. The flow curve measured in this work is in the same range of values as the 1 mg/mL HA solution (HA with a molecular weight of 2.48 MDa). Bingol *et al.* [125] characterised the rheological properties of sodium hyaluronate samples with different concentrations and of synovial fluid taken *post mortem* from different patients. Similarly to the results presented here, those authors also observed a shear-thinning behaviour of the biofluid and variability from donor to donor.

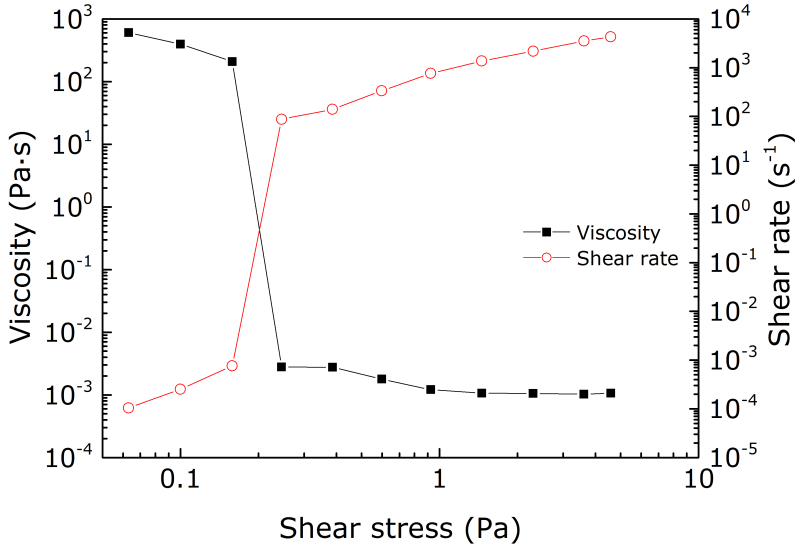

(a)

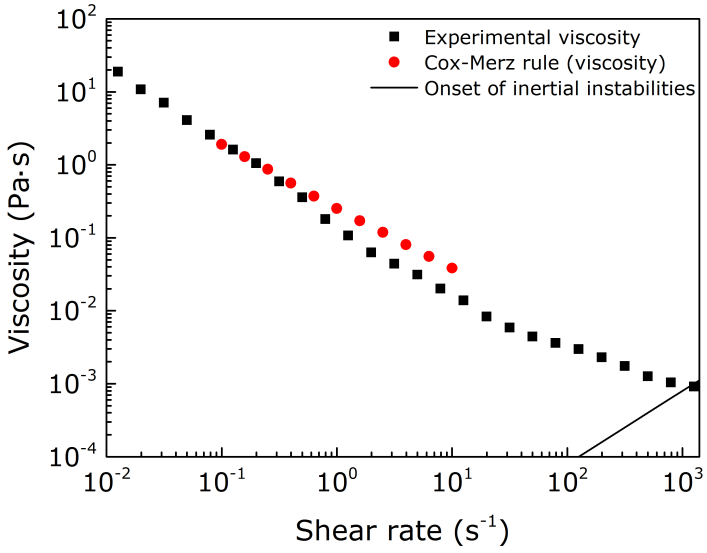

(b)

Figure 4.2. Shear measurements with the VH liquid phase, measured at $T = 37\ ^{\circ}\mathrm{C}$. (a) Shear viscosity and shear rate as function of shear stress for a stress-controlled experiment; (b) shear viscosity as function of shear rate for shear rate-controlled experiment and comparison with the shear viscosity predicted using the Cox-Merz rule using the SAOS measurements. The onset of inertial instabilities was calculated with Eq. (3.22).

4.3 SAOS experiments

Small amplitude oscillatory shear measurements (SAOS) were performed using different samples with the gel and liquid phases and repeated at different elapsed times after dissection. A strain sweep was carried out at constant frequency, $\omega = 10$ rad/s (for the liquid phase and the gel phase 4 ± 1 h after dissection). The effect of the imposed oscillatory strain on the viscous and elastic moduli is illustrated in Fig. 4.3, where it is possible to observe that both the liquid and the gel phases are in the linear regime (G' and G'' constant) at least up to $\gamma \cong 1\%$.

Fig. 4.4 shows the frequency sweep response for the three different types of sample under a strain amplitude of $\gamma = 1\%$, selected to be in the linear regime based on the strain sweep experiments (cf. Fig. 4.3): the gel phase immediately after dissection; the gel phase 4 ± 1 h after dissection, and the liquid phase.

Fig. 4.4a also shows G' measurements performed with water (which ideally should be zero) for comparison and to determine the instrument baseline. It is clear that the G' values of the VH samples are at least 3 orders of magnitude higher than the baseline of

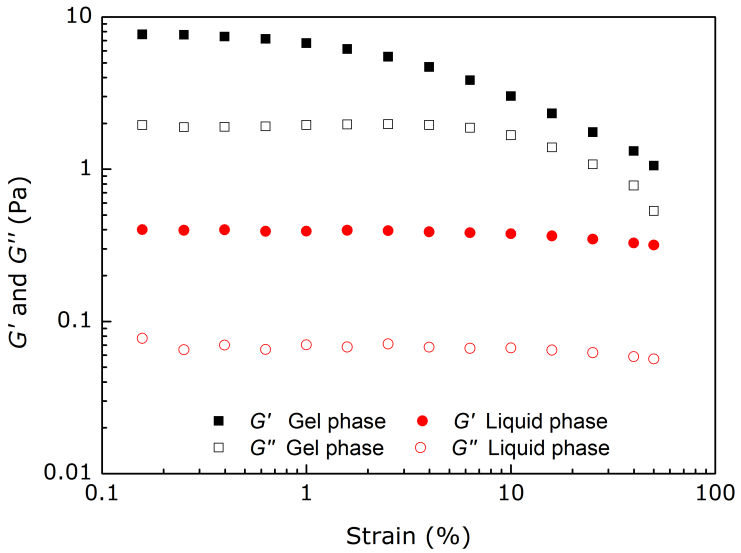

Figure 4.3. SAOS measurements at different strains conducted with the liquid and the gel phases at $T = 37$ °C and constant frequency, $\omega = 10$ rad/s.

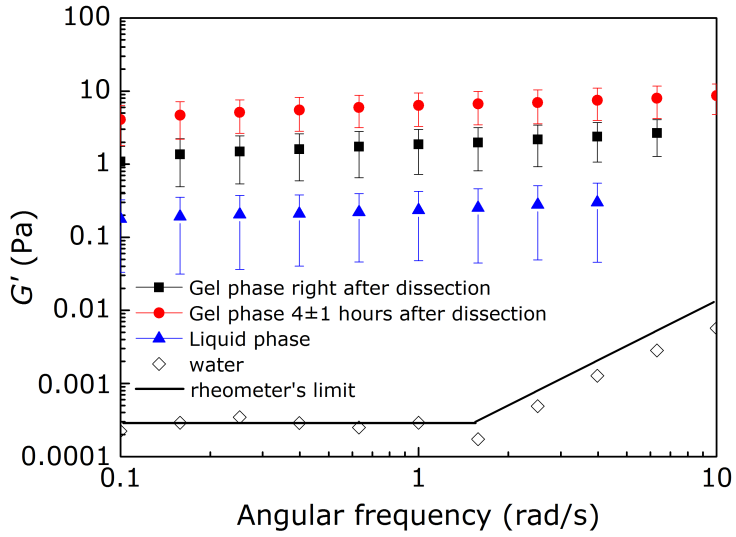

(a)

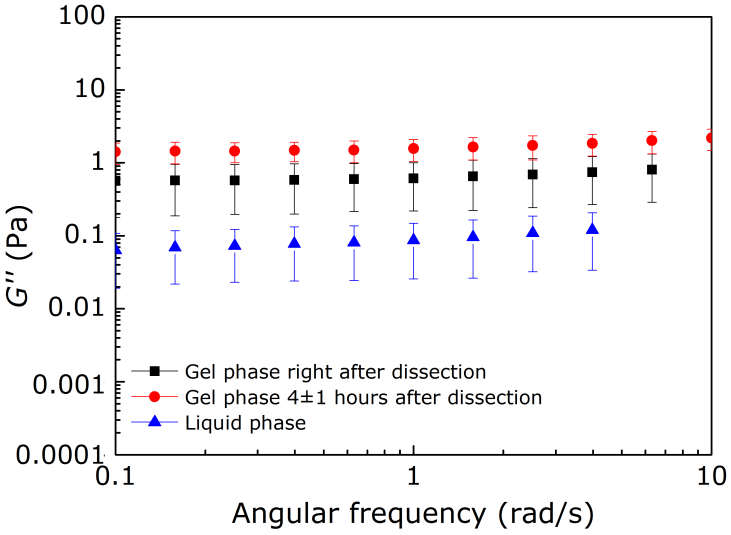

(b)

Figure 4.4. (a) Storage (G') and (b) loss (G'') moduli of the gel phase of VH as function of frequency for constant strain amplitude, $\gamma = 1\%$, measured at $T = 37$ °C.

the equipment, thus being reliable. Additionally, only data exhibiting a raw phase below 90° is presented in Fig. 4.4 [129]. The VH gel phase right after dissection is the sample with the properties most similar to the VH in its natural environment [10]. Even if the

shape and conformation of the fluid during the experiment is not exactly the same as in the vitreous cavity, it is the closest to the conformation of VH in the vitreous cavity that is possible to study *ex vivo*. In this conformation, the collagen networks actively interact with the hyaluronan molecules, which are responsible for the VH properties: it is believed that the hyaluronan molecules are bound to the collagen fibrils, stabilising the collagen conformation and reinforcing the vitreous structure [10, 130]. Nickerson *et al.* [10] hypothesised that the hyaluronan increases the moduli by placing the collagen network under internal tension.

The average and standard deviation of G' and G'' for all samples analysed are shown in Fig. 4.4. As expected for biofluids there is donor to donor variability and, as a result, the measurements repeated with samples from different rabbit eyes and in different days, even under similar experimental conditions, present some variability. The oscillatory measurements show that G' and G'' are higher in the gel phase measured 4 ± 1 h after dissection than right after dissection. Measurements with the gel phase (both right after dissection and 4 ± 1 h after the dissection) show that for all the frequencies, G' is in average higher than G'', indicating that a solid-like behaviour dominates [95]. For the liquid phase, both G' and G'' are lower than the gel phase, and the elapsed time after dissection does not seem to significantly influence the linear viscoelasticity of the fluid for the time-frame investigated. Nevertheless, G' is also higher than G'' for the range of frequencies tested and the fluid can be considered as a weak gel [131]. In this work, however, the notation *liquid phase* is still used for consistency with previous works [16, 37–39]. Nickerson *et al.* [10] showed that for variable frequency experiments, the broad plateau modulus region expected for gels occurs below $\omega = 5$ rad/s. As such, the analysis is based on values obtained for $\omega = 1$ rad/s (see Table 4.2). Using the Cox-Merz rule [132] it is possible to estimate the shear viscosity in steady shear flow from the SAOS measurements. The results obtained are included in Fig. 4.2b, showing the applicability of this empirical rule for VH liquid phase at lower shear rates (between $\dot{\gamma} = 0.1$ and 10 s^{-1}).

Fam *et al.* [126] performed SAOS experiments with hyaluronic acid/bovine calf serum solutions. For solutions with concentrations of HA between 3 and 4 mg/ml,

Table 4.2. Average values obtained for storage and loss moduli for the VH liquid phase and VH gel phase right after dissection and 4 ± 1 h after dissection. The values presented were obtained for a strain amplitude $\gamma = 1\%$ and a constant frequency, $\omega = 1$ rad/s.

Samples		Number of samples tested	G' (Pa)		G'' (Pa)	
			Average	Standard deviation	Average	Standard deviation
Liquid phase		13	0.23	0.19	0.09	0.06
Gel phase	Immediately after dissection	14	1.86	1.14	0.61	0.39
	4 ± 1 h after dissection	9	6.35	3.05	1.57	0.52

the storage modulus is in the same range of values of the VH liquid phase, but the loss modulus is not (G' between 0.1 and 0.8 Pa and G'' around 1 Pa, for $\omega = 1$ rad/s), indicating that the elastic behaviour is similar, but the VH liquid phase shows a less viscous character than the HA solutions. For the VH gel phase measured right after dissection and for a constant frequency of $\omega = 1$ rad/s, G' shows an average value of 1.86 Pa (standard deviation of 1.14 Pa) and G'' presents an average value of 0.61 Pa (std. deviation of 0.39 Pa) (see Table 4.2). The moduli results are in the same range of those presented by Sharif-Kashani *et al.* [11], Nickerson *et al.* [10] and Filas *et al.* [36]: in the measurements performed by Sharif-Kashani *et al.* [11] right after dissection, the storage modulus varies between 1 and 2 Pa and the loss modulus between 0.2 and 0.3 Pa; Nickerson *et al.* [10] obtained an elastic modulus $G' \simeq 2$ Pa and a viscous modulus $G'' \simeq 0.1$ Pa for a frequency of $\omega = 1$ rad/s, also immediately after dissection; finally, Filas *et al.* measured $G' \simeq 3$ Pa and $G'' \simeq 1$ Pa for porcine eyes. These small differences may be explained by the difference in the amount of HA and collagen content between rabbit and porcine eyes: collagen content in the eyes of rabbits varies between 75-900 μg/mL while in pig's eyes is ~ 20 μg/mL, while HA content varies in the range 20-60 μg/mL in rabbit eyes and 70-80 μg/mL in porcine eyes [22]. As shown by Filas *et al.* [36], the differences in HA and collagen content can significantly change the moduli of the samples. The SAOS measurements with VH gel 4 ± 1 h after dissection (Table 4.2) compare well with the measurements of Shayegan and Forde [133] with collagen solutions: G' varies between 3 and 20 Pa, while G'' varies between 0.01 and 1 Pa for a frequency of $\omega = 1$ rad/s.

Oscillatory measurements along time were also performed to investigate the time dependency of the storage and loss moduli for a low frequency, $\omega = 1$ rad/s (see Fig. 4.5). The measurements were started right after dissection as described previously. For all samples, G' increases slightly in the beginning of the experiment while G'' remains approximately constant. On the other hand, Nickerson *et al.* [9, 10] reported that for a strain amplitude of $\gamma = 3\%$ and a frequency of $\omega = 10$ rad/s both the elastic and viscous moduli decrease over time. We found a similar behaviour only for high frequencies ($\omega = 10$ rad/s, see Fig. 4.6). However, after some time (around 60 min) both moduli started to vary suddenly suggesting that the sample network was destroyed. As such, it is not guaranteed that the decrease in the moduli at the beginning of the experiment was not a result of a degradation process.

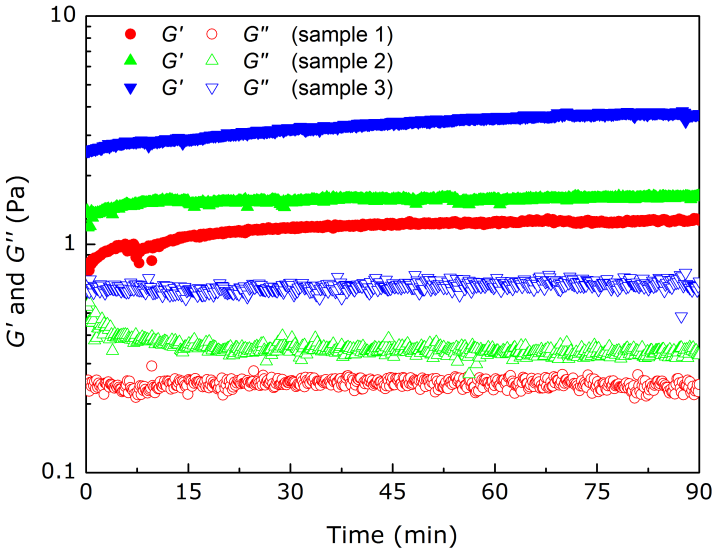

Figure 4.5. Elastic (G') and viscous (G'') moduli variation with time for three independent experiments with the vitreous gel phase right after dissection. The measurements were performed at $T = 37$ °C for constant strain, $\gamma = 1\%$, and frequency, $\omega = 1$ rad/s.

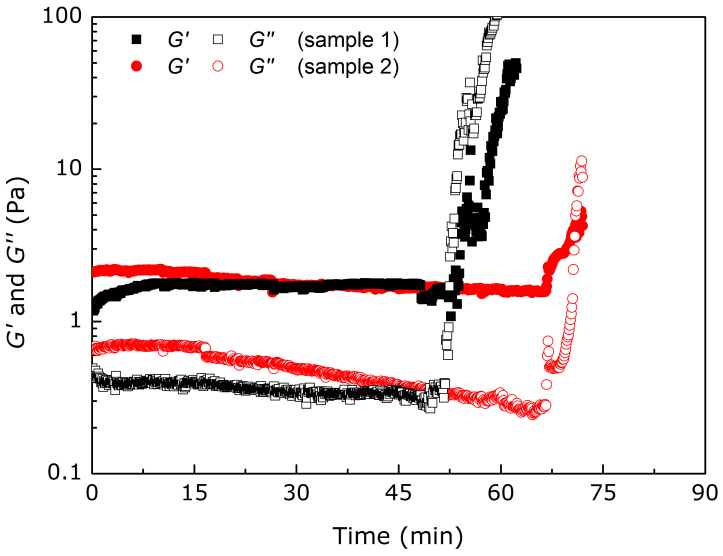

Figure 4.6. Elastic (G') and viscous (G'') moduli variation with time for three independent experiments with the vitreous gel phase right after dissection. The measurements were performed at $T = 37$ °C for constant strain, $\gamma = 1\%$, and frequency, $\omega = 10$ rad/s.

4.4 Creep experiments

Fig. 4.7 shows the results of creep tests performed with the liquid phase for two different applied shear stresses, $\tau_0 = 1.0$ Pa and 2.0 Pa. The compliance, J , is defined as the ratio between the deformation and the applied shear stress, $J(t) = \gamma(t)/\tau_0$. For small times ($t < 30$ s) an unsteady behaviour is observed (where instrument inertia can be significant [129]), but for larger times, a steady shear flow is approached, with a linear increase of J with time as shown in the inset of Fig. 4.7. The slope of J as function of time is approximately 10^3 Pa^{-1} s^{-1} , which is approximately the inverse of the shear viscosity at high shear rates shown in Fig. 4.2.

For the gel phase, creep tests were also performed and the results are shown in Fig. 4.8 for two different shear stresses ($\tau_0 = 1.0$ Pa and 2.0 Pa). Different shear stresses were tested, and following the methodology presented by Evans *et al.* [134] and Tassieri *et al.* [135], the compliance values were converted to storage and loss moduli. The compliance results measured for shear stresses of 1.0 Pa and 2.0 Pa when converted to storage and loss moduli are consistent with G' and G'' measured experimentally in

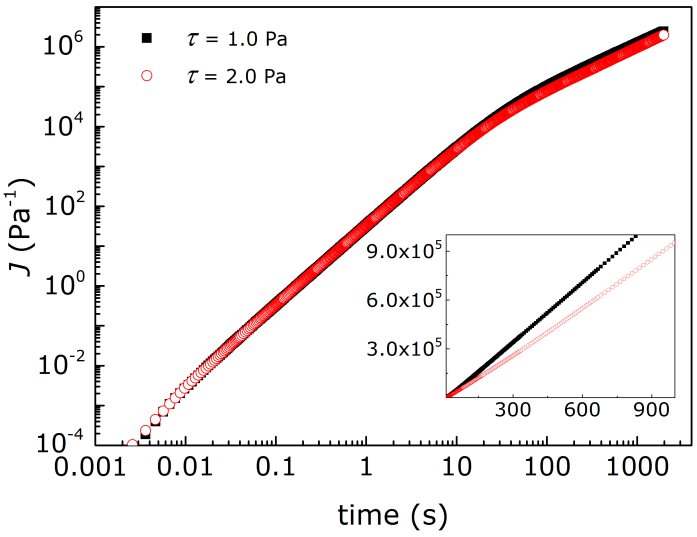

Figure 4.7. Compliance of the liquid phase of VH for two different applied shear stresses as function of time, measured at $T = 37$ °C using the cone-plate geometry with 60 mm diameter.

SAOS: Fig. 4.9 shows the agreement between the experimental SAOS data and the values converted from compliance data measured with a shear stress of 2 Pa.

Fig. 4.8 shows that the gel phase of VH behaves as a viscoelastic material and the response for the two different applied shear stresses is qualitatively similar: there is a first elastic region that occurs immediately after the shear stress is applied, and a second delayed region [105]. The first region corresponds to the elastic response of the vitreous gel phase to a sudden increase of the shear stress (but instrument inertia can also be important in this region) and occurs for a short time: $t \leq 0.2$ s for the delayed experiments, and $t \leq 1$ s for experiments performed immediately after dissection. The elastic region is quickly followed by a delayed elastic region until steady state is reached. The results presented here show that the compliance is higher right after dissection (maximum values are $J = 4.85$ Pa^{-1} for $\tau_0 = 1.0$ Pa and $J = 3.77$ Pa^{-1} for $\tau_0 = 2.0$ Pa) than a few hours after dissection ($J = 0.35$ Pa^{-1} for $\tau_0 = 1.0$ Pa and $J = 0.12$ Pa^{-1} for $\tau_0 = 2.0$ Pa). Based on these SAOS experiments, this behaviour was expected since the compliance plateau is characteristic of the inverse of the elasticity or stiffness of the VH [134].

Sharif-Kashani *et al.* [11] performed similar measurements for three different applied shear stresses ($\tau_0 = 0.5,\ 1.0$ and 2.0 Pa) using porcine eyes, and their results show that lower shear stresses produce higher compliance values. Their maximum compliance

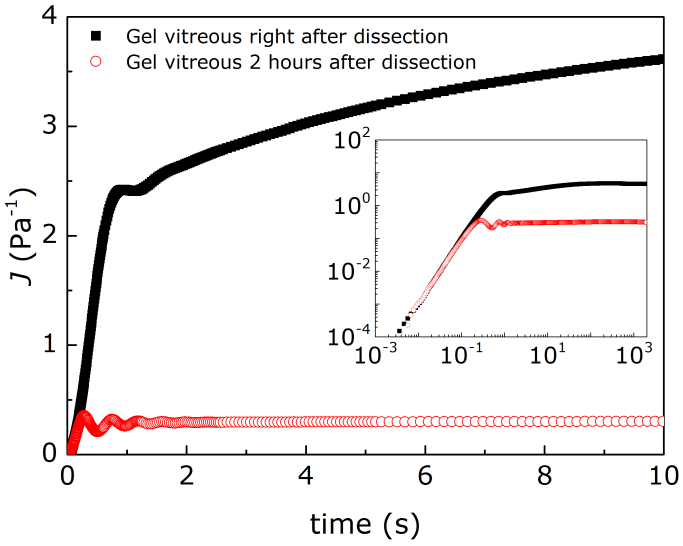

(a)

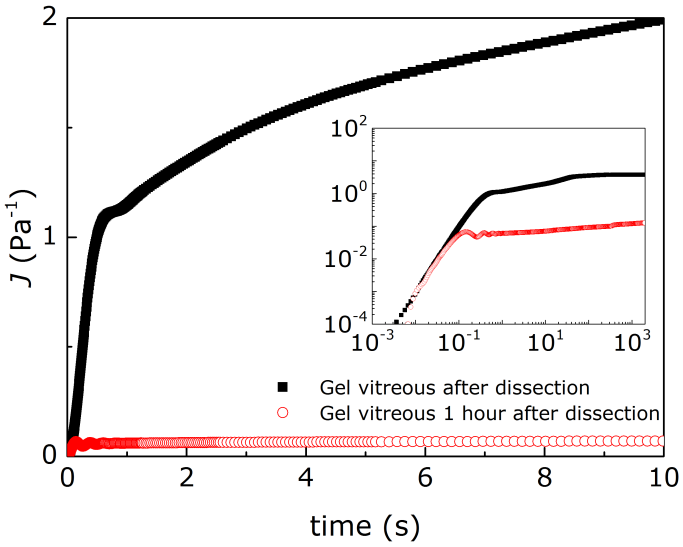

(b)

Figure 4.8. Compliance of the VH gel phase at $T = 37$ °C plotted as function of time for different applied shear stress values: (a) $\tau_0 = 1.0$ Pa and (b) $\tau_0 = 2.0$ Pa.

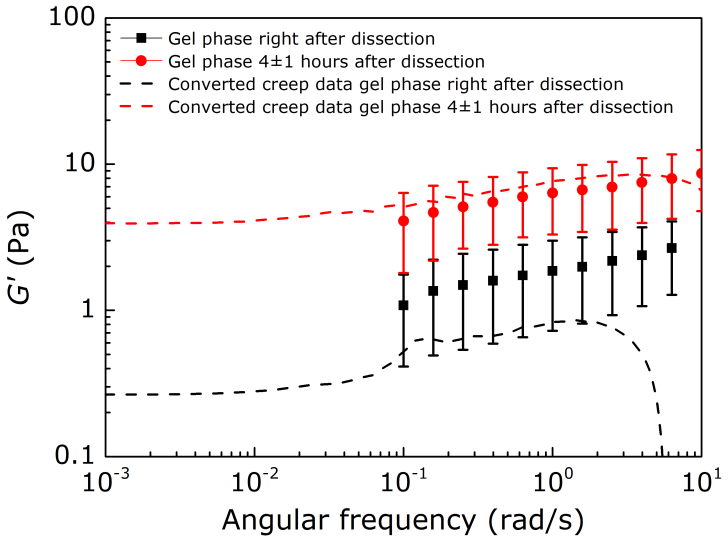

(a)

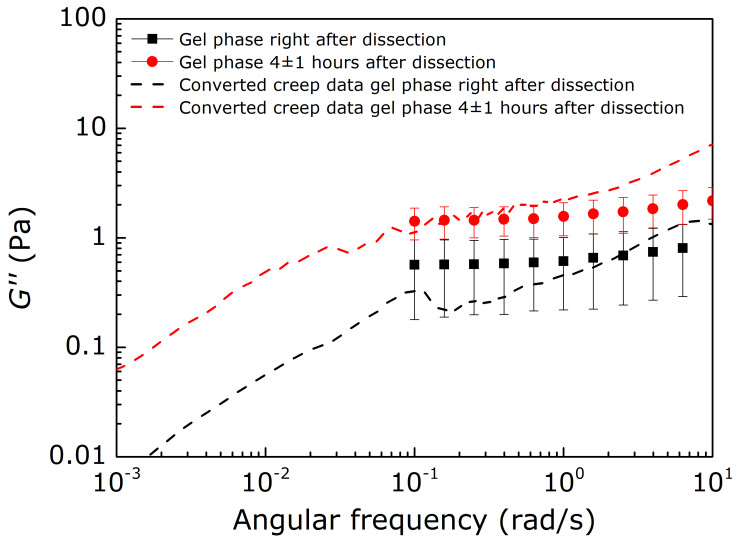

(b)

Figure 4.9. Comparison between the storage and loss moduli values measured experimentally with SAOS experiments and the values calculated from compliance data, measured at a shear stress of $\tau_0 = 2.0$ Pa, following the methodology presented by Evans *et al.* [134] and Tassieri *et al.* [135].

values are around $J = 2$ Pa^{-1} and 1 Pa^{-1} for shear stresses of $\tau_0 = 1.0$ Pa and 2.0 Pa, respectively. Kavehpour *et al.* [136], measured the compliance values of four distinct pairs of porcine eyes. Although the results are very similar for the same pair of eyes,

different values of compliance for different pairs varied in a range between approximately $J = 0.02$ Pa^{-1} and 1 Pa^{-1}.

The compliance value for collagen gel solutions with concentrations of 1% w/w is in the range between $J = 1.5$ Pa^{-1} and 2.8 Pa^{-1} [137]. Similarly to what happens with G' and G'', the compliance values for collagen are comparable to the values obtained for the vitreous gel phases. These results corroborate the idea that the gel properties are mainly established by the collagen fibrils. Additionally, the study performed by Sakuma *et al.* [138], where the authors digested VH with collagenase (destroying collagen fibrils) and consequently obtained a reduction in vitreous gel elasticity (which in that case was associated with a short time scale in creep experiments), supports the idea that the elastic properties of VH are mainly caused by the collagen fibrils.

4.5 Extensional flow experiments

Two examples of the time evolution of the liquid filament diameter measured with the CaBER are shown in Fig. 4.10. The extensional relaxation times were obtained based on the model for a viscoelastic fluid in the elasto-capillary thinning regime, where the filament diameter decays exponentially with time [109], $D(t) \propto e^{-t/3\lambda}$, where λ is the fluid relaxation time. The results show a good agreement between samples from different rabbit eyes. Two exemplifying cases obtained for different strains are shown in Fig. 4.10 and exhibit approximately the same gradient in a semi-log plot in the exponentially thinning region. The average relaxation time obtained is $\lambda = 9.7 \pm 2.2$ ms (based on 12 samples).

A set of extensional flow measurements was performed at a temperature of $T \approx 34$ °C, for specific times between 5 min and 150 min after the dissection of the eye and the relaxation time was found to be nearly independent of time (see Fig. 4.11).

Bingol *et al.* [125] studied the extensional behaviour of sodium hyaluronate and synovial fluid samples. The authors found that the biofluid relaxation time depends strongly of the hyaluronan molecular weight and the concentration of HA. Haward *et al.* [128] used an Optimised Shape Cross-slot Extensional Rheometer (OSCER), to

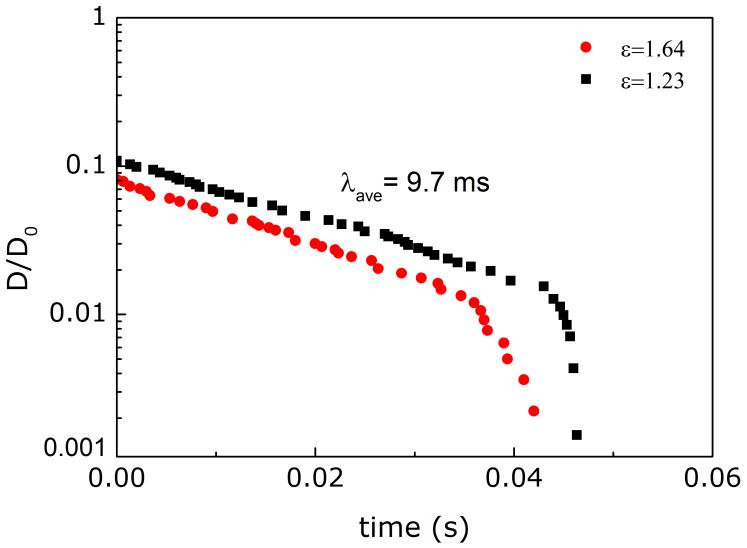

Figure 4.10. Time evolution of filament diameter of VH liquid phase, measured with the CaBER at $T = 37$ °C. The imposed Hencky strains are $\varepsilon = 1.23$ and 1.64, and the samples were submitted to a strike time of 50 ms for plate separation. The two samples exhibit approximately the same relaxation time obtained from the exponentially thinning region is similar for both samples.

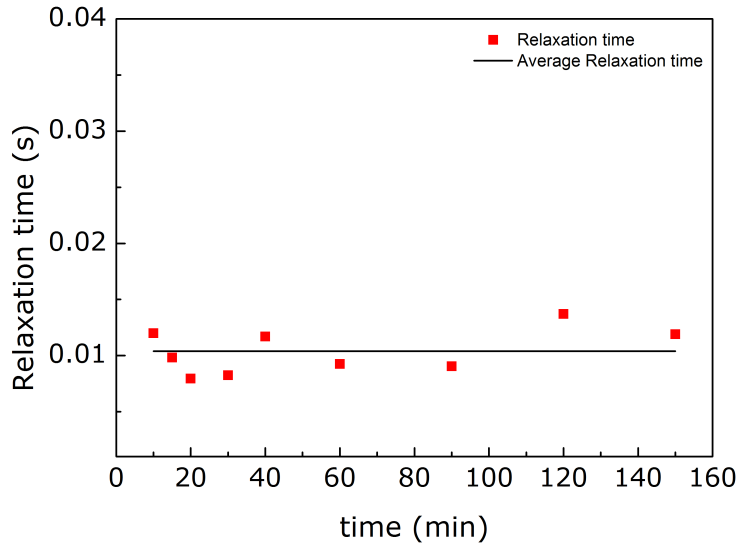

Figure 4.11. Evolution of relaxation time of VH liquid phase measured with CaBER at $T \approx 34$ °C and for different times after the dissection of the eye, using initial and final aspect ratios of $\Lambda_i = D_i/D_p = 0.33$ and $\Lambda_f = D_f/D_p = 1.5$ and an imposed strain of $\varepsilon = 1.51$.

study the elongational flow behaviour and the rheological properties of HA solutions representative of the synovial fluid in the knee joint. The authors tested 3 different solutions: HA solutions of 0.1 wt.% and 0.3 wt.% in a physiological phosphate buffered saline (PBS) and a model synovial fluid formed from a solution of 0.3 wt. % HA combined with 1.1 wt.% BSA, and 0.7 wt.% γ-globulin. The relaxation times of the three solutions were 6.8, 16.8, and 17.2 ms, respectively, which are similar to the relaxation times of the VH samples measured in the present work.

4.6 Conclusions

The shear and extensional rheological properties of vitreous humour were characterised in the liquid and gel phases, both immediately after dissection and several hours after dissection. Both phases showed viscoelastic behaviour, but significant differences between them were found: the liquid phase exhibits the lowest elastic and viscous moduli, while the gel phase 4 ± 1 h hours after dissection shows the highest values. Creep experiments show that the VH gel phase behaves like a typical viscoelastic gel, presenting an elastic region, followed by a delayed elastic region until steady state is reached. When submitted to steady shear, the liquid phase exhibits a shear thinning behaviour achieving a viscosity plateau of $\sim 10^{-3}$ Pa s. Experiments with the liquid phase under extensional flow yielded an average relaxation time of $\lambda = 9.7$ ms, which was found not to change significantly with time after dissection. The surface tension of the liquid phase was also found to be nearly constant within the timeframe of the experiments.

The properties of VH liquid phase and VH gel phase are consistent with literature data obtained for solutions of HA and collagen, respectively, suggesting that the rheological properties are dictated mainly by the collagen content in the case of the gel phase, and by the HA content in the liquid phase.

The detailed rheological characterisation data provided here for the different phases of VH are key to understand the differences in VH properties due to the liquefaction process that occurs along the different stages of the eye's life, as well as the changes caused in the biofluid structure as a consequence of some diseases. The rheological

insight is also crucial for the improvement and development of new drug delivery systems as well as for the development of a new class of vitreous humour substitutes to be used in eye surgery than can mimic its mechanical functionality.

"Things are not always what they seem; the first appearance deceives many."

Phaedrus

Chapter 5

Characterisation of pharmacological fluids

A detailed rheological characterisation of commercial fluids used in eye surgery under shear and extensional flow conditions is presented in this chapter. Surface tension and interfacial tension measurements, and microfluidics flow visualisations are also presented. Pharmacological fluids with different compositions were tested, including perfluorocarbons (PFLC), silicone oils (SiO), and a heavy SiO (HSiO) (a mixture of 70% of silicone oil with 30% of perfluorohexyloctane). Surface and interfacial tension results show that all the pharmacological fluids investigated have a surface tension lower than the one of vitreous humour (VH). Shear rheology experiments showed a constant viscosity for all the fluids. Extensional rheological experiments of all the pharmacological fluids under study show that Siluron 2000 is the only fluid exhibiting elastic behaviour.

5.1 Surface and interfacial tension

Surface tension (ST) experiments using the pendant drop method were performed for all the pharmacological fluids under study. The ST values measured are presented

in Table 5.1 for all the test fluids. The ST of the PFLC fluids HPF8 and HPF10 show a difference of 4.9 mN/m between them, with HPF10 presenting a higher value. Note that HPF8 is a linear perfluorocarbon and HPF10 a cyclic one (see Fig. 3.6). Freire *et al.* [139] showed that cyclic PFLCs have higher surface tension than the linear chain with the same number of carbon units. These authors measured the surface tension of different PFLCs, including a linear perfluorooctane (HPF8) and a cyclic perfluorodecalin (HPF10). For a temperature of $T = 20$ °C the values measured were $\sigma = 14.92 \pm 0.04$ mN/m and $\sigma = 19.85 \pm 0.07$ mN/m, for the linar perfluorooctane and the cyclic perfluorodecalin, respectively, which are approximately 0.7 mN/m lower than the values measured in this work. The SiO-based fluids also have similar surface tensions between them, and the values vary between 21.7 and 22.0 mN/m. The Densiron 68 (a mixture of 70% of SiO and 30% of perfluorohexyloctane (F6H8)) presents a lower surface tension (average value of 20.8 mN/m) when compared with the SiOs. For all the fluids investigated, only the surface tension of Densiron 68 (19.13 mN/m) is provided by the manufacturer. However, Kim *et al.* [140] measured the surface tension of a silicone oil with a viscosity of approximately 5 Pa s and Densiron 68, using the Du Nuoy-ring method. Their values are approximately 1 mN/m lower than the values measured in this work. In Ref. [140], the authors investigated different concentrations of mixtures of SiO and perfluorohexyloctane until the ratio of Densiron 68. Their results show that the surface tension of those mixtures decreases with the increase of F6H8. In summary, all the pharmacological fluids studied present surface tension values lower than VH liquid phase ($\sigma = 47.8 \pm 0.04$ mN/m).

Table 5.1. Surface tension of the pharmacological fluids analysed in this study, at temperatures between $T = 20$ and 22 °C.

Fluid	Average surface tension (mN/m)	Standard deviation (mN/m)
HPF8	15.6	0.4
HPF10	20.5	0.4
Densiron 68	20.8	0.2
RS-Oil 1000	21.9	0.3
Siluron 2000	22.0	0.3
Siluron 5000	21.7	0.6

As mentioned previously, the pharmacological fluids are used in vitreoretinal detachment surgeries with the goal of reattaching the retina [141, 142]. When a pharmacological fluid is inserted in the VH cavity it will interact with the retina and due to its specific gravity it will be able to push the retina back to the choroid tissue. Note that due to their specific gravity, SiOs are mostly used in the treatment of superior retinal detachment (RD), while HSiOs are mostly used to treat inferior RD [143]. However, during the whole process the VH substitute will also be in contact with VH, and the way they interact is important for the success of the medical procedure. Therefore, it is relevant to study the properties in the interface between the two fluids. To the best of the author knowledge, there are no published studies presenting the interfacial tension (IFT) between the pharmacological fluids and VH. Nevertheless, it is possible to find the values of the interfacial tension between some pharmacological fluids and water. At $T = 25$ °C, Densiron 68 has an interfacial tension in water of 40.82 mN/m [140, 144]. For SiOs, different studies show different values: Kim *et al.* [140] presented a value of 43.01 mN/m and Wetterqvist *et al.* [144] reported a value of 35.4 mN/m. HPF8 has an ITF in water of 55.0 mN/m [144].

In this work, the IFT of the surgical fluids under study was measured in the VH liquid phase extracted from rabbit eyes. The drop formed for the different pharmacological fluids and VH liquid phase are shown in Fig. 5.1. The average IFT and standard deviation values are presented in Table 5.2. The results show that the SiO-based fluids present an average IFT of around 30 mN/m, while the PFLCs have an average IFT between 33 and 34 mN/m. The HPF8 fluid presents the highest value (average of 34.0 mN/m) and Siluron 5000 shows the lowest value (average of 28.3 mN/m). The IFT measurements were repeated at least five times, and the standard deviation associated with the experiments is considerable. The drop shape method accuracy depends on the size of the droplet formed: the dropled must be as large as possible, but stable. During the experiments presented here, it was challenging to create a stable and large droplet and that may have contributed for the large standard deviations obtained. Nevertheless, all the measurements considered had similar droplets with similar volumes. Analysing Table 5.2 it is possible to find a relation between the viscosity of the fluis (which are

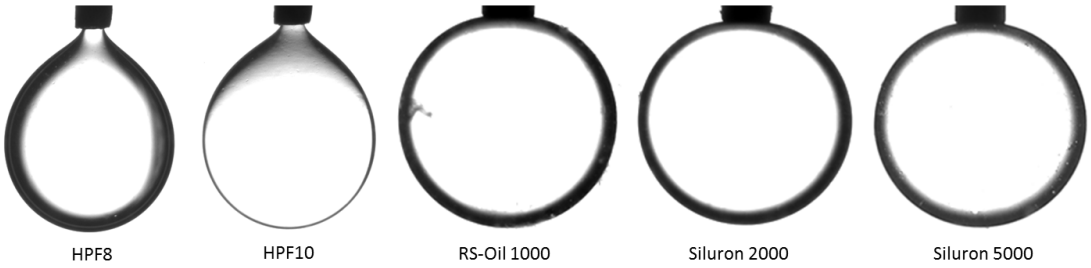

Figure 5.1. Pendant drop shape during the interfacial tension experiments for the pharmacological fluids in contact with VH liquid phase from rabbit eyes. The drop is formed by the pharmacological fluid and the environment is VH fluid. The measurements were made at temperatures between $T = 21$ and 23 °C.

Table 5.2. Interfacial tension of the pharmacological fluids analised when in contact with VH, measured at temperatures between $T = 21$ and 23 °C.

Fluid	Average interfacial tension (mN/m)	Standard deviation (mN/m)
HPF8	34.0	4.6
HPF10	33.1	6.9
RS-Oil 1000	31.6	7.3
Siluron 2000	29.8	6.7
Siluron 5000	28.3	8.7

presented in the next section) and the interfacial tension values: the last one decreases with the increase of the shear viscosity of the pharmacological fluid. There are no results for the IFT between the fluid Densiron 68 and VH because it was not possible, using the pendant drop method, to create stable droplets to perform the measurements.

The success of the implantation of the VH substitutes is directly related with the fluid ST (or IFT) and specific gravity, and together with the shear viscosity it will dictate how easily a fluid can emulsify [145, 146]. SiO-based fluids presented IFT values around 30 mN/m while the PFLCs have an average value around $33 - 34$ mN/m. For the SiOs, considering that the values are close enough to be considered similar, the differences in emulsification between different SiOs found in the literature (see descripion in Section 2.2.2) must be mainly due to viscosity and specific gravity differences.

5.2 Steady shear flow experiments

The flow curves for the fluids under study are shown in Fig. 5.2 for a constant temperature of $T = 37$ °C, and Table 5.3 summarises the viscosity values for a constant shear rate of $\dot{\gamma} = 100$ s^{-1} for both temperatures under study ($T = 20$ and 37 °C). All the pharmacological fluids show a constant viscosity as function of the shear rate. The viscosity decreases with temperature and the most discrepant values were recorded for the Perfluorocarbons that present differences higher than 50% for a variation in temperature of 17 °C. SiOs and HSiO show differences between 30 and 35%, except Siluron 2000 which is the fluid that shows the lowest difference (21%).

Previous results (see Section 4.2) show that VH liquid phase viscosity decreases with the increase of shear rate (shear-thinning behaviour). The fact that the pharmacological fluids do not present a shear-thinning viscosity affects their flow behaviour when compared with the VH and that may be one of the reasons why those fluids cannot be used as a permanent VH substitute, since they cannot mimic properly the VH behaviour under deformation.

As mentioned in the previous section, the tendency of a substance to emulsify and

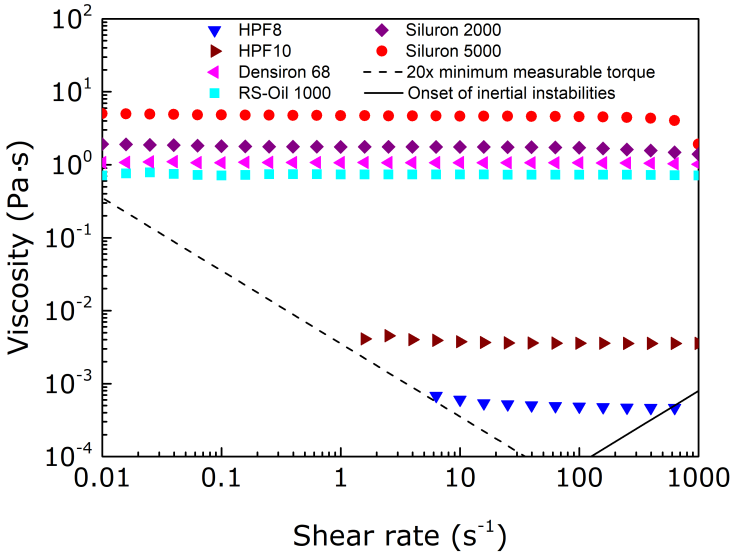

Figure 5.2. Flow curve of VH substitutes, measured at $T = 37$ °C. The minimum measurable torque was calculated with Eq. (3.19), and the onset of inertial instabilities was calculated with Eq. (3.21).

Table 5.3. Shear viscosity of the pharmacological VH substitutes measured at $T = 20$ °C and $T = 37$ °C for a constant shear rate of $\dot{\gamma} = 100$ s^{-1}.

Fluid	Viscosity (Pa s)		Difference (%)
	20 °C	37 °C	
HPF8	8.82x10^{-4}	4.85x10^{-4}	58.0
HPF10	6.04x10^{-4}	3.57x10^{-3}	51.4
Densiron 68	1.51	1.07	34.1
RS-Oil 1000	1.00	0.73	31.2
Siluron 2000	2.12	1.71	21.4
Siluron 5000	6.33	4.57	32.2

disperse into droplets over time depends on several properties, including the shear viscosity of the fluid. The less viscous a substance is, the lower the energy that is required to disperse a large bubble of the substance into small droplets [145]. However, during eye surgery fluids with a higher viscosity have the disadvantage of taking longer to be injected in the eye, and also the need of larger needles during the injection process. The SiOs viscosity is related with the average molecular weight (MW) of the molecules. Formulations with high molecular weight (HMW) will emulsify less than formulations with low molecular weight (LMW). Nevertheless, as explained in Section 2.2, it is possible to formulate mixtures of SiOs with different MW (e.g. Siluron 2000), or SiOs with other fluids (e.g. Densiron 68) that decrease the fluid's viscosity but have similar resistance to emulsification when compared with the main SiO presented in the solution. Based on that, the two SiO-based fluids with intermediate viscosities are the ones with higher acceptance nowadays in surgery: they show similar resistance to emulsification and are easier and faster to inject (and extract) in the eye during the surgical procedure than SiO with a viscosity around 5 Pa s. The SiOs and HSiO have a clinical acceptance higher than the PFLCs. In fact, nowadays the PFLCs are rarely used in eye surgery, being a choice only in extreme cases. The discrepancies in their shear viscosities when compared with the HSiO and SiOs may be one of the reasons why their residence time in the eye is so low.

5.3 SAOS experiments

All the pharmacological fluids tested were subjected to oscillatory shear experiments. Fig. 5.3 shows the storage and loss moduli measured for all the fluids under study. Additionally, Fig. 5.3a presents the baseline of the rheometer, measured with water, to illustrate the lower limit of G' that can be measured. Table 5.4 presents the storage and loss moduli values measured at a constant frequency of $\omega = 1$ rad/s. The results show that HPF8, HPF10 and Densiron 68 fluids have G' values closer to the baseline. As the values are in the same range as the ones measured with water, it seems that those fluids do not present elasticity, or the values are so low that it is not possible to measure with SAOS. Siluron 2000 and Siluron 5000 are the fluids that present a measurable G' value, but even those fluids present low G' values: for a frequency of $\omega = 1$ rad/s, Siluron 5000 shows a value of $G' = 0.027$ Pa and for Densiron 2000 $G' = 0.005$ Pa. For frequencies above $\omega = 10$ rad/s the phase angle is higher than 90°, which means that the values are not reliable and inertial effects are significant [129]. The loss modulus of the two Perfluorocarbons are the lowest of all the fluids studied and specifically for HPF8 it was not possible to measure G'' for a frequency below $\omega = 0.7$ rad/s. All the SiOs and Densiron 68 present a linear increase of the loss modulus with the increase of the frequency (unitary slope in log-log scale).

Feng *et al.* [84] tested the efficacy of a PVA hydrogel as a VH substitute. In their study, SAOS experiments were also performed with a SiO with a viscosity of 5 Pa s used as a Vitreous substitute (Oxane 5700, Bauch and Lomb, Roshester, New York). As expected, the storage and loss moduli results for the Oxane 5700 are similar to those

Table 5.4. Storage and loss moduli of the pharmacological VH substitutes for a temperature of $T = 37$ °C, and a frequency of $\omega = 1$ rad/s.

Fluid	Storage modulus (Pa)	Loss modulus (Pa)
HPF8	–	$3.6\text{x}10^{-3}$
HPF10	–	$5.8\text{x}10^{-3}$
Densiron 68	–	1.09
RS-Oil 1000	$5.6\text{x}10^{-3}$	0.71
Siluron 2000	$5.2\text{x}10^{-3}$	1.78
Siluron 5000	$2.7\text{x}10^{-2}$	4.73

presented here for the Siluron 5000 fluid. Furthermore, the authors believed that the SiO fluids studied behaved as purely viscous solutions.

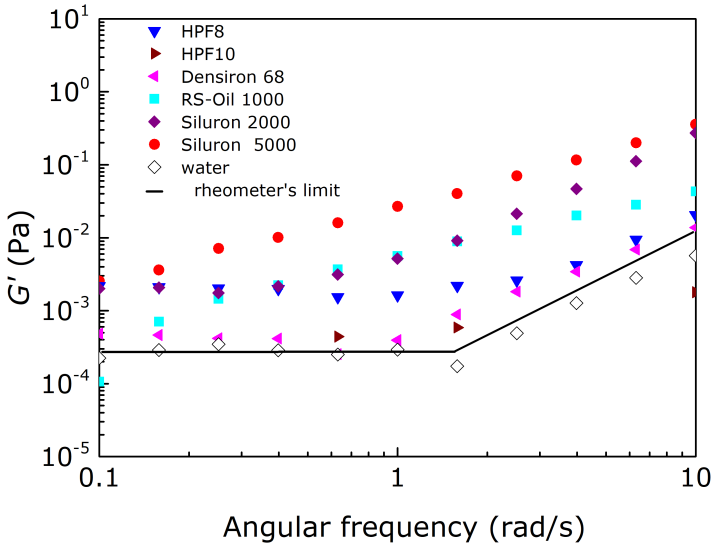

(a)

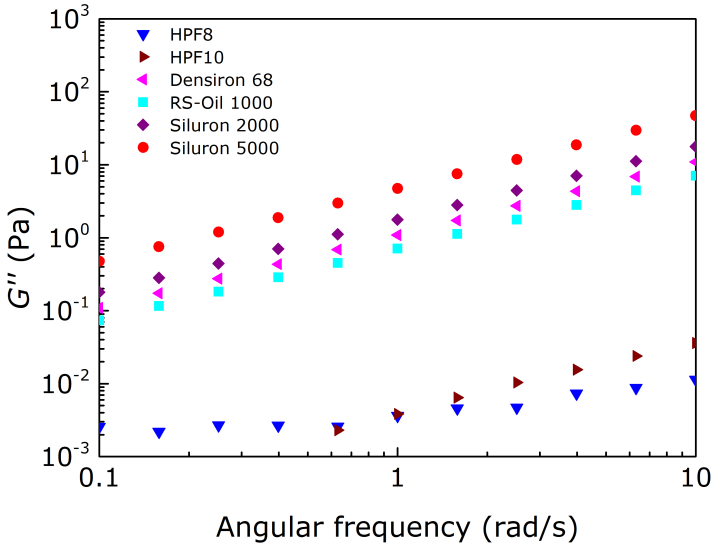

(b)

Figure 5.3. (a) Storage and (b) loss moduli of the VH substitutes plotted as a function of angular frequency. Measurements were performed at a constant strain amplitude $\gamma = 1$ % for the PFLCs or constant strain amplitude of $\gamma = 40$ % for the SiO and Densiron 68. Measurements were performed at $T = 37$ °C.

Caramoy *et al.* [58] developed new blends of SiO based on HMW chains for use as an endotamponade in vitreoretinal surgery. They measured the shear viscosity and both storage and loss moduli of Siluron 1000, Siluron 2000 and Siluron 5000. The authors measured the flow curve for shear rates between $\dot{\gamma} = 6$ and 100 s^{-1} and the results obtained for the three silicone oils are similar to the results presented here. The storage and loss moduli presented by the authors were measured with a piezoelectric axial vibrator system, and a comparison between their results and the results obtainded in this work are presented in Fig. 5.4. Note that the SiO with a viscosity around 1 Pa s measured by Caramoy *et al.* [58] is from a different pharmaceutical company than the one used in this work. However, the rheological properties are expected to be similar. They performed the G' measurements for frequencies above $\omega = 60$ rad/s, while in this work only the measurements performed for angular frequencies below about 10 rad/s are reliable. Nevertheless, when plotted together both data sets seem to follow the same trend. The G'' measurements were performed for a frequency between $\omega = 6$ and 60000 rad/s and their results increase linearly with frequency and are in agreement with the results presented in this work (see Fig. 5.4b). Caramoy *et al.* concluded that the SiO under study presented viscoelastic behaviour, with Siluron 1000 exhibiting the smallest elastic component, which could not be measured at low frequencies.

It is known that depending on the SiO MW, the fluid may or may not have elasticiy. For the SiOs used in eye surgery, it is possible to find works that assume that they are viscoelastic [58, 147] and others that consider that they behave as Newtonian fluids [84]. However, it is not possible to find in the literature works that objectively show and quantify the elasticity (or lack of it) of those fluids.

The company Fluoron, that produces most of pharmacological fluids studied here, presents the parameter linear elastic compliance J_e (see Section 3.4.1) for their SiO in the product specification table [148]. Even if this parameter is mostly used in solid mechanics, it can be obtained from SAOS experiments by the ratio G'/G''^2 when $\omega \to 0$ [149]. Table 5.5 compares the values presented by Fluoron and the values calculated based on the SAOS experiments presented here. The results are of the same order of magnitude as the ones reported by the company. The problem associated with these

measurements is the fact that even for Newtonian fluids it is possible to measure a G' value at low frequencies (due to the equipment limitations), and consequently calculate an apparent elastic compliance J_e.

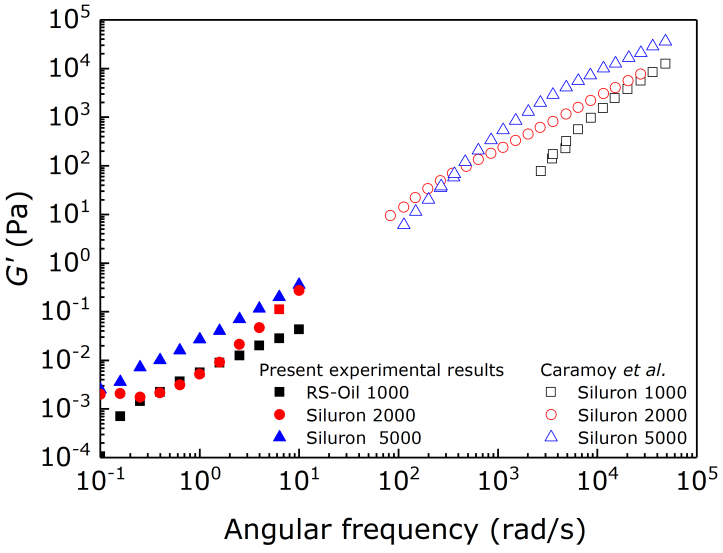

(a)

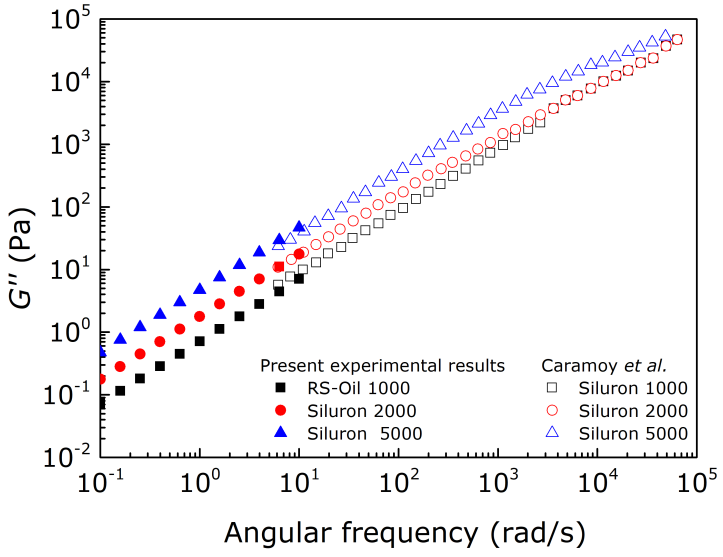

(b)

Figure 5.4. Comparison of the (a) storage and (b) loss moduli measurements performed in this work and the results presented by Caramoy *et al.* [58] for the SiO used in eye surgery.

Table 5.5. Comparison of the linear steady state elastic compliance J_e presented by Fluoron [148] and the values calculated based on the SAOS experiments presented in this work.

Fluid	Elasticity in the equilibrium compliance J_e (Pa^{-1})	
	Fluoron	Present experimental results
RS-Oil 1000	–	2.1×10^{-6}
Siluron 1000	2×10^{-5}	–
Densiron 68	–	2.0×10^{-5}
Siluron 2000	6.5×10^{-5}	5.45×10^{-5}
Siluron 5000	1×10^{-5}	2.8×10^{-5}

So far, the results presented here are inconclusive about the presence or not of elasticity in the tested pharmacological fluids. Consequently, more experiments need to be performed, ideally using other measurement techniques.

5.4 Extensional flow experiments

All the pharmacolgical fluids under study were also tested in extensional flow experiments. As explained in Section 3.5, for a Newtonian fluid the thread thins linearly in time in a CaBER-type experiment. When elastic effects become important, the dynamics of necking change significantly due to the large elastic normal stresses and the filament diameter decay with time before the breakup is nearly exponential (instead of linear), following Eq. (3.45) [110]. With the pharmacological fluids, instead of imposing a fast axial step strain to create an unstable filament (as performed with the VH liquid phase), the slow retraction method (SRM) technique was adopted. The SRM allows to investigate filament thinning of fluids with low viscosity and/or low relaxation times, applying a plate separation with a very low velocity, allowing to positioning the plates close to the critical point when a stable liquid bridge still exists [110, 112]. As explained in the methodology, a miniaturized filament breakup device was used in these extensional experiments [111].

When subjected to a plate separation with a velocity of 5 μm/s, the filaments of the PFLCs fluids breakup close to the plates (see Fig. 5.5), showing the typical behaviour of a low viscosity Newtonian fluid. Based on that, and in the results presented in the previous sections, the author concludes that the PFLCs show a Newtonian fluid

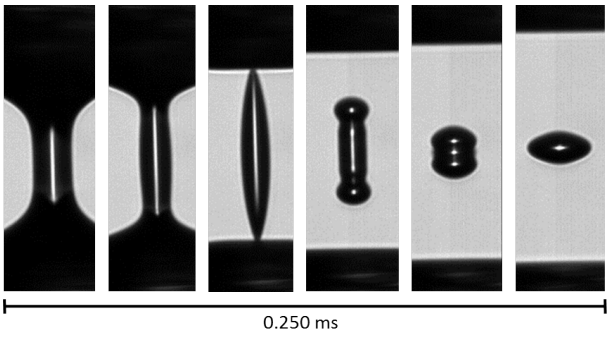

(a)

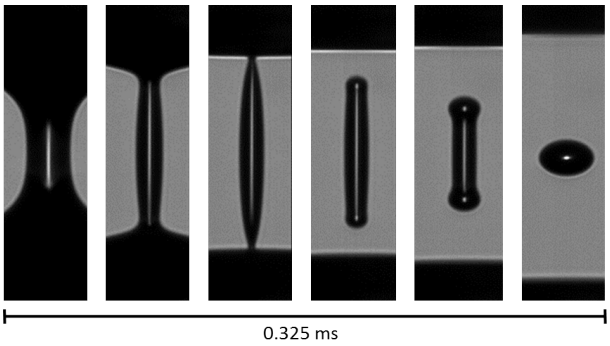

(b)

Figure 5.5. Filament thinning dynamics induced by the SRM for (a) HPF8 and (b) HPF10 fluids. All the measurements were performed at $T = 21 \pm 2$ °C, the plates were separated with a velocity of 5 μm/s and the plate diameter is D_p= 2 mm.

behaviour.

During the SRM experiments, the SiO and HSiO create a stable filament that breaks in the middle. Fig. 5.6a shows the minimum filament diameter (D_{min}/D_0) for three different experiments performed with the Siluron 2000 fluid right before the filament breakup. It is possible to observe that for a time between 40 and 20 ms before the filament breakup, the minimum filament thinning diameter (D_{min}/D_0) deviates from the linear behaviour and decays exponentially with time. Fig. 5.6b illustrates the filament thinning and breakup for some representative times, marked in Fig. 5.6a from (i) to (vi). For the time interval between 40 and 20 ms before the filament breakup, the filament diameter forms a quasi-cylindrical thread that decays exponentially with time $D(t) \propto e^{-t/3\lambda}$ [109], corresponding to the elasto-capillary thinning regime. Additionally, Fig. 5.6b shows the behaviour of the filament right before the breakup (grey box),

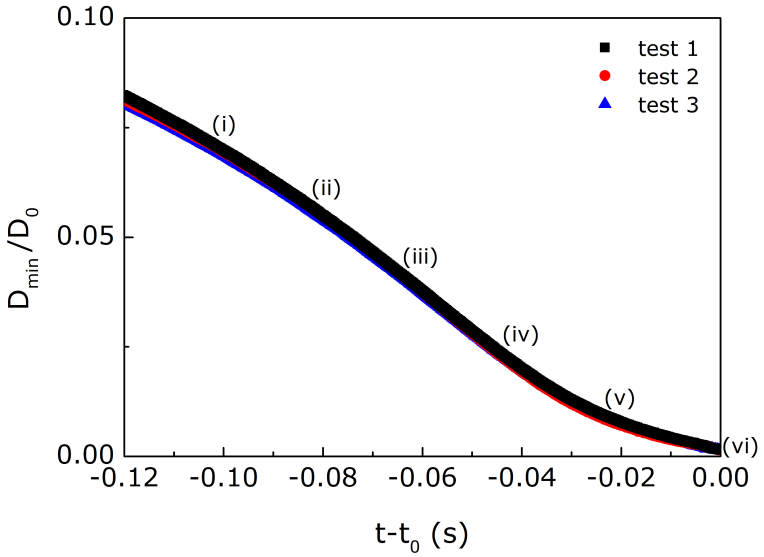

(a)

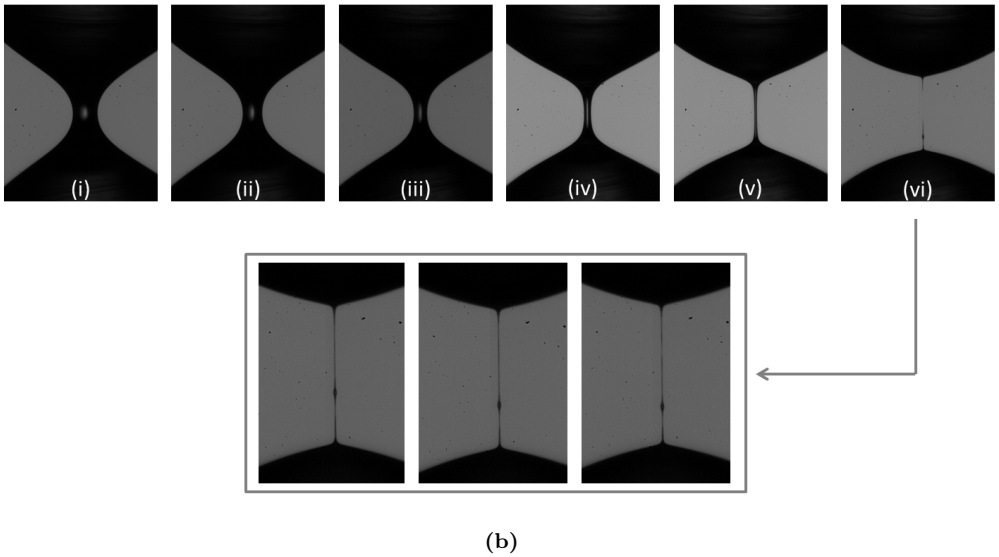

(b)

Figure 5.6. (a) Filament thinning dynamics (D_{min}/D_0) induced by the SRM for the Siluron 2000 fluid. t_0 is the time of the filament breakup. All the measurements were performed at $T = 21 \pm 2$ °C, the plates were separated with a velocity of 5 μm/s and the plate diameter is D_p= 2 mm. (b) Shape of the filament for the times marked in (a) from (i) to (vi), and an inset of the filament right before the breakup showing the formation of a bead.

where it is possible to observe the formation of a small bead along the filament. There is a general agreement that during the breakup of a filament, small beads occur only for viscoelastic fluids [150].

As explained in the begining of this section, for a Newtonian fluid the thread breaks linearly in time and according to Papageorgiou [151] the midpoint radius decreases as

$$R_{min} = 0.0709\frac{\sigma}{\eta}(t_0 - t) \tag{5.1}$$

Based on the shear viscosity and the surface tension measurements, Eq. (5.1) was tested for all SiO based fluids. A comparison between the miminum radius R_{min} of the studied fluids filament before the breakup and the theoretical behaviour predicted by the Papageorgiou solution is presented in Fig. 5.7.

Note that the Papageorgiou solution is calculated based on the shear rheology and

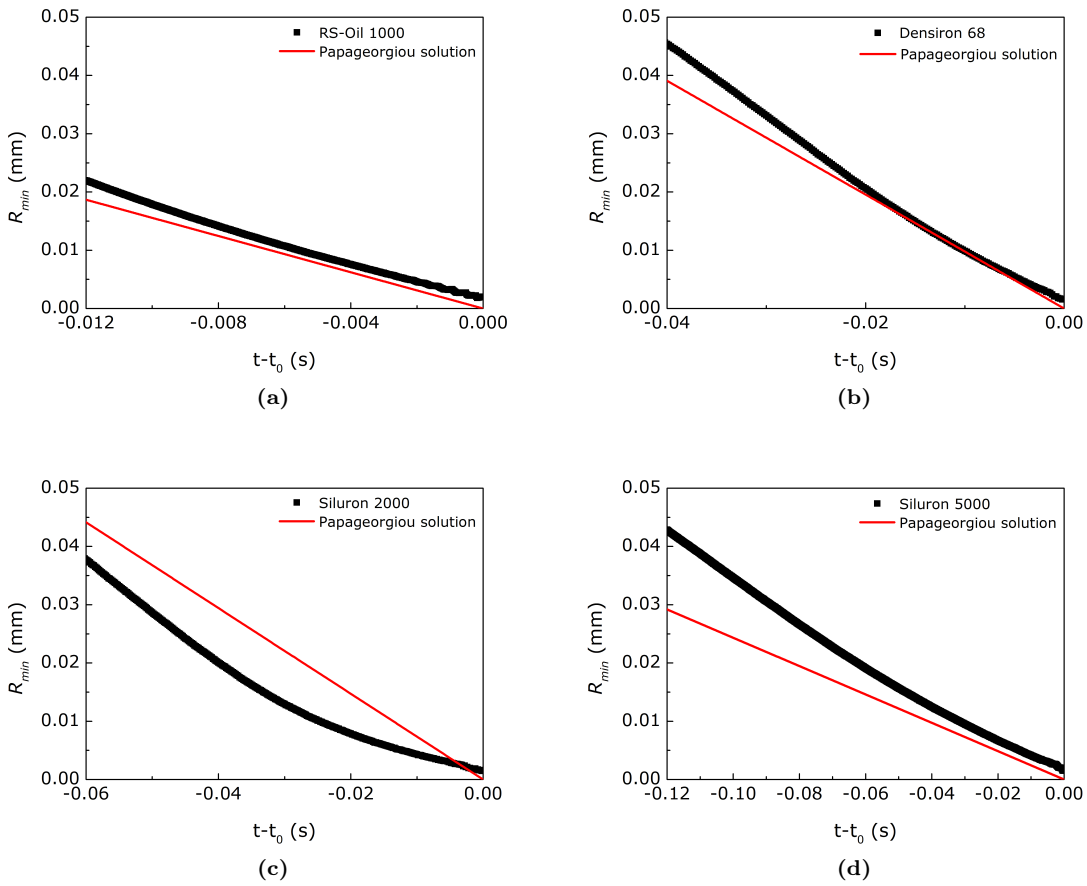

Figure 5.7. Time evolution of the minimum radius (R_{min}) close to breakup and the Papageorgiou solution for Siluron 2000 fluid. t_0 is the time of the filament breakup. All the measurements were performed at $T = 21 \pm 2$ °C, with a plate with diameter $D_p = 2$ mm and an initial gap of $D_i = 0.5$ mm.

average surface tension measurements previously presented in this chapter. As a consequence, the accuracy of the Papageorgiou solution depends on those measurements and slight differences may occur. The results presented in Fig. 5.7 show that close to the filament breakup, the diameter decay with time for the RS-Oil 1000, Densiron 68 and Siluron 5000 fluids is linear, with the same slope as the Papageorgiou solution, indicating that those fluids behave as Newtonian fluids. However, the Siluron 2000 fluid does not follow the Papageorgiou solution behaviour, and it is possible to observe a distinct slope between the experiments and the theoretical Newtonian profile. Based on the information presented in Chapter 2, of all the SiO under study Siluron 2000 is the only which includes HMW molecules in its constitution, and it seems that, even a small amount of HMW molecules is enough to give elasticity to the fluid. This fluid shows elastic behaviour and it is possible to calculate an extensional relaxation time. Fig. 5.8 shows the evolution of the minimum filament thinning diameter (D_{min}/D_0) close to breakup, and the exponential fit performed with Siluron 2000 fluid. Note that just one case is shown here. However, experiments were repeated three times to assess repeatibility, and the average relaxation time obtained was 6.8 ms with a standard deviation of 0.2 ms.

To the best of the author knowledge, there is only one study available that performed extensional measurements with SiO fluids used in eye surgery. Day *et al.* [61] used a CaBER device for testing a SiO with a viscosity of 1 Pa s plus the same fluid with different additions of a HMW SiO (1%, 5%, 10%, 15% and 20%). They concluded that the mid-filament diameter of all the fluids tested decayed linearly with time, as expected for a Newtonian fluid. Additionally, on a study with the goal to demostrate how to correctly analyse extensional measurements for Newtonian fluids, McKinley and Tripathi [152] tested a SiO with a higher shear viscosity ($\eta = 10.5$ Pa s) than the SiOs tested here and showed that for the last stages of the filament breakup, the SiO also followed the Papageorgiou solution.

This study shows, based on extensional rheological experiments, that all pharmacological fluids under study, except Siluron 2000, behave as Newtonian fluids. Siluron 2000 fluid behaves as a Boger fluid, as it presents a constant shear viscosity but also a

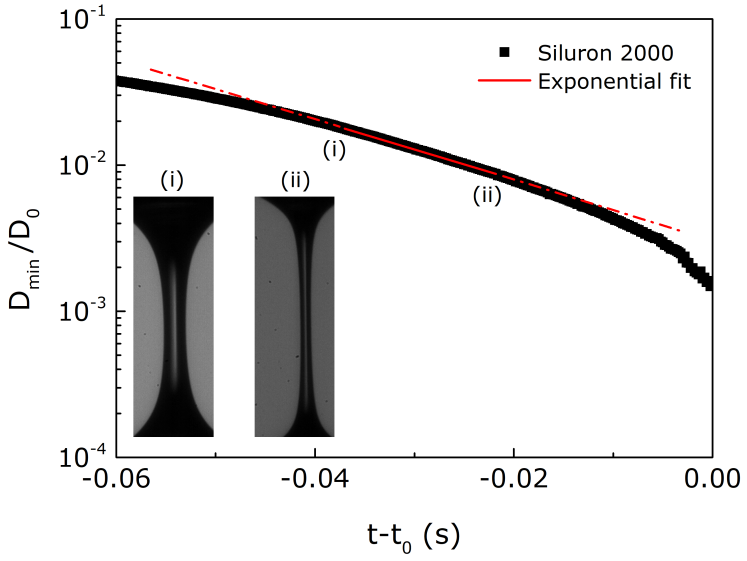

Figure 5.8. Time evolution of the minimum filament diameter (D_{min}/D_0) close to breakup and the exponential fit used to calculate the extensional relaxation time λ for Siluron 2000 fluid. t_0 is the time of the filament breakup. (i) and (ii) represent the first and last points, respectively, used in the exponential fit and the shape of the filament is shown for those two times. The measurement was performed at $T = 21 \pm 2$ °C, with a plate with diameter $D_p = 2$ mm and an initial gap of $D_i = 0.5$ mm.

measurable elastic component, more specifically with an extensional relaxation time of $\lambda = 6.8$ ms.

5.5 Microfluidics

The extensional measurements presented in the previous section showed that the Siluron 2000 fluid has a low elastic behaviour, and all the other SiO behave as Newtonian fluids. Based on the knowledge that the small length-scales used in microfluidic devices allow to access a wide range of deformation rates and consequently viscoelastic effects can be enhanced in fluids that would behave essentially as Newtonian fluids in macroscale flows, a set of microfluidic experiments were performed with the Siluron 2000, Densiron 68 and Siluron 5000 fluids. The goal of the microfluidic experiments was to access if there is formation of corner vortices in the upstream channel as a consequence of the elasticity of the fluid, as typically observed in contraction flows of polymer solutions above a critical Wi, and also check if there is formation of corner vortices in the downstream channel

due to inertial effects for Newtonian fluids [153, 154].

A contration-expansion geometry with a contraction ratio $CR = 7.8$ was used in the microfluidic experiments. The flow field visualised for the Siluron 2000 fluid is presented in Fig. 5.9. The fluid Siluron 2000 reached a maximum flow rate of $Q = 80$ μl/min, corresponding to a Reynolds number of Re $= 0.006$ and a Deborah number of De $=$ 62.2. During the experiments, with the increase of the flow rate the metallic tips from where the fluid was injected into the microchannels suffered lubrication and it was not possible to keep them attached to the entrance of the channels. Also, increasing the flow rate above a certain value leads to structural problems of the PDMS microchannels. Therefore, the flow rate presented here is the maximum flow rate that was possible to reach without having lubrication or pressure problems. The experimental results show that for the Siluron 2000 fluid no vortices were generated in the corners at the upstream channels, and the flow is symmetric (or reversible) which is characteristic of creeping flows of Newtonian fluids.

Fig. 5.10 presents flow fields observed with Densiron 68 and Siluron 5000 fluids. The fluid Densiron 68 reached a maximum flow rate of $Q = 80$ μl/min, corresponding to a Reynolds number of Re $= 0.009$, while the Siluron 5000 fluid reached a maximum flow rate of $Q = 40$ μl/min, corresponding to a Reynolds number of Re $= 0.001$. Similarly to what happened with Siluron 2000 fluid, the flow rates presented here were the maximum

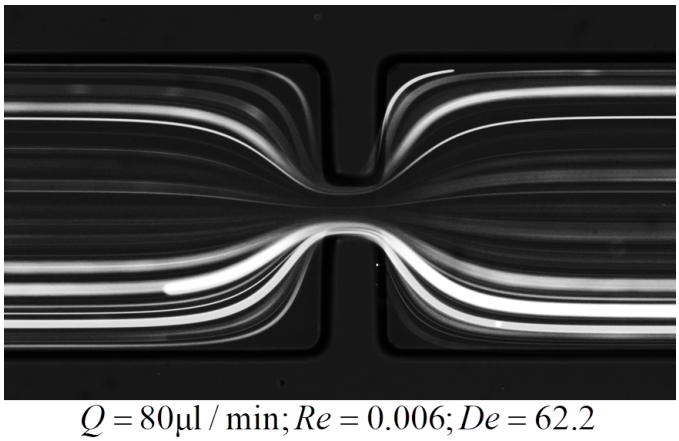

Figure 5.9. Flow patterns observed with the Siluron 2000 fluid. The flow direction is from left to right. The experiments were performed at temperature $T = 24 \pm 1$ °C.

reached without having lubrication problems. Results show that none of fluids generated vortices in the corners of the downstream channel, and again a symmetric flow field is observed, without differences in the upstream and downstream regions.

It was not possible to find in the literature studies in microfluidic contraction-expansion geometries for fluids with such high viscosities and a low relaxation time (corresponding to a very dilute Boger fluid) as in the fluids studied in this work. Fluids with viscosities as high as the ones presented in this work are not common in microfluidics, as it is not easy to apply high flow rates without damaging the structural integrity of the deformable PDMS microchannels [154, 155]. Nevertheless, several studies show the formation of upstream vortices, with viscoelastic dilute solutions, for Deborah num-

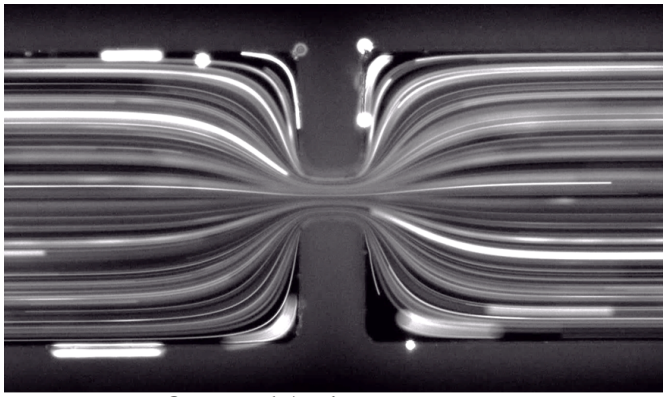

$Q = 80\mu l / \min; Re = 0.009$

(a)

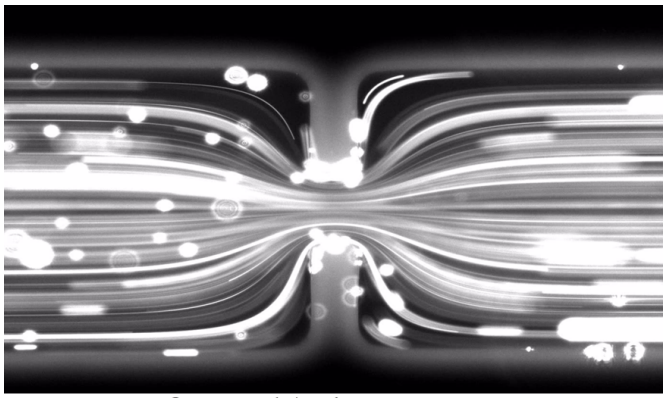

$Q = 40\mu l / \min; Re = 0.001$

(b)

Figure 5.10. Flow patterns observed with (a) the Densiron 68 and (b) the Siluron 5000 fluids. The flow direction is from left to right. The experiments were performed at temperature $T = 21.5 \pm 1$ °C.

ber lower than the one reached here, and the formation of downstream vortices, with Newtonian solutions, for Reynolds numbers significantly higher than the ones reached in this study. Sousa *et al.* [153] studied the flow of two polymeric solutions, polyacrylamide (PAA) and xanthan gum, through microfluidic channels containing both hyperbolic and abrupt contractions-expansions. The viscoelastic fluids studied showed a shear-thinning behaviour and viscosities around 0.2 Pa s for a shear rate of 0.1 s^{-1} and 0.003 Pa s for a shear rate of 1000 s^{-1}. The PAA solution had a relaxation time of $\lambda = 38$ ms and for xanthan gum the relaxation time was $\lambda = 3.8$ ms. For the abrupt contraction, at a Deborah number of 1.19, both fluids show an upstream vortex, formed as consequence of the elasticity of the fluid. They also performed flow visualisations with de-ionised water flowing through an abrupt expansion, and downstream recirculations were observed for Reynolds numbers higher than Re = 53.8. Campo Deano *et al.* [154] developed low viscosity Boger fluids and assessed their elasticity analysing the flow through a microfluidic hyperbolic contraction. Different PAA aqueous solution with 1% of sodium chloride (NaCl) were tested, and their shear viscosities varied between aproximately 0.004 and 0.001 Pa s. For the more viscous solution, which had a relaxation time of 29 ms, recirculations were observed for a De = 4.57 and above. In their study, it is shown that increasing the viscosity of the solution also increased the value of the Deborah number required to generate the onset of corner vortices. The authors also performed flow visualisations with a Newtonian fluid (de-ionised water) and downstream lip vortices were observed for Reynolds numbers above Re = 30.

Based on the available information from the literature, the author of this work believes that the flow rates and consequently the Reynolds numbers reached with Densiron 68 and Siluron 5000 fluids are too low to observe the onset of inertial effects. Likewise, for Siluron 2000 fluid, higher flow rates are needed to be achieved in order to observe the onset of elastic effects of this low elasticity fluid.

5.6 Conclusions

Vitreous humour is a key component for the proper operation of the eye. This biofluid presents viscoelastic behaviour (as demonstrated in Chapter 4) that plays an important role during rapid eye movements. For the treatment of some eye diseases, the injection of a vitreous substitute in the vitreous cavity is often necessary. We studied the rheological properties of typical substitute fluids as well as the interaction of those fluids with VH collected from rabbit eyes. The surface tension of all the fluids are below 22.0 mN/m. The highest value was measured with Siluron 2000 ($\sigma = 22$ mN/m) and the lowest with HPF8 ($\sigma = 15.6$ mN/m). The average interfacial tension values for the VH substitutes in contact with VH are between 28.3 mN/m for Siluron 2000 and 34.0 mN/m for HPF8.

All the pharmacological fluids investigated show a constant viscosity in shear flow, and the viscosities of the fluids varies between 4.85×10^{-4} Pa s for HPF8 and 4.57 Pa s for Siluron 5000 at $T = 37$ °C. The PFLCs are the fluids with lower viscosities. SAOS experiments showed that the loss modulus of the SiO-based fluids increase linearly with frequency. Furthermore, for HPF8, HPF10, RSOil 1000 and Densiron 68 fluids the storage modulus is close to the rheometer sensitivity limit, leading to inconclusive results regarding whether or not they present elasticity.

The extensional experiments show that from all the pharmacological fluids under study, Siluron 2000 is the only fluid that presents viscoelastic behaviour, with an average extensional relaxation time of 6.8 ms.

Finally, the microfluidic experiments were unable to corroborate the extensional experiments. However, due to experimental setup limitations, it is believed that the flow rates necessary to start observing the onset of elastic effects for Siluron 2000 or the onset of inertial effects of the Newtonian fluids were not reached.

Recent studies have attempted to create new VH substitutes, such as polymeric solutions and hydrogels (see Section 2.3), that in addition to be biocompatible also present viscoelastic behaviour. The fact that the pharmacological fluids studied here present a Newtonian behaviour, or a very low viscoelastic behaviour, can be one of the causes why they cannot be used as a permanent VH substitute and cannot mimic

adequately the complex rheological properties of VH and consequently its behaviour during fast eye movements.

"Everything flows and nothing stays."

Homer

Chapter 6

Flow dynamics of VH during saccadic eye movements

This chapter describes saccadic eye movements, the most common movements of the eye. A literature review is also presented, discussing experimental and numerical work related with the flow behaviour of VH and other fluids in the eye during saccadic movements. The need for new computacional fluid dynamics (CFD) studies that can resemble more accurately the flow dynamics of VH in the eye is also discussed.

6.1 Saccadic movements

The human eye has one of the fastest muscles in the body, being able to produce rotations of 40 degrees in approximately 100 ms [2]. In the different situations of daily life, the eyes are able to produce different, voluntary or involuntary, movements with distinct anatomy and physiology. How those movements affect the dynamics of the eye, especially the VH flow dynamics, is not yet fully understood. Many of the eye's diseases are directly or indirectly associated with the morphological changes of this biofluid with age, and consequent changes in its flow behaviour: based on Repetto *et al.* [156], medical literature suggests that retinal detachment (RD) occurrence and progression is

largely related to mechanical phenomena. In particular, the shear stress exerted by the vitreous (or by tamponade fluids in vitrectomised eyes) on the retina is thought to be an important factor in inducing RD [157]. So far, several experimental and numerical studies have been performed with the aim of understanding the flow dynamics of VH, as well as to study the effect of the movements of the eye in the VH flow behaviour. However, more research in the area that can lead to a better understanding of the VH flow behaviour is crucial to help in the development of new health solutions.

In order to study the flow dynamics in the eye, it is important to fully understand and be able to characterise the eye movements. It is accepted that healthy eye movements can be classified in four types [158]:

- vestibulo-ocular movements;
- vergence movements;
- smooth pursuit movements;
- saccadic movements.

The vestibulo-ocular movements are involuntary movements produced as a consequence of changes in the head position, in order to allow the eyes to remain in focus on a specific target when the head moves. The disjuntive movements of the eye (both convergence or divergence) that point the fovea of both eyes to a specific target, which can be located at different distances from the observer, are called vergence movements. Smooth pursuit movements are the movements produced by the eyes when following a moving object, and are considered slow movements (angular velocity below $100°/s$) [158, 159]. However, the majority of the eye movements are not smooth, happening instead in saccades [159]. The saccades are very quick and ballistic movements produced by both eyes simultaneously and in the same direction when fixating an object [160, 161]. In fact, the eyes are never completely at rest, because they are constantly producing saccades. These movements are the fastest and the most common type of eye movements [159]. According to Sparks [162] the saccadic movements are the most studied of the oculomotor subsystem.

The parameters usually employed in the analysis of saccadic movements are latency, the angular and peak velocity, amplitude and duration, as shown in Fig. 6.1. Latency is the time taken from the appearance of the target to the beginning of the saccade in response to that target; amplitude is given in terms of the angle of the eye movement during the saccade, usually measured in degrees; peak velocity corresponds to the highest velocity achieved during the saccadic movement; and duration is the time taken to complete the saccadic movement, wich is most easily measured from the velocity profile. Note that the trajectory and velocity of saccades cannot be voluntarily altered.

Studies regarding the movements of the eye can be found in the literature since the beginning of the 20th century, as for example the work published in 1901 from Dogde and Cline entitled *"The angle of velocity of eye movements"* [163], where the authors developed a device to record photographies of the eye movements. However, an increase of studies in the area started in the 1950's (as for example [164, 165]). More recent studies characterising and predicting the magnitude of saccadic movements have been

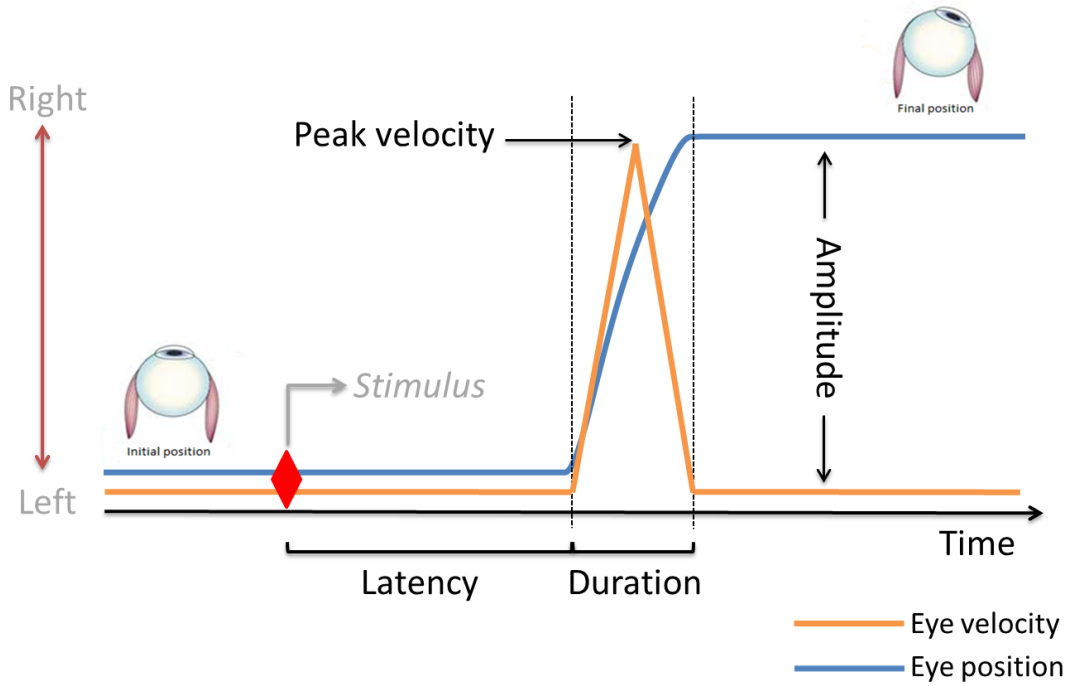

Figure 6.1. Schematic representation of the eye response to a stimulus: to reach a new position, and after a latency period, the eye acquires a velocity in order to perform a movement with a specific amplitude.

published [166–172]. Even if sacaddic movements are involuntary and, as a consequence, for the same amplitude its duration and velocity vary (even for the same person), it is possible to recognise a pattern for these movements [173].

In 1988, Collewijn *et al.* [167] measured the horizontal saccades of 4 individuals with perfect visual acuity. The authors were able to measure saccades from 5 to 80°, and they observed that the acceleration and the peak velocity increased until an amplitude up to 40°, but larger amplitudes had mostly the same peak velocity and were reached by an extension of the deceleration phase. The saccadic movements had a duration between around 50 ms (for 10° saccade) and 300 ms (for a 80° saccade). Saccades up to 30° were mostly symmetrical, with identical acceleration and deceleration times, whereas saccades with amplitudes higher than 30° showed a longer deceleration time, and consequently exhibited an asymmetric profile. Wilson *et al.* [168] measured saccades from 122 normal volunteers of different ages, performed at different times of the day. Measurements were performed for saccades of 15°, 25° and 35°. The average peak velocity of the three amplitudes of movement were 322°/s, 445°/s, and 507°/s, respectively. Interestingly, this study also showed that the peak velocity of the same amplitude of movement decreases with age.

Geest and Frens [171] measured the sacaddes produced by 4 individuals, with the goal of comparing two different recording methods. They recorded the amplitude, duration and peak velocity of the saccades. An example of the peak velocity and duration as a function of the amplitude of the movement for the left eye of one of the individuals tested is shown in Fig. 6.2. The results showed that a saccadic movement with an amplitude of 10° had a duration of $\sim$ 50 s and a peak velocity between 200 and 400°/s, and a 40° saccade had a peak velocity close to 500°/s for a duration of $\sim$ 130 ms.

More recently, Issen and Knill [174] performed a study based on the fact that when catching an object, the eyes perform saccades to fix the object before the hands begin to move. Eleven participants with normal visual acuity were subjected to the experiment. Two stimulus conditions were tested: approximately 14.5° of movement and approximately 28° of movement. The results showed that the saccades took around 40 ms to perform the 14.5° of movement with an average velocity close to 300°/s, and around

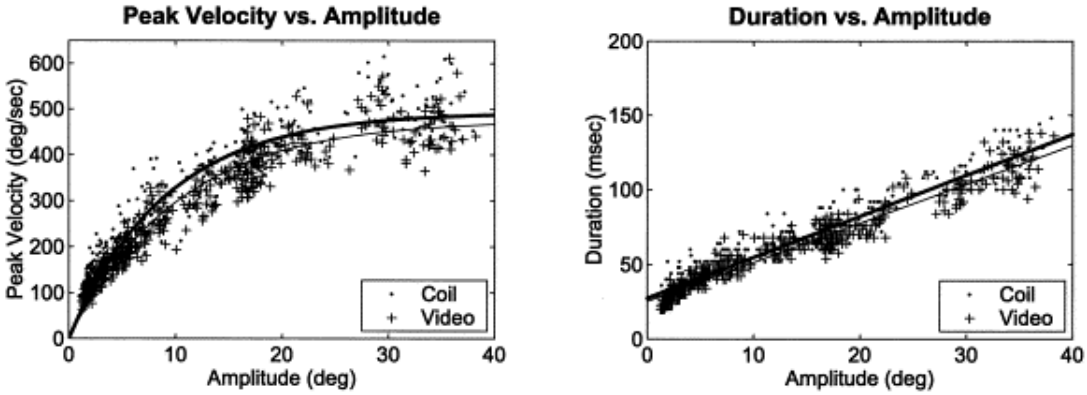

Figure 6.2. An example of the peak velocity and duration as a function of the amplitude of saccadic movements obtained with two different recording methods. Each point represents one saccade. (reprinted from [171] with permission from Elsevier).

80 ms to perform 28° of movement, reaching a peak velocity around 400°/s.

Other different values for peak velocity, amplitude and duration of saccades can be found in the literature. For example, Sparks [162] states that saccadic movements can have peak velocities between 400 and 800°/s, and Collewijn *et al.* [167] reports peak velocities as high as 900°/s for a 15° displacement. Nevertheless, there is an agreement among the different studies about the main characteristics of saccadic movements: the movements have commonly an amplitude between 10 and 50° (larger saccades are associated with head movements); the peak velocities are usually between 200 and 600°/s, and even large saccades do not last much longer than 100 ms, which is the time for the visual system to process the information [173]; there is a relationship between amplitude, velocity and duration of the movement; small saccades show a symmetric velocity profile over time, whereas larger saccades have a deceleration time higher than the acceleration time; for smaller saccades, the peak velocity of a saccade increases with the increase of the magnitude of the saccade, but for larger saccades when increasing the degree of movement, the peak velocity remains mostly the same. Based on this knowledge, it is possible to mathematically reproduce the typical saccadic movements to use in both numerical and experimental research.

6.2 Flow dynamics of vitreos humour

The numerical and experimental study of the VH flow dynamics and fluids used in eye surgery during saccadic eye movements have been under special attention since the end of the 1990's [175]. In this section, the most relevant analytical, numerical and experimental research works developed in the area are described, and in Table 6.1 a summary with the key points of those studies is presented.

In 2005, Repetto *et al.* [176] presented an experimental study of the VH motion induced by saccadic eye movements. A model of the vitreous cavity consisting of a simple spherical cavity carved in a perspex cylindrical container was used. Instead of the real vitreous cavity dimensions (radius of ~ 12 mm), the model had more than the double of the average eye diameter and was able to rotate with a prescribed time law that reproduced real saccadic eye movements (the prescribed time law will be described in Chapter 7). The spherical cavity was filled with a Newtonian fluid, glycerol, and the flow field was measured with the particle image velocimetry (PIV) technique. The authors found that the maximum value of the wall shear stress (WSS), which is thought to play an important role in the pathogenesis of retinal detachment, does not significantly depend on the amplitude of the saccadic movements. This finding suggested that as small eye rotations are more common than large movements, the former are the main responsible for vitreous stresses on the retina. Another important finding from this study was that the maximum WSS increases with the fluid viscosity, leading the authors to conclude that from a mechanical point of view, in order to minimize the shear stresses on the retina, low viscosity tamponade fluids should be adopted after vitrectomy. This study was a start point to try to understand the flow patterns during saccadic movements; however, considering the eye as a perfect sphere and VH as a Newtonian fluid may lead to significant differences in the resulting shear stresses and consequently biased conclusions.

Table 6.1. Summary of relevant numerical, analytical and experimental studies performed regarding the flow dynamics of VH.

Reference	Type	Geometry	Fluid rheology	Movement
Repetto *et al.* 2005 [176]	Experimental	Sphere ($R = 40.8$ mm)	Newtonian	Saccades
Repetto *et al.* 2006 [156]	Analytical	Weakly deformed sphere	Newtonian	Saccades
Stocchino *et al.* 2007 [157]	Experimental	Weakly deformed sphere ($R = 40.8$ mm)	Newtonian	Sinusoidal
Repetto *et al.* 2010 [177]	Analytical	Weakly deformed sphere	Newtonian	Sinusoidal
Stocchino *et al.* 2010 [178]	Experimental	Weakly deformed spheres ($R = 40.8$ mm)	Newtonian	Sinusoidal
Repetto *et al.* 2011 [179]	CFD (Comsol Multiphysics®)	2D sphere ($R = 12$ mm)	Newtonian and viscoelastic model based on data from [10, 21]	Saccades
Meskauskas *et al.* 2011 [23]	CFD	Sphere	Newtonian and viscoelastic models based on data from [10, 19, 21]	Sinusoidal
Balachandran and Barocas 2011 [180]	CFD	Simplified eye geometry (see Fig. 6.4)	Newtonian	Sinusoidal
Meskauskas *et al.* 2012 [24]	CFD	Sphere and different ellipsoids with an indentation	Newtonian and viscoelastic models based on data from [10, 19, 21]	Sinusoidal
Abouali *et al.* 2012 [25]	CFD (Fluent®)	Simplified eye geometry ($R = 12$ mm)	Newtonian	Saccades
Isakova *et al.* 2014 [181]	Analytical	Sphere	Newtonian and viscoelastic model based on data from [21]	Sinusoidal
Modarreszadeh and Abouali 2014 [26]	CFD (OpenFOAM®)	Simplified eye geometry ($R = 12$ mm)	Viscoelastic model based on data from [10]	Sinusoidal
Bonfiglio *et al.* 2015 [182]	Experimental	Sphere ($R = 12.5$ mm)	Viscoelastic model	Sacaddes

Repetto *et al.* [156,177] and Stocchino *et al.* [157,178] performed analytical and experimental studies, respectively, of the dynamics of the VH induced by saccadic movements. The eye models were created based in the same assumptions as in [176], but to try to resemble the real vitreous chamber an improved non-spherical shape was considered (see Fig. 6.3). In the studies performed by Stocchino *et al.* [157,178], different ratios of concavity were tested, and sinusoidal oscillations with different amplitudes were studied. In all the cases, VH was assumed to be a Newtonian incompressible fluid. Their results showed that the non-spherical shape of the cavity generates flow fields and stresses on the boundary significantly different with respect to the case of motion within a sphere, and vortices were formed in the area of the lenses indentation, which the authors believed might play a role in the generation of retinal detachments. In addition, in [157] the authors found a strong shear stress concentration in the region close to the lens that may be related to the larger velocities reached by the fluid in that region due to the concavity of the wall.

Balachandran and Barocas [180] used the finite element model (FEM) to simulate drug dispersion in the vitreous cavity. Their goal was to study the effect of vitreous sloshing during the insertion of drugs in the eye, the effect of drug retention in the VH and the effect of the concentration of transcleral and intra-vitreal drug sources for

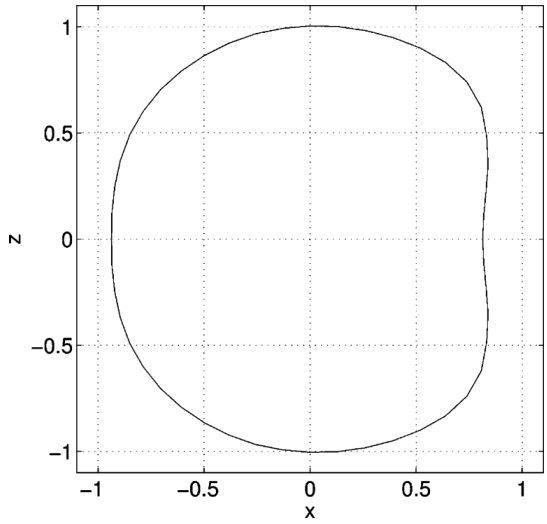

Figure 6.3. Eye model used in the study of Repetto *et al.* [156] (reprinted from [156] with permission from Springer).

different degrees of vitreous liquefaction. They used a simplified eye geometry (see Fig. 6.4) but despite recognising that liquefied VH probably exhibits a non-Newtonian behaviour, the authors simulated the liquefied vitreous as a Newtonian fluid. Moreover, the saccades were simulated as a simple sinusoidal movement. Their results showed that the transport of drugs in the vitreous cavity is significantly different if the eye is moving when compared with a static eye. The authors also found that increasing the fluid viscosity has an impact in the drug distribution as it takes longer for the drug to spread into the cavity. The model can be used as a predictive tool for drug delivery systems, even though the authors believe that to increase the accuracy of the model the simplifications assumed need to be overcomed.

Abouali *et al.* [25] published a study where saccadic movements with amplitudes from 10 to 50° were analysed. The saccadic movements were simulated as in [176]. The eye model had the size of the real human eye, with a radius of 12 mm and with different degrees of indentation resembling the lenses shape in the anterior part of the eye. The governing equations with no-slip boundary conditions were solved using FLUENT® 6.2.13 CFD solver package. Three different Newtonian fluids were studied: water, glycerol and a silicone oil, with kinematic viscosities of 10^{-6}, 5×10^{-4}, 10^{-3} m^2/s, and densities of 998.2, 1260 and 970 kg/m^3, respectively. The authors found that the

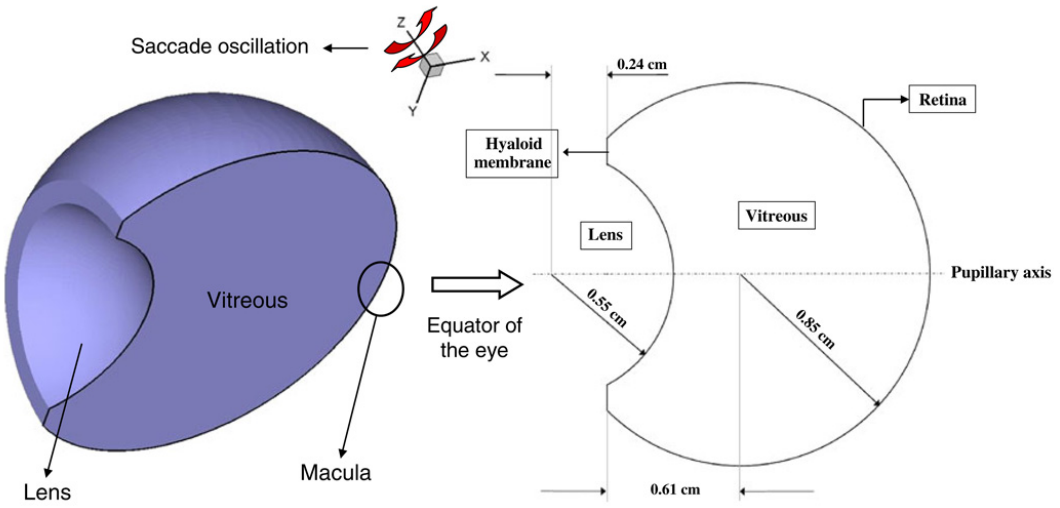

Figure 6.4. Representation of the simplified eye geometry used by Balachandran and Barocas (reprinted from [180] with permission from Springer).

maximum WSS depends on the density of the liquid, rotation amplitude, kinematic viscosity, angular frequency and radius of the sphere, although differently with different parameters. Interestingly, it was observed that the WSS of a more viscous fluid can be lower than for a fluid with lower viscosity due to its higher density: results showed the WSS for glycerol is slightly higher than for a more viscous liquid such as silicone oil (see Fig. 6.5). Results also showed that the change in the lens indentation did not change significantly the WSS values on the cavity wall.

All the studies previously described actively helped to understand the flow dynamics of the biofluid during saccadic eye movements, and/or provided an insight on understanding the importance of considering the lenses indentation. However, all of those works were performed using Newtonian fluids. As showed in Chapter 4, both VH

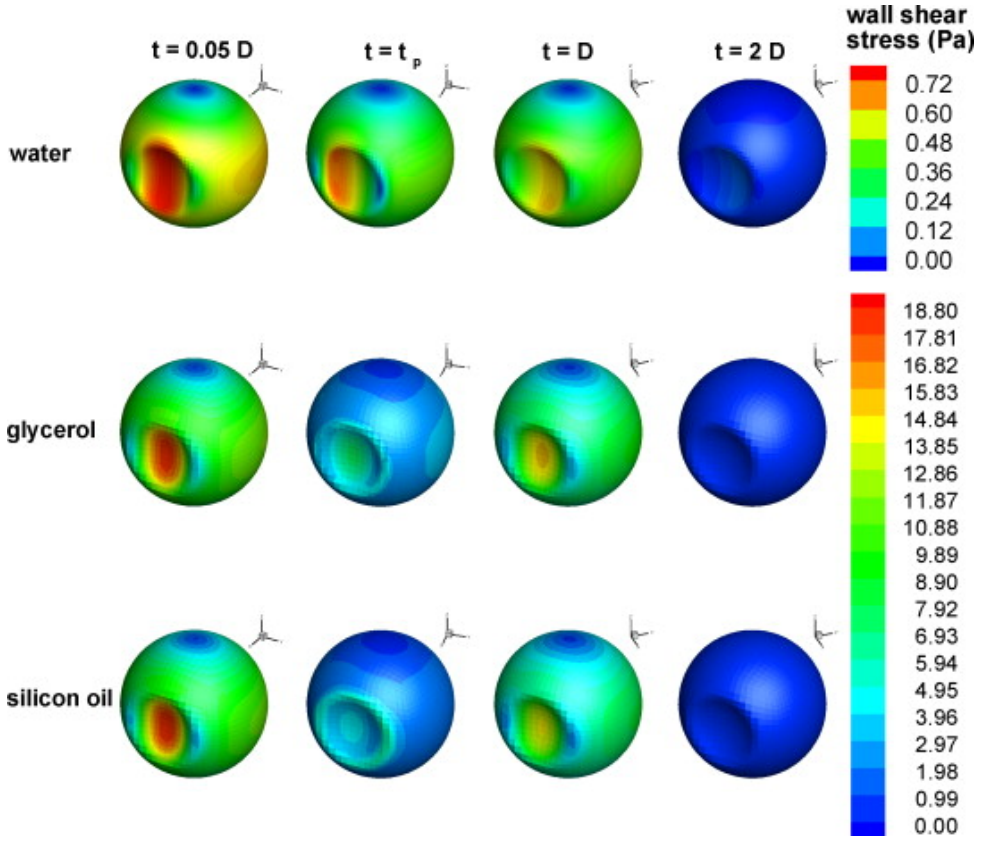

Figure 6.5. Wall shear stress (WSS) contours on the vitreous chamber, for a displacement of 50° at different times of the movement, for the three different fluids under study (reprinted from [25] with permission from Elsevier).

phases exhibit viscoelastic rheological behaviour. Therefore, assuming that the biofluid has a Newtonian behaviour can lead to significant differences in the flow behaviour, as a Newtonian fluid does not show the same complexity as a viscoelastic fluid.

In 2011, the first studies about eye movements considering fluids with viscoelastic properties were published [23, 179]. Taking into account that posterior vitreous detachment (PVD) is a common condition in elderly people, and the traction exerted by the detached vitreous on the retina may result in retinal tears and detachments, Repetto *et al.* [179] tried to estimate the magnitude of those tractions using the software Comsol Multiphysics®. The saccadic movements were based in the mathematical model presented in [176]. The vitreous chamber was split into two regions, one occupied by the detached vitreous, modelled as an elastic viscous solid, and the other occupied by the liquefied vitreous, modelled as a Newtonian fluid. The viscoelastic properties of VH were based in the works of Nickerson *et al.* [10] and Swindle *et al.* [34]. Numerical simulations were performed on a 2D rigid sphere. Twelve different configurations of the interface were tested and the results showed that the generated tractions between the fluid and the retina may be of the same order of magnitude as the adhesive force between the retina and the pigment epithelium. Therefore, the model gives a physical explanation for the hypothesis that saccadic movements, in the presence of PVD, could be responsible for high tractions on the retina. Despite all the simplifications, the model gave some insight on the dynamics of the detached vitreous and suggested that the problem was worth attention from a mechanical point of view.

In 2011, Meskauskas *et al.* [23] tried to understand how the mechanical properties of VH can affect the stresses exerted on the retina during eye rotations. VH was modelled as a viscoelastic fluid and different viscoelastic models were studied: three based on the experimental data measured by Nickerson *et al.* [10] and Swindle *et al.* [21], and one based on the experimental data measured by Lee [19]. The vitreous chamber was modeled as a sphere. Their results showed that the maximum velocity inside the eye cavity can be twice the maximum wall velocity, and that resonance effects related with the viscoelasticity of the fluids generate larger wall shear stresses, and could be relevant for the occurrence of retinal detachment. Those results were later corroborated by

Isakova *et al.* [181], that using an analytical approach obtained the same trend of results, and also by Bonfiglio *et al.* [182] that based on an experimental study also obtained similar results. In 2012, Meskauskas *et al.* [24] used the same model as in [23] to study the retinal detachment in myopic eyes: since the shape of myopic eyes is different from healthy eyes, different conformations of an ellipsoid eye shape were studied. The results showed that the VH and the retina in highly myopic eyes are continuously subjected to significantly larger shear stresses when compared with emmetropic eyes.

Modarreszadeh and Abouali [26] also studied the eye movements, with the same geometry presented by Abouali *et al.* [25], but this time using a viscoelastic fluid model subjected to sinusoidal oscillations. The opensource software OpenFOAM® was used and the viscoelastic solver developed by Favero *et al.* [183] was adapted to handle dynamic meshes. To model the viscoelastic behaviour of VH, a 2-mode Giesekus model was chosen, based on the experimental rheological measurements performed by Nickerson *et al.* [10]. The paper focused in providing a reliable numerical procedure for the study of VH under oscillatory movements, and only a few results are presented. Still, preliminary results showed that for a simplified eye globe rotating at 10 rad/s with an amplitude of 3%, the WSS is 10 times higher for the viscoelastic model resembling the VH properties when compared with the cavity filled with the liquefied vitreous simulated as a Newtonian fluid.

As discussed before, Repetto *et al.* and Stocchino *et al.* [156, 157, 177, 178] showed that, in the case of a Newtonian fluid, a weak departure of the domain from the spherical shape significantly affects the fluid motion. However, in most of the studies performed with viscoelastic fluids, and described here, for simplicity the authors considered the eye as a sphere. The author of this work believes that using a sphere to model the vitreous chamber while simulating viscoelastic fluids will also produce significant differences in the flow patterns.

In summary, over the years several studies regarding VH flow behaviour have been performed using numerical, analytical, or experimental approaches. However, most of those works dismiss at least one crucial point: the ones that consider the lens indentation in the vitreous chamber modelled VH as a Newtonian fluid (expect Modarreszadeh and

Abouali [26]), and those that consider VH as a viscoelastic fluid consider the vitreous chamber as a sphere; the experiments that took into account the indentation, ended up using simplified deformed spheres that do not accurately resemble the vitreous chamber shape; and some works use sinusoidal movements instead of proper saccades, which is not an accurate approximation. Therefore, a proper CFD study using adequate viscoelastic rheological models that are able to model the VH behaviour and the properties of the fluids used in eye surgery, using geometries that take into account the real shape of the vitreous chamber and real saccade profiles, will give a better insight about the flow dynamics of those biofluids during saccadic eye movements.

"All models are wrong, but some models are useful."

G. P. E. Box

Chapter 7

Numerical method

This chapter starts with the description of the mass conservation, momentum and constitutive laws required to simulate the flow of VH and pharmacological fluids during saccadic eye movements using computational fluid dynamics (CFD). The methodology followed in the CFD simulations is described in detail: the eye model used; the saccadic eye movement computation; the constitutive equations used to model the rheological behaviour of VH and pharmacological fluids; as well as the numerical method and boundary conditions. The different validations performed, in order to show the solver stability and the method accuracy, close this chapter.

7.1 Background

According to the kinetic theory, matter is made up of molecules that are constantly in random motion, and strongly attract each other when close to one another [184]. Fluids are a combination of molecules that move and interact with each other, and also with the domain boundaries. There are two extreme ways to model the fluid state: the molecular (or microscopic) approach; and the continuum (or macroscopic) approach. In the molecular approach, the process is described from a molecular point of view. The fluid is considered as a group of discrete particles, the intermolecular forces

are taken into account and the positions of individual molecules are calculated. The continuum approach considers the fluid as an infinitely divisible substance, in which every element of the fluid contains a large number of molecules that can be represented by the average statistical properties of the molecules contained in an element of volume. As the fluid properties have a unique value at each point in the whole volume, the fluid properties can vary as function of position and time [185]. Even though researchers have started connecting molecular dynamics with classical CFD computations, CFD still works mostly assuming a continuum medium. The treatment of a fluid as a continuum has firmly been established for the fluids and length scales considered in this work, therefore justifying the use of the continuum approach is this study.

In this work, the behaviour of the VH biofluid and the pharmacological fluids (characterised experimentally in Chapter 4 and Chapter 5, respectively) as the vitreous cavity is subjected to saccadic eye movements is simulated using the opensource finite-volume code OpenFOAM®. The fluids under study are enclosed in a vitreous chamber, that resembles the human vitreous cavity in the eye, and different degrees of saccadic eye movements are considered.

Newtonian fluid flow modelling is typically based on three conservation laws: mass, encoded by the continuity equation; momentum, described by the Cauchy momentum equation; energy, given by the conservation of energy equation [186, 187]. The flows studied here are considered *isothermal*, i.e. the flow motion occurs at constant temperature, which means that the conservation of energy equation does not need to be solved. Additionally, the fluids used can be considered incompressible. The continuity equation is a scalar equation, the momentum balance is a vector equation, and the extra-stress constitutive equations required for non-Newtonian fluids are tensorial equations. All the equations are presented in vector/tensor notation (Gibbs notation); however, they can also be written in any coordinate system.

For isothermal incompressible fluid flows, the continuity equation can be written as

$$\nabla \cdot \mathbf{u} = 0 \tag{7.1}$$

where $\mathbf{u}$ is the velocity vector with components u_x, u_y and u_z in the x, y and z directions, respectively.

The Cauchy momentum equation can be written as

$$\rho(\frac{\partial \mathbf{u}}{\partial t} + \mathbf{u} \cdot \nabla \mathbf{u}) = -\nabla p + \nabla \cdot \boldsymbol{\tau} + \rho \mathbf{g} \tag{7.2}$$

where ρ is the fluid density, p the pressure, t represents time and $\mathbf{g}$ the acceleration of gravity. In order to solve the momentum equation, the extra-stress tensor $\boldsymbol{\tau}$ is calculated based on an adequate rheological constitutive equation. For an inelastic fluid, the extra-stress tensor describes the molecular stresses at a specific point in the flow as a function of the local velocity gradient. For viscoelastic fluids, the flow history is important, due to the memory of the fluid, and it is a common approach to split the total extra-stress tensor in a polymeric contribution $\boldsymbol{\tau}_p$ and a solvent contribution $\boldsymbol{\tau}_s$: $\boldsymbol{\tau} = \boldsymbol{\tau}_s + \boldsymbol{\tau}_p$. The Newtonian solvent contribution is given by

$$\boldsymbol{\tau}_s = \eta_s(\nabla \mathbf{u} + \nabla \mathbf{u}^{\mathrm{T}}) \tag{7.3}$$

while the polymeric contribution can be described by a differential-type system of partial equations, which can be written in a generic form as

$$f(\boldsymbol{\tau}_p)\boldsymbol{\tau}_p + \lambda(\dot{\gamma})\overset{\nabla}{\boldsymbol{\tau}}_p + \mathbf{h}(\boldsymbol{\tau}_p) = \eta_p(\dot{\gamma})(\nabla \mathbf{u} + \nabla \mathbf{u}^{\mathrm{T}}) \tag{7.4}$$

where η_s and η_p are the solvent and the polymer viscosity contributions, respectively, λ is the relaxation time, $\dot{\gamma}$ the shear-rate, $f(\boldsymbol{\tau}_p)$ is a scalar function depending on an invariant of $\boldsymbol{\tau}_p$, $\mathbf{h}(\boldsymbol{\tau}_p)$ is a tensor-valued function depending on $\boldsymbol{\tau}_p$, and $\overset{\nabla}{\boldsymbol{\tau}}_p$ represents the upper-convected time derivative of the polymeric contribution [188]. For GNF fluids (see Section 3.2), which are inelastic, $\boldsymbol{\tau}_p$ is zero and the stress tensor is $\boldsymbol{\tau} = \eta_s(\dot{\gamma})(\nabla \mathbf{u} + \nabla \mathbf{u}^T)$, where $\eta_s(\dot{\gamma})$ is a function of the shear rate.

Constitutive equations are an approximation of the material response obtained by arguments corroborated by experiments. Depending on the fluid behaviour (Newtonian, GNF, viscoelastic, etc − see Section 3.2), different rheological models, and consequently different constitutive equations, can be used. Some common models are:

- Newtonian fluid
- GNF models
  - Power law
  - Carreau-Yasuda
  - Herschel-Bulkley
  - Casson
  - Bingham
- Viscoelastic fluid models
  - upper-convected Maxwell
  - Oldroyd-B
  - Giesekus
  - Phan-Thien–Tanner (PTT)
  - Finite Extendable Non-linear Elastic (FENE): Chilcott and Rallison closure (FENE-CR); Peterlin closure (FENE-P)
  - White-Metzner

In Section 7.2, the constitutive equations for the models chosen to describe the rheological behaviour of the fluids under study will be presented in detail.

7.2 Methodology

7.2.1 Eye model

The eye geometry used in the simulations was based on the real eye shape and size of an adult Human eye [189]. According to *Encyclopedia Britannica Macropedia: Sensory Reception*, the dimensions of the eye are reasonably constant, with a variation of one or two millimetres between individuals, and with a vertical diameter of about 24 mm.

The geometry was drawn with the 3D CAD design software SolidWorks® v.15 and all the dimensions considered are shown in Fig. 7.1.

Additionally, a magnetic resonance image (MRI) of a Human eye was used as a model for the vitreous chamber considered in the simulations, which is shown in Fig. 7.2a. In Fig. 7.2b, the midplane of the vitreous chamber used in the simulations is superimposed onto the MRI of the Human eye, showing that the geometry created and used in this work resembles the shape of a real VH cavity.

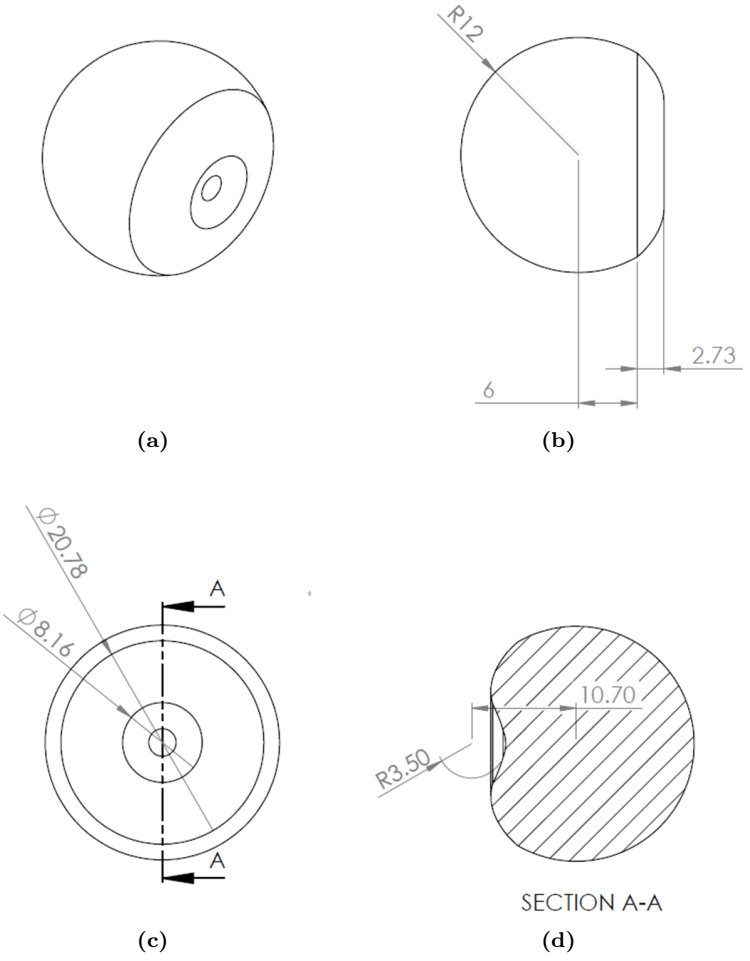

Figure 7.1. Computational model of the vitreous cavity (a) 3D view, (b) side view, (c) front view, and (d) midplane view based on section A-A presented in (c). All the dimensions presented are in millimetres.

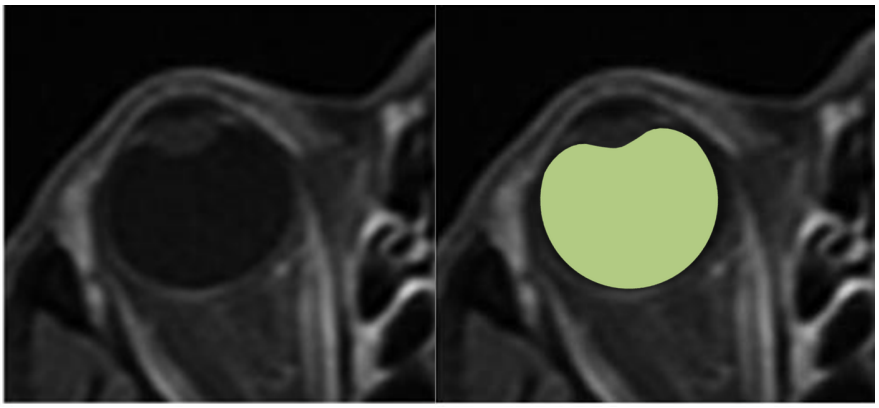

(a) (b)

Figure 7.2. (a) Magnetic resonance image of an adult Human eye, and (b) comparison between the real human eye and the midplane of the geometry used in the CFD work (MRI reprinted from [190] with permission from Creative Commons).

7.2.2 Saccadic Movements

As discussed in Chapter 6, the vitreous cavity is subjected to different types of movements. The sacaddic movements are the most common movements of the eye [159], and due to their fast nature they are also the ones that most affect the VH flow behaviour.

Saccadic movements are defined based on the saccade amplitude A, the saccade duration t_D, the peak angular velocity v_p and the acceleration time t_p. The fifth order polynomial equation presented by Reppeto *et al.* [176] (based in the experimental measurements of Becker [191]) was used in this work to define the saccadic movements:

$$\theta(t) = c_0 + c_1 t + c_2 t^2 + c_3 t^3 + c_4 t^4 + c_5 t^5 \tag{7.5}$$

The six coefficients were obtained imposing the following constraints: $\theta(0) = 0$, $\theta(t_D) = A$, $\theta'(0) = 0$, $\theta'(t_D) = 0$, $\theta'(t_p) = \Omega_p$ and $\theta''(t_p) = 0$.

The variable t_D is the saccade duration (measured in seconds) and is defined as

$$t_D = t_0 + dA \tag{7.6}$$

where A is the saccade amplitude measured in degrees (in the range $5° < A < 50°$) and d is the slope that assumes approximately a value of 0.0025 s/deg, while t_0 varies

between 0.02 and 0.03 s. The average angular velocity is defined as $\bar{\Omega} = A/t_D$ and measurements of Becker [191] showed that the ratio between the peak and the mean velocities can be considered constant,

$$\Omega_p/\bar{\Omega} = 1.64 \tag{7.7}$$

Finally, the experimental data from Becker [191] shows that saccades with amplitudes below 10° follow an acceleration time approximately equal to $t_p/t_D \sim 0.45$. The dimensionless acceleration time t_p/t_D decreases linearly with increasing saccade amplitude, to the value of $t_p/t_D \sim 0.25$ for a 50° displacement saccade.

In this work, the angular displacements under study are between 10° and 40°, as saccadic movements with a displacement higher than 40° are typically associated with head movements. The saccadic movement profiles, as well as the angular velocities related with each degree of displacement, are shown in Fig. 7.3. The fifth degree polynomial equation coefficients associated with each degree of movement where computed using MATLAB® software version R2014b (MathWorks), and are presented in Table 7.1.

Table 7.1. Coefficients for the polynomial function describing the saccadic movements (see Eq. (7.5)).

	Angular displacement (°)			
	10	20	30	40
c_0 (°)	0	0	0	0
c_1 (°/s)	0	0	0	0
c_2 (°/s^2)	11864	14947	16354	17200
c_3 (°/s^3)	-4478.5	-167250	-225050	-246330
c_4 (°/s^4)	-6057100	-350950	1094800	1458000
c_5 (°/s^5)	60026000	7412200	-1796900	-3394900
t_p (s)	0.0225	0.03	0.035	0.0375
t_D (s)	0.05	0.075	0.1	0.1250

7.2.3 Constitutive models

The models used to simulate the rheological properties of VH and of the commercial fluids used in eye surgery are described in this section. Their rheological properties were extensively described in Chapter 4 and Chapter 5, respectively. Based on those data, adequate constitutive models that are able to reproduce their rheological behaviour

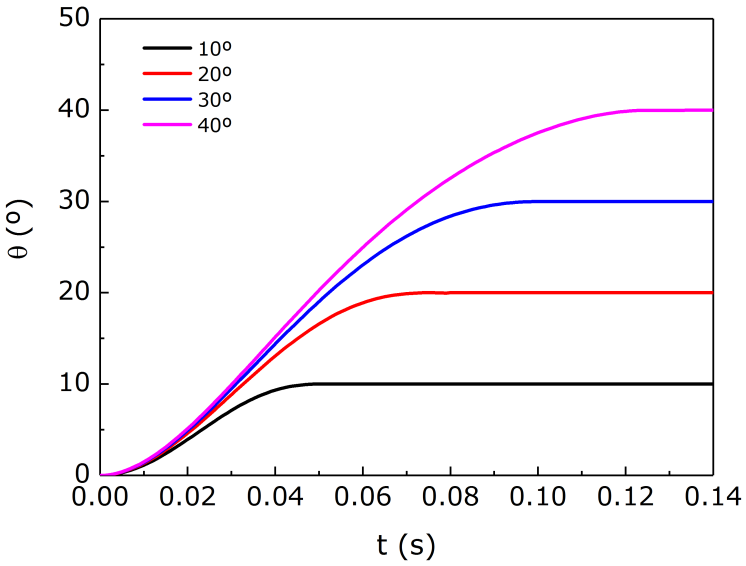

(a)

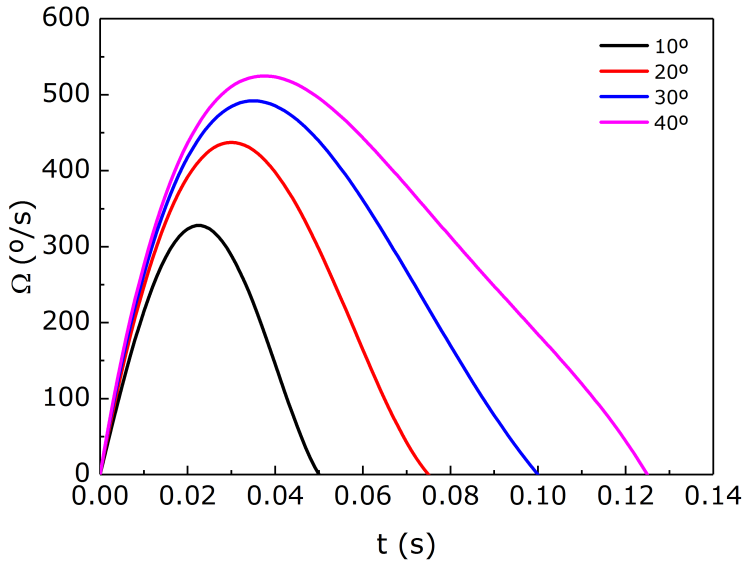

(b)

Figure 7.3. (a) Angular displacement and (b) angular velocity of the saccadic eye movements under study.

were chosen.

i) Vitreous humour

The Giesekus model was used to fit the rheological behaviour of both the VH liquid and gel phases. The Giesekus model was originally developed to describe the nonlinear response of polymeric solutions [192]. However, this model has been proven suitable for gel-like solutions [26, 193–196] and it has subsequently been used in several studies to model their rheological behaviour. Due to the complex VH phases characteristics, a single mode model was not capable of fitting accurately the experimental rheological data, and several modes were required to reproduce the fluids behaviour: a 3-mode Giesekus model was able to accurately capture the experimental VH gel phase rheological data, while a 4-mode Giesekus model was used to fit the VH liquid phase rheology presented in Chapter 4.

For the multimode Giesekus model, the shear viscosity is given by

$$\eta(\dot{\gamma}) = \eta_s + \sum_k \frac{\eta_{p,k}(1-f_k)^2}{1+(1-2\alpha_k)f_k} \tag{7.8}$$

where the function f_k of mode k is given by

$$f_k = \frac{1-X_k}{1+(1-2\alpha_k)X_k} \quad \text{with} \quad X_k^2 = \frac{\sqrt{1+16\alpha_k(1-\alpha_k)(\lambda_k\dot{\gamma})^2}-1}{8\alpha_k(1-\alpha_k)(\lambda_k\dot{\gamma})^2} \tag{7.9}$$

The storage and loss moduli in SAOS are given by

$$G' = \sum_k \frac{\eta_{p,k}\lambda_k\omega^2}{1+(\lambda_k\omega)^2} \tag{7.10}$$

$$G' = \eta_s\omega + \sum_k \frac{\eta_{p,k}\omega}{1+(\lambda_k\omega)^2} \tag{7.11}$$

where k is the mode index, varying from one to the number of modes used in the model, η_s and $\eta_{p,k}$ are the solvent and polymer viscosities of mode k respectively, λ_k is the relaxation time of mode k, ω is the angular frequency and α_k is the nonlinear parameter of mode k that is related with the anisotropy of the drag between the flow

and the polymer segments [103].

To solve the momentum equation (Eq. (7.2)), the Newtonian constitutive extra-stress tensor $\boldsymbol{\tau}_s$ is given by Eq. (7.3) and the viscoelastic extra-stress $\boldsymbol{\tau}_p$ is solved based on the Giesekus equation, which for mode k is given by

$$\boldsymbol{\tau}_{p,k} + \lambda_k \overset{\triangledown}{\boldsymbol{\tau}}_{p,k} + \alpha_k \frac{\lambda_k}{\eta_{p,k}} (\boldsymbol{\tau}_{p,k} \boldsymbol{\tau}_{p,k}) = \eta_{p,k} (\nabla \mathbf{u} + \nabla \mathbf{u}^{\mathrm{T}}) \tag{7.12}$$

where $\overset{\triangledown}{\boldsymbol{\tau}}_{p,k}$ is the upper-convective time derivative of $\boldsymbol{\tau}_{p,k}$, defined as $\overset{\triangledown}{\boldsymbol{\tau}}_{p,k} = \frac{\partial \boldsymbol{\tau}_{p,k}}{\partial t} + \mathbf{u} \cdot \nabla \boldsymbol{\tau}_{p,k} - \boldsymbol{\tau}_{p,k} \cdot \nabla \mathbf{u} - \nabla \mathbf{u}^{\mathrm{T}} \cdot \boldsymbol{\tau}_{p,k}$. Fig. 7.4 shows the experimental VH data and the data fit with the multimode Giesekus model. The coefficients for each mode of the model are presented in Table 7.2.

The data in Fig. 7.4a refers to the biofluid in its normal conformation right after dissection, when it looks like a gel, while the data in Fig. 7.4b refers to the liquid part of the sample, that correlates with the VH in later ages. The density of both phases is 1006 kg/m^3.

ii) Perfluorocarbons

The pharmaceutical fluids HPF8 and HPF10 were modeled as incompressible Newtonian fluids. Their viscosity curves are presented in Fig. 5.2 and, for a temperature of 37 °C, HPF8 has a shear viscosity of $\eta = 4.85 \times 10^{-4}$ Pa s and HPF10 has a shear viscosity

Table 7.2. Giesekus model parameters used to fit the rheological data of VH gel and liquid phases.

Gel phase				
	mode 1	mode 2	mode 3	
λ_k (s)	35	2	0.2	
$\eta_{p,k}$ (Pa s)	45	1.7	0.2	
η_s (Pa s)				0.05
α_k	0.5	0.5	0.5	
Liquid phase				
	mode 1	mode 2	mode 3	mode 4
λ_k (s)	35	2	0.2	0.01
$\eta_{p,k}$ (Pa s)	6	0.2	0.035	0.006
η_s (Pa s)				0.0007
α_k	0.5	0.5	0.5	0.5

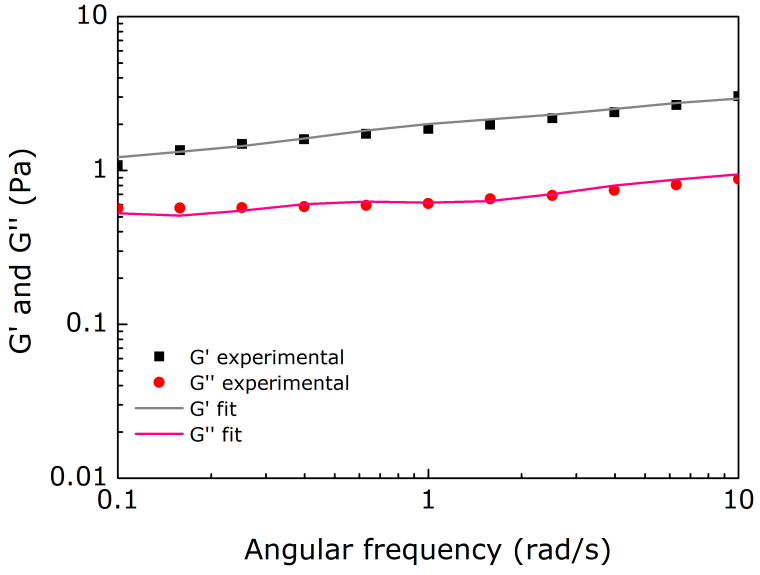

(a)

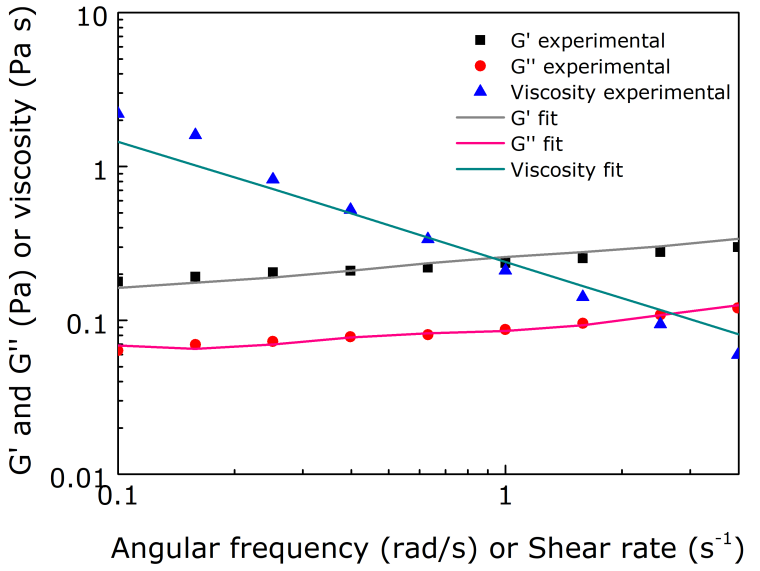

(b)

Figure 7.4. Average storage and loss moduli as function of angular frequency, and shear viscosity as function of shear rate at $T = 37$ °C for (a) the gel phase of VH and the fit with a 3-mode Giesekus model, and (b) liquid phase of VH and the fit with a 4-mode Giesekus model.

of $\eta = 3.57 \times 10^{-3}$ Pa s. For these fluids the constitutive equation is given by Eq. (7.3) and the momentum equation becomes

$$\rho(\frac{\partial \mathbf{u}}{\partial t} + \mathbf{u}.\nabla\mathbf{u}) = -\nabla p + \eta\nabla^2\mathbf{u} + \rho\mathbf{g} \tag{7.13}$$

where the shear viscosity η is constant.

iii) Silicone oils

As discussed in Chapter 5, the fluids used in eye surgery Densiron 68, RS-Oil 1000 and Siluron 5000 behave as Newtonian fluids. Therefore, those fluids were simulated as Newtonian fluids. The Siluron 2000 fluid exhibits a very low elastic behaviour. To assess if such a low value of elasticiy affects the fluid flow when compared with the Newtonian fluid behaviour, Siluron 2000 fluid was simulated both as a Newtonian fluid and as a viscoelastic fluid using an Oldroyd-B model. This model is frequently used in the simulation of Boger fluids, and predicts a constant shear viscosity and a quadratic increase of the first normal-stress difference with shear rate in a steady viscometric flow [103]. For the Oldroyd-B model, the constant shear viscosity is $\eta_0 = \eta_s + \eta_p$. To solve the momentum equation (Eq. (7.2)), the Newtonian constitutive stress tensor $\boldsymbol{\tau}_s$ is given by Eq. (7.3) and $\boldsymbol{\tau}_p$ is solved based on the UCM constitutive equation,

$$\boldsymbol{\tau}_p + \lambda\overset{\triangledown}{\boldsymbol{\tau}}_p = \eta_p(\nabla\mathbf{u} + \nabla\mathbf{u}^T) \tag{7.14}$$

For the Siluron 2000 fluid, two different solvent viscosities ratios were tested: $\beta = \eta_s/\eta_0 = 0.98$ and 0.95. The viscosity values used in the simulations for all the SiOs are presented in Table 7.3.

7.2.4 Numerical method

The open source finite-volume code OpenFOAM® version 2.2.2 was used to solve the governing equations with no-slip boundary conditions, in a Cartesian coordinate system. OpenFOAM uses the object oriented C++ programming language. The rheoTool package [188] with some modifications, in order to handle dynamic meshes, was used

Table 7.3. Viscosity values for the Newtonian and the Oldroyd-B models, used in the CFD simulations with the fluids RS-Oil 1000, Densiron 68, Siluron 2000 and Siluron 5000.

Fluids	Newtonian model	Oldroyd-B model				
	η (Pa s)	$\beta = 0.98$		$\beta = 0.95$		λ (s)
		η_p (Pa s)	η_s (Pa s)	η_p (Pa s)	η_s (Pa s)	
RS-Oil 1000	0.73	–	–	–	–	–
Densiron 68	1.07	–	–	–	–	–
Siluron 2000	1.71	0.0342	1.6758	0.0855	1.6245	0.0068
Siluron 5000	4.57	–	–	–	–	–

in the present investigation. The rheoTool package is able to solve transient, incompressible and single-phase flows of Newtonian and viscoelastic fluids. More information about the solver is presented in Pimenta and Alves [188].

A second-order implicit backward scheme was used to solve the temporal discretisation. The backward scheme uses the information from the two previous time steps, and the temporal derivative at time n is calculated as

$$\frac{\partial}{\partial t}(\phi^n) = \frac{3\phi^n - 4\phi^{n-1} + \phi^{n-2}}{2\Delta t} \tag{7.15}$$

where Δt is the time-step and ϕ the variable calculated on the three time levels, $n-2 = t - \Delta t$, $n-1 = t$ and $n = t + \Delta t$.

Second-order discretisation schemes were used, allowing larger time steps when compared with first-order schemes without compromising the numerical accuracy. However, it may also increase the computational time and lead to stability issues. Fig. 7.5 presents a comparison between the results obtained with the first-order Euler scheme, and the second-order Backward scheme used in this work, for the VH liquid phase subjected to a 40° diplacement as described in Section 7.2.2. The figure shows the velocity magnitude profiles in the midplane (line $z = 0$) of the vitreous cavity for three different times, $t = 0.0063$ s, $t = t_p = 0.0375$ s and $t = t_D = 0.125$ s. The numerical results show that the flow field is not very sensitive to the temporal schemes because of the very small time step ($\Delta t = 1 \times 10^{-4}$ s) used. Notwithstanding, as the computational time was similar using both schemes, the second-order backward scheme was chosen for all the remaining simulations performed in this work.

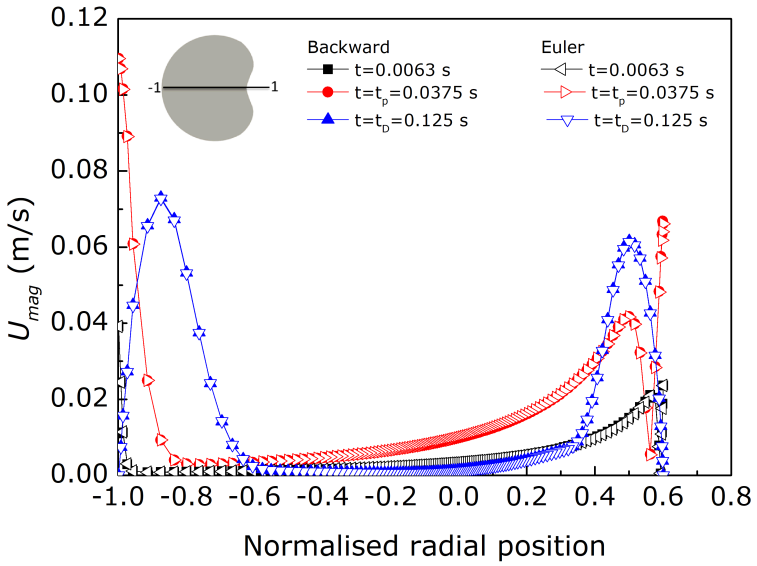

Figure 7.5. Comparison between different time schemes, Backward and Euler, with the VH liquid phase, for a 40° diplacement movement at $t = 0.0063$ s, $t = t_p = 0.0375$ s and $t = t_D = 0.125$ s. VH liquid phase was simulated with the Giesekus model, with the parameters given in Table 7.2.

To ensure the velocity-pressure coupling in a segregated way, the semi-implicit method for pressure-linked equations-Consistent (SIMPLEC) algorithm was selected. As shown in Fig. 7.6, with the SIMPLEC algorithm, an approximation of the velocity field is first obtained by solving the momentum equation. Then, the pressure field is calculated by enforcing the continuity equation and using the pressure field from the previous time step or an initial guess. The velocity and pressure fields are then corrected and conservative fluxes (if necessary) are calculated. The pressure correction is solved implicitly, whereas the velocity correction is computed explicitly. The main advantage of the SIMPLEC methodology, when compared with the semi-implicit method for pressure-linked equations (SIMPLE), is the fact that SIMPLEC does not require under-relaxation of pressure, which is important particularly for unsteady flow calculations. As mentioned in [188], for the benchmark cases tested with RheoTool, the SIMPLEC algorithm showed good results for transient viscoelastic fluid flows at low Reynolds numbers.

The discretisation of the governing equations was performed based on a third-order

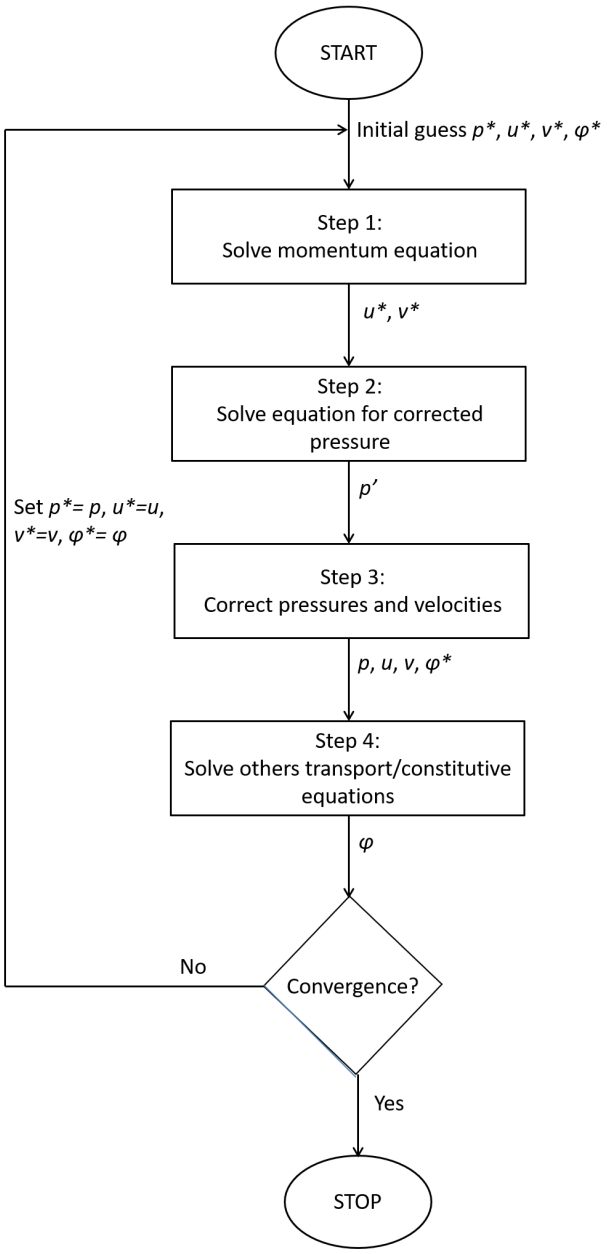

Figure 7.6. Stages of the methodology used in rheoTool based on the SIMPLEC algorithm (adapted from [197]).

accurate high-resolution scheme, known as the Convergent and Universally Bounded Interpolation Scheme for the Treatment of Advection (CUBISTA) [198], for the convective terms both of the momentum and constitutive equations. Unlike classical third order schemes that are not bounded, which may give rise to oscillations in the solution in

regions where there are strong gradients of the variable being solved, in high resolution schemes as CUBISTA the imposition of the boundedness property allow for good resolution of steep gradients without introducing oscillations in the solution and enhancing numerical stability. CUBISTA has the advantage over other higher-order schemes of promoting enhanced iterative convergence when used with implicit methods. The CUBISTA scheme is accurate and stable, being particularly adequate for the simulation of viscoelastic flows [198].

To show the importance of selecting an appropriate scheme for the spatial discretisation of the convective terms in the simulation of viscoelastic fluids, Fig. 7.7 presents a comparison between the fist-order Upwind scheme, and the third-order CUBISTA scheme. The velocity magnitude profiles in the midplane of the vitreous cavity for three different times, $t = 0.0063$ s, $t = t_p = 0.0375$ s and $t = t_D = 0.125$ s, are shown. The simulations were performed with the VH liquid phase for a movement of 40° diplacement, as described in Section 7.2.2, using the four mode Giesekus model (see Table 7.2). When the flow is aligned with the mesh, the first-order Upwind discretisation scheme may be acceptable. However, when the flow is not aligned with the mesh, the first-order scheme generates significant numerical errors. The results show small differences between the two schemes used, mostly close to the lens, due to the use of a refined mesh and the smoothness of the flow. Nevertheless, the use of CUBISTA scheme increases the numerical accuracy and will be used in the remaining simulations.

The vitreous cavity was moved with a specified velocity profile as described in Section 7.2.2. The no-slip boundary condition was considered at the wall, meaning that the fluid adjacent to the walls moves with the same velocity as the wall. A zero pressure gradient normal to the walls was assumed. The log-conformation tensor approach was used to solve the constitutive equation, which is known to increase the numerical stability [188, 199].

For the fluids and flow conditions under study, the maximum Reynolds number reached during the simulation is presented in Table 7.4 for each fluid. Here, the maximum Reynolds number is defined as $\mathrm{Re} = \frac{\rho U_{max} R}{\eta_0}$, where R is the eye radius, U_{max} is the maximum velocity reached for each degree of movement, and η_0 is the zero shear

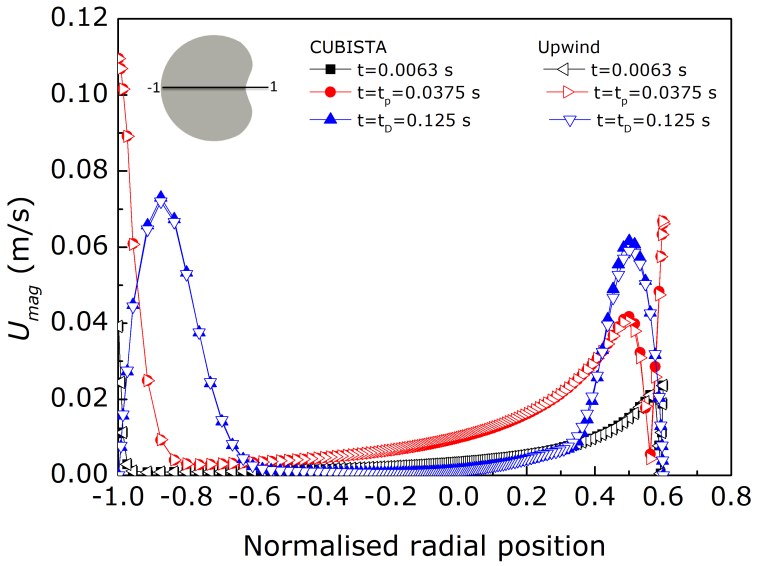

Figure 7.7. Comparison between different discretisation schemes, CUBISTA and Upwind, with the VH liquid phase, for a 40° diplacement movement at $t = 0.0063$ s, $t = t_p = 0.0375$ s and $t = t_D = 0.125$ s. VH liquid phase was simulated with the Giesekus model, with the parameters given in Table 7.2.

viscosity of the fluid. Independently of the degree of movement, the maximum Reynolds number reached is below Re = 2, except for the low viscosity PFLCs: HPF8 can reach Re≈ 4790, while the maximum value for HPF10 is Re≈ 717.

The maximum Weissenberg number for the viscoelastic fluids was estimated as $\mathrm{Wi} = \frac{\lambda_p U_{max}}{R}$ where λ_p is the average relaxation time, calculated as $\lambda_p = \frac{\sum_k \lambda_k \eta_k}{\sum_k \eta_k}$ with λ_k and η_k presented in Table 7.2 ($\lambda_k = 33.66$ s for both fluids). Fig. 7.8 shows the nominal Weissenberg number variation with time, for all the displacements studied: 10°, 20°, 30°, and 40°.

Table 7.4. Maximum Reynolds number, based on the peak velocity, for the fluids under study for the following displacements: $A = 10°$, $20°$, $30°$ and $40°$.

				$A = 10°$		$A = 20°$		$A = 30°$		$A = 40°$	
	Density (kg/m^3)	Zero shear viscosity (Pa s)	Radius (m)	Max U (m/s)	Max Re	Max U (m/s)	Max Re	Max U (m/s)	Max Re	Max U (m/s)	Max Re
VH gel	1006	46.95	0.012	0.069	0.018	0.092	0.024	0.103	0.026	0.110	0.028
VH liquid	1006	6.25			0.133		0.178		0.199		0.212
HPF8	1760	4.85×10^{-4}			3005		4006		4485		4790
HPF10	1940	3.57×10^{-3}			450		560		672		717
RS Oil 1000	970	0.73			1.116		1.487		1.665		1.778
Densiron 68	1060	1.07			0.813		1.084		1.213		1.296
Siluron 2000	970	1.71			0.470		0.626		0.701		0.749
RS Oil 5000	970	4.57			0.176		0.234		0.262		0.280

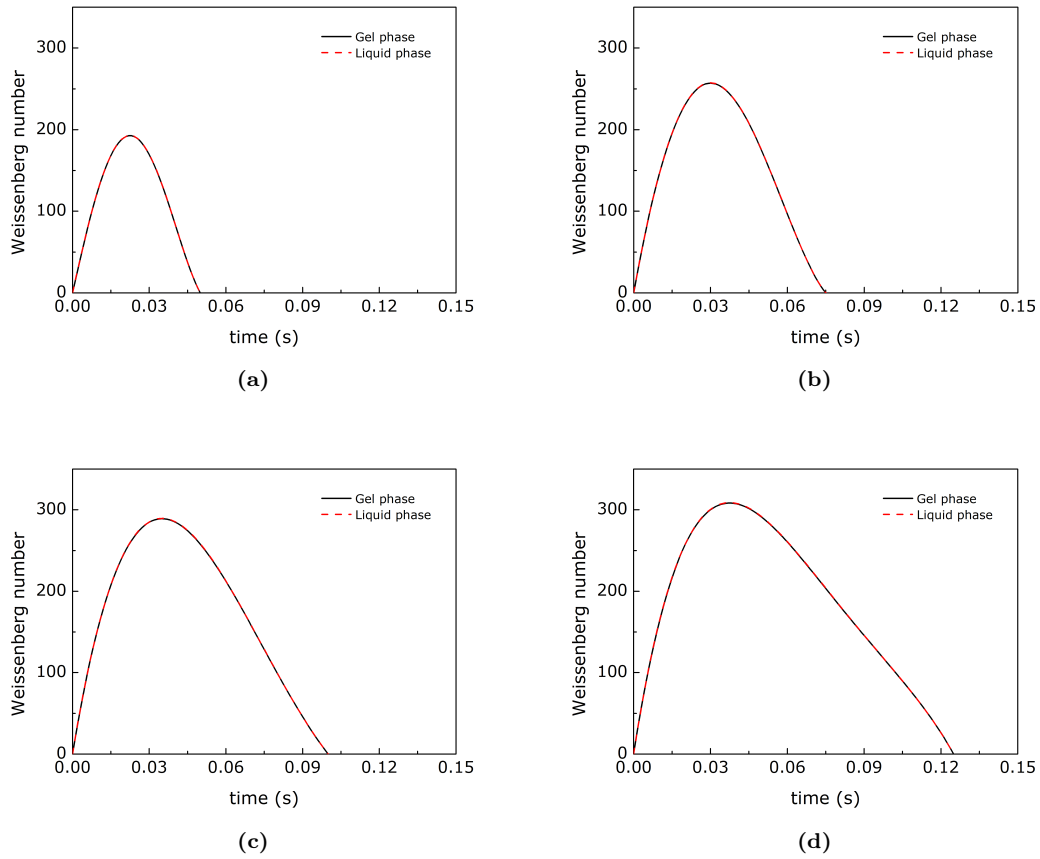

Figure 7.8. Nominal Weissenberg number estimated as a function of time for the different phases of VH for a displacement of (a) 10°, (b) 20°, (c) 30°, and (d) 40°.

7.3 Numerical method validation

This section presents several validations to assess the validity and accuracy of the solver and the followed methodology. The validity of the solver used is shown in the next subsection, and the mesh refinement studies close this chapter.

7.3.1 Solver validation

The RheoTool package has been validated for several benchmark cases, and more information can be found in Pimenta and Alves [188]. However, the original package is

not prepared to work with dynamic meshes as used in this work. The necessary modifications in order to RheoTool handle dynamic meshes where kindly performed by the rheoTool's developer F. Pimenta, and validations with a relevant test case for this work was performed. For the cases under study in this work, the whole eye model needs to move with a prescribed mesh motion, guaranteeing that the mesh does not suffer any topological change. In order to include the effect of the dynamic mesh, a term defining the velocity of the grid $\mathbf{u}_g$ must be subtracted from the differential equations. In this moving mesh framework, the continuity and momentum equations become

$$\frac{\partial \rho}{\partial t} + \nabla \cdot (\mathbf{u} - \mathbf{u}_g) = 0 \tag{7.16}$$

$$\rho \left[\frac{\partial \mathbf{u}}{\partial t} + \mathbf{u} \cdot \nabla (\mathbf{u} - \mathbf{u}_g) \right] = -\nabla p + \nabla \cdot \boldsymbol{\tau} + \rho \mathbf{g} \tag{7.17}$$

The results obtained with RheoTool working with dynamic meshes (named RheoDyMFoam) are compared in this section with theoretical results from David *et al.* [169]. Note that besides the chosen moving mesh technique, applying the velocity as a boundary condition was also tested. However, while it works well for such cases as a 2D circle, it becomes problematic for more complex geometries. To set the velocity as a boundary condition in stationary grids when in presence of generic boundaries leads to issues related to the need to set normal velocity components to the boundaries, which is not numerically straightforward for an enclosed stationary grid. The vitreous chamber studied in this thesis shows non-circular boundaries (e.g. in the lens indentation) and based on that using the velocity as a boundary condition was excluded.

i) Sphere filled with a Newtonian fluid

David *et al.* [169] presented an analytical solution for Newtonian fluid motion of a sphere during oscillatory and saccadic movements. As mentioned in Chapter 6, Repetto *et al.* [176] studied experimentally the vitreous motion induced by saccadic eye movements. A model of the vitreous cavity was used in their work, consisting of a spherical cavity with a radius of 40.8 mm carved in a perspex cylindrical container. The spherical cavity

was filled with a Newtonian fluid, glycerol. Abouali *et al.* [25] used the same geometry and fluid to validate their numerical setup for the simulation of Newtonian fluids, during saccadic movements, in a simplified eye geometry using FLUENT software.

In this study, the same geometry, fluid and saccadic movement profile were chosen to validate our solver for Newtonian fluids: a saccadic movement with an amplitude $A = 40°$ and a period $t_D = 0.247$ s (see Fig. 7.9 and Table 7.5) was applied to a Newtonian fluid with a kinematic viscosity of $8.19\text{x}10^{-4}$ m^2/s and a density of 1260 kg/m^3.

The mesh used in this test is shown in Fig. 7.10, and consists of 56000 cells splitted in 7 blocks.

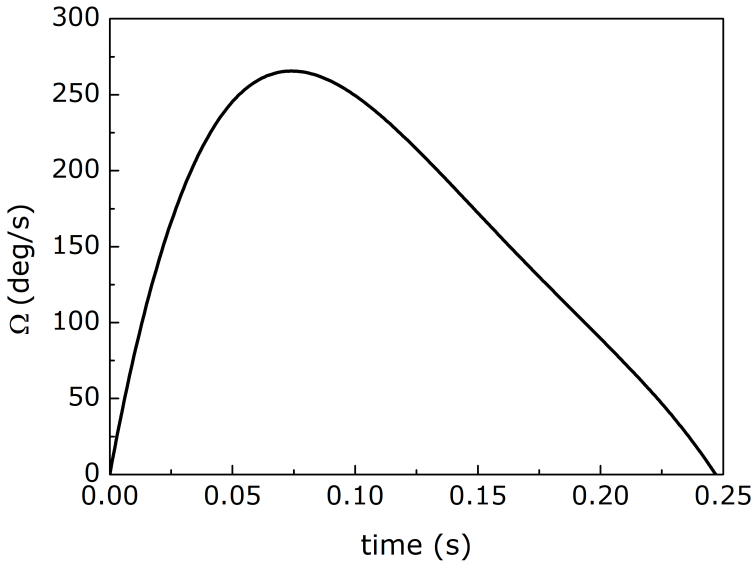

Figure 7.9. Angular velocity of the saccadic eye movement under study.

Table 7.5. Coefficients for the polynomial function describing the saccadic movement (see Eq. (7.5)) for a 40° movement, with a duration of $t_D = 0.247$ s.

Constant	Value
c_0 (deg)	0
c_1 (deg/s)	0
c_2 (deg/s^2)	4405
c_3 (deg/s^3)	-31925
c_4 (deg/s^4)	95629
c_5 (deg/s^5)	-112690
t_D (s)	0.247

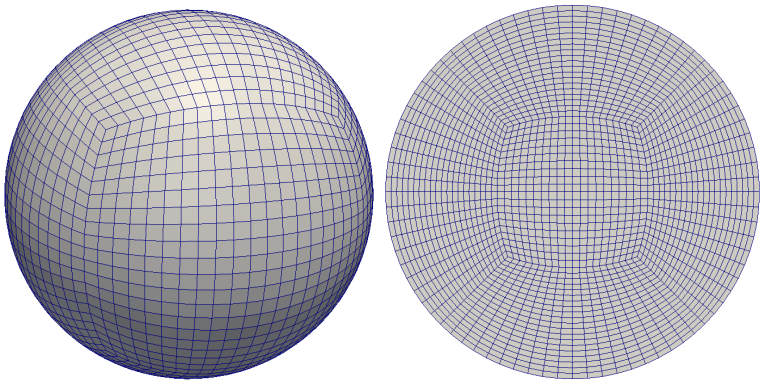

(a) (b)

Figure 7.10. Computational mesh used in the validation with a sphere filled with a Newtonian fluid: (a) surface mesh and (b) mesh in the plane $z = 0$.

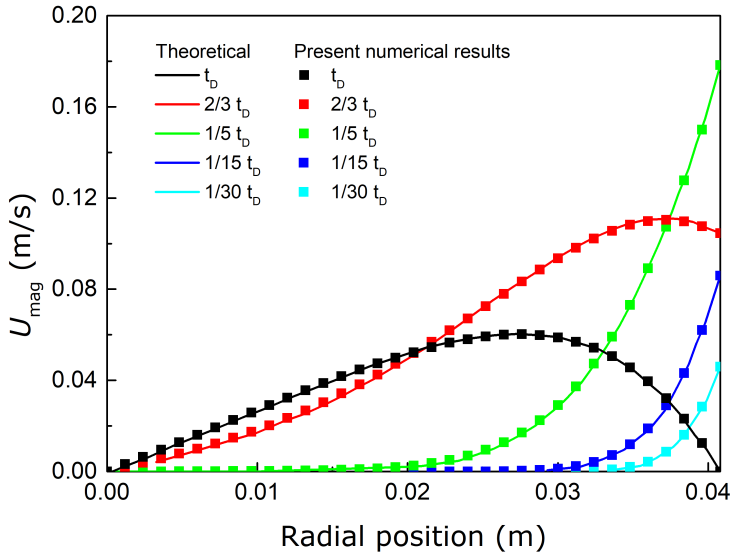

Figure 7.11. Comparison between theoretical (from [25, 169, 176]) and numerical velocity magnitude U_{mag} during a saccadic movement with $A = 40°$ and duration $t_D = 0.247$ s.

The velocity magnitude profiles for the imposed saccadic movement and the theoretical profiles obtained based in the work from David [169] are shown in Fig. 7.11. The results of the numerical model are in perfect agreement with the theoretical solution, confirming the validity of RheoTool handling dynamic meshes.

7.3.2 Mesh and time step validations

To ensure good accuracy of the CFD results presented in this work, different levels of mesh refinement and different time steps were tested. If the order of accuracy is constant as the grid is refined and the time step reduced, the results can be considered mesh and time step independent above a certain level of refinement (in space and time) that needs to be determined, and that is crucial to obtain stable and reliable results.

For meshing purposes, the geometry was split in seven different blocks: a cube in the middle and six blocks around the central cube that meet the surface of the eye geometry. All the cells are tetrahedric and different levels of refinements were used. The total number of cells in each mesh generated is shown in Table 7.6 and the surface and midplane of the meshes are shown in Fig. 7.12. *Mesh1* has 10 cells, *mesh2* has 20 cells, *mesh3* has 40 cells and *mesh4* has 80 cells per block and in each direction. Additionally, *mesh2*, *mesh3* and *mesh4* were locally refined close to the walls, and those meshes are designated *mesh2b*, *mesh3b* and *mesh4b*, respectively. For all of the last three meshes, the cells adjacent to the wall were divided in four or three new cells, assuring that the skewness was the same as the corresponding mesh without refinements near the wall.

Taking into account the differences in the characteristics of the fluids under study, different fluid rheologies require different degrees of mesh refinement. Based on that, the mesh validations were divided in 3 groups: the SiO and HSiO, the PFLCs and the

Table 7.6. Details of the meshes used in the simulations.

	mesh1	mesh2	mesh2b	mesh3	mesh3b	mesh4	mesh4b
Number of cells	7000	56000	63200	448000	476800	3584000	3660800
Number of points	7351	57301	64507	453001	481807	3603601	3680405
Number of faces	21300	169200	190800	1348800	1435200	10771200	11001600
Number of internal faces	20700	166800	188400	1339200	1425600	10732800	10963200
Max. skewness	0.35	0.38	0.39	0.42	0.42	0.47	0.47

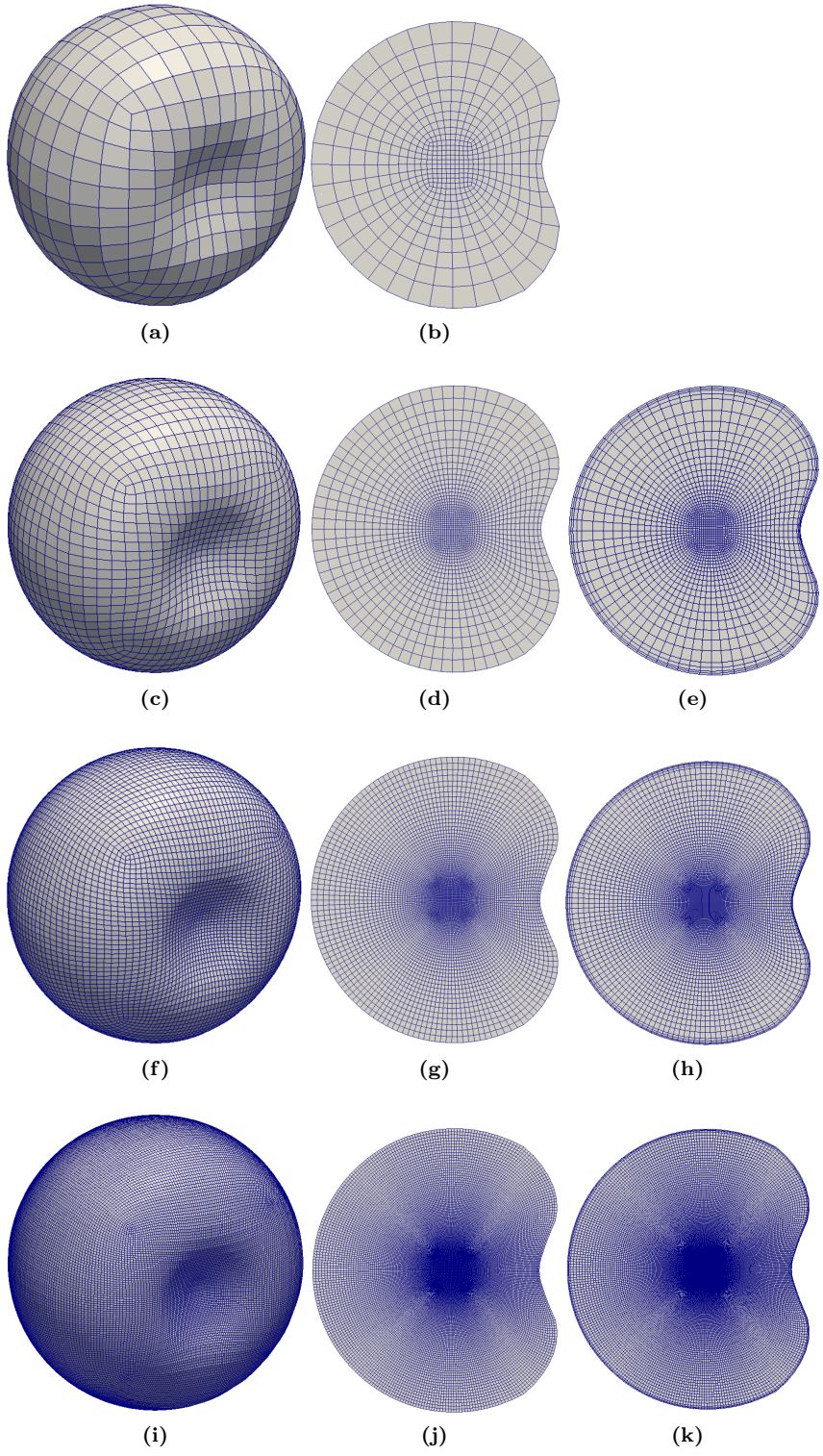

Figure 7.12. Numerical meshes studied. (a),(c),(f) and (i) correspond to the mesh in the surface for *mesh1*, *mesh2*, *mesh3* and *mesh4*, respectively. (b),(d),(g) and (j) show the plane $z = 0$ for *mesh1*, *mesh2*, *mesh3* and *mesh4*, respectively. (e),(h) and (k) are a representation of plane $z = 0$ for *mesh2b*, *mesh3b* and *mesh4b*, respectively.

viscoelastic fluids. As the properties of the SiO are similar, validations were performed for the SiO with the lower viscosity (RS-Oil 1000, $\eta = 0.73$ Pa s), and the same mesh was used for all the remaining SiO based fluids. Both PFLCs show Newtonian behaviour and a very low viscosity (see Table 5.3), which means that the difusive time scale is high and the velocity gradients occur primarily very close to the walls. Thus, special attention was devoted to the boundary layer close to the walls, and validations were performed with the HPF8 fluid. Finally, for the VH, due to the large normal stresses, a more complex flow field than the fluids used in eye surgery is expected, and it may require the use of a different mesh refinement level when compared with the previous fluids. For the VH samples, validations were performed with the VH liquid phase.

For the three fluids subjected to mesh refinement validations, a 40° diplacement movement was imposed, as described in Section 7.2, and the velocity magnitude profiles in the midplane of the vitreous cavity for three different times, $\sim 0.05t_D = 0.0063$ s, $t_p = 0.0375$ s and $t_D = 0.125$ s were compared. Finally, for the meshes selected, different time steps were tested and the comparison of the velocity magnitude profiles in the midplane for the same times used in the mesh validations are also presented.

i) Silicone oils

As explained in Section 7.2.3, RS-Oil 1000, Densiron 68 and Siluron 5000 fluids were simulated as Newtonian fluids, and Siluron 2000 fluid was simulated both as Newtonian fluid and as a viscoelastic fluid using the Oldroyd-B model. The validations presented here were obtained with the simulations performed with the RS-Oil 1000 fluid. *Mesh1*, *mesh2* and *mesh3* were tested, and the velocity magnitude profiles in the midplane, at the line $z = 0$, are shown in Fig. 7.13. Note that the points represented in the plots correspond to the centre of the cells, thus not requiring any sort of interpolation.

The numerical results show that the three meshes tested have similar velocity magnitude profiles for the different times shown in Fig. 7.13. However, *mesh1* shows a slight difference in the velocity profiles for the time corresponding to zero velocity applied at the walls, $t = t_D = 0.125$ s. *Mesh2* and *mesh3* present velocity profiles with no meaningful differences between them, which means that the level of refinement of *mesh2* is

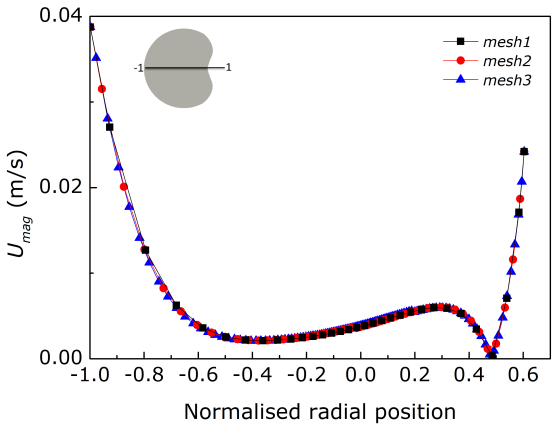

(a)

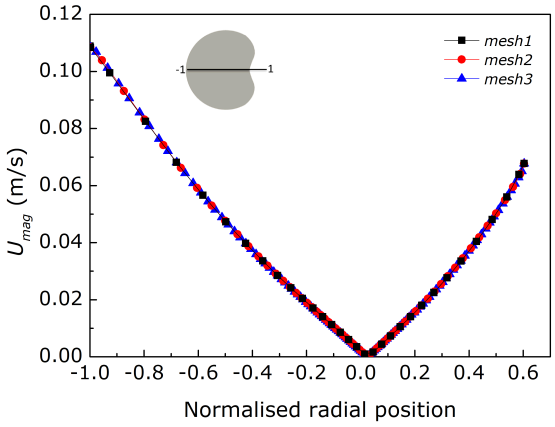

(b)

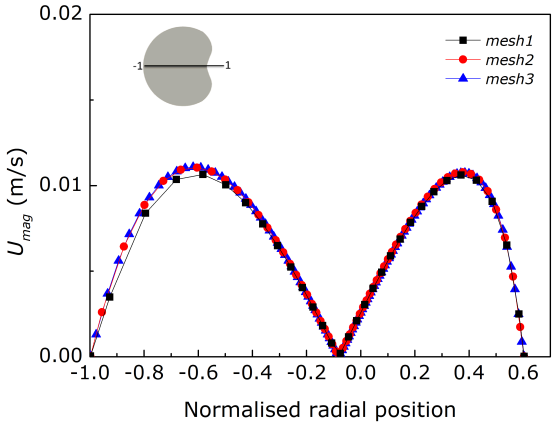

(c)

Figure 7.13. Comparison of velocity magnitude as function of normalised radial position in different meshes for a 40° diplacement movement at (a) $t = 0.0063$ s, (b) $t = t_p = 0.0375$ s and (c) $t = t_D = 0.125$ s, for the fluid RS-Oil 1000.

enough to obtain reliable results which are already independent of the computational grid.

Two different fixed time steps were also tested, $\Delta t = 1 \times 10^{-4}$ s and 1×10^{-5} s, and the results presented in Fig. 7.14 show that a time step of $\Delta t = 1 \times 10^{-5}$ s causes no meaningful differences between the converged numerical results when compared with the larger time step of $\Delta t = 1 \times 10^{-4}$ s. Based on that, a fixed time step of $\Delta t = 1 \times 10^{-4}$ s was adopted for all the CFD work performed with the SiO fluids.

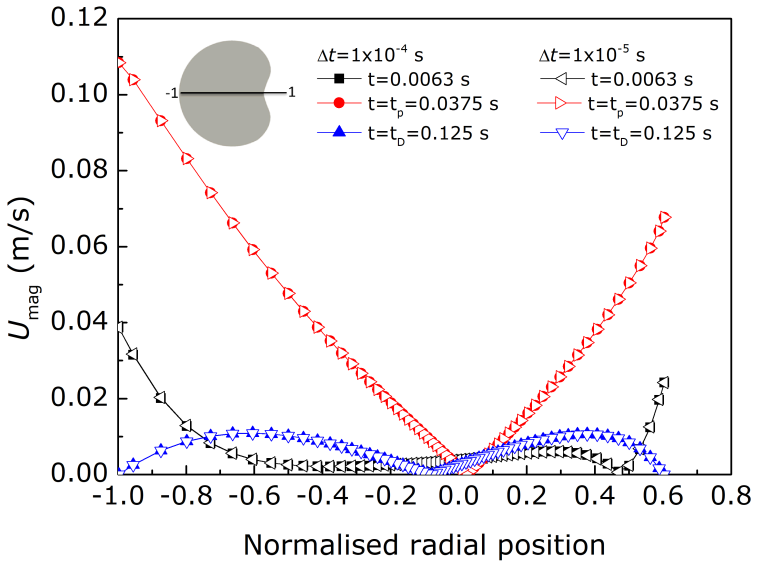

Figure 7.14. Comparison of velocity magnitude as function of normalised radial position for a 40° diplacement movement, at $t = 0.0063$ s, $t = t_p = 0.0375$ s and $t = t_D = 0.125$ s, for the fluid RS-Oil 1000, using different time steps.

ii) Perfluorocarbons

Between the two PFLCs under study, HPF8 is the one with the lowest viscosity (see Table 5.3), and it was selected to perform the validations of the PFLCs.

Mesh2b, *mesh3b* and *mesh4b* were tested and the velocity profiles in the midplane, at the line $z = 0$, are shown in Fig. 7.15. The velocity profiles obtained are similar for the three meshes tested. However, from the analysis of Fig. 7.15c it is possible to see that *mesh2b* shows some inconsistencies when compared with the other two more refined

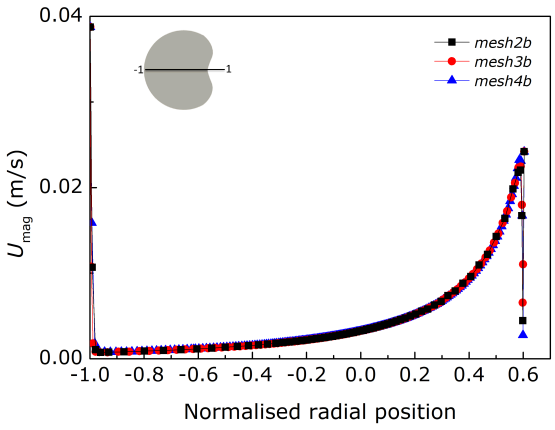

(a)

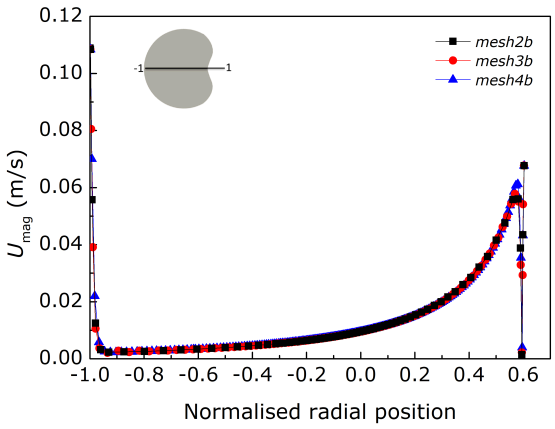

(b)

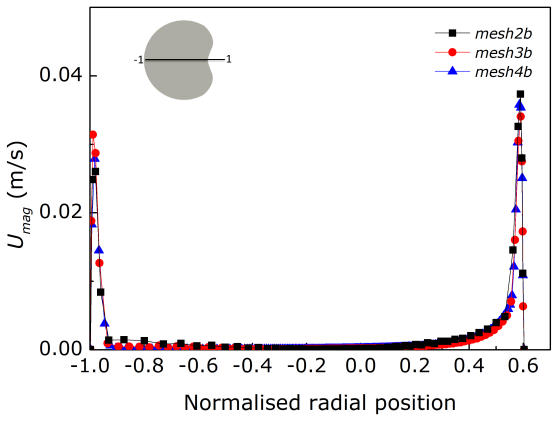

(c)

Figure 7.15. Comparison of velocity magnitude as function of normalised radial position in different meshes for a 40° diplacement movement at (a) $t = 0.0063$ s, (b) $t = t_p = 0.0375$ s and (c) $t = t_D = 0.125$ s, for the fluid HPF8.

meshes. *Mesh3b* and *mesh4b* show similar velocity profiles and *mesh3b* was considered to have a level of refinement that allows to obtain reliable results which are independent of the computational grid.

Once again, two different time steps were tested, $\Delta t = 1 \times 10^{-4}$ s and 1×10^{-5} s. The results presented in Fig. 7.16 show that there are no meanigful differences in the velocity profiles between these two time steps. Therefore, the time step $\Delta t = 1 \times 10^{-4}$ s was chosen in all the remaining numerical work performed with the PFLCs fluids.

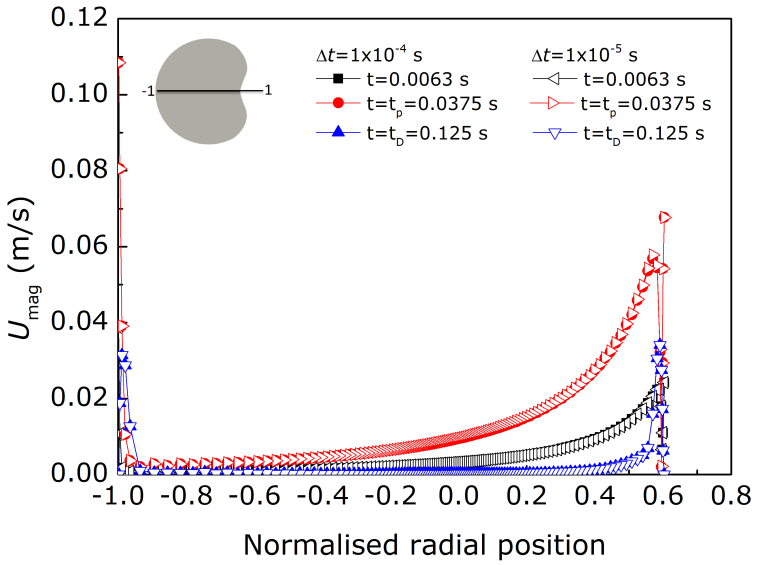

Figure 7.16. Comparison of velocity magnitude as function of normalised radial position for a 40° diplacement movement, at $t = 0.0063$ s, $t = t_p = 0.0375$ s and $t = t_D = 0.125$ s, for the fluid HPF8, using different time steps.

iii) Vitreous humour

Finally, the mesh validations for the VH cases were performed. VH shows a shear-thinning behaviour. Due to the variable viscosity and the memory of the fluid, the velocity gradients may occur very close to the walls and in other regions of the domain. Based on that, meshes without and with refinement near the walls were tested: *mesh2*, *mesh2b*, *mesh3*, *mesh3b* and *mesh4b*. From the analysis of Fig. 7.17, it is possible to see that spliting the cell next to the wall in four cells in *mesh2* increases the accuracy of

the solution (the black squares refer to *mesh2* and the red circles to *mesh2b*). However, comparing *mesh2b* with the more refined meshes shows that *mesh2b* presents some oscilations for a normalised radial position between -0.6 and -0.2 for $t = t_D = 0.125$ s (Fig. 7.17c). *Mesh3*, *mesh3b* and *mesh4b* all show similar profiles, even though in the area close to the lens indentation there is a better agreement in the velocity profiles obtained with *mesh3b* and *mesh4b* than with *mesh3*. As such, and since the computational time is similar for both *mesh3* and *mesh3b*, *mesh3b* was chosen to perform further simulations with both VH liquid and gel phases.

Finally, the same time steps studied for the RS-oil 1000 and HPF8 were also tested and results are shown in Fig. 7.18. Once again, a time step of $\Delta t = 1 \times 10^{-4}$ s was chosen since the numerical results show that the differences between this time step and a smaller time step of $\Delta t = 1 \times 10^{-5}$ s are negligible.

Summarising, the numerical work performed in this section allows to conclude that *mesh2* is adequate for simulating the SiOs, while *mesh3b* was selected to simulate the PFLCs and VH flow. All the simulations were performed with a time step $\Delta t = 1 \times 10^{-4}$ s, which was found to be low enough to achieve high temporal accuracy in all tested fluids.

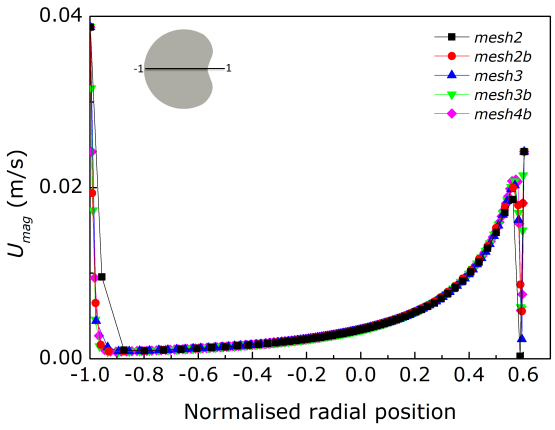

(a)

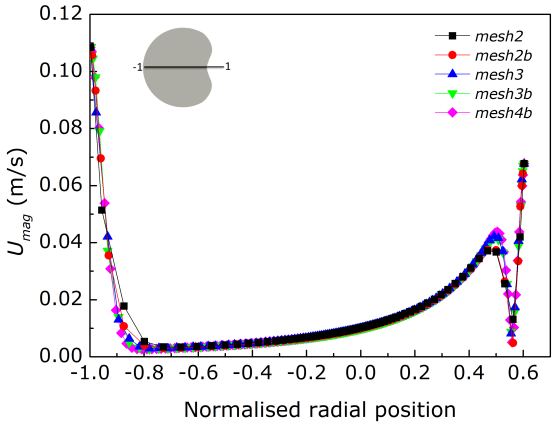

(b)

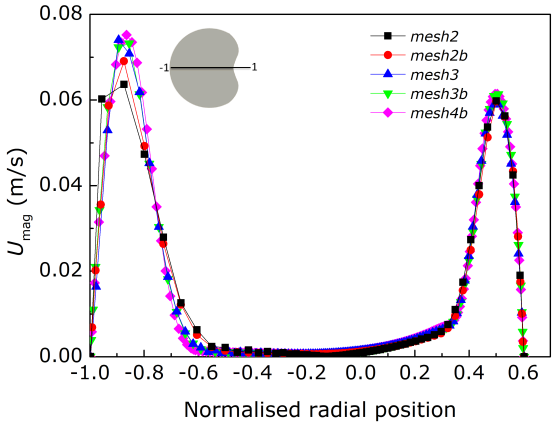

(c)

Figure 7.17. Comparison of velocity magnitude as function of normalised radial position in different meshes for a 40° diplacement movement at (a) $t = 0.0063$ s, (b) $t = t_p = 0.0375$ s and (c) $t = t_D = 0.125$ s, for VH liquid phase biofluid.

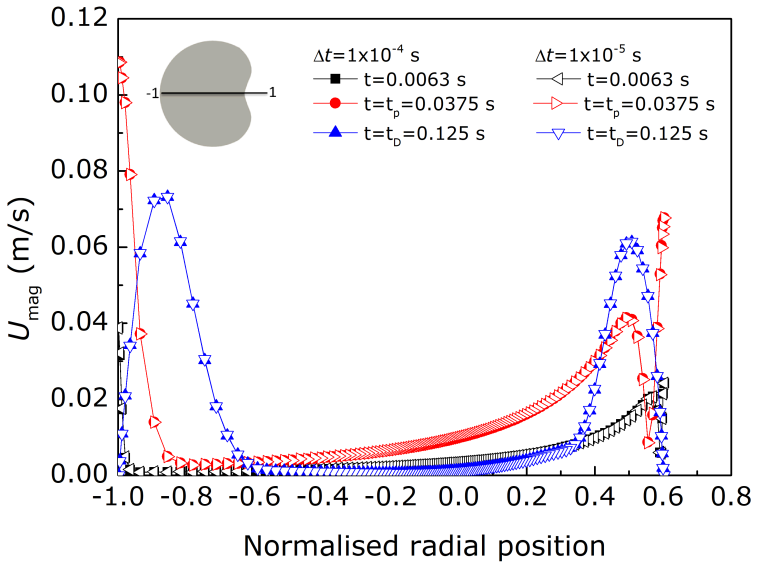

Figure 7.18. Comparison of velocity magnitude as function of normalised radial position for a 40° diplacement movement, at $t = 0.0063$ s, $t = t_p = 0.0375$ s and $t = t_D = 0.125$ s, for VH liquid phase biofluid, using different time steps.

"The great thing about science is that you can get it wrong over and over again because what you're after - call it truth or understanding - waits patiently for you. Ultimately, you'll find the answer because it doesn't change."

Dudley Herschbach

Chapter 8

Numerical results

This chapter presents the numerical simulations of flow behaviour of VH and pharmacological fluids for different degrees of saccadic movements. Firstly, a comparison between the flow behaviour of Siluron 2000 simulated as a Newtonian fluid and as a viscoelastic fluid is presented. The results show that, for the degree of elasticity considered, only very small differences are predicted in terms of the velocity and WSS profiles. The impact of the different rheological properties of all fluids under study is also studied. SiO-based fluids show higher velocities along the vitreous cavity and higher WSS when compared with both VH and the PFLCs. To conclude the chapter, the differences in the flow behaviour of the fluids are investigated when subjected to different degrees of saccadic movements. The results show that both velocity along the vitreous cavity and the shear stresses on the cavity walls increase with the increase of the saccadic movement displacement.

8.1 Siluron 2000: assessing the impact of elasticity

As shown in Chapter 5, Siluron 2000 is a viscoelastic fluid, but its elasticity is very low and the shear viscosity is high. To try to understand how the elasticity can affect the flow behaviour of this fluid, Siluron 2000 fluid was simulated both as a Newtonian fluid and

as a viscoelastic fluid using the Oldroyd-B model, with solvent viscosity ratios $\beta = 0.98$ and $\beta = 0.95$. A high value of β, close to $\beta = 1$, was used due to the negligible shear-thinning of the fluid in steady shear flow. For the viscoelastic simulations, the relaxation time used was $\lambda = 6.8$ ms, as measured with an in-house miniaturised filament breakup device (see Chapter 5). The velocity magnitude in the midline at the plane $z = 0$, for saccadic movements with amplitudes $A = 10°$ and $40°$, are shown in Fig. 8.1. For both amplitudes, it is possible to observe a minor effect of the fluid viscoelasticity for the time where the wall velocity is zero, $t = t_D$ (see Fig. 8.1e and Fig. 8.1f). Additionally, for time $t = 0.04t_D$ it is also possible to observe a very small difference in the velocity magnitude when the Siluron 2000 fluid is subjected to a saccadic movement with $A = 10°$ (see Fig. 8.1b). The differences observed are small and overall the velocity profiles follow the same trend. For time $t = t_p$, the velocity magnitudes are mostly the same for the Newtonian fluid and the Oldroyd-B fluids, for both amplitudes under study (see Fig. 8.1c and Fig. 8.1b). Finally, there are no significant differences between the two different solvent viscosity ratios studied ($\beta = 0.98$ and $\beta = 0.95$).

The average WSS along time was also computed for Siluron 2000 fluid for saccadic movements with amplitudes $A = 10°$ and $40°$, and the numerical results are shown in Fig. 8.2. The results show that the Newtonian model presents slightly lower average WSS values in the maximum peak: for an amplitude $A = 10°$, the Newtonian model has a maximum peak of 7.23 Pa while for the Oldroyd-B model with $\beta = 0.95$ the value is 7.37 Pa; and for an amplitude $A = 40°$ the Newtonian model has a maximum peak of 9.20 Pa while for the Oldroyd-B model with $\beta = 0.95$ the value is 9.38 Pa. Similarly to the velocity magnitude results, there are no significant differences in the WSS results between the two different solvent viscosity ratios studied for the Oldroyd-B model.

Siluron 2000 is composed of two different MW molecules: 95% of PDMS with a shear viscosity of 1 Pa s and 5% of PDMS with a shear viscosity of 2500 Pa s. The manufacturer claims that due to this mixture, Siluron 2000 can modify its viscous properties depending on the shear forces, such as the ones generated in the eye due to its constant movements [148]. The results presented here show that for typical movements that the eye is subjected to, the differences in the flow behaviour between

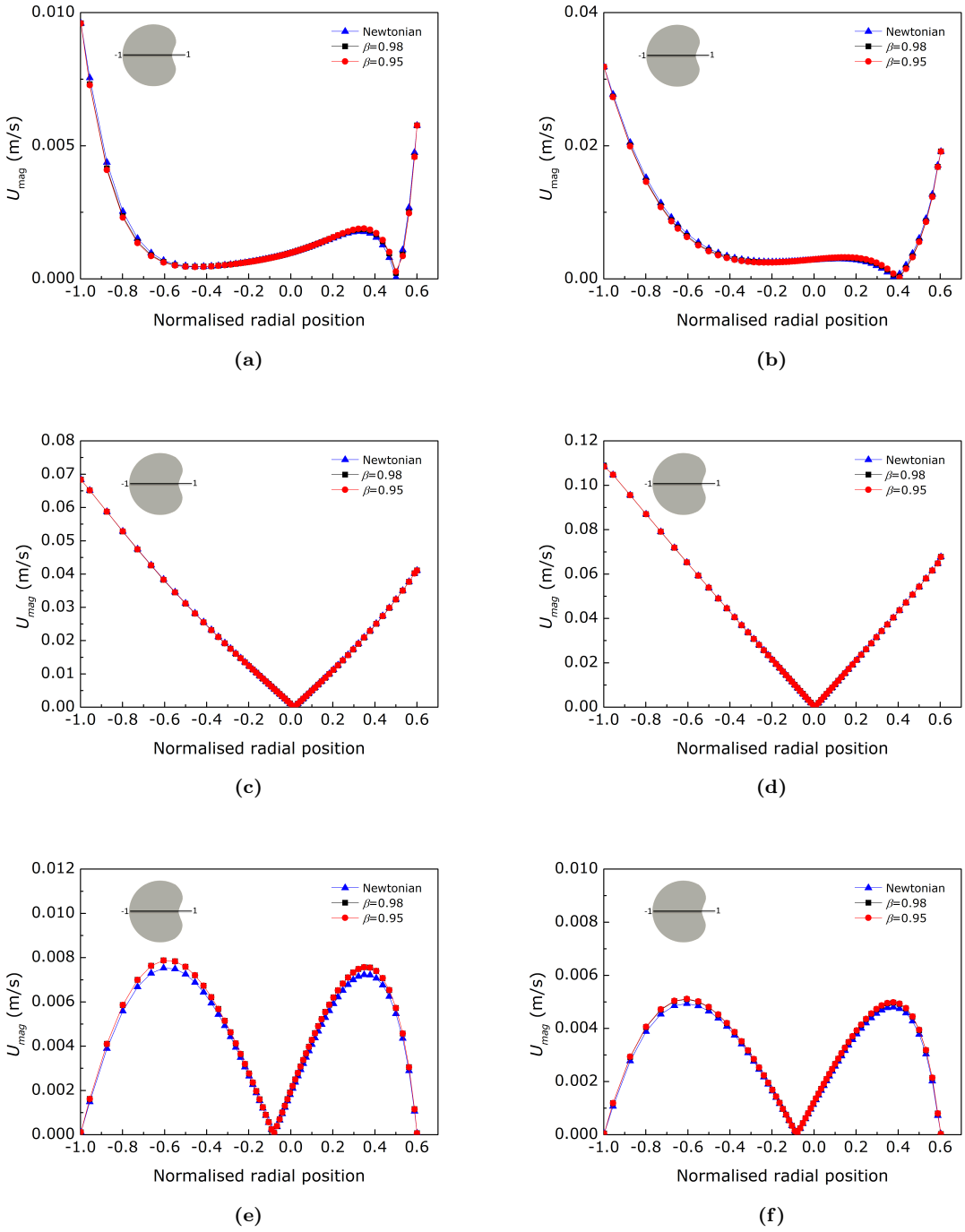

Figure 8.1. Comparison of velocity magnitude along the normalised radial position in the plane $z = 0$ for Siluron 2000 fluid for a saccadic movement of (a)(c)(e) $A = 10°$ and (b)(d)(f) $A = 40°$ at (a)(b) $t = 0.04t_D$, (c)(d) $t = t_p$ and (e)(f) $t = t_D$. A Newtonian fluid and two Oldroyd-B fluids with $\beta = 0.98$ and $\beta = 0.95$ were considered.

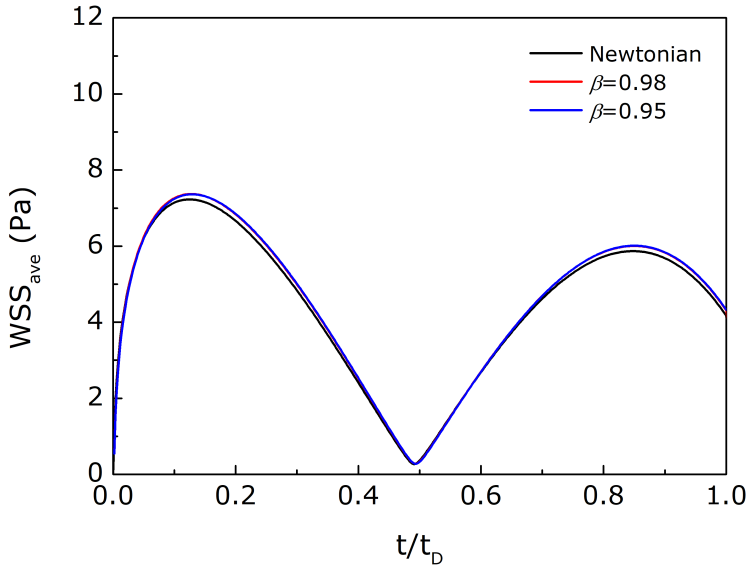

(a)

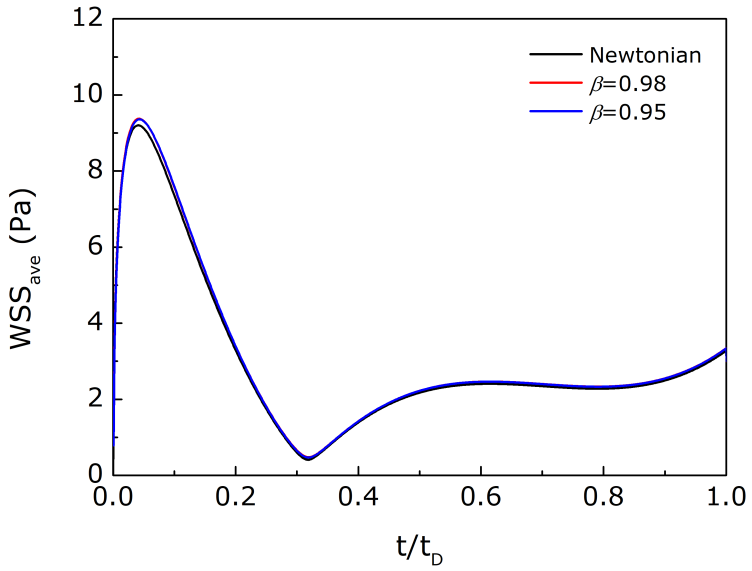

(b)

Figure 8.2. Comparison of the time variation of the average WSS for Siluron 2000 fluid for saccadic movements of (a) $A = 10°$ and (b) $A = 40°$, for a Newtonian fluid and two Oldroyd-B fluids with $\beta = 0.98$ and $\beta = 0.95$.

the Newtonian model and the Oldroyd-B model tested are very small. The low elasticity of Siluron 2000 is not sufficient to affect significantly its flow behaviour during typical saccadic movements. For all the remaining results shown in this chapter, the Siluron 2000 fluid is simulated as a viscoelastic fluid with $\beta = 0.95$.

8.2 Impact of different rheological properties

As presented in Chapter 4, both VH phases present significant elasticity, and more specifically a solid-like behaviour, but the gel phase presents a stronger elastic behaviour than the liquid phase. It is believed that the decrease of the elastic properties with the liquefaction process of the VH is the main reason for the appearance of diseases such as retinal detachment (RD) and retinal tears (RT) [42, 46]. To treat such diseases, a pharmacological fluid is inserted in the vitreous cavity. Studies showed that, depending on the fluid, the pharmacological fluids can remain in the vitreous cavity for a period of up to 6 months [45]. However, as shown previously, VH rheological behaviour is significantly different from that of the pharmacological fluids under study. Additionally, SiO-based fluids have distinct rheological behaviour when compared with PFLCs fluids. PFLCs behave as Newtonian fluids and have viscosities close to the viscosity of water, while the SiO-based fluids under study present a high shear viscosity and Newtonian behaviour, apart from Siluron 2000 fluid which is a Boger fluid, with low elasticity. Therefore, it is necessary to study the differences in the flow behaviour between both VH phases, and also between the pharmacological fluids and VH.

As shown in chapter 6, there is a body of research work on the flow behaviour of vitreous humour, however most of those studies rely on assumptions (e.g. simplified eye geometry, assumption of VH as a Newtonian fluid) that may lead to differences in the flow behaviour when compared with the real VH behaviour. In this work a geometry that is a better approximation of the vitreous humour chamber than others found in the literature is used. Additionally, the simulations use more complex rheological models that better reproduce the viscoelastic VH gel and liquid behaviour measured experimentally in this work (for example, in all previous works the VH liquid phase is

modelled as a Newtonian fluid). The author believes that the methodology followed allows to obtain results that enhance the understanding of the actual VH behaviour in the eye.

This section presents a comparative study of the flow behaviour of both VH phases and the pharmacological fluids under study. Velocity and WSS profiles are presented and discussed for all the fluids under study, when subjected to a saccadic movement with amplitude $A = 40°$ (see details on Section 7.2.2).

It must be noted that the Giesekus model used to simulate the VH flow is mostly used in the simulation of viscoelastic liquids, and its applicability in the simulation of gel deformations is arguable. Nevertheless, as mentioned in Section 7.2.3, this model has been proven suitable for gel-like solutions [26,193–196]. Based on that, and the fact that the model provided a good fit to the experimental data, the Giesekus model was chosen for this study.

8.2.1 Velocity field

The velocity magnitude contours in the plane $z = 0$ for all the fluids under study are presented in Fig. 8.3. The vitreous cavity rotates anti-clockwise around the z axis. PFLCs present very low viscosities (at $T = 37$ °C, HPF8 has a viscosity of 4.85×10^{-4} Pa s and the viscosity of HPF10 is 3.57×10^{-3} Pa s), which means that the diffusive time scale is high and the velocity gradients occur primarily close to the walls. Considering the eye as a perfect sphere with a diameter of $D = 0.024$ m, the diffusive time scale can be estimated as $t_{diff} = \frac{\rho D^2}{\eta}$, and Table 8.1 presents the diffusive time scales computed for the pharmacological fluids under study. Note that the values are not accurate for the real geometry under study, but they still provide an indication of the differences in the diffusive time scales between the tested fluids. Comparing the two PFLCs under study, the diffusive time scale of the fluid HPF10 is much lower than that of HPF8 and the momentum diffuses faster in the vitreous cavity due to the HPF10 viscosity being much higher than the HPF8 viscosity. For both PFLC fluids, the lens indentation significantly affects the flow: for times $t = 0.1t_D$ and $t = t_p$ the velocity magnitude right behind the lens indentation is considerable when compared to the rest of the vitreous

cavity. Finally, it is possible to observe that for $t = 2t_D$, due to inertial effects, there is still fluid motion close to the walls.

The SiO-based fluids show a distinct velocity profile when compared to the PFLCs. Due to their high shear viscosity, the diffusive time scale is low (see Table 8.1) and for $t = t_p$ there is fluid motion all across the vitreous cavity, except at the centre. It is possible to consider that these fluids move similarly to a rigid body, where individual fluid particles display a rotational motion, without being significantly deformed. With the increase of the SiO viscosity, the momentum propagates faster in the vitreous cavity (see the velocity contours for $t = 0.1t_D$). For time $t = t_D$ there is almost no fluid motion in the vitreous cavity and the flow stops right after $t = t_D$. Based on the results presented in Fig. 8.3, it seems that the lens indentation affects the velocity magnitude contours of the SiO-based fluids mostly in the beginning of the movement.

From the analysis of Fig. 8.3, it is possible to observe two main differences between the flow behaviour of VH and the pharmacological fluids: for times $t = 0.1t_D$ and $t = t_p$, right behind the lens indentation, a region where the velocity magnitude is close to zero (in fact there is a recirculation of fluid in that area) is formed; and for times higher than $t = t_D$ there are considerable velocity gradients inside the vitreous cavity. Note that the recirculation of fluid behind the centre of the lens indentation occurs for all the fluids under study (not shown here); however, for SiO-based fluids and PFLCs that happens during a short period of time, while for both VH phases the recirculation lasts longer. The VH liquid phase initially shows a flow behaviour similar to HPF10. However, for $t \geq t_D$ the flow pattern changes significantly. For $t = 2t_D$ the fluid velocity magnitude reaches a value around 0.06 m/s, that is more than half of the maximum

Table 8.1. Diffusive time of all the pharmacological fluids under study, calculated considering the geometry as a perfect sphere with a diameter $D = 0.024$ m.

Fluid	Diffusive time scale (s)
HPF8	2090
HPF10	313
RS-Oil 1000	0.776
Densiron 68	0.565
Siluron 2000	0.327
Siluron 5000	0.122

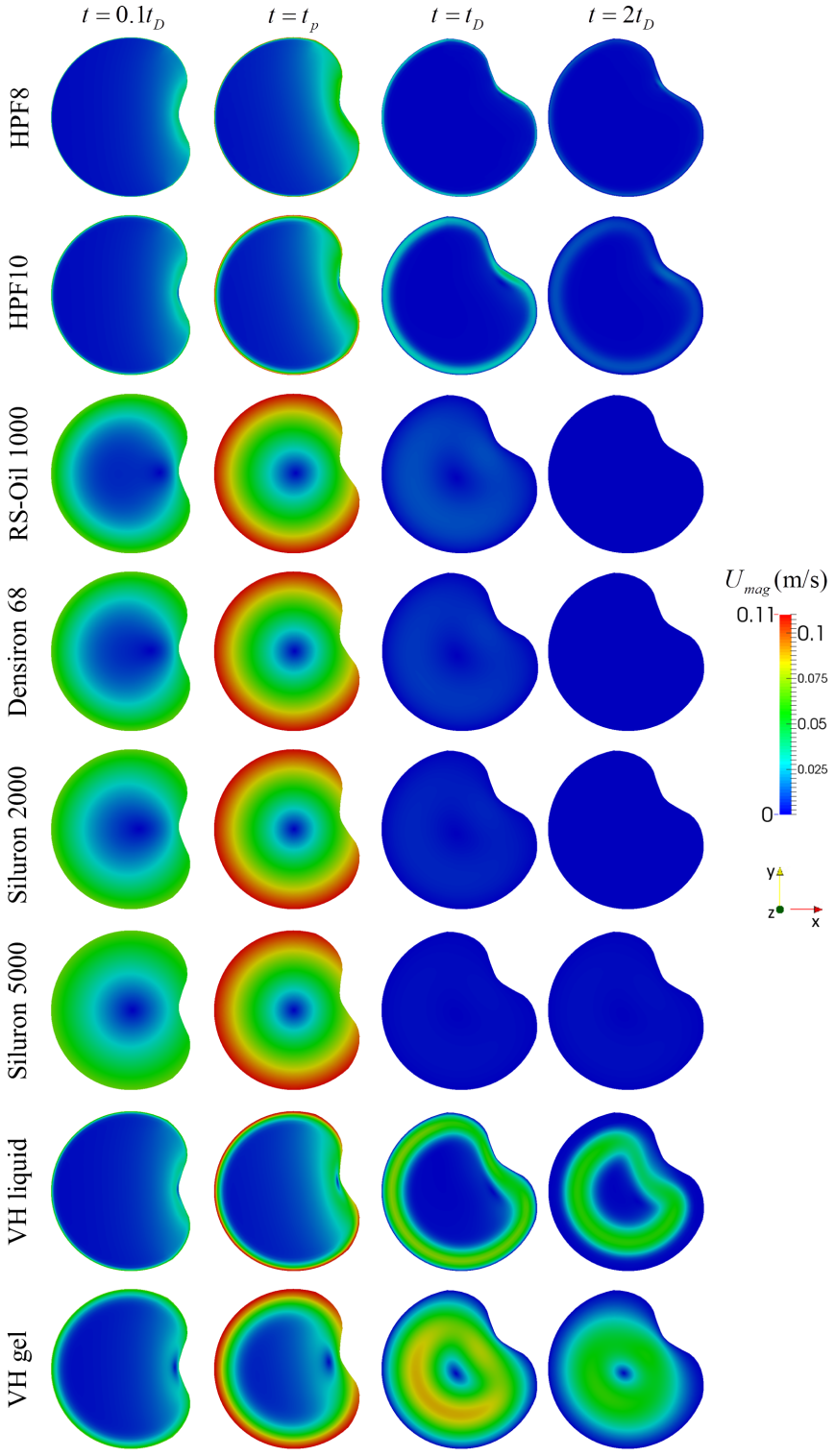

Figure 8.3. Velocity magnitude contour plots on the plane $z = 0$ for a saccadic movement with 40° displacement at times $t = 0.1t_D = 0.0125$ s, $t = t_p = 0.0375$ s, $t = t_D = 0.125$ s and $t = 2t_D = 0.25$ s, for all the fluids under study.

velocity reached at the walls at $t = t_p$. Even with obvious differences, the VH gel phase follows the same trend as the VH liquid phase, since for $t > t_D$ the flow motion inside the vitreous cavity is still considerable.

Note that a brief analysis of different cross-sections in the z-plane parallels to the one showed in Fig. 8.3 (not presented here) showed that in general, and for all the fluids under study, the velocity profiles follow similar trends to those observed in the central plane. Based on that, the velocity profile analysis and discussions in this section and following sections are based on the velocity in the midplane $z = 0$.

Due to their Newtonian behaviour, for $t > t_D$ the pharmacological fluids keep flowing in the same direction as the original flow, a consequence of inertia. However, it was expected that due to memory effects, VH would flow in the opposite direction of the movement (recoil). In Fig. 8.4, the velocity vectors are superimposed onto the velocity contours for both VH phases at times $t = t_D$ and $t = 2t_D$. The numerical results show that the VH liquid phase does not show significant memory effects, as the flow keeps the original direction (inertial effects are more significant than elastic effects), while the VH gel phase shows considerable memory effects as the flow happens in the opposite direction (elastic effects are dominant).

Abouali *et al.* [25] also studied the flow behaviour of three different Newtonian fluids when subjected to saccadic movements with amplitudes between $A = 10°$ and $50°$. Their geometry was a simplified vitreous cavity and did not show the complexity of the vitreous cavity studied here. Nevertheless, for a saccadic movement of $A = 50°$ the flow behaviour of water and a SiO with a shear viscosity of 0.97 Pa s followed the same trend as the results presented here.

As discussed in Chapter 4, the VH gel phase has the closest properties to those of the VH in its natural environment. Therefore, a pharmacological fluid with the goal to be used as a permanent VH substitute should have flow properties similar to the VH gel phase. Overall, the velocity contour results show that both PFLCs and SiO-based fluids exhibit a distinct flow behaviour from that predicted for the VH gel phase.

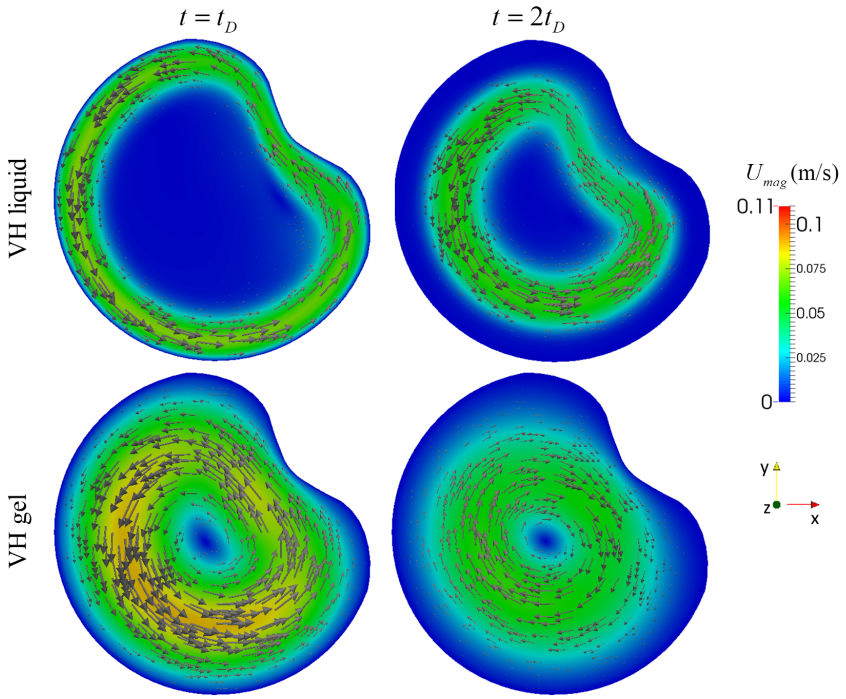

Figure 8.4. Velocity magnitude contours with vectors (grey arrows) on the plane $z = 0$ for a saccadic movement with 40° displacement at times $t = t_D = 0.125$ s and $t = 2t_D = 0.25$ s, for VH liquid and gel phases.

8.2.2 Wall shear stress

The time variation of the average WSS, WSS_{ave}, for all the fluids under study is presented in Fig. 8.5. Note that for both VH phases and for Siluron 2000 fluid the WSS include both the Newtonian and polymeric components. Additionaly, the time and value of the peak WSS_{ave} reached by each fluid is presented in Table 8.2. For the SiO-based fluids, the peak WSS_{ave} occurs in the beginning of the movement for $t < 0.1t_D$, and these fluids present the highest values, between 7.78 Pa for RS-Oil 1000 and 10.81 Pa for Siluron 5000. All the SiOs present their lowest WSS_{ave} at $t = t_p$, or right after that time. The PFLCs present the peak WSS_{ave} for $t > 0.1t_D$, with HPF10 presenting the highest value of the PFCLs (0.92 Pa). VH liquid and gel phases reach the peak WSS_{ave} for times $t = 0.0237$ s and $t = 0.0197$ s, respectively.

The WSS contours of all the fluids under study for a saccadic movement of $A = 40°$ are presented in Fig. 8.6. Due to the high WSS values reached in the beginning of

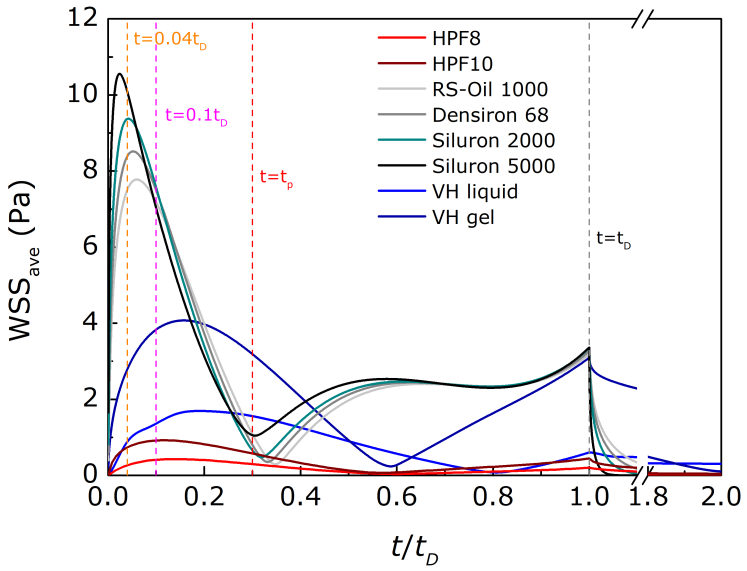

Figure 8.5. Time variation of the average WSS on the vitreous cavity for a saccadic movement of 40°, for all the fluids under study.

the movement with the SiO-based fluids, the WSS contours for $t = 0.04t_D$ are also presented. Note that due to the differences in the maximum WSS values, three different scales were used. The results show that, for all the fluids, the maximum values of WSS occur around the centre of the lens indentation. The PFLCs show an interesting WSS profile along the lens indentation, with higher values concentrated along the z axis reaching the outer area of the lens indentation (see the figures at $t = 0.04t_D$ and $t = 0.1t_D$), while all the other fluids show a constant WSS in the region around the

Table 8.2. Peak WSS_{ave} during a saccadic movement with 40° displacement.

Fluid	time (s)	Peak WSS_{ave} (Pa)
HPF8	0.0180	0.43
HPF10	0.0140	0.92
RS-Oil 1000	0.0075	7.78
Densiron 68	0.0065	8.52
Siluron 2000	0.0053	9.38
Siluron 5000	0.0030	10.56
VH liquid phase	0.0237	1.70
VH gel phase	0.0197	4.07

lens indentation. For $t = t_p$, the PFLCs also show WSS contours lower in one side of the indentation ($y < 0$) than in the other ($y > 0$). The maximum WSS obtained for the HPF8 fluid is around 0.8 Pa, while the HPF10 fluid presents a maximum WSS of approximately 1.5 Pa. From all the fluids under study, SiO-based fluids show the higher WSS values. Siluron 5000 fluid reaches a maximum WSS in the centre of the lens indentation around 30 Pa, while RS-Oil 1000 reaches a maximum WSS around 18 Pa. VH gel phase shows higher values of WSS when compared with VH liquid phase, and curiously for $t = 0.1t_D$ the average WSS is higher than for $t = t_p$. However, the maximum WSS in the lens indentation occurs at $t = t_p$. For $t = 2t_D$, all the fluids show WSS contours very close to zero.

In the study performed by Abouali *et al.* [25], the WSS contours are presented for water, glycerol and a SiO, and the values are in agreement with the ones presented here. However, in their study the WSS contours in the borders of the lens indentation show considerable differences when compared to the values inside and outside the lens indentation (see Fig. 6.5). Such phenomenon seems to be a consequence of the geometry in that area. Here, the geometry used presents a smoother transition between the lens indentation and the rest of the vitreous cavity, and no discrepancy was found between the WSS values on that area and in the neighbour areas.

As explained in the beginning of this section, the pharmacological fluids are mostly used in eye surgery to reattach the retina or close retinal tears that are created in the VH fluid as a consequence of the degradation of the collagen and HA structures. The forces generated between the fluid and the retina are key to keep the retina in its proper position. The VH liquid phase shows WSS values much lower than VH gel phase, which may explain the increase of cases of RD and RT with VH liquefaction. It seems that the stresses generated by VH liquid phase on the vitreous cavity walls are not enough to keep the retina in its proper position. The PFLCs present WSS values much lower than the VH gel phase, which might compromise their effectiveness to reattach the retina or eliminate retinal tears. In fact, as explained in Chapter 2, the use of these fluids in eye surgery is rare, as SiO-based fluids are the main choice for the treatment of RD and RT. The SiO-based fluids present WSS values much higher than VH gel phase, which seems

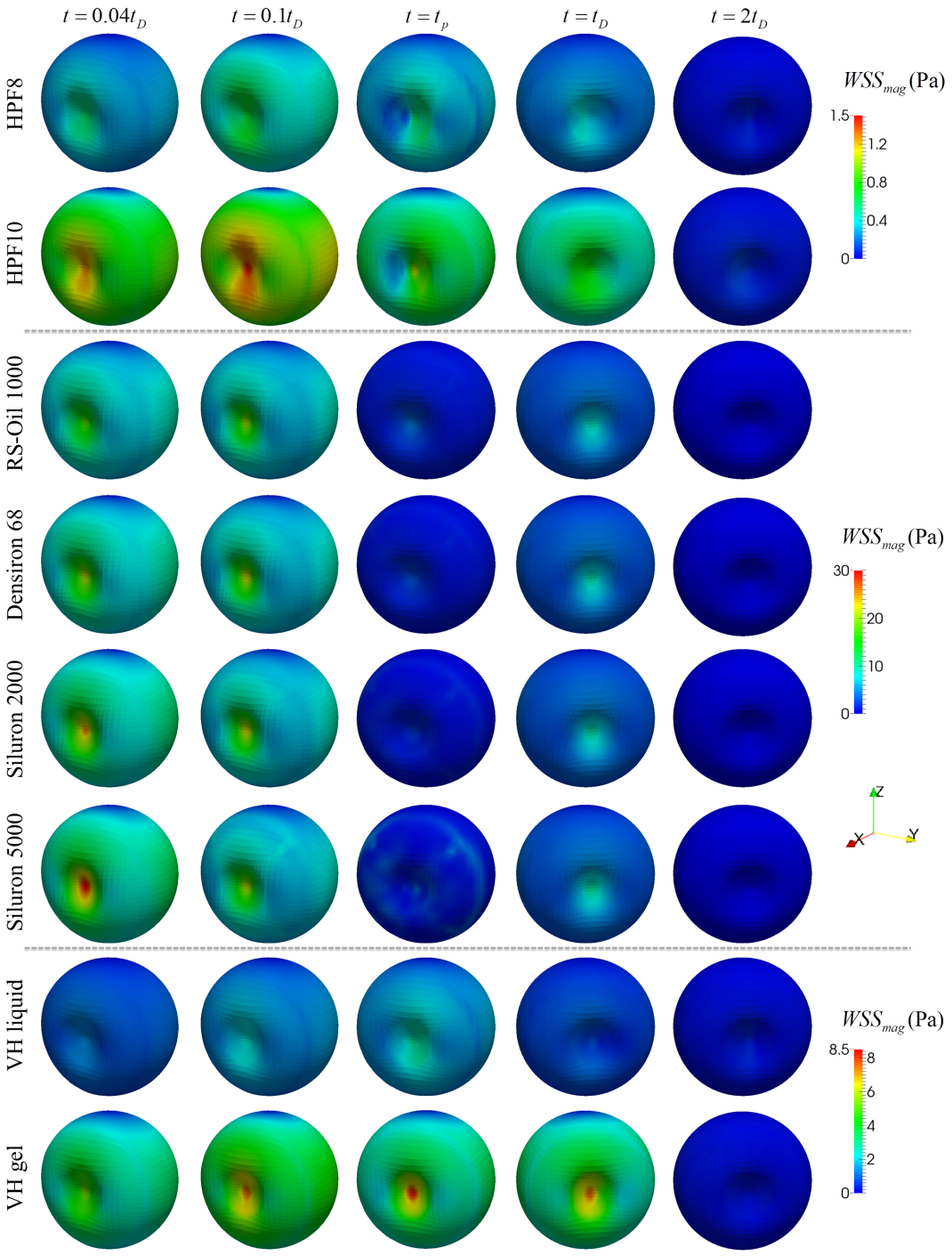

Figure 8.6. Wall shear stress contours for a saccadic movement with 40° displacement at times $t = 0.04t_D = 0.005$ s, $t = 0.1t_D = 0.0125$ s, $t = t_p = 0.0375$ s, $t = t_D = 0.125$ s and $t = 2t_D = 0.25$ s, for all the fluids under study.

appropriate to reattach the retina, as higher forces will pull and keep the retina in its proper position. However, it can be found in the literature that the use of SiO-based fluids for long periods often leads to complications such as cataracts, glaucoma, and corneal damage among others [18, 49, 200]. Since the WSS values produced by the SiO are much higher than the ones produced by VH gel phase, a long exposure of the retina to these fluids could be responsible for corneal and retina damage. From a mechanical point of view, a fluid with a similar behaviour as VH gel phase, that would be able to produce stresses in the walls with similar magnitudes as the ones produced by VH gel phase, would be ideal to be used as a permanent VH substitute.

8.3 Impact of different degrees of movement

A comparison of the velocity magnitude and WSS contours for different saccadic movement amplitudes, $A = 10$, 20, 30 and 40°, are presented in this section. Results for HPF10, Siluron 2000, VH gel phase and VH liquid phase fluids are shown. Due to the similarities between HPF10 and HPF8, and among the SiO-based fluids, the results for HPF8, RS-Oil 1000, Densiron 68 and Siluron 5000 fluids are not presented here, but can be found in Appendix A.

8.3.1 Velocity field

The velocity contours when the vitreous cavity is subjected to different degrees of movement, A, are presented in Fig. 8.7, Fig. 8.8, Fig. 8.9 and Fig. 8.10, for HPF10, Siluron 2000, VH liquid phase and VH gel phase, respectively. As discussed in Section 8.2.1, the velocity contours show significant differences between those fluids; however, the same trend is observed for all the fluids when comparing different degrees of movement. With the increase of the saccadic movement amplitude, A, the angular velocity applied in the vitreous cavity walls also increases (see Fig. 7.3) and, consequently, the velocities reached in the vitreous cavity increase. The momentum diffusion of the fluid across the vitreous cavity also increases, and the more considerable differences between different degrees of movement can be found in the VH gel phase (see Fig. 8.10). For times $t = t_D$

and $t = 2t_D$, the portion of VH gel that exhibits very little deformation (in the centre of the cavity) decreases significantly with the increase of the saccadic amplitude, A, which is due to the higher elastic effects (higher Wi) observed at higher amplitudes, causing an increase of the fluid memory effects. As described before, the VH gel phase is a network composed of collagen and HA molecules, and when subjected to deformation the molecules adjust their conformation. This rearrangment will eventually cause degradation of the molecules for higher deformations. Therefore, the fact that the amount of VH gel in motion inside the vitreous cavity increases significantly with the increase of the saccadic amplitude leads the author to believe that larger saccades affect more the VH degradation than smaller saccades.

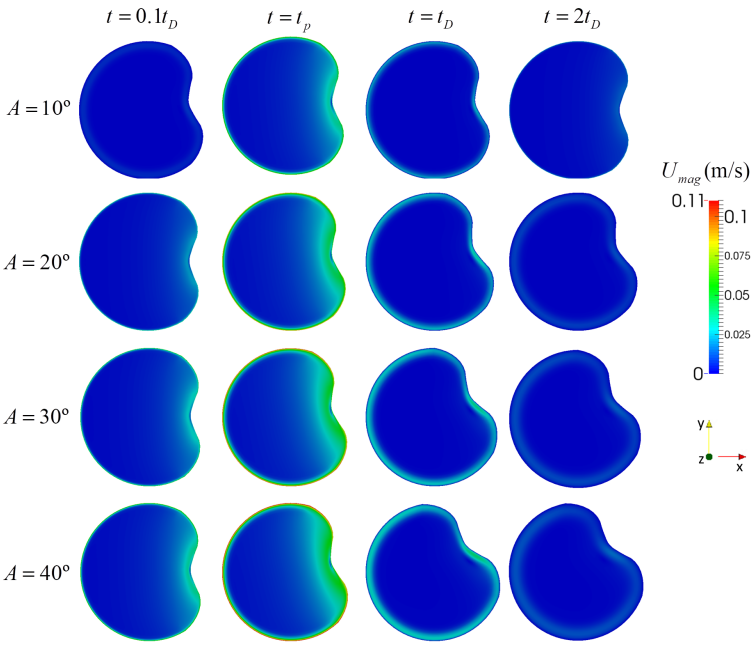

Figure 8.7. Velocity magnitude contours on plane $z = 0$ for saccadic movements of 10, 20, 30 and 40° displacement and times $t = 0.1t_D$, $t = t_p$, $t = t_D$ and $t = 2t_D$, for HPF10 fluid.

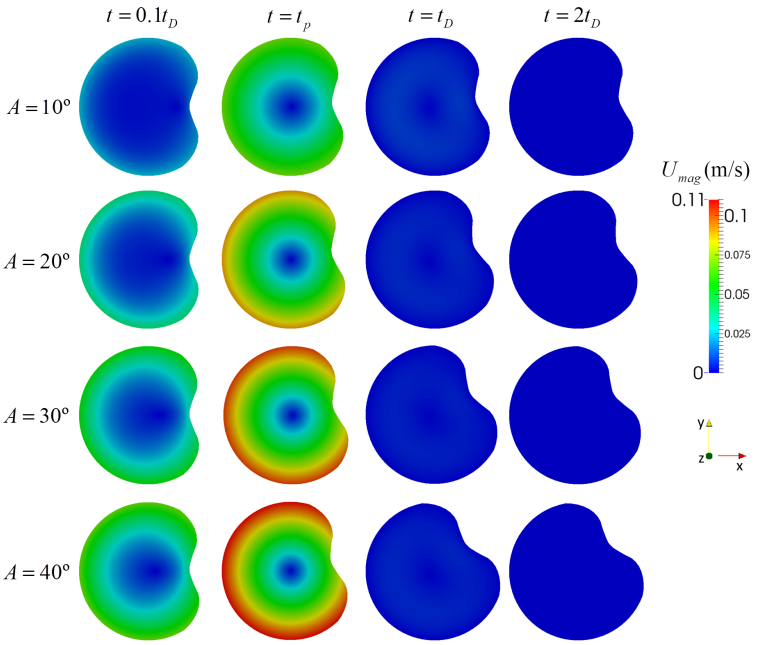

Figure 8.8. Velocity magnitude contours on plane $z = 0$ for saccadic movements of 10, 20, 30 and 40° displacement and times $t = 0.1t_D$, $t = t_p$, $t = t_D$ and $t = 2t_D$, for Siluron 2000 fluid.

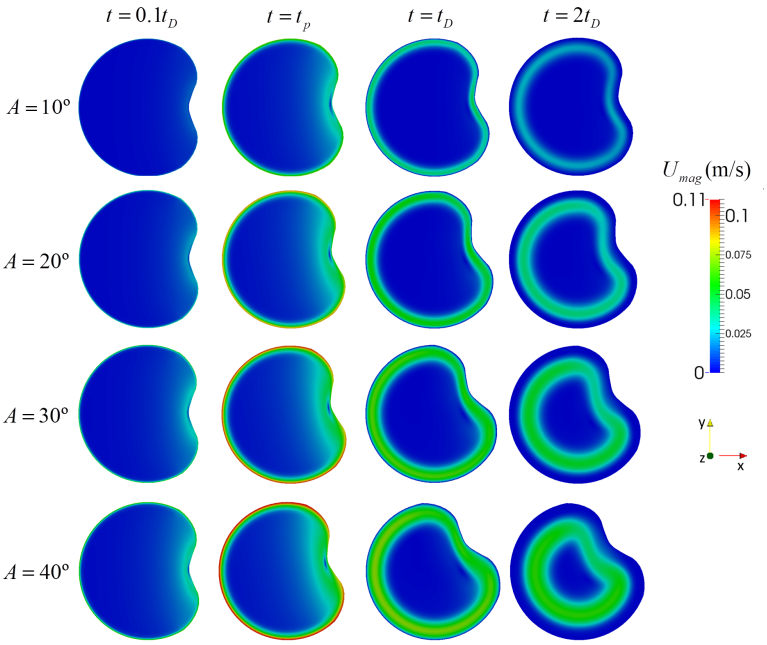

Figure 8.9. Velocity magnitude contours on plane $z = 0$ for saccadic movements of 10, 20, 30 and 40° displacement and times $t = 0.1t_D$, $t = t_p$, $t = t_D$ and $t = 2t_D$, for VH liquid phase.

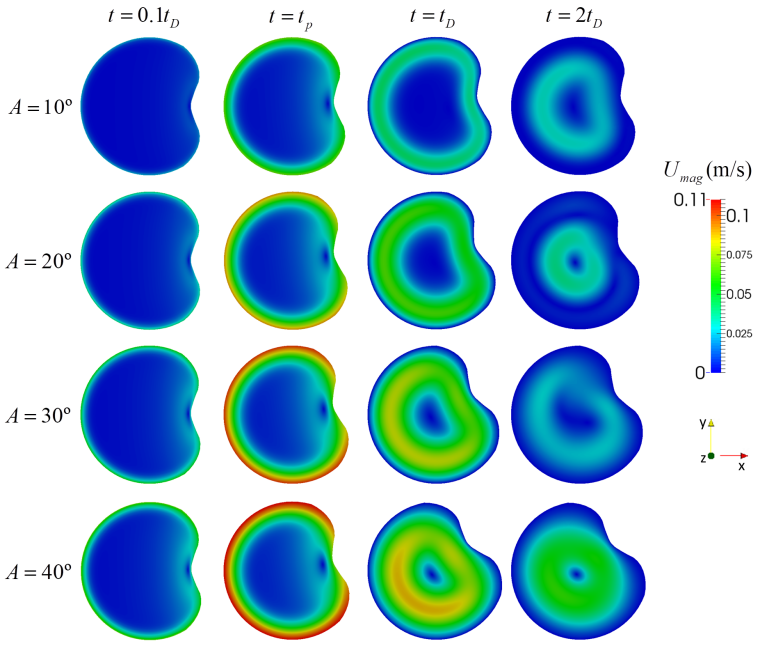

Figure 8.10. Velocity magnitude contours on plane $z = 0$ for saccadic movements of 10, 20, 30 and 40° displacement and times $t = 0.1t_D$, $t = t_p$, $t = t_D$ and $t = 2t_D$, for VH gel phase.

8.3.2 Wall shear stress

Unlike the velocity field analysis, not all fluids investigated in this section follow the same WSS pattern while comparing different degrees of movement. Therefore, an individual analysis of the WSS patterns for each fluid will be performed.

The time variation of the average WSS in the vitreous cavity and the WSS contours for HPF10 fluid, for different degrees of movement and at different times, are shown in Fig. 8.11 and Fig. 8.12, respectively. The numerical results show that the peak WSS_{ave} increases with the increase of the saccadic amplitude up to a maximum of 0.92 Pa for a saccadic movement with amplitude $A = 40°$. Also, with the increase of the saccadic movement amplitude, the peak value of WSS_{ave} is reached faster. After reaching the peak value, for times between $t = 0.1t_D$ and $t = t_p$, WSS_{ave} decreases to a minimum, and by the end of the saccadic movement it increases again reaching a similar value for all the amplitudes studied. For $t > t_D$ the WSS_{ave} follows the same trend and values for all the amplitudes under study. From the analysis of Fig. 8.12, it is possible to observe that for $t = t_p$ the region of the lens indentation where $y > 0$ shows higher WSS values

than the $y < 0$ region, for all the degrees of movement under study.

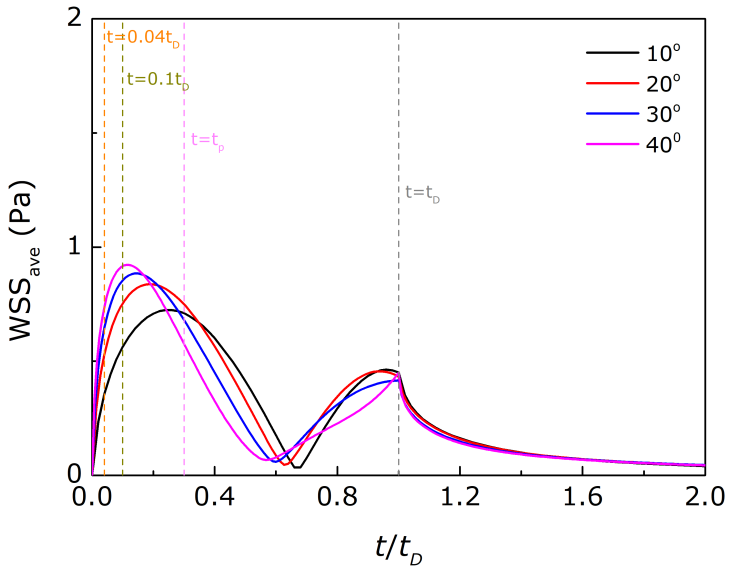

Figure 8.11. Time variation of the average WSS on the vitreous cavity for diplacements of 10, 20, 30 and 40°, for HPF10 fluid.

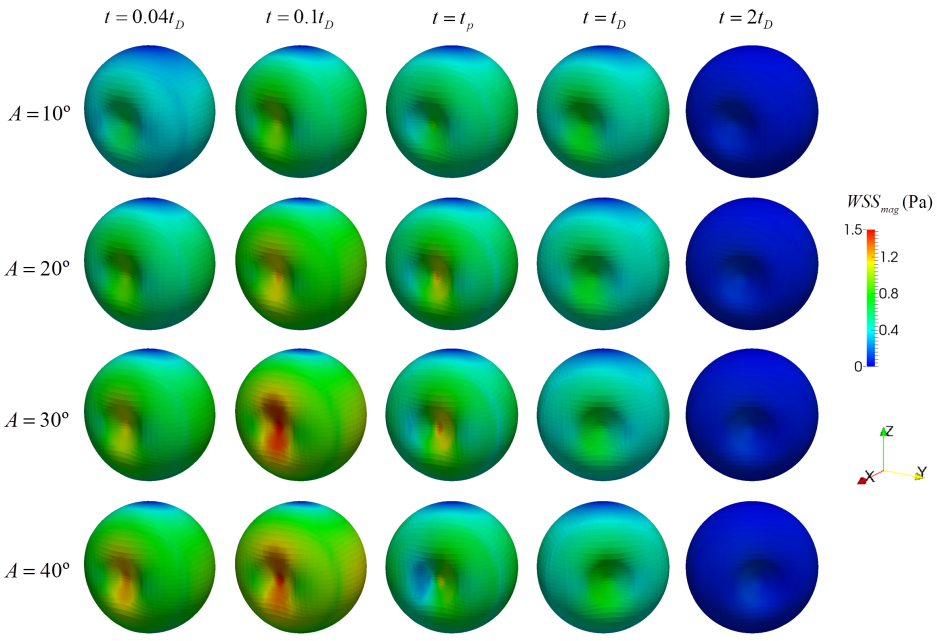

Figure 8.12. Wall shear stress contours on the vitreous cavity for for saccadic movements of 10, 20, 30 and 40° displacement and times $t = 0.04t_D$, $t = 0.1t_D$, $t = t_p$, $t = t_D$ and $t = 2t_D$, for HPF10 fluid.

Fig. 8.13 and Fig. 8.14 show the time variation of WSS_{ave} in the vitreous cavity and the WSS contours for Siluron 2000 fluid, for different degrees of movement and at different times. For $t < t_p$, WSS_{ave} follows the same trend as observed for the HPF10 fluid, but the values are around ten times higher. However, significant differences can be found for the second WSS_{ave} peak: the movement with an amplitude of $A = 10°$ shows a larger WSS_{ave} peak than all the other movement amplitudes tested. Movements with amplitude $A = 20$ and $30°$ follow the same trend as the saccadic movement with $A = 10°$; however, a different profile is obtained for a movement with $A = 40°$. The difference in the WSS_{ave} profiles may be related to the saccadic profile applied (see Section 7.2.2), as small saccades are characterised by a quasi-symmetric profile, while for higher saccadic amplitudes the deviations from a symmetric profile are considerable, and especially for a saccadic movement with $A = 40°$ the velocity profile in the final stages of the movement follows a different trend than all the other amplitudes tested. For all the amplitudes of movement studied, the maximum WSS is reached in the centre of the lens indentation and a smooth transition between the lens indentation area and the rest of the vitreous cavity is observed.

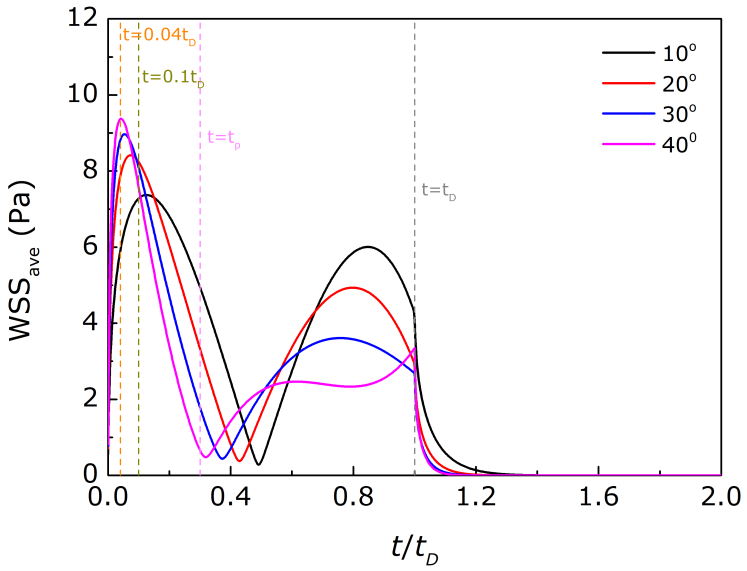

Figure 8.13. Time variation of the average WSS on the vitreous cavity for diplacements of 10, 20, 30 and 40°, for Siluron 2000 fluid.

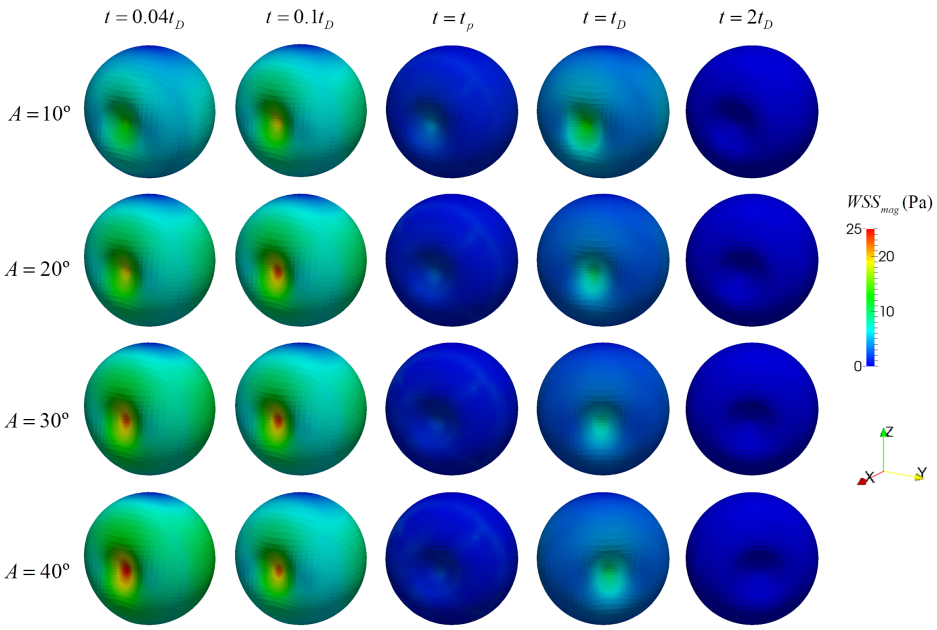

Figure 8.14. Wall shear stress contours on the vitreous cavity for for saccadic movements of 10, 20, 30 and 40° displacement and times $t = 0.04t_D$, $t = 0.1t_D$, $t = t_p$, $t = t_D$ and $t = 2t_D$, for Siluron 2000 fluid.

The time variation of WSS_{ave} on the vitreous cavity and the WSS contours for VH liquid phase, for different degrees of movement, are presented in Fig. 8.15 and Fig. 8.16. The response to the different degrees of movement follows the same trend: with the increase of the movement amplitude, the first peak of the WSS_{ave} occurs faster and the corresponding values are higher (the WSS_{ave} peak for a movement of $A = 40°$ is 1.7 Pa, while for $A = 10°$ is 1.2 Pa); the second peak occurs for $t \approx t_D$ and again larger saccades lead to higher WSS_{ave} values. After $t = t_D$, WSS_{ave} starts decreasing, but for $t = 2t_D$ the value is still not zero. Similarly to HPF10, for $t = t_p$, VH liquid phase presents higher WSS values in the region of the lens indentation where $y > 0$ than in the $y < 0$ region. (see Fig. 8.16). However, the opposite trend is observed for $t = t_D$.

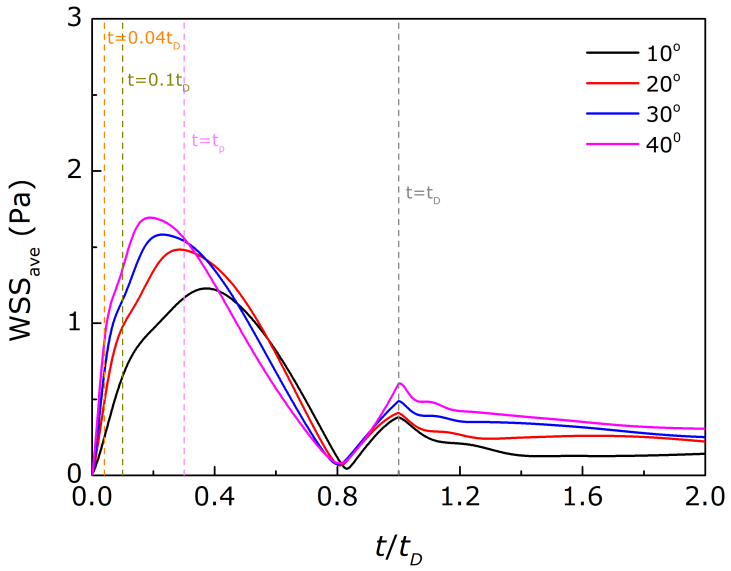

Figure 8.15. Time variation of the average WSS on the vitreous cavity for diplacements of 10, 20, 30 and 40°, for VH liquid phase.

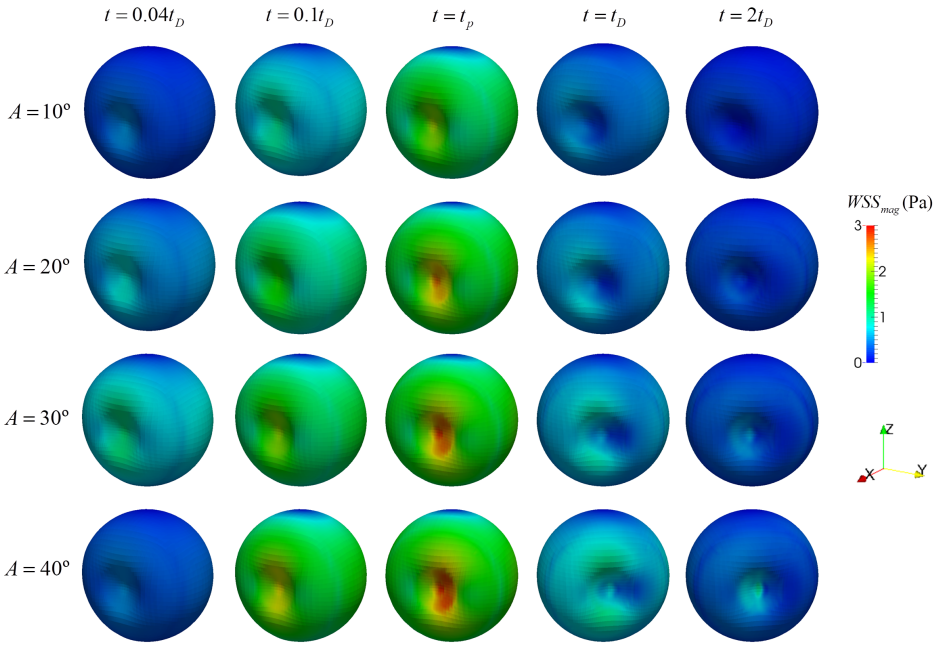

Figure 8.16. Wall shear stress contours on the vitreous cavity for for saccadic movements of 10, 20, 30 and 40° displacement and times $t = 0.04t_D$, $t = 0.1t_D$, $t = t_p$, $t = t_D$ and $t = 2t_D$, for VH liquid phase.

Finally, the WSS_{ave} time variation and the WSS contours for VH gel phase are presented in Fig. 8.17 and Fig. 8.18, for different degrees of movement. For $t < t_D$, and for the different saccadic movement amplitudes, the WSS_{ave} time variation follows the same trend as described for the VH liquid phase. However, for $t > t_D$ it is possible to observe that for the larger saccades the average WSS decreases faster, and curiously for $t = 2t_D$ it is close to zero for a movement with an amplitude of $A = 40°$. That fact is better seen in Fig. 8.18, since for $t = 2t_D$ it is possible to observe considerable WSS in the centre of the lens indentation for $A = 10$, 20 and 30°, but not for $A = 40°$. Analysing Fig. 8.18, it is also possible to observe that for all the degrees of movement the maximum WSS values are reached in the centre of the lens indentation.

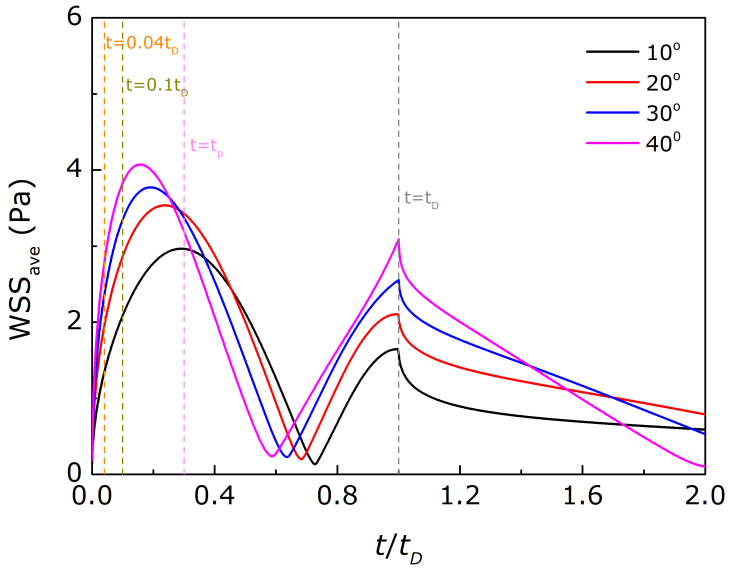

Figure 8.17. Time variation of the average WSS on the vitreous cavity for diplacements of 10, 20, 30 and 40°, for VH gel phase.

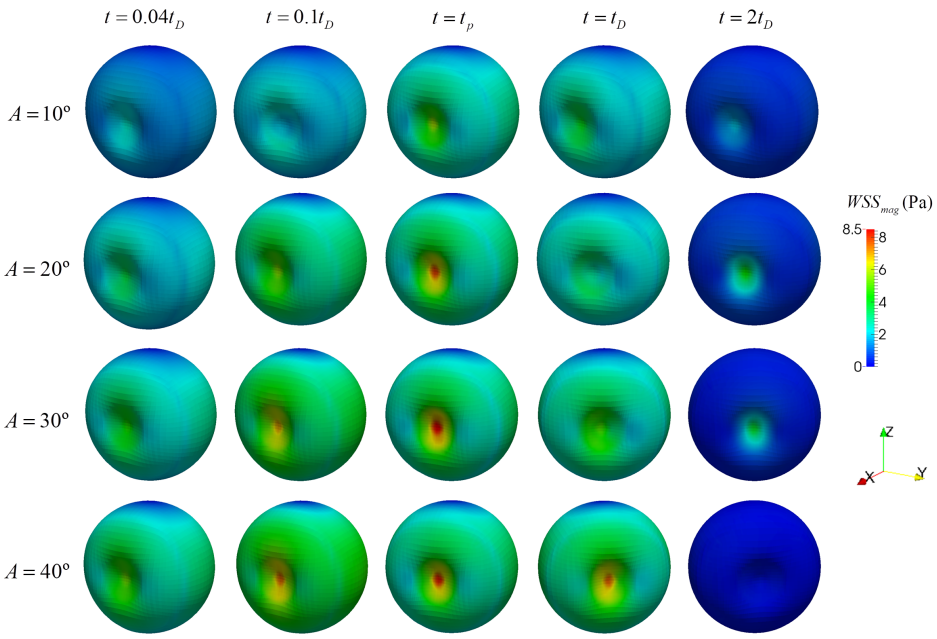

Figure 8.18. Wall shear stress contours on the vitreous cavity for for saccadic movements of 10, 20, 30 and 40° displacement and times $t = 0.04t_D$, $t = 0.1t_D$, $t = t_p$, $t = t_D$ and $t = 2t_D$, for VH gel phase.

In general, the results show that for all the fluids, increasing the amplitude of the saccadic movement increases the WSS_{ave} and magnitude values.

8.3.3 Conclusions

The main goal of this chapter was to quantify the differences in the flow behaviour between VH and the pharmacological fluids under study, and also the differences between VH gel and VH liquid phases. To this end, a detailed numerical study comparing the flow behaviour of different VH phases and the pharmacolgical fluids under study was performed.

Results show that VH gel and liquid phases have distinct flow behaviour and the WSS values produced by the VH gel phase are more than the double than the ones generated by the VH liquid phase. Such difference may play an important role in RD and RT diseases, as the stresses applied to the walls may not be enough to keep the retina in its proper position.

PFLCs and SiO show distinct flow behaviour between them and also distinct flow

behaviour when compared with VH. In fact, all the SiO present WSS much higher than VH gel phase, while PFLCs present lower values. None of those pharmacological fluids are able to mimic VH gel phase flow behaviour. The author of this work believes that a fluid with the aim of being used as a permanent VH substitute needs to properly mimic the VH flow behaviour. The eye is constantly subjected to fast movements, among other movements, and finding a fluid that presents a similar behaviour with similar velocities and WSS magnitudes as VH gel phase (the healthy VH conformation) is key to find a permanent VH substitute.

This chapter also presented a comparison between the Siluron 2000 flow behaviour simulated as a low elasticity viscoelastic fluid and as a Newtonian fluid. The results showed that since the elastic component of the fluid is weak, only minor differences were observed in the velocity and WSS profiles. Therefore, it seems that during usual saccadic eye movements, the elastic component of Siluron 2000 fluid does not generate significant stresses due to elasticity and a behaviour similar to that of all the other SiO-based fluids that present a Newtonian rheology is observed.

"It is good to have an end to journey toward; but it is the journey that matters, in the end."

Ernest Hemingway

Chapter 9

Conclusions and Future work

9.1 Thesis conclusions

The work developed in this thesis contributed to a better understanding of the rheological and flow behaviour of VH and pharmaceutical replacement fluids. For this purpose, this research work was divided in two main parts with specific objectives: in the first part, an extensive experimental rheological study was performed using the VH fluid from rabbit eyes and fluids used in eye surgery; the second part presents the numerical study of the flow of VH and pharmacological fluids during saccadic eye movements.

9.1.1 Experimental studies

The first part of this thesis focused on the rheological characterisation of the biofluid VH from rabbit eyes and pharmacological fluids used in eye surgery.

VH biofluid is an avascular fluid that is generated during the embryonic stage and is never replaced during lifetime. It has been observed that in adults and elder people, two distinct VH phases are found in the eye: a liquid and a gel phase. The study of the different phases of VH is key to understand the differences in VH properties originating from the liquefaction process. To the best of the author's knowledge, there are no rheological studies in the literature that investigate both phases separately. A better insight of the VH rheological properties is crucial for the improvement and development of new VH substitutes to be used in eye surgery, which can mimic its mechanical functionality.

A systematic rheological study, under shear and extensional flow, of both phases was performed separately. Results show that both VH phases present viscoelastic behaviour, with significant differences in the degree of elasticty: SAOS experiments showed that VH gel is characterised by a strong solid-like behaviour, while VH liquid phase shows a weaker solid-like behaviour. Those results were confirmed by creep experiments, and for the gel phase it was possible to distinguish an elastic region, followed by a delayed elastic region until steady-state was reached. Creep measurements with the VH liquid phase showed the typical behaviour of a weak elastic fluid. Extensional rheological experiments were only performed with the VH liquid phase, and an average relaxation time of $\lambda = 9.7$ ms was measured.

In order to quantify the rheological differences between the VH gel phase and fluids used in eye surgery, six pharmacological fluids (two PFLCs and 4 SiO-based fluids) were tested under shear and extensional rheological experiments, and the surface and interfacial tension were measured. The results obtained show that all the pharmacological fluids show a distinct rheological behaviour when compared with VH gel phase. The PFLCs behave as Newtonian fluids with viscosity values close to that of water. All the SiO-based fluids also behave as Newtonian fluids, except Siluron 2000, which under extensional flow presented a relaxation time of $\lambda = 6.8$ ms. Siluron 2000 is a mixture of 95% of PDMS with a viscosity of 1 Pa s and 5% of PDMS with a viscosity of 2500 Pa s, and the HMW molecules provide elastic properties to the fluid. The IFT between the pharmacological fluids and the VH liquid phase extracted from rabbit eyes were also measured. The average ITF values measured are between 28.3 mN/m for Siluron 5000 and 34.0 mN/m for HPF8. The fact that the pharmacological fluids under study present a distinct rheological behaviour compared to VH can be one of the causes why they cannot be used as a permanent VH substitute and therefore their behaviour during saccadic eye movements is different.

9.1.2 CFD studies

In order to assess how the rheological differences between both VH phases and the pharmacological fluids under study affect the flow behaviour of the fluids, when the

eyes are subjected to saccadic movements, numerical simulations of the fluid flow were performed in a realistic vitreous chamber cavity subjected to saccadic movements of different amplitudes.

In the numerical work, in order to study the fluid flow behaviour, appropriate rheological models were chosen to fit the experimental rheological data obtained in the first part of this thesis. The Giesekus model was used to fit both VH phases rheological behaviour; the PFLCs fluids were simulated as Newtonian fluids; RS-Oil 1000, Densiron 68 and Siluron 5000 were simulated as Newtonian fluids; and Siluron 2000 fluid rheology was fitted with the Oldroyd-B model with solvent viscosity ratios $\beta = 0.98$ and $\beta = 0.95$, and was also simulated as a Newtonian fluid for comparison.

Firstly, numerical simulations with Siluron 2000 fluid showed that due to its low elasticity, only minor differences were found in the velocity magnitude and average WSS between the simulations performed with the Oldroyd-B model and the Newtonian model. It seems that for the typical saccadic eye movements, the deformation rates are not large enough for the low elasticity of this fluid to change significantly its flow behaviour.

The numerical results also showed that VH liquid phase presents a distinct behaviour from VH gel phase. In the liquid phase, the elasticity and the viscosity are lower than in the gel phase and consequently the flow behaviour changes. The most important difference is the fact that the WSS produced by the VH gel phase is more than the double of the values generated by VH liquid phase: for a saccadic movement with an amplitude $A = 40°$, the VH gel phase can reach an average WSS along the vitreous cavity of 4.07 Pa, while the maximum average WSS obtained for the VH liquid phase was 1.70 Pa. This difference may play an important role in RD phatologies.

None of the pharmacological fluids tested can mimic adequately the rheological behaviour of VH gel phase. The fact that their rheology and consequent flow behaviour are distinct from the VH gel phase behaviour shows, from a mechanical point of view, why they cannot be used as a permanent substitute. Additionally, the fact that SiO-based fluids show significantly higher wall shear stresses than VH gel phase can explain why a long exposure of those fluids in the eye is associated with complications such as

corneal and retinal damage.

Finally, the study of the effect of different degrees of movement shows that larger saccadic movements produce higher velocity gradients inside the vitreous cavity and also higher values of WSS.

9.2 Future work

Important results for a better understanding of the rheological and flow behaviour of VH, as well as common replacement fluids used in eye surgery, were produced during this work. Nevertheless, further work in the area needs to be conducted in order to fill the medical need for approriate fluids to be used as permanent VH substitutes. Given the current scenario, future work both from an experimental and numerical approaches are proposed.

There is a considerable range of polymers that were tested over the years with the goal of being used as a permanent VH substitute. Even if some of the fluids previously studied show biocompatibility, good tamponade effect, transparency, or have buffer capacity, somehow until now they have all failed to work as a permanent VH substitute. The author believes that the lack of understanding of the rheological properties of those formulations leads to solutions with rheological properties significantly different from the real VH, which can be an important factor for the failure of the proposed formulations. Furthermore, a rheological characterisation of the new VH analogues, which have already shown promising results from a physiological point of view, is crucial. Adjusting the rheology of those polymeric solutions/hydrogels, so they can match the VH rheological behaviour, would be important for their success as a permanent VH substitute.

The rheological properties of the interface created by the contact between the VH analogues and VH must also be investigated. Interfacial rheology is a growing research topic, and interfacial rheology experiments would be crucial to a better understanding of the properties in the interface between VH and VH substitutes. Interfaces between two fluids are often made to deform and the relationships between the associated surface

stresses, strains, and strain rates are nontrivial and must be studied. This will provide important information for the fluid replacement during surgery.

For all the new fluids previously mentioned, numerical simulations of their flow behaviour in the eye cavity must be done to quantify and compare it to the VH behaviour. It is essential to know how the different fluids respond when subjected to common eye movements. Moreover, the numerical study of VH flow behaviour when in contact with the pharmacological substitutes would be of great interest. A two-phase solver that would be able to accurately investigate two-phase flows related to non-Newtonian fluids would be necessary. The two-phase simulations between VH and the pharmacological fluids under study in this work can be important to quantify the stresses in the interface and quantify the fluid deformation in the interface. Finally, for the new VH formulations, two-phase flow simulations could be used as a predictive tool to aid the understanding of how those fluids will interact with VH biofluid when subjected to typical saccadic eye movements.

Appendix A

Impact of different degrees of movement

The study of the impact of different degrees of movement in the flow behaviour was performed for all the fluids under study. The SiO based fluids show similar behaviour between them. The same is found for the PFLCs. Based on that, in Section 8.3 only the results for the Siluron 2000 and HPF10 fluids were presented. Here, the velocity profiles in the midplane $z = 0$, the time variation of the average WSS, and the WSS on the vitreous cavity walls are presented for the fluids HPF8, RS-Oil 1000, Densiron 68 and Siluron 5000.

A.1 HPF8 fluid

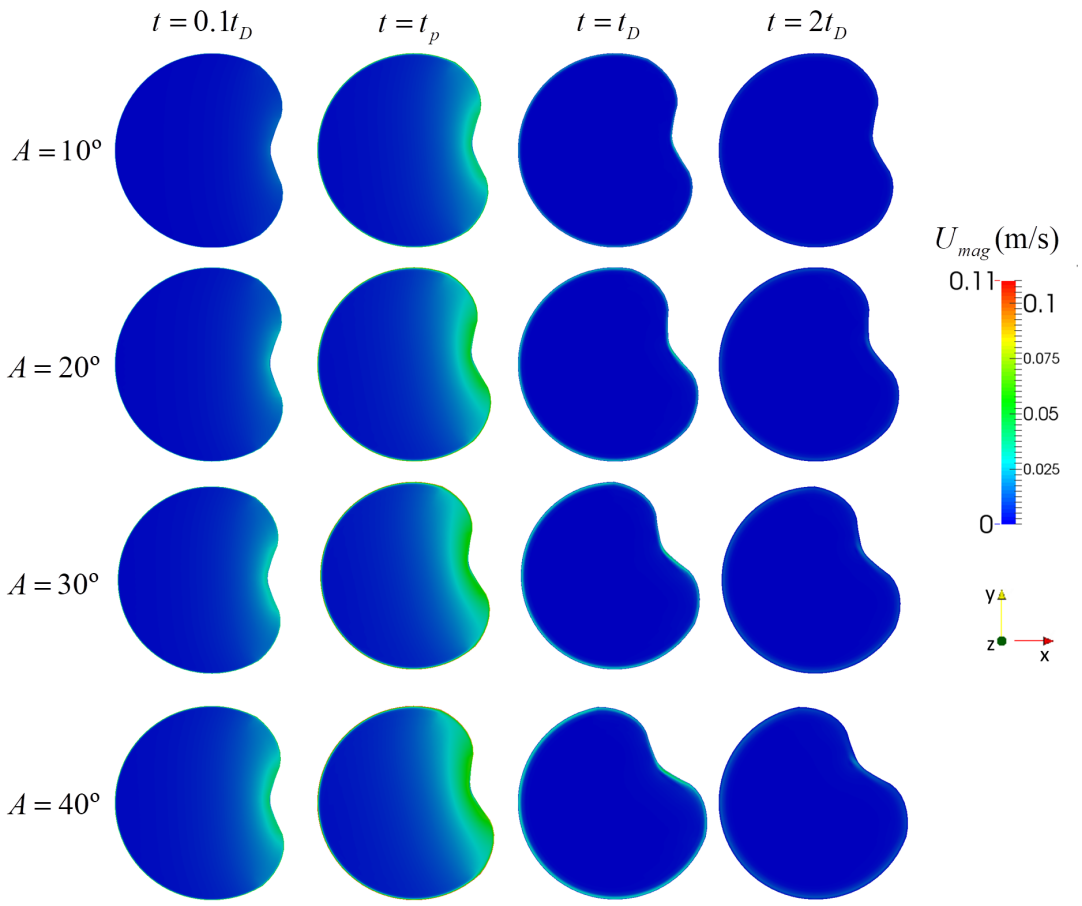

Figure A.1. Velocity magnitude contours on plane $z = 0$ for saccadic movements of 10°, 20°, 30° and 40° displacement, at times $t = 0.1t_D$, $t = t_p$, $t = t_D$ and $t = 2t_D$, for HPF8 fluid.

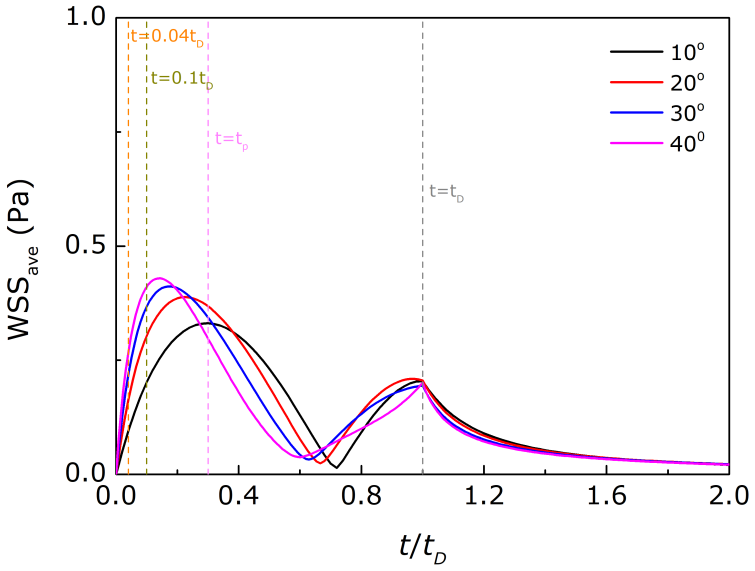

Figure A.2. Time variation of the average WSS on the vitreous cavity for diplacements of 10, 20, 30 and 40°, for HPF8 fluid.

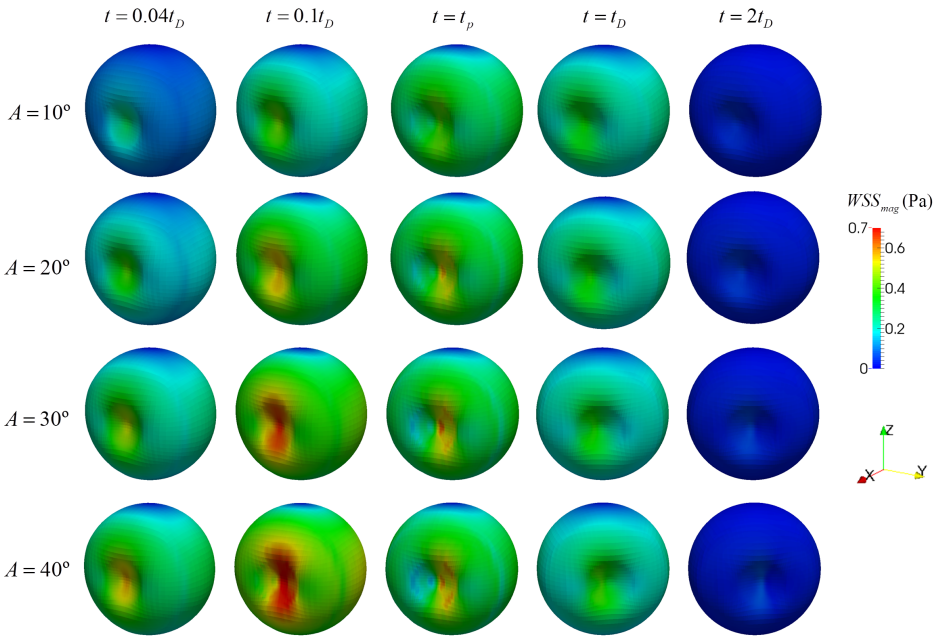

Figure A.3. Wall shear stress contours on the vitreous cavity for saccadic movements of 10, 20, 30 and 40° displacement and times $t = 0.04t_D$, $t = 0.1t_D$, $t = t_p$, $t = t_D$ and $t = 2t_D$, for HPF8 fluid.

A.2 RS-Oil 1000 fluid

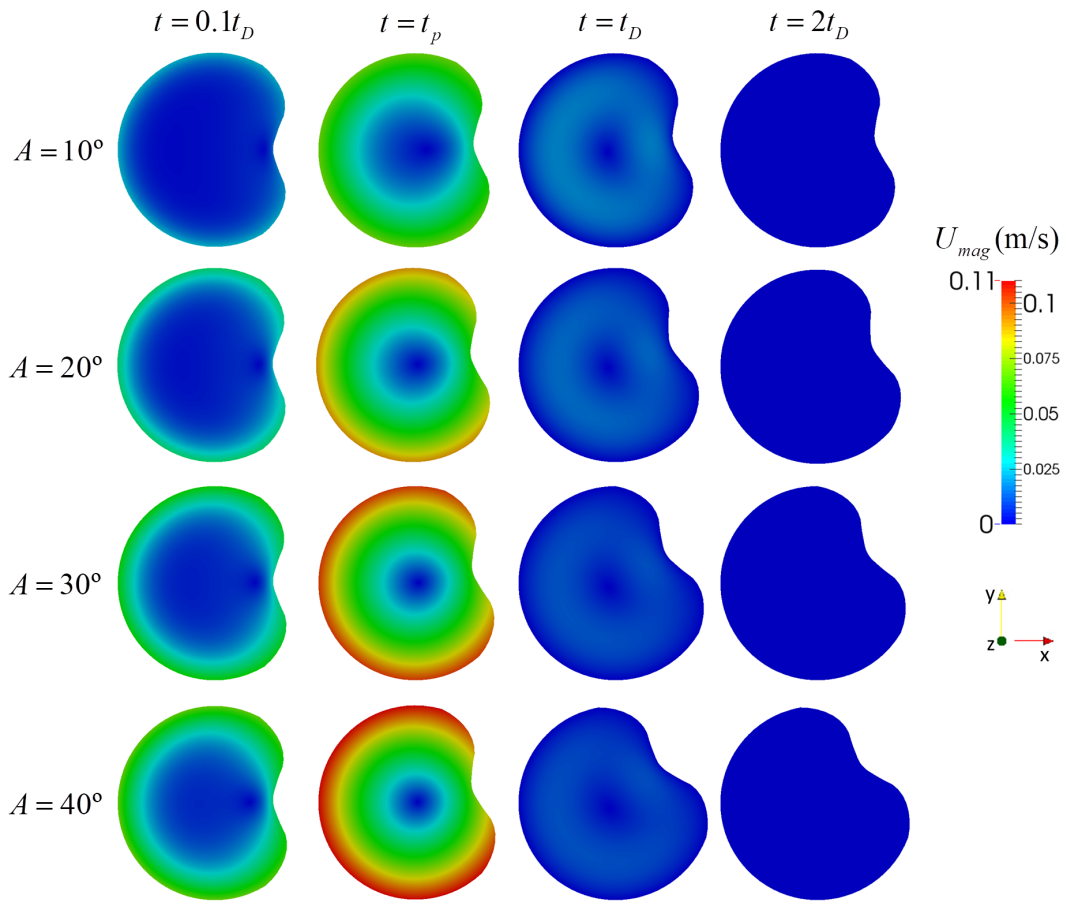

Figure A.4. Velocity magnitude contours on plane $z = 0$ for saccadic movements of 10°, 20°, 30° and 40° displacement, at times $t = 0.1t_D$, $t = t_p$, $t = t_D$ and $t = 2t_D$, for RS-Oil 1000 fluid.

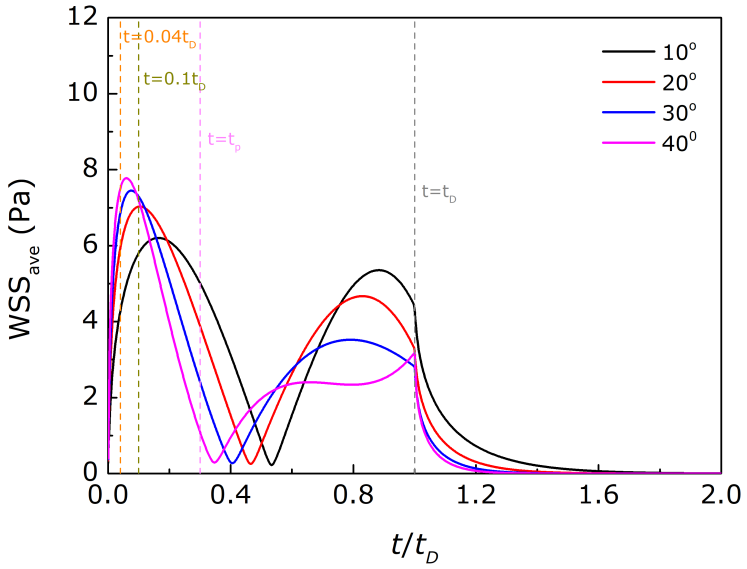

Figure A.5. Time variation of the average WSS on the vitreous cavity for diplacements of 10, 20, 30 and 40°, for RS-Oil 1000 fluid.

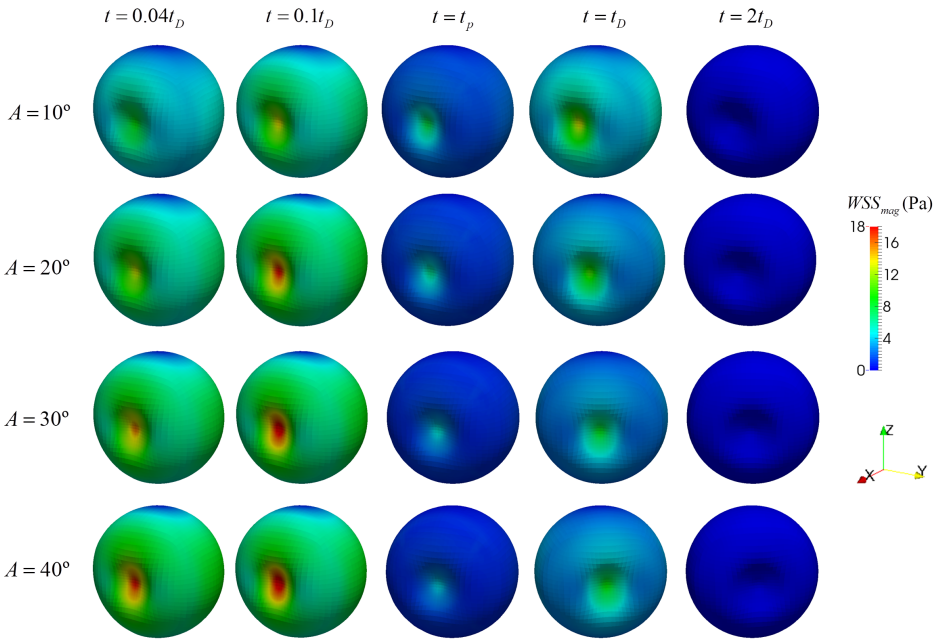

Figure A.6. Wall shear stress contours on the vitreous cavity for saccadic movements of 10, 20, 30 and 40° displacement and times $t = 0.04t_D$, $t = 0.1t_D$, $t = t_p$, $t = t_D$ and $t = 2t_D$, for RS-Oil 1000 fluid.

A.3 Densiron 68 fluid

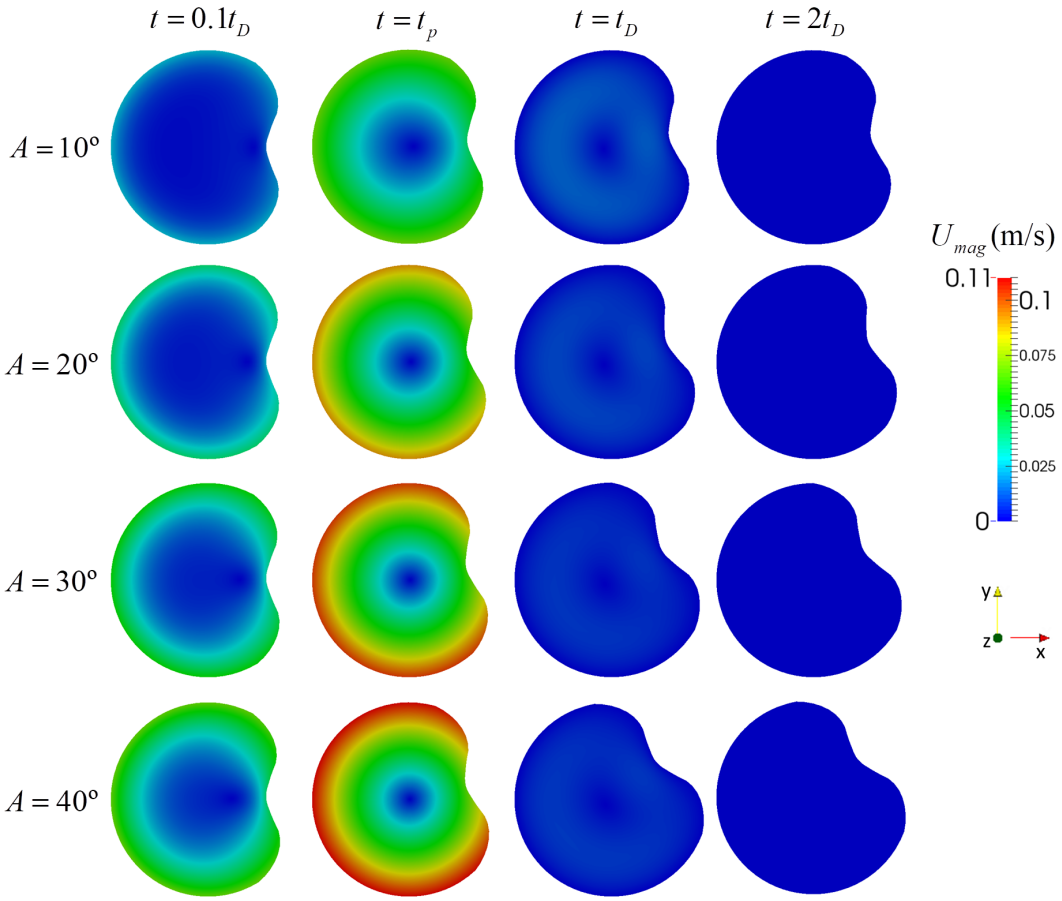

Figure A.7. Velocity magnitude contours on plane $z = 0$ for saccadic movements of 10°, 20°, 30° and 40° displacement, at times $t = 0.1t_D$, $t = t_p$, $t = t_D$ and $t = 2t_D$, for Densiron 68 fluid.

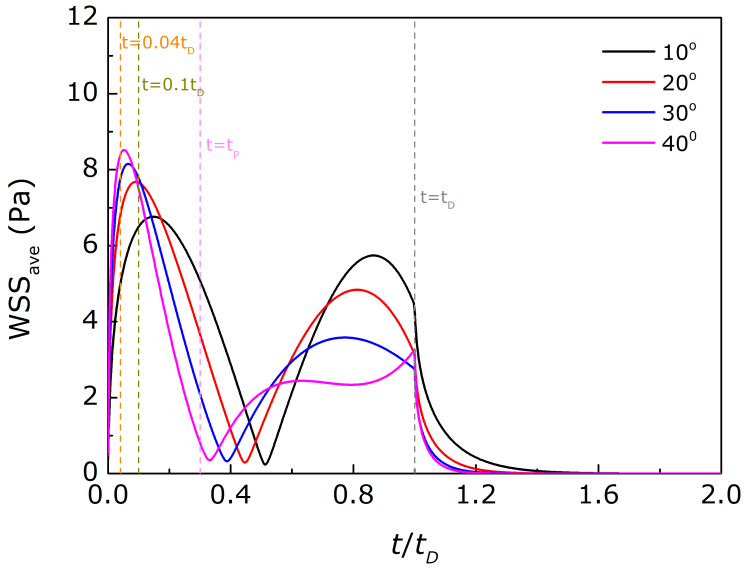

Figure A.8. Time variation of the average WSS on the vitreous cavity for diplacements of 10, 20, 30 and 40°, for Densiron 68 fluid.

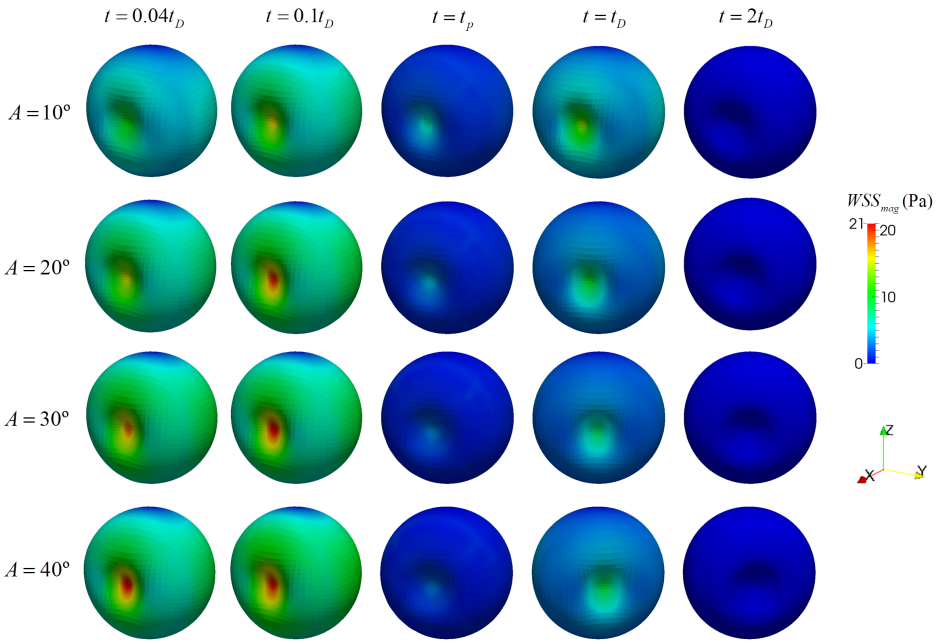

Figure A.9. Wall shear stress contours on the vitreous cavity for saccadic movements of 10, 20, 30 and 40° displacement and times $t = 0.04t_D$, $t = 0.1t_D$, $t = t_p$, $t = t_D$ and $t = 2t_D$, for Densiron 68 fluid.

A.4 Siluron 5000 fluid

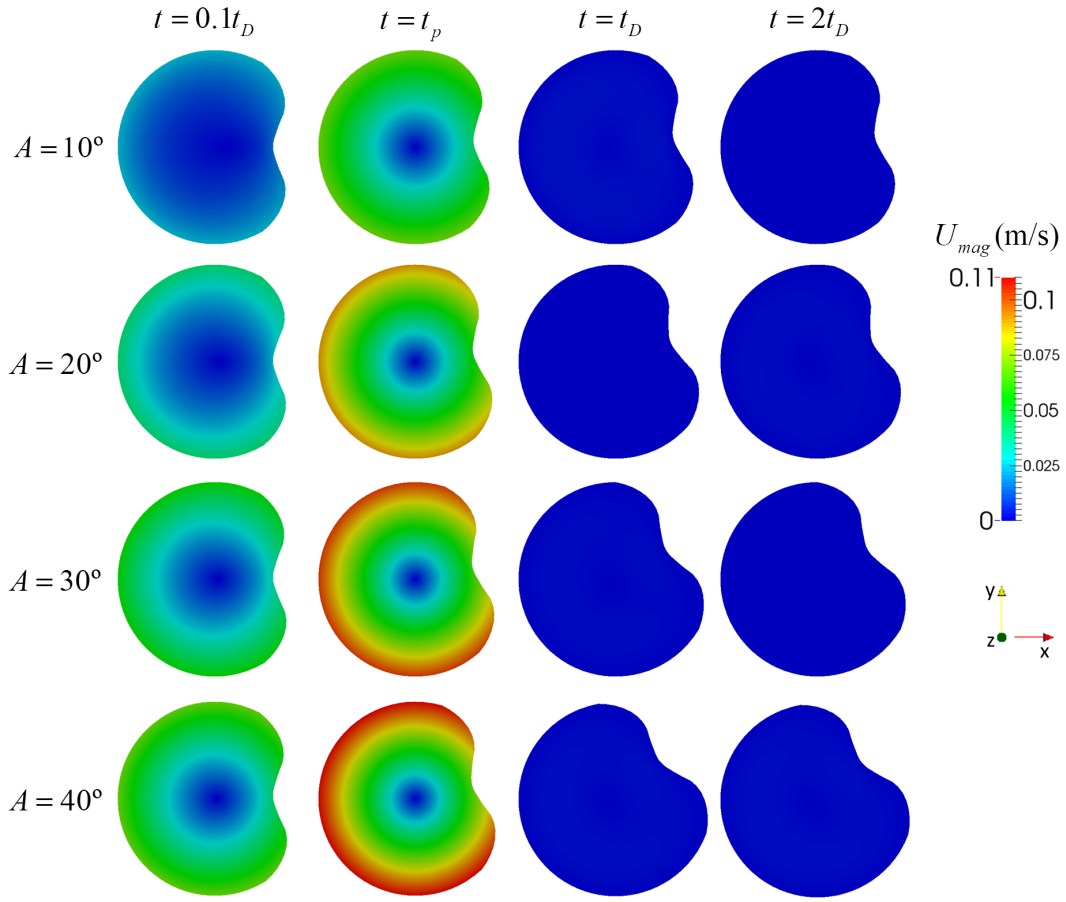

Figure A.10. Velocity magnitude contours on plane $z = 0$ for saccadic movements of 10°, 20°, 30° and 40° displacement, at times $t = 0.1t_D$, $t = t_p$, $t = t_D$ and $t = 2t_D$, for Siluron 5000 fluid.

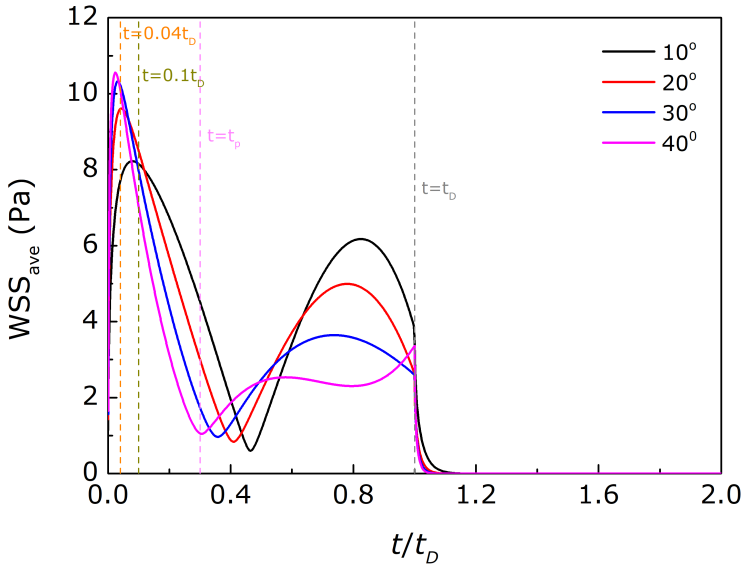

Figure A.11. Time variation of the average WSS on the vitreous cavity for diplacements of 10, 20, 30 and 40°, for Siluron 5000 fluid.

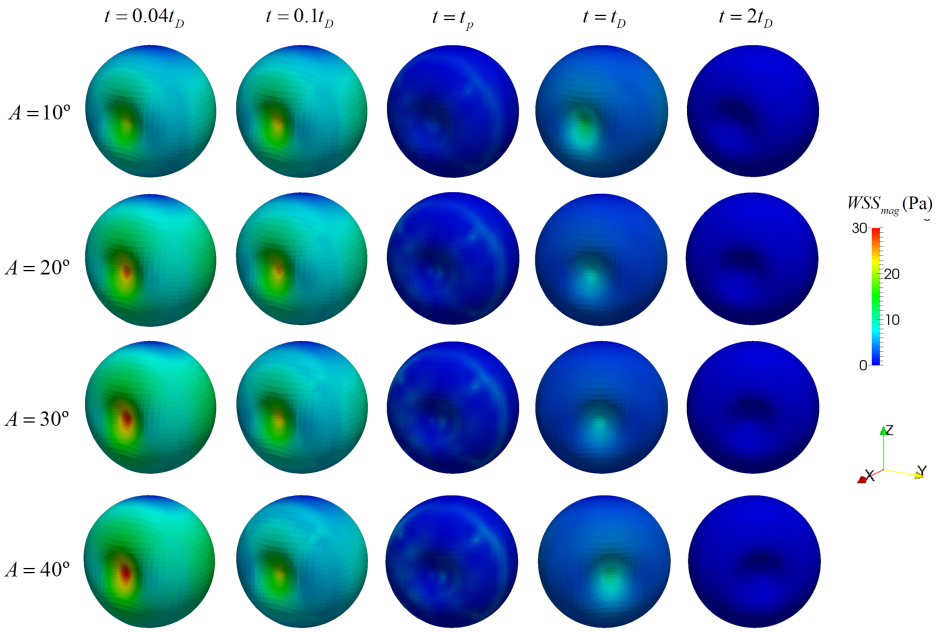

Figure A.12. Wall shear stress contours on the vitreous cavity for saccadic movements of 10, 20, 30 and 40° displacement and times $t = 0.04t_D$, $t = 0.1t_D$, $t = t_p$, $t = t_D$ and $t = 2t_D$, for Siluron 5000 fluid.

Bibliography

[1] H. R. Taylor and J. E. Keeffe, "World blindness: a 21st century perspective," *British Journal of Ophthalmology*, vol. 85, no. 3, pp. 261–266, 2001.

[2] J. D. Enderle, *Models of Horizontal Eye Movements: Early models of saccades and smooth pursuit.* No. pt. 1 in Synthesis lectures on biomedical engineering, Morgan & Claypool, 2010.

[3] E. Marieb, *Human Anatomy & Physiology.* Pearson Education, 2004.

[4] J. V. Forrester, A. D. Dick, P. G. McMenamin, F. Roberts, and E. Pearlman, "Chapter 1 - anatomy of the eye and orbit," in *The Eye (Fourth Edition)*, pp. 1–102.e2, Saunders, W.B., 2016.

[5] K. Cholkar, S. R. Dasari, D. Pal, and A. K. Mitra, "1 - eye: anatomy, physiology and barriers to drug delivery," in *Woodhead Publishing Series in Biomedicine*, pp. 1–36, Woodhead Publishing, 2013.

[6] E. E. Pastorino and S. M. Doyle-Portillo, *Cengage Advantage Books: What is Psychology? Essentials.* Cengage Learning, 2012.

[7] L. A. Harris, *CliffsAP Psychology.* John Wiley & Sons, 2007.

[8] T. V. Chirila, Y. Hong, P. D. Dalton, I. J. Constable, and M. F. Refojo, "The use of hydrophilic polymers as artificial vitreous," *Progress in Polymer Science*, vol. 23, no. 3, pp. 475–508, 1998.

[9] C. S. Nickerson, H. L. Karageozian, J. Park, and J. A. Kornfield, "Internal tension: A novel hypothesis concerning the mechanical properties of the vitreous humor," *Macromolecular Symposia*, vol. 227, no. 1, pp. 183–190, 2005.

[10] C. S. Nickerson, J. Park, J. A. Kornfield, and H. Karageozian, "Rheological properties of the vitreous and the role of hyaluronic acid," *Journal of Biomechanics*, vol. 41, no. 9, pp. 1840–1846, 2008.

[11] P. Sharif-Kashani, J. P. Hubschman, D. Sassoon, and H. P. Kavehpour, "Rheology of the vitreous gel: effects of macromolecule organization on the viscoelastic properties," *Journal of Biomechanics*, vol. 44, no. 3, pp. 419–23, 2011.

[12] J. H. Siggers and C. R. Ethier, "Fluid mechanics of the eye," *Annual Review of Fluid Mechanics*, vol. 44, no. 1, pp. 347–372, 2012.

[13] A. W. Fromm, *The vitreous body, its origin, development, and structure as observed in the eye of the pig, by Aloisius William Fromm.* 1921.

[14] J. Sebag, "Imaging vitreous," *Eye*, vol. 16, no. 4, pp. 429–39, 2002.

[15] J. Sebag and E. A. Balazs, "Human vitreous fibres and vitreoretinal disease," *Trans Ophthalmol Soc U K*, vol. 104, no. Pt 2, pp. 123–8, 1985.

[16] P. N. Bishop, "Structural macromolecules and supramolecular organisation of the vitreous gel," *Progress in Retinal and Eye Research*, vol. 19, no. 3, pp. 323–344, 2000.

[17] J. Black and G. W. Hastings, *Handbook of Biomaterial Properties.* Chapman & Hall, 1998.

[18] F. Baino, "Towards an ideal biomaterial for vitreous replacement: Historical overview and future trends," *Acta Biomaterialia*, vol. 7, no. 3, pp. 921–935, 2011.

[19] B. Lee, "Comparative rheological studies of the vitreous body of the eye," *Dissertations available from ProQuest. Paper AAI9227704. http://repository.upenn.edu/dissertations/AAI9227704*, 1992.

[20] C. Cavallotti and L. Cerulli, *Age-Related Changes of the Human Eye*. Aging Medicine, Humana Press, 2008.

[21] K. E. Swindle, P. D. Hamilton, and N. Ravi, "In situ formation of hydrogels as vitreous substitutes: Viscoelastic comparison to porcine vitreous," *Journal of Biomedical Materials Research Part A*, vol. 87A, no. 3, pp. 656–665, 2008.

[22] T. T. Kleinberg, R. T. Tzekov, L. Stein, N. Ravi, and S. Kaushal, "Vitreous substitutes: A comprehensive review," *Survey of Ophthalmology*, vol. 56, no. 4, pp. 300–323, 2011.

[23] J. Meskauskas, R. Repetto, and J. H. Siggers, "Oscillatory motion of a viscoelastic fluid within a spherical cavity," *Journal of Fluid Mechanics*, vol. 685, pp. 1–22, 2011.

[24] J. Meskauskas, R. Repetto, and J. H. Siggers, "Shape change of the vitreous chamber influences retinal detachment and reattachment processes: Is mechanical stress during eye rotations a factor?vitreous stress on the retina," *Investigative Ophthalmology & Visual Science*, vol. 53, no. 10, pp. 6271–6281, 2012.

[25] O. Abouali, A. Modareszadeh, A. Ghaffariyeh, and J. Tu, "Numerical simulation of the fluid dynamics in vitreous cavity due to saccadic eye movement," *Medical Engineering and Physics*, vol. 34, no. 6, pp. 681–92, 2012.

[26] A. Modarreszadeh and O. Abouali, "Numerical simulation for unsteady motions of the human vitreous humor as a viscoelastic substance in linear and non-linear regimes," *Journal of Non-Newtonian Fluid Mechanics*, vol. 204, pp. 22–31, 2014.

[27] A. F. Silva, M. A. A. Alves, and M. S. N. OAlves, "Rheological behaviour of vitreous humour," *Rheologica Acta*, pp. 1–10, 2017.

[28] A. Laude, L. E. Tan, C. G. Wilson, G. Lascaratos, M. Elashry, T. Aslam, and B. Patton, N.and Dhillon, "Intravitreal therapy for neovascular age-related macular degeneration and inter-individual variations in vitreous pharmacokinetics," *Progress in Retinal and Eye Research*, vol. 29, no. 6, pp. 466–475, 2010.

[29] S. Grabherr, C. Widmer, K. Iglesias, F. Sporkert, M. Augsburger, P. Mangin, and C. Palmiere, "Postmortem biochemistry performed on vitreous humor after postmortem ct-angiography," *Legal Medicine*, vol. 14, no. 6, pp. 297–303, 2012.

[30] A. Thierauf, F. Musshoff, and B. Madea, "Post-mortem biochemical investigations of vitreous humor," *Forensic Science International*, vol. 192, no. 1–3, pp. 78 – 82, 2009.

[31] J. Kokavec, S. H. Min, M. H. Tan, J. S. Gilhotra, H. S. Newland, S. R. Durkin, J. Grigg, and R. J. Casson, "Biochemical analysis of the living human vitreous," *Clinical & Experimental Ophthalmology*, vol. 44, no. 7, pp. 597–609, 2016. CEO-15-11-0983.R1.

[32] M. D. de Smet, A. M. Gad Elkareem, and A. H. Zwinderman, "The vitreous, the retinal interface in ocular health and disease," *Ophthalmologica*, vol. 230, no. 4, pp. 165–78, 2013.

[33] P. N. Bishop, "The biochemical structure of mammalian vitreous," *Eye*, vol. 10, no. 6, pp. 664–670, 1996.

[34] K. E. Swindle and N. Ravi, "Recent advances in polymeric vitreous substitutes," *Expert Review of Ophthalmology*, vol. 2, no. 2, pp. 255–265, 2007.

[35] F. A. Bettelheim and T. J. Y. Wang, "Dynamic viscoelastic properties of bovine vitreous," *Experimental Eye Research*, vol. 23, no. 4, pp. 435–441, 1976.

[36] B. A. Filas, Q. Zhang, R. J. Okamoto, Y. B. Shui, and D. C. Beebe, "Enzymatic degradation identifies components responsible for the structural properties of the vitreous body," *Investigative Ophthalmology & Visual Science*, vol. 55, no. 1, pp. 55–63, 2014.

[37] E. A. Balazs and J. L. Denlinger, "Ageing changes in the vitreous," *Dismukes K and Sekular R (eds). Ageing and human visual function*, p. pp 45–57, 1982.

[38] L. I. Los, R. J. van der Worp, M. J. A. van Luyn, and J. M. M. Hooymans, "Age-related liquefaction of the human vitreous body: Lm and tem evaluation

of the role of proteoglycans and collagen," *Investigative Ophthalmology & Visual Science*, vol. 44, no. 7, pp. 2828–2833, 2003.

[39] J. Sebag, "Ageing of the vitreous," *Eye*, vol. 1, no. 2, pp. 254–262, 1987.

[40] K. A. Walton, C. H. Meyer, C. J. Harkrider, T. A. Cox, and C. A. Toth, "Age-related changes in vitreous mobility as measured by video b scan ultrasound," *Experimental Eye Research*, vol. 74, no. 2, pp. 173–180, 2002.

[41] F. Watts, L. E. Tan, C. G. Wilson, J. M. Girkin, M. Tassieri, and A. F. Wright, "Investigating the micro-rheology of the vitreous humor using an optically trapped local probe," *Journal of Optics*, vol. 16, no. 1, p. 015301, 2014.

[42] M. M. Le Goff and P. N. Bishop, "Adult vitreous structure and postnatal changes," *Eye*, vol. 22, no. 10, pp. 1214–1222, 2008.

[43] C. Oyster, *The Human Eye: Structure and Function.* Sinauer Associates, 2006.

[44] J. Sebag, "Abnormalities of human vitreous structure in diabetes," *Graefes Arch Clin Exp Ophthalmol*, vol. 231, no. 5, pp. 257–60, 1993.

[45] F. Baino, "Scleral buckling biomaterials and implants for retinal detachment surgery," *Medical Engineering & Physics*, vol. 32, no. 9, pp. 945–956, 2010.

[46] J. Sebag, S. Nie, K. Reiser, M. A. Charles, and N. T. Yu, "Raman spectroscopy of human vitreous in proliferative diabetic retinopathy," *Invest Ophthalmol Vis Sci*, vol. 35, no. 7, pp. 2976–80, 1994.

[47] O. Lundquist and S. Osterlin, "Glucose concentration in the vitreous of nondiabetic and diabetic human eyes," *Graefes Arch Clin Exp Ophthalmol*, vol. 232, no. 2, pp. 71–4, 1994.

[48] A. W. Stitt, J. E. Moore, J. A. Sharkey, G. Murphy, D. A. Simpson, R. Bucala, H. Vlassara, and D. B. Archer, "Advanced glycation end products in vitreous: Structural and functional implications for diabetic vitreopathy," *Invest Ophthalmol Vis Sci*, vol. 39, no. 13, pp. 2517–23, 1998.

[49] G. G. Giordano and M. F. Refojo, "Silicone oils as vitreous substitutes," *Progress in Polymer Science*, vol. 23, no. 3, pp. 509–532, 1998.

[50] X. Su, M. J. Tan, Z. Li, M. Wong, L. Rajamani, G. Lingam, and X. J. Loh, "Recent progress in using biomaterials as vitreous substitutes," *Biomacromolecules*, vol. 16, no. 10, pp. 3093–3102, 2015. PMID: 26366887.

[51] P. M. Jacobs, J. M. Twomey, and P. K. Leaver, "Behaviour of intraocular gases," *Eye*, vol. 2, pp. 660–663, nov 1988.

[52] Y. Imamura, M. Minami, M. Ueki, B. Satoh, and T. Ikeda, "Use of perfluorocarbon liquid during vitrectomy for severe proliferative diabetic retinopathy," *British Journal of Ophthalmology*, vol. 87, no. 5, pp. 563–566, 2003.

[53] W. J. Stone, "Alloplasty in surgery of the eye," *New England Journal of Medicine*, vol. 258, no. 12, pp. 596–602, 1958. PMID: 13517524.

[54] P. A. Cibis, B. Becker, E. Okun, and S. Canaan, "The use of liquid silicone in retinal detachment surgery," *Archives of Ophthalmology*, vol. 68, no. 5, pp. 590–599, 1962.

[55] R. L. Williams, M. J. Day, M. J. Garvey, G. Morphis, C. Irigoyen, D. Wong, and T. Stappler, "Injectability of silicone oil-based tamponade agents," *British Journal of Ophthalmology*, vol. 95, no. 2, pp. 273–276, 2011.

[56] D. J. Light, "Silicone oil emulsification in the anterior chamber after vitreoretinal surgery," *Optometry - Journal of the American Optometric Association*, vol. 77, no. 9, pp. 446 – 449, 2006.

[57] Y. K. Chan, C. O. Ng, P. C. Knox, M. J. Garvey, R. L. Williams, and D. Wong, "Emulsification of silicone oil and eye movements," *Investigative Ophthalmology & Visual Science*, vol. 52, no. 13, p. 9721, 2011.

[58] A. Caramoy, S. Schröder, S. Fauser, and B. Kirchhof, "In vitro emulsification assessment of new silicone oils," *British Journal of Ophthalmology*, vol. 94, no. 4, pp. 509–512, 2010.

[59] A. Caramoy, N. Hagedorn, S. Fauser, W. Kugler, T. Groß, and B. Kirchhof, "Development of emulsification-resistant silicone oils: Can we go beyond 2000 mpas silicone oil?," *Investigative Ophthalmology & Visual Science*, vol. 52, no. 8, 2011.

[60] R. L. Williams, M. Day, M. J. Garvey, R. English, and D. Wong, "Increasing the extensional viscosity of silicone oil reduces the tendency for emulsification," *RETINA*, vol. 30, no. 2, pp. –, 2010.

[61] M. Day, R. Blanchard, R. English, T. Dobbie, R. Williams, M. Gavey, and D. Wong, "Shear and extensional rheometry of pdms tamponade agents used in vitroretinal surgery," *AIP Conference Proceedings*, vol. 1027, no. 1, pp. 1411–1413, 2008.

[62] B. Macías-Murelaga, M. Ruiz, L. Bascarán, A. Gibelalde, M. Aldazabal, and C. Irigoyen, "Heavy silicone oil (densiron® 68) in proliferative vitreoretinopathy: 4 years of experience," *Archivos de la Sociedad Española de Oftalmología (English Edition)*, vol. 88, no. 11, pp. 445–449, 2013.

[63] H. Schwarzer, B. Mazinani, N. Plange, M. Fuest, P. Walter, and G. Roessler, "Clinical observations and occurrence of complications following heavy silicone oil surgery," *BioMed Research International*, vol. 2014, p. 706809, mar 2014.

[64] S. Ozdek, N. Yuksel, G. Gurelik, and B. Hasanreisoglu, "High-density silicone oil as an intraocular tamponade in complex retinal detachments," *Canadian Journal of Ophthalmology / Journal Canadien d'Ophtalmologie*, vol. 46, no. 1, pp. 51 – 55, 2011.

[65] C. M. Gremillion, G. A. Peyman, K. R. Liu, and K. S. Naguib, "Fluorosilicone oil in the treatment of retinal detachment," *British Journal of Ophthalmology*, vol. 74, no. 11, pp. 643–646, 1990.

[66] S. Rizzo, F. Genovesi-Ebert, A. Vento, F. Cresti, E. Di Bartolo, and C. Belting, "A new heavy silicone oil (hws 46-3000) used as a prolonged internal tamponade

agent in complicated vitreoretinal surgery: a pilot study," *Retina*, vol. 27, no. 5, pp. 613–620, 2007.

[67] C. Liang, G. A. Peyman, P. Serracarbassa, N. Calixto, A. A. Chow, and P. Rao, "An evaluation of methylated collagen as a substitute for vitreous and aqueous humor," *International Ophthalmology*, vol. 22, no. 1, pp. 13–18, 1998.

[68] M. J. Colthurst, R. L. Williams, P. S. Hiscott, and I. Grierson, "Biomaterials used in the posterior segment of the eye," *Biomaterials*, vol. 21, no. 7, pp. 649–665, 2000.

[69] N. Soman and R. Banerjee, "Artificial vitreous replacements," *Bio-Medical Materials And Engineering*, vol. 13, no. 1, pp. 59–74, 2003.

[70] T. V. Chirila, S. Tahija, Y. Hong, S. Vijayasekaran, and I. J. Constable, "Synthetic polymers as materials for artificial vitreous body: Review and recent advances," *Journal of Biomaterials Applications*, vol. 9, no. 2, pp. 121–137, 1994.

[71] T. V. Chirila and Y. Hong, "Poly(1-vinyl-2-pyrrolidinone) hydrogels as vitreous substitutes: a rheological study," *Polymer International*, vol. 46, no. 3, pp. 183–195, 1998.

[72] Y. Hong, T. V. Chirila, M. J. H. Cuypers, and I. J. Constable, "Polymers of 1-vinyl-2-pyrrolidinone as potential vitreous substitutes: Physical selection," *Journal of Biomaterials Applications*, vol. 11, no. 2, pp. 135–181, 1996.

[73] Y. Hong, T. V. Chirila, S. Vijayasekaran, P. D. Dalton, S. G. Tahija, M. J. H. Cuypers, and I. J. Constable, "Crosslinked poly(1-vinyl-2-pyrrolidinone) as a vitreous substitute," *Journal of Biomedical Materials Research*, vol. 30, no. 4, pp. 441–448, 1996.

[74] Y. Hong, T. V. Chirila, S. Vijayasekaran, W. Y. Shen, X. Lou, and P. D. Dalton, "Biodegradation in vitro and retention in the rabbit crosslinked poly(1-vinyl-2-pyrrolidinone) hydrogel as a vitreous substitute," *Journal of Biomedical Materials Research*, vol. 39, no. 4, pp. 650–659, 1998.

[75] S. Daniele, M. F. Refojo, C. L. Schepens, and H. Freeman, "Glyceryl methacrylate hydrogel as a vitreous implant: An experimental study," *Archives of Ophthalmology*, vol. 80, no. 1, pp. 120–127, 1968.

[76] M. F. Refojo, "Polymers in ophthalmic surgery," *Journal of Biomedical Materials Research*, vol. 5, no. 1, pp. 113–119, 1971.

[77] T. V. Chirila, I. J. Constable, Y. Hong, S. Vijayasekaran, M. F. HUMPHREY, P. D. Dalton, S. G. Tahija, M. Maley, M. J. H. Cuypers, C. Sharp, S. R. Moore, and M. J. Davies, "Syntethic hydrogel as an artificial vitreous body - a one-year study of its effects on the retina," *Cells and materials*, vol. 5, pp. 83–96, MAR 1995.

[78] K. Muller-Jensen and H. Kohler, "An attempt to replace the vitreous body by polyacrylamide," *Bericht uber die Zusammenkunft. Deutsche Ophthalmologische Gesellschaft*, vol. 68, pp. 181–4, 1968.

[79] K. Mueller-Jensen, "Polyacrylamide as an alloplastic vitreous implant," *Albrecht von Graefes Archiv für klinische und experimentelle Ophthalmologie*, vol. 189, no. 2, pp. 147–158, 1973.

[80] K. E. Swindle, P. D. Hamilton, and N. Ravi, "Advancements in the development of artificial vitreous humor utilizing polyacrylamide copolymers with disulfide crosslinkers," *Abstracts of Papers of the American Chemical Society*, vol. 231, 2006.

[81] W. J. Foster, H. A. Aliyar, P. Hamilton, and N. Ravi, "Internal osmotic pressure as a mechanism of retinal attachment in a vitreous substitute," *Journal of Bioactive and Compatible Polymers*, vol. 21, no. 3, pp. 221–235, 2006.

[82] S. Lamponi, G. Leone, M. Consumi, G. Greco, and A. Magnani, "In vitro biocompatibility of new pva-based hydrogels as vitreous body substitutes," *Journal of Biomaterials Science, Polymer Edition*, vol. 23, no. 1-4, pp. 555–75, 2012.

[83] G. Leone, M. Consumi, M. Aggravi, A. Donati, S. Lamponi, and A. Magnani, "Pva/stmp based hydrogels as potential substitutes of human vitreous," *Journal of Materials Science: Materials in Medicine*, vol. 21, no. 8, pp. 2491–2500, 2010.

[84] S. Feng, H. Chen, Y. Liu, Z. Huang, X. Sun, L. Zhou, X. Lu, and Q. Gao, "A novel vitreous substitute of using a foldable capsular vitreous body injected with polyvinylalcohol hydrogel," *Scientific Reports*, vol. 3, 2013.

[85] S. Maruoka, T. Matsuura, K. Kawasaki, M. Okamoto, H. Yoshiaki, M. Kodama, and M. Sugiyama, M.and Annaka, "Biocompatibility of polyvinylalcohol gel as a vitreous substitute," *Current Eye Research*, vol. 31, no. 7-8, pp. 599–606, 2006.

[86] M. H. Alves, B. E. Jensen, A. A. Smith, and A. N. Zelikin, "Poly(vinyl alcohol) physical hydrogels: new vista on a long serving biomaterial," *Macromol Biosci*, vol. 11, no. 10, pp. 1293–313, 2011.

[87] C. D. Pritchard, S. Crafoord, S. Andréasson, K. M. Arnér, T. M. O'Shea, R. Langer, and F. K. Ghosh, "Evaluation of viscoelastic poly(ethylene glycol) sols as vitreous substitutes in an experimental vitrectomy model in rabbits," *Acta Biomaterialia*, vol. 7, no. 3, pp. 936 – 943, 2011.

[88] M. Annaka, K. Mortensen, M. E. Vigild, T. Matsuura, S. Tsuji, T. Ueda, and H. Tsujinaka, "Design of an injectable in situ gelation biomaterials for vitreous substitute," *Biomacromolecules*, vol. 12, no. 11, pp. 4011–4021, 2011. PMID: 21988210.

[89] U. Laurent, P. Törnquist, K. Granath, K. Lilja-Englind, and D. Ytterberg, "Molecular weight and concentration of hyaluronan in vitreous humour from diabetic patients," *Acta Ophthalmologica*, vol. 68, no. S195, pp. 109–112, 1990.

[90] M. J. Yaszemski, D. J. Trantolo, K. U. Lewandrowski, V. Hasirci, D. E. Altobelli, and D. L. Wise, *Tissue Engineering And Novel Delivery Systems*. CRC Press, 2003.

[91] L. I. Los, "The rabbit as an animal model for post-natal vitreous matrix differentiation and degeneration," *Eye*, vol. 22, pp. 1223–1232, 2008.

[92] E. M. del Amo and A. Urtti, "Rabbit as an animal model for intravitreal pharmacokinetics: Clinical predictability and quality of the published data," *Experimental Eye Research*, vol. 137, pp. 111–124, 2015.

[93] R. I. Tanner, *Engineering Rheology*. Oxford Engineering Science Series, OUP Oxford, 2000.

[94] F. Irgens, *Rheology and Non-Newtonian Fluids*. Springer International Publishing, 2013.

[95] H. Barnes, *A Handbook of Elementary Rheology*. University of Wales, Institute of Non-Newtonian Fluid Mechanics, 2000.

[96] M. P. Krafft and J. G. Riess, "Perfluorocarbons: Life sciences and biomedical uses dedicated to the memory of professor guy ourisson, a true renaissance man.," *Journal of Polymer Science Part A: Polymer Chemistry*, vol. 45, no. 7, pp. 1185–1198, 2007.

[97] K. Waxman, "Perfluorocarbons as blood substitutes," *Annals of Emergency Medicine*, vol. 15, no. 12, pp. 1423 – 1424, 1986.

[98] O. Reynolds, "An experimental investigation of the circumstances which determine whether the motion of water shall be direct or sinuous, and of the law of resistance in parallel channels," *Philosophical Transactions of the Royal Society of London*, vol. 174, pp. 935–982, 1883.

[99] M. Reiner, "The deborah number," *Physics Today*, vol. 17, p. 1, 1964.

[100] J. L. White, "Dynamics of viscoelastic fluids, melt fracture and the rheology of fiber spinning," *J. Appl. Polymer Sci.*, vol. 8, pp. 2339–2357, 1964.

[101] J. M. Dealy, "Weissenberg and deborah numbers - their definition and use," *Rheology Bulletin - Society of Rheology*, vol. 79 (2), pp. 14–18, 2010.

[102] L. E. Rodd, T. P. Scott, D. V. Boger, J. J. Cooper-White, and G. H. McKinley, "The inertio-elastic planar entry flow of low-viscosity elastic fluids in microfabricated geometries," *Journal of Non-Newtonian Fluid Mechanics*, vol. 129, no. 1, pp. 1 – 22, 2005.

[103] F. A. Morrison, *Understanding Rheology*. Oxford University Press, 2001.

[104] H. P. Sdougos, S. R. Bussolari, and C. F. Dewey, "Secondary flow and turbulence in a cone-and-plate device," *Journal of Fluid Mechanics*, vol. 138, p. 379–404, 1984.

[105] T. Mezger, *The Rheology Handbook: For Users of Rotational and Oscillatory Rheometers*. Vincentz Network, 2014.

[106] W. P. Cox and E. H. Merz, "Correlation of dynamic and steady flow viscosities," *Journal of Polymer Science*, vol. 28, no. 118, pp. 619–622, 1958.

[107] F. Snijkers and D. Vlassopoulos, "Appraisal of the cox-merz rule for well-characterized entangled linear and branched polymers," *Rheologica Acta*, vol. 53, no. 12, pp. 935–946, 2014.

[108] G. H. McKinley, "Visco-elasto-capillary thinning and break-up of complex fluids," 2005.

[109] V. M. Entov and E. J. Hinch, "Effect of a spectrum of relaxation times on the capillary thinning of a filament of elastic liquid," *Journal of Non-Newtonian Fluid Mechanics*, vol. 72, no. 1, pp. 31 – 53, 1997.

[110] L. Campo-Deano and C. Clasen, "The slow retraction method (srm) for the determination of ultra-short relaxation times in capillary breakup extensional rheometry experiments," *Journal of Non-Newtonian Fluid Mechanics*, vol. 165, no. 23, pp. 1688–1699, 2010.

[111] P. C. Sousa, E. J. Vega, R. G. Sousa, J. M. Montanero, and M. A. Alves, "Measurement of relaxation times in extensional flow of weakly viscoelastic polymer solutions," *Rheologica Acta*, vol. 56, no. 1, pp. 11–20, 2017.

[112] D. C. Vadillo, W. Mathues, and C. Clasen, "Microsecond relaxation processes in shear and extensional flows of weakly elastic polymer solutions," *Rheologica Acta*, vol. 51, no. 8, pp. 755–769, 2012.

[113] J. D. Berry, M. J. Neeson, R. R. Dagastine, D. Y. C. Chan, and R. F. Tabor, "Measurement of surface and interfacial tension using pendant drop tensiometry," *Journal of Colloid and Interface Science*, vol. 454, pp. 226 – 237, 2015.

[114] M. Stamm, *Polymer Surfaces and Interfaces: Characterization, Modification and Applications*. Springer ebook collection / Chemistry and Materials Science 2005-2008, Springer Berlin Heidelberg, 2008.

[115] A. Baszkin and W. Norde, *Physical Chemistry of Biological Interfaces*. Taylor & Francis, 1999.

[116] R. Jones and R. Richards, *Polymers at Surfaces and Interfaces*. Cambridge University Press, 1999.

[117] M. S. N. Oliveira, L. E. Rodd, G. H. McKinley, and M. A. Alves, "Simulations of extensional flow in microrheometric devices," *Microfluidics and Nanofluidics*, vol. 5, p. 809, Apr 2008.

[118] F. J. Galindo-Rosales, L. Campo-Deaño, F. T. Pinho, E. van Bokhorst, P. J. Hamersma, M. S. N. Oliveira, and M. A. Alves, "Microfluidic systems for the analysis of viscoelastic fluid flow phenomena in porous media," *Microfluidics and Nanofluidics*, vol. 12, pp. 485–498, Jan 2012.

[119] Y. Xia and G. M. Whitesides, "Soft lithography," *Annual Review of Materials Science*, vol. 28, no. 1, pp. 153–184, 1998.

[120] J. Friend and L. Yeo, "Fabrication of microfluidic devices using polydimethylsiloxane," *Biomicrofluidics*, vol. 4, no. 2, p. 026502, 2010.

[121] A. Ross, n. Blake, R. C., and R. S. Ayyala, "Surface tension of aqueous humor," *J Glaucoma*, vol. 19, no. 7, pp. 456–9, 2010.

[122] J. Li, A. He, C. C. Han, B. S. Fang, D.and Hsiao, and B. Chu, "Electrospinning of hyaluronic acid (ha) and ha/gelatin blends," *Macromolecular Rapid Communications*, vol. 27, no. 2, pp. 114–120, 2006.

[123] L. Ambrosio, A. Borzacchiello, P. A. Netti, and L. Nicolais, "Rheological study in hyaluronic acid and its derivative solutions," *Journal of Macromolecular Science, Part A*, vol. 36, no. 7-8, pp. 991–1000, 1999.

[124] A. Maleki, A. Kjøniksen, and B. Nyström, "Anomalous viscosity behavior in aqueous solutions of hyaluronic acid," *Polymer Bulletin*, vol. 59, no. 2, pp. 217–226, 2007.

[125] A. O. Bingol, D. Lohmann, K. Puschel, and W. M. Kulicke, "Characterization and comparison of shear and extensional flow of sodium hyaluronate and human synovial fluid," *Biorheology*, vol. 47, no. 3-4, pp. 205–24, 2010.

[126] H. Fam, M. Kontopoulou, and J. T. Bryant, "Effect of concentration and molecular weight on the rheology of hyaluronic acid/bovine calf serum solutions," *Biorheology*, vol. 46, no. 1, pp. 31–43, 2009.

[127] S. J. Haward, "Synovial fluid response to extensional flow: Effects of dilution and intermolecular interactions," *PLoS ONE*, vol. 9, no. 3, p. e92867, 2014.

[128] S. J. Haward, A. Jaishankar, M. S. N. Oliveira, M. A. Alves, and G. H. McKinley, "Extensional flow of hyaluronic acid solutions in an optimized microfluidic cross-slot devicea)," *Biomicrofluidics*, vol. 7, no. 4, p. 044108, 2013.

[129] R. H. Ewoldt, M. T. Johnston, and L. M. Caretta, *Experimental Challenges of Shear Rheology: How to Avoid Bad Data*, pp. 207–241. New York, NY: Springer New York, 2015.

[130] K. J. Bos, D. F. Holmes, R. S. Meadows, K. E. Kadler, D. McLeod, and P. N. Bishop, "Collagen fibril organisation in mammalian vitreous by freeze etch/rotary shadowing electron microscopy," *Micron*, vol. 32, no. 3, pp. 301–6, 2001.

[131] D. R. Picout and S. B. Ross-Murphy, "Rheology of biopolymer solutions and gels," *ScientificWorldJournal*, vol. 3, pp. 105–21, 2003.

[132] O. Manero, F. Bautista, J. F. A. Soltero, and J. E. Puig, "Dynamics of worm-like micelles: the cox–merz rule," *Journal of Non-Newtonian Fluid Mechanics*, vol. 106, no. 1, pp. 1–15, 2002.

[133] M. Shayegan and N. R. Forde, "Microrheological characterization of collagen systems: From molecular solutions to fibrillar gels," *PLoS ONE*, vol. 8, no. 8, p. e70590, 2013.

[134] R. M. L. Evans, M. Tassieri, D. Auhl, and T. A. Waigh, "Direct conversion of rheological compliance measurements into storage and loss moduli," *Physical Review E*, vol. 80, no. 1, p. 012501, 2009.

[135] M. Tassieri, M. Laurati, D. J. Curtis, D. W. Auhl, S. Coppola, A. Scalfati, K. Hawkins, P. R. Williams, and J. M. Cooper, "i-rheo: Measuring the materials ' linear viscoelastic properties "in a step"!," *Journal of Rheology*, vol. 60, no. 4, pp. 649–660, 2016.

[136] P. Kavehpour, R. Freeman, R. Vedadghavami, S. Shah, R. Amini, and J. Hubschman, "Mechanical properties of vitreous humor in eye pairs," *Investigative Ophthalmology & Visual Science*, vol. 54, no. 6, pp. 3321–, 2013.

[137] M. T. Sheu, J. C. Huang, G. C. Yeh, and H. O. Ho, "Characterization of collagen gel solutions and collagen matrices for cell culture," *Biomaterials*, vol. 22, no. 13, pp. 1713–9, 2001.

[138] T. Sakuma, Y.-Y. Won, J. Sueda, N. Usumoto, D. Weitz, and T. Hirose, "Rheology of vitreous : Effects of enzymes," *Invest. Ophthalmol. Vis. Sci.*, vol. 45, no. 5, pp. 1948–, 2004.

[139] M. G. Freire, P. J. Carvalho, A. J. Queimada, I. M. Marrucho, and J. A. P. Coutinho, "Surface tension of liquid fluorocompounds," *Journal of Chemical & Engineering Data*, vol. 51, no. 5, pp. 1820–1824, 2006.

[140] Y. K. Kim, B. Gunther, and H. Meinert, "A new, heavier-than-water silicone oil: A solution of perfluorohexyloctane in polydimethylsiloxane," *European Journal of Ophthalmology*, vol. 15, no. 5, pp. 627–637, 2008.

[141] J. Mackiewicz, B. Mühling, W. Hiebl, H. Meinert, K. Maaijwee, N. Kociok, Z. Lüke, C.and Zagorski, B. Kirchhof, and A. M. Joussen, "In vivo retinal tolerance of various heavy silicone oils," *Investigative Ophthalmology & Visual Science*, vol. 48, no. 4, pp. 1873–1883, 2007.

[142] M. R. Romano, T. Stappler, J. Marticorena, C. Groenewald, I. Pearce, S. K. Gibran, D. Wong, and H. Heimann, "Primary vitrectomy with densiron-68 for rhegmatogenous retinal detachment," *Graefe's Archive for Clinical and Experimental Ophthalmology*, vol. 246, no. 11, pp. 1541–1546, 2008.

[143] A. M. Joussen and D. Wong, "The concept of heavy tamponades - chances and limitations," *Graefe's Archive for Clinical and Experimental Ophthalmology*, vol. 246, pp. 1217–1224, Sep 2008.

[144] C. Wetterqvist, D. Wong, R. Williams, T. Stappler, E. Herbert, and S. Freeburn, "Tamponade efficiency of perfluorohexyloctane and silicone oil solutions in a model eye chamber," *British Journal of Ophthalmology*, vol. 88, no. 5, pp. 692–696, 2004.

[145] F. Barca, T. Caporossi, and S. Rizzo, "Silicone oil: Different physical proprieties and clinical applications," *BioMed Research International*, vol. 2014, p. 7, 2014.

[146] P. Schneider, T. Telger, P. Niesel, and G. Eisner, *Eye Surgery: An Introduction to Operative Technique*. Springer Berlin Heidelberg, 2012.

[147] M. R. Romano, C. Groenwald, R. Das, T. Stappler, D. Wong, and H. Heimann, "Removal of densiron-68 with a 23-gauge transconjunctival vitrectomy system," *Eye*, vol. 23, p. 715–717, jan 2009.

[148] "Long-term tamponades, ultrapurified silicone oils and gases for intraocular use." http://www.fluoron.de/, 2016.

[149] A. Frank, "Creep recovery measurements of polymers," *77th Annual Meeting of the American Society of Rheology*, 2005.

[150] P. P. Bhat, S. Appathurai, M. T. Harris, M. Pasquali, G. H. McKinley, and O. A. Basaran, "Formation of beads-on-a-string structures during break-up of viscoelastic filaments," *Nature Physics*, vol. 6, pp. 625–631, Aug. 2010.

[151] D. T. Papageorgiou, "On the breakup of viscous liquid threads," *Physics of Fluids*, vol. 7, no. 7, pp. 1529–1544, 1995.

[152] G. H. McKinley and A. Tripathi, "How to extract the newtonian viscosity from capillary breakup measurements in a filament rheometer," *Journal of Rheology*, vol. 44, no. 3, pp. 653–670, 2000.

[153] P. C. Sousa, F. T. Pinho, M. S. N. Oliveira, and M. A. Alves, "Extensional flow of blood analog solutions in microfluidic devices," *Biomicrofluidics*, vol. 5, no. 1, p. 014108, 2011.

[154] L. Campo-Deaño, F. J. Galindo-Rosales, F. T. Pinho, M. A. Alves, and M. S. N. Oliveira, "Flow of low viscosity boger fluids through a microfluidic hyperbolic contraction," *Journal of Non-Newtonian Fluid Mechanics*, vol. 166, no. 21, pp. 1286 – 1296, 2011.

[155] S. L. Perry, J. J. L. Higdon, and P. J. A. Kenis, "Design rules for pumping and metering of highly viscous fluids in microfluidics," *Lab on a Chip*, vol. 10, pp. 3112–3124, 2010.

[156] R. Repetto, "An analytical model of the dynamics of the liquefied vitreous induced by saccadic eye movements," *Meccanica*, vol. 41, no. 1, pp. 101–117, 2006.

[157] A. Stocchino, R. Repetto, and C. Cafferata, "Eye rotation induced dynamics of a newtonian fluid within the vitreous cavity: the effect of the chamber shape," *Physics in Medicine & Biology*, vol. 52, no. 7, pp. 2021–34, 2007.

[158] D. Purves, G. Augustine, D. Fitzpatrick, L. C. Katz, A. LaMantia, J. O. McNamara, and S. M. Williams, *Neuroscience*. Sunderland (MA): Sinauer Associates, 2001.

[159] S. Liversedge, I. Gilchrist, and S. Everling, *The Oxford Handbook of Eye Movements*. Oxford Library of Psychology, OUP Oxford, 2011.

[160] V. Kumari, E. Antonova, B. Wright, A. Hamid, E. M. Hernandez, A. Schmechtig, and U. Ettinger, "The mindful eye: Smooth pursuit and saccadic eye movements in meditators and non-meditators," *Consciousness and Cognition*, vol. 48, pp. 66 – 75, 2017.

[161] J. Bronzino, *Biomedical Engineering Handbook 2*. The electrical engineering handbook series, Springer Berlin Heidelberg, 2000.

[162] D. L. Sparks, "The brainstem control of saccadic eye movements," *Nature Reviews Neuroscience*, vol. 3, no. 12, pp. 952–964, 2002.

[163] R. Dodge and T. S. Cline, "The angle velocity of eye movements.," *Psychological Review*, vol. 8, pp. 145–157, mar 1901.

[164] H. B. Barlow, "Eye movements during fixation," *The Journal of Physiology*, vol. 116, p. 290–306, mar 1952.

[165] R. W. Ditchburn and B. L. Ginsborg, "Involuntary eye movements during fixation," *The Journal of Physiology*, vol. 119, p. 1–17, jan 1953.

[166] A. T. Bahill, M. R. Clark, and L. Stark, "The main sequence, a tool for studying human eye movements," *Mathematical Biosciences*, 1975.

[167] H. Collewijn, C. J. Erkelens, and R. M. Steinman, "Binocular co-ordination of human horizontal saccadic eye movements," *The Journal of Physiology*, vol. 404, no. 1, pp. 157–182, 1988.

[168] S. J. Wilson, P. Glue, D. Ball, and D. J. Nutt, "Saccadic eye movement parameters in normal subjects," *Electroencephalography and Clinical Neurophysiology*, vol. 86, no. 1, pp. 69 – 74, 1993.

[169] T. David, S. Smye, T. Dabbs, and T. James, "A model for the fluid motion of vitreous humour of the human eye during saccadic movement," *Physics in Medicine and Biology*, vol. 43, no. 6, p. 1385, 1998.

[170] C. M. Harris and D. M. Wolpert, "Signal-dependent noise determines motor planning," *Nature*, vol. 394, pp. 780–784, Aug. 1998.

[171] J. N. van der Geest and M. A. Frens, "Recording eye movements with video-oculography and scleral search coils: a direct comparison of two methods," *Journal of Neuroscience Methods*, vol. 114, no. 2, pp. 185–195, 2002.

[172] M. A. Frens and J. N. Van der Geest, "Scleral search coils influence saccade dynamics," *Journal of Neurophysiology*, vol. 88, p. 692, aug 2002.

[173] R. Leigh and D. Zee, *The Neurology of Eye Movements*. Contemporary neurology series, Oxford University Press, 2015.

[174] L. A. Issen and D. C. Knill, "Decoupling eye and hand movement control: Visual short-term memory influences reach planning more than saccade planning," *Journal of Vision*, vol. 12, no. 1, p. 3, 2012.

[175] R. P. G. van Gompel, *Eye Movements: A Window on Mind and Brain*. Educational psychology, Elsevier Science, 2007.

[176] R. Repetto, A. Stocchino, and C. Cafferata, "Experimental investigation of vitreous humour motion within a human eye model," *Physics in Medicine and Biology*, vol. 50, no. 19, p. 4729, 2005.

[177] R. Repetto, J. H. Siggers, and A. Stocchino, "Mathematical model of flow in the vitreous humor induced by saccadic eye rotations: effect of geometry," *Biomechanics and Modeling in Mechanobiology*, vol. 9, no. 1, pp. 65–76, 2010.

[178] A. Stocchino, R. Repetto, and J. H. Siggers, "Mixing processes in the vitreous chamber induced by eye rotations," *Physics in Medicine & Biology*, vol. 55, no. 2, pp. 453–67, 2010.

[179] R. Repetto, A. Tatone, A. Testa, and E. Colangeli, "Traction on the retina induced by saccadic eye movements in the presence of posterior vitreous detachment," *Biomechanics and Modeling in Mechanobiology*, vol. 10, no. 2, pp. 191–202, 2011.

[180] R. K. Balachandran and V. H. Barocas, "Contribution of saccadic motion to intravitreal drug transport: Theoretical analysis," *Pharmaceutical Research*, vol. 28, no. 5, pp. 1049–1064, 2011.

[181] K. Isakova, J. O. Pralits, R. Repetto, and M. R. Romano, "Mechanical models of the dynamics of vitreous substitutes," *BioMed Research International*, vol. 2014, p. 10, 2014.

[182] A. Bonfiglio, A. Lagazzo, R. Repetto, and A. Stocchino, "An experimental model of vitreous motion induced by eye rotations," *Eye and Vision*, vol. 2, no. 1, pp. 1–10, 2015.

[183] J. L. Favero, A. Secchi, N. Cardozo, and H. Jasak, "Viscoelastic flow simulation: Development of a methodology of analysis using the software openfoam and differential constitutive equations," *Computer Aided Chemical Engineering*, vol. 27, pp. 915 – 920, 2009. 10th International Symposium on Process Systems Engineering: Part A.

[184] S. Pople, *Explaining Physics*. Oxford University Press, 1987.

[185] P. Balachandran, *Fundamental of compressible fluid dynamics*. PHI Learning, 2006.

[186] S. Richardson, *Fluid Mechanics*. Series in Chemical and Mechanical Engineering, Taylor & Francis, 1989.

[187] C. Gallegos, *Rheology - Volume I:*. 2010.

[188] F. Pimenta and M. A. Alves, "Stabilization of an open-source finite-volume solver for viscoelastic fluid flows," *Journal of Non-Newtonian Fluid Mechanics*, vol. 239, pp. 85 – 104, 2017.

[189] E. Y. K. Ng, J. H. Tan, U. R. Acharya, and J. S. Suri, *Human Eye Imaging and Modeling*. CRC Press, 2012.

[190] J. T. P. D. Hallinan, P. Pillay, L. H. L. Koh, K. Y. Goh, and W. Yu, "Eye globe abnormalities on mr and ct in adults: An anatomical approach," *Korean Journal of Radiology*, vol. 17, pp. 664–673, June 2016.

[191] W. Becker, *The neurobiology of saccadic eye movements. Metrics*. PHI Learning, 2006.

[192] H. Giesekus, "A simple constitutive equation for polymer fluids based on the concept of deformation-dependent tensorial mobility," *Journal of Non-Newtonian Fluid Mechanics*, vol. 11, no. 1–2, pp. 69 – 109, 1982.

[193] M. Pflaumbaum and H. Rehage, "Myristyl dimethylamine oxide surfactant solutions: Model systems for rheological research," *ChemPhysChem*, vol. 4, no. 7, pp. 705–713, 2003.

[194] S. Kheirandish, I. Gubaydullin, and N. Willenbacher, "Shear and elongational flow behavior of acrylic thickener solutions. part ii: effect of gel content," *Rheologica Acta*, vol. 48, no. 4, pp. 397–407, 2009.

[195] M. Keshavarz and B. Kaffashi, "The ability of retention, drug release and rheological properties of nanogel bioadhesives based on cellulose derivatives," *Pharmaceutical Development and Technology*, vol. 19, no. 8, pp. 952–959, 2014.

[196] P. A. Vasquez, Y. Jin, E. Palmer, D. Hill, and M. G. Forest, "Modeling and simulation of mucus flow in human bronchial epithelial cell cultures - part i: Idealized axisymmetric swirling flow," *PLoS Computational Biology*, vol. 12, aug 2016.

[197] H. K. Versteeg and W. Malalasekera, *An Introduction to Computational Fluid Dynamics: The Finite Volume Method*. Pearson Education Limited, 2007.

[198] M. A. Alves, P. J. Oliveira, and F. T. Pinho, "A convergent and universally bounded interpolation scheme for the treatment of advection," *International Journal for Numerical Methods in Fluids*, vol. 41, no. 1, pp. 47–75, 2003.

[199] A. Afonso, P. Oliveira, F. Pinho, and M. Alves, "The log-conformation tensor approach in the finite-volume method framework," *Journal of Non-Newtonian Fluid Mechanics*, vol. 157, p. 55–65, mar 2009.

[200] J. L. Federman and H. D. Schubert, "Complications associated with the use of silicone oil in 150 eyes after retina-vitreous surgery," *Ophthalmology*, vol. 95, no. 7, pp. 870 – 876, 1988.